

Martin-Luther-Universität Halle-Wittenberg
Naturwissenschaftliche Fakultät I - Biowissenschaften
Institut für Pharmazie



Structure-Based Design, Synthesis, and Biological Characterization of Potential Novel Anticancer Agents

**“Hunting for different targets in prevailing adults' and children's
cancer types”**

DISSERTATION

zur Erlangung des akademischen Grades

Doctor rerum naturalium (Dr. rer. nat.)

der Naturwissenschaftlichen Fakultät I Biowissenschaften

der Martin-Luther-Universität Halle-Wittenberg

Vorgelegt von

Frau M.Sc. Nehal Hany Aly Elghazawy

Gutachter:

- 1- Prof. Dr. Wolfgang Sippl, Halle
- 2- Prof. Dr. Mike Schutkowski, Halle
- 3- Assoc. Prof. Dr. Nermin Salah, Cairo

Date of Defence: 19 November 2024

Abstract

Cancer represents a global health challenge, impacting millions annually, with mortality rates surpassing global pandemics. Its nature harnesses complexity in initiation, mechanism, progression, outcomes, and treatment. As cancer types vary in prevalence, our focus on breast cancer, most common in females, and neuroblastoma in infants, drives our pursuit to identify potential anticancer molecules. Our approach blends computational studies, chemical synthesis, biochemical assays, and cellular testing to identify these compounds.

This work's initial focus is on PKMYT-1, a member of the WEE kinase family linked with various cancer types. Employing various in silico methods, we pursued novel diaminopyrimidines as PKMYT-1 inhibitors. Simultaneously, those diaminopyrimidines were synthesized and tested for their impact on PKMYT-1 inhibition and anticancer activity against hepatoma and neuroblastoma cell lines. While promising, the PKMYT-1 inhibition and anticancer results didn't align. Computational studies suggested the possibility of the synthesized compounds favoring other kinases like WEE1 and Aurora kinases, suggesting alternative pathways.

The second part of the work targets breast cancer, focusing on the Estrogen Receptor (ER) and MCF-7 cells representing ER+ breast cancer via multiple approaches. The first approach involves designing analogs of Tamoxifen, known for metabolism variations due to CYP2D6 polymorphism. Synthesized analogs displayed potent anticancer effects and confirmed ER binding, revealing alternative metabolic pathways. In the second approach, we explored isoeugenol and its derivatives' anticancer properties on MCF-7 cells, aiming for mechanistic validation and in vivo efficacy verification. Lastly, 5,7-dibromoquinoline derivatives with antiproliferative effects on MCF-7 cells were synthesized. To modify their physicochemical parameters, they were encapsulated in nanomicelles, which improved their solubility, cell penetration and ensured sustained release for potential therapy.

These findings could be starting points for enhancing these compounds and validating their biological outcomes using in vivo models in future projects.

Keywords: Cancer, WEE kinases, PKMYT-1, Diaminopyrimidines, Neuroblastoma, Anticancer, Molecular Docking, Computer-aided drug design, Breast Cancer, Estrogen receptor, Tamoxifen, MCF-7 cells, Isoeugenol.

Kurzfassung

Krebs ist ein globales Gesundheitsproblem, von dem jährlich Millionen Menschen betroffen sind und dessen Sterblichkeitsrate die von Pandemien übertrifft. Krebs ist von Natur aus sehr komplex, was seine Entstehung, seinen Mechanismus, sein Fortschreiten, seine Folgen und seine Behandlung angeht. Da es unterschiedliche Krebsarten gibt, konzentriert sich diese Arbeit auf Brustkrebs, der bei Frauen am häufigsten auftritt, und auf Neuroblastome bei Säuglingen. Unser Ansatz kombiniert computergestützte Studien, chemische Synthese, biochemische Assays und zelluläre Tests, um diese Verbindungen zu identifizieren.

Der Schwerpunkt dieser Arbeit liegt zunächst auf PKMYT-1, einem Mitglied der WEE-Kinase-Familie, das mit verschiedenen Krebsarten in Verbindung gebracht wird. Mithilfe verschiedener In-silico-Methoden haben wir neue Diaminopyrimidine als PKMYT1-Inhibitoren untersucht. Gleichzeitig wurden diese Diaminopyrimidine synthetisiert um auch ihre Auswirkungen auf die PKMYT-1-Hemmung und ihre krebshemmende Wirkung gegen Hepatom- und Neuroblastom-Zelllinien zu testen. Obwohl die Ergebnisse vielversprechend waren, korrelierten die PKMYT-1-Hemmung und die krebshemmende Wirkung zunächst nicht. Computergestützte Studien legten die Möglichkeit nahe, dass die synthetisierten Verbindungen andere Kinasen wie WEE1 und Aurora-Kinasen begünstigen, was auf alternative Wirkmechanismen hindeutet.

Der zweite Teil der Arbeit zielt auf Brustkrebs ab und konzentriert sich auf den Östrogenrezeptor (ER) und MCF-7-Zellen, die ER+-Brustkrebs repräsentieren. Der erste Ansatz umfasst die Entwicklung von Tamoxifen-Analoga, die aufgrund des CYP2D6-Polymorphismus unterschiedlich verstoffwechselt werden. Die synthetisierten Analoga zeigten starke krebshemmende Wirkungen und bestätigten die ER-Bindung, was alternative Stoffwechselwege aufzeigte. Im zweiten Ansatz untersuchten wir die krebshemmenden Eigenschaften von Isoeugenol und seinen Derivaten auf MCF-7-Zellen mit dem Ziel der mechanistischen Validierung und der Überprüfung der in vivo-Wirksamkeit. Schließlich wurden 5,7-Dibromchinolinderivate mit antiproliferativer Wirkung auf MCF-7-Zellen synthetisiert. Um ihre physikochemischen Parameter zu verändern,

wurden sie in Nanomikroben eingekapselt, wodurch ihre Löslichkeit und Zellpenetration verbessert und eine nachhaltige Freisetzung für eine potenzielle Therapie gewährleistet wurde.

Diese Erkenntnisse könnten Ausgangspunkt für die Verbesserung dieser Verbindungen und die Validierung ihrer biologischen Ergebnisse anhand von In-vivo-Modellen in künftigen Projekten sein.

Schlüsselwörter: Krebs, WEE-Kinasen, PKMYT-1, Diaminopyrimidine, Neuroblastom, Krebsbekämpfung, molekulares Docking, computergestütztes Wirkstoffdesign, Brustkrebs, Östrogenrezeptor, Tamoxifen, MCF-7-Zellen, Isoeugenol.

Acknowledgments

While the Ph.D. journey is a purely scientific achievement, mine has enriched my personal and professional skills and bestowed upon me invaluable people to whom I am always grateful.

First, I would like to thank my supervisor, **Prof. Wolfgang Sippl**, for welcoming me as a Ph.D. student in his group. I appreciate the amount of responsibility he gave me, which was the right push for my scientific future and academic career. His utmost support helped me through the challenges, bringing me this far with my degree. Finally, he was a great mentor who nourished my interest in different projects with collaborators worldwide, leading to multiple publications.

Second, I would like to thank **Dr. habil Matthias Schmidt** for trusting me with the project he had worked on for years. My close work with him has shown me the true meaning of a leader. He has made our very international lab a warm place for all of us. I can't show enough gratitude to him for his sincere compassion in hard times and genuine joy for our success.

Also, a special thanks goes to **Dr. Dina Robaa** for being that important person in my life. She has been there from day one of this journey until the thesis's final revisions. Whenever everything is stuck, she always comes with the torch that lights the way for all of us around her. She has been a mentor in computational chemistry, academic career, and life.

I want to thank **Dr. Ehab Ghazy**, who has greatly supported my Ph.D. journey. He never saved any advice, whether in the lab or in life. His opinions were always a trustworthy guide. While Dr. Ehab was considered a colleague, the support I received from him and his lovely family has made them a second family to me.

A big thank goes to all the colleagues I met in the lab who have always been nice and helpful. A special thanks to my Italian sister **Chiara** and my Guatemalan sister **Yarden**. I am grateful for our great times together that helped me to pass the hard times.

Dedication

To my parents, Thanks for your unconditional love and endless support over the years. Thanks to my mother, who has known my passion for chemistry since I was thirteen years old, and for her encouragement to pursue it. Thanks to my father for never saving money and making the effort to make me the person I am today.

Thanks to my sisters, Nour and Dalia, for your love and endless support. Thanks to my nephew Yazeed, for making me laugh whenever things get tough for me.

To my late grandparents, who have always been asking when I will finish the Ph.D., I dedicate that work to you.

Finally, to my life partner and husband, Mahmoud, thanks for being there through every minute of this journey. Thanks for the support that you give me. I hope that you and our future kids are proud of me.

Table of Contents

ABSTRACT	II
KURZFASSUNG	IV
ACKNOWLEDGMENTS	VI
DEDICATION	VII
TABLE OF CONTENTS	VIII
LIST OF FIGURES	X
LIST OF ABBREVIATIONS	XII
1. INTRODUCTION	1
1.1. CANCER.....	2
1.2. NEUROBLASTOMA	2
1.2.1. <i>Epidemiology and Classification</i>	2
1.2.2. <i>Pathophysiology</i>	3
1.2.3. <i>Management</i>	3
1.3. BREAST CANCER	4
1.3.1. <i>Epidemiology and classification</i>	4
1.3.2. <i>Pathophysiology</i>	5
1.3.3. <i>Management</i>	6
1.4. RELEVANCE OF THE INVESTIGATED PROTEIN TARGETS	6
1.4.1. <i>WEE1 and PKMYT-1 kinases</i>	6
1.4.1.1. Mitotic cell cycle	6
1.4.1.2. Physiological role WEE kinases in the cell cycle.....	8
1.4.1.3. WEE Kinases and Cancer	9
1.4.1.4. WEE1 and PKMYT-1 Inhibition.....	11
1.4.1.4.1. Designing WEE and PKMY1 Inhibitors	11
1.4.1.4.2. WEE1 Inhibitors	13
1.4.1.4.3. PKMYT-1 inhibitors.....	14
1.4.2. <i>Estrogen Receptor</i>	19
1.4.2.1. Characterization and Physiological Role of Estrogen Receptor	19
1.4.2.2. Estrogen receptor signaling pathway:	20
1.4.2.3. Estrogen Receptor and Breast Cancer	22

1.4.2.4.	Estrogen receptor ligands for breast cancer treatment	23
1.4.2.4.1.	Selective Estrogen Receptor Modulators:	23
1.4.2.4.2.	Tamoxifen.....	24
1.4.2.4.3.	Metabolism of Tamoxifen:	25
1.4.2.4.4.	Tamoxifen mechanism of action:	26
1.4.2.4.5.	Tamoxifen Structure-Activity Relationship.....	27
1.4.2.4.6.	CYP2D6 enzyme.....	28
2.	AIM OF THE WORK.....	30
3.	RESULTS	34
4.	SUMMARY OF THE RESULTS.....	105
5.	GENERAL CONCLUSIONS	123
6.	REFERENCES	127
7.	APPENDIX	135

List of Figures

FIGURE 1: CLASSIFICATIONS OF BREAST CANCER	5
FIGURE 2: EUKARYOTE CELL CYCLE	8
FIGURE 3: CELL CYCLE CONTROL	10
FIGURE 4: SUPERPOSITION OF CRYSTAL STRUCTURES FROM THE PROTEIN DATA BANK (PDB) OF WEE1 (PDB ID: 1X8B) AND PKMYT-1 (PDB ID: 3P1A).....	13
FIGURE 5: MOST PROMISING WEE1 INHIBITORS UNDER INVESTIGATION CLASSIFIED BASED ON THEIR CHEMICAL STRUCTURES	14
FIGURE 6: CHEMICAL STRUCTURES OF SELECTED PKMYT-1 INHIBITOR	15
FIGURE 7: STRUCTURES FOR THE TEN PKMYT-1 INHIBITORS DERIVED FROM SCREENING GSK PKIs AND PKIIs	16
FIGURE 8: RATIONALE OF DESIGN OF RP-6306	18
FIGURE 9: ESTROGEN RECEPTOR DOMAIN STRUCTURE LANDSCAPE.....	20
FIGURE 10: LIGAND-DEPENDENT AND LIGAND-INDEPENDENT MECHANISM OF ESTROGEN RECEPTOR SIGNALING	22
FIGURE 11: STRUCTURES OF SELECTED SERMS.....	24
FIGURE 12: TAMOXIFEN METABOLISM TO ITS ACTIVE METABOLITES.....	26
FIGURE 13: E2 (A) vs. 4-OHTAM (B) COMPLEX WITH HELIX 12 AND EXPOSURE TO D351	27
FIGURE 14: STILBENE SKELETON.....	27
FIGURE 15: HYDROXYTAMOXIFEN INTERACTIONS IN THE ER PDB ID (3ERT)	28
FIGURE 16: STRUCTURES FOR TEN PKMYT-1 INHIBITORS DERIVED FROM SCREENING GSK PKIs AND PKIIs	39
FIGURE 17: DOCKING RESULTS OF THE THREE MOST POTENT INHIBITORS FOUND FOR PKMYT-1 (PDB ID 5VD1).	48
FIGURE 18: . DOCKING RESULTS OF THE THREE MOST POTENT INHIBITORS FROM THE CANCER CELL TESTING FOR WEE1 (PDB ID 5Y5V).....	49
FIGURE 19: DOCKING RESULTS OF THE THREE MOST POTENT INHIBITORS FROM THE CANCER CELL TESTING FOR AURORA A KINASE (PDB ID 4DEB).....	50
FIGURE 20: SCHEME OF THE ATP-BINDING POCKET OF PKMYT-1.....	107
FIGURE 21: DIPHENYLDIAMINOPYRIMIDINE SCAFFOLD AND THREE POSSIBLE VECTORS TO START A FRAGMENT GROWING PROCESS	108
FIGURE 22: THE MOST PROMISING SYNTHESIZED PKMYT-1 INHIBITORS	109
FIGURE 23: DESIGN STRATEGY OF TAM DERIVATIVES.....	113
FIGURE 24: MOST ACTIVE COMPOUND IN FLEXIBLE TAM ANALOGUES (COMPOUND 3)	113
FIGURE 25: OVERLAY OF COMPOUND 3 (RED) ON 4-OHTAM (GREEN).....	114
FIGURE 26: COMPOUND 3 AND COMPOUND 10 STRUCTURES AND IC50 VALUES	115
FIGURE 27: OVERLAY OF COMPOUND 3 (RED) ON 4-OHTAM (GREEN).....	116
FIGURE 28: EXTRACTED ION CHROMATOGRAM OF COMPOUND 10 AFTER INCUBATION IN HL OR CYP2D6 SUPERSOMES, BOTH WITH AND WITHOUT NADPH.	117

FIGURE 29: MOST ACTIVE COMPOUNDS 2,8,10 AND THEIR IC ₅₀ S AGAINST MCF-7 AND MCF-10A CELLS	118
FIGURE 30: DOWNREGULATION OF ER GENES (A) AND PROTEINS(B) IN CASE OF COMPOUND 2 TREATED CELLS VS CONTROL	119
FIGURE 31: SUMMARY OF MIXED MECHANISMS OF ACTION OF COMPOUND 2.....	119
FIGURE 32: DESIGN STRATEGY FOR QUINOLINE-BASED DERIVATIVES	120
FIGURE 33: MOST ACTIVE COMPOUND OF THE 5,7-DIBROMQUINOLINE DERIVATIVES.	121
FIGURE 34: FREE COMPOUNDS VS THEIR CORRESPONDING NANOMICELLS FORMATION	121
FIGURE 35: FREE FORM VS. LOADED NP IC ₅₀ S AGAINST MCF-7 AND MDA-MB231 CELLS.....	122
FIGURE 36: DEGRADATION PATTERN OF THE PLURONIC NANOMICELLES, AND THE RELEASE PROFILES OF THE SYNTHESIZED BIOACTIVE COMPOUNDS FROM THE NANOMICELLES.	122

List of abbreviations

4-OHTAM	4-hydroxytamoxifen
5-FU	5-Fluorouracil
AF1	Transcriptional activation function 1
AF2	Transcriptional activation factor 2
Akt	Protein kinase B
ALK	Anaplastic Lymphoma Kinase
AP-1	Activator protein 1
BC	Breast Cancer
CCAAT	cytosine-cytosine-adenosine-adenosine-thymidine
C/EBPβ	CCAAT-enhancer-binding protein beta
Cdks	Cyclin-dependent kinases
CDC25	Cell division cycle 25
CREB	cAMP response element-binding protein
CYP	Cytochrome P450
DBD	DNA binding domain
E1	Estrone
E2	Estradiol
E3	Estriol
E4	Estetrol
Elk-1	ETS Like-1 protein
EM	Extensive metabolizers
ER	Estrogen Receptor
ERα	Estrogen Receptor alpha
ERβ	Estrogen Receptor beta
ERE	Estrogen Response Element
ERK1/2	Extracellular signal-regulated protein kinases 1 and 2
FP	Fluorescence polarization
GPβER1	G protein-coupled estrogen receptor 1

hHep	human hepatocytes
HLM	human liver microsomes
HER2	Human Epidermal Growth Factor Receptor 2
HSP90	Heat Shock Protein 90
IM	Intermediate Metabolizers
LBD	ligand-binding domain
MAPK	Mitogen-activated protein kinase
MBC	Male breast cancer
MCF-7	Michigan Cancer Foundation-7
MEK1/2	Mitogen-activated protein kinase kinase 1/2
mERs	membrane Estrogen Receptors
mTOR	Mammalian target of rapamycin
NADPH	Nicotinamide Adenine Dinucleotide Phosphate
NB	Neuroblastoma
NF-κB	Nuclear Factor Kappa B
NP	Nano Particles
NSCLS	Non-small-cell lung cancer
NTD	N-Terminal A/B domain
(PAM50)	Prediction Analysis of Microarray 50
PI3K	Phosphoinositide 3-kinases
PKMYT-1	Membrane-associated tyrosine- and threonine-specific cdc2-inhibitory kinase
PM	Poor Metabolizers
PR	Progesterone receptor
P53	Tumor protein P53
RAF	Rapidly Accelerated Fibrosarcoma.
RAS	Rat sarcoma
SAC	Spindle assembly checkpoint
SERDs	Selective Estrogen Receptor Down-regulators
SERMs	Selective Estrogen Receptor Modulators

SP-1	Specificity Protein 1
SNPs	Single-nucleotide polymorphisms
SSRIs	Selective Serotonin Reuptake Inhibitors
TAM	Tamoxifen
TNBC	Triple-negative breast cancer
UM	Ultrarapid Metabolizers

1. Introduction

1.1. Cancer

Cancer represents an escalating global public health challenge, standing among the leading causes of mortality worldwide. As per GLOBOCAN 2020, the number of new cancer cases diagnosed in 2020 was 19.3 million, and almost 10.0 million died due to cancer. GLOBOCAN predicts that the number of cancer cases will increase to 28.4 million in 2040 [1, 2]. While cancer pathophysiology may be multifactorial, at its core lies the abnormal growth and spread of cells as an outcome of genetic mutations that disrupt the delicate balance between cell division and regulation. These mutated cells, which should be detected and eliminated through immune surveillance, manage to evade the body's natural regulatory mechanisms. Consequently, they form tumors and interfere with normal bodily functions, contributing to the diverse spectrum of conditions encompassed within the broader category of cancer [3, 4]. Tumors can be classified in various ways, with one standard approach organizing them based on the tissue of origin or anatomical location. For instance, some tumors are associated with specific organs, such as breast cancer, lung cancer, prostate cancer, etc. Others, like neuroblastoma, osteosarcoma, and leukemia, are categorized by their originating tissues [5, 6]. The heterogeneity across cancer types necessitates tailored approaches to diagnosis, treatment, and management, considering factors such as growth patterns and responses to therapy. Therefore, cancer research advancements have revolutionized detection and treatment paradigms [7-9].

1.2. Neuroblastoma

1.2.1. Epidemiology and Classification

Neuroblastoma (NB) stands as the most prevalent and life-threatening tumor occurring in infancy, contributing to around 8-10% of all childhood cancer cases and 15% of childhood cancer-related fatalities. It is typically a tumor of early childhood, where the median age for diagnosis is 18 months, and more than 90% of all neuroblastoma cases are diagnosed before 10 years of age [10-12]. The annual incidence of NB in the United States is approximately 650 cases, i.e., 10.2 per million children (65 per million infants), with little change (0.4%) over time [13].

Given the heterogeneous nature of neuroblastoma, establishing a classification system for prognosis and tailored treatment is imperative. Over recent decades, the neuroblastoma risk classification system has integrated numerous clinical and biological factors. To address the challenge of non-uniform risk grouping, the International Neuroblastoma Risk Group (INRG) classification emerged as a solution. This classification introduced a novel staging system based on image-defined risk factors inherent to the original tumor. Subsequently, a refined risk stratification system was developed, identifying key predictive factors such as INRG stage, patient age, histologic category, degree of differentiation, MYCN status, 11q aberration, and tumor cell ploidy. Utilizing these parameters, 17 distinct cohorts were defined and categorized into very low, low, intermediate, or high-risk groups [14, 15].

1.2.2. Pathophysiology

Neuroblastoma's tumorigenesis originates from disrupted development in sympatho-adrenergic precursors of the neural crest. While no prevalent genetic or epigenetic abnormality explains most NB cases, specific structural genomic changes like MYCN amplification, anaplastic lymphoma kinase (ALK) activating mutations, 1p36 deletion, or 17q gain are linked to tumorigenesis and reduced survival [16-20].

1.2.3. Management

The treatment spectrum for neuroblastoma varies widely based on the patient's risk status, ranging from observation alone to cytoreductive surgery, either with or without low-intensity chemotherapy for low-risk disease, to intensive multimodal therapies for high-risk disease. Recently, the identification of neuroblastoma biology drivers has introduced disease-directed therapies targeting specific oncogenic factors. These targeted therapy options include addressing genetic aberrations, disrupted signaling molecules, immunology-based approaches, radiopharmaceutical targeting of norepinephrine and somatostatin receptors, regulating epigenetic factors, and concentrating on Bcl-2 family

proteins. Notably, cancer immunotherapy emerged as an effective strategy with reduced toxicity compared to genotoxic therapies [21-23].

Understanding the genetics of neuroblastoma is crucial, facilitating tailored medical approaches aligned with each patient's genetic predisposition. Moreover, continuous efforts must continue uncovering novel signaling pathways pivotal in NB's development and resistance to treatment, presenting potential avenues for therapy.

1.3. Breast cancer

1.3.1. Epidemiology and classification

Breast Cancer (BC) ranks as the most prevalent diagnosed cancer type and remains one of the leading causes of mortality among female cancer patients. In 2020, a distressing 2.3 million cases of female breast cancer were reported worldwide, with approximately 685,000 women losing their lives to this disease. Disturbingly, projections reveal an alarming surge in the burden of breast cancer, with estimations suggesting that by 2040, the global count of new cases will escalate to over 3 million, accompanied by a staggering 1 million fatalities. While breast cancer is a typical malignancy in women, it is noteworthy that nearly 1% of all breast cancer cases are observed in males (MBC), accentuating the susceptibility of male breast tissue to carcinogenic transformation [24-26].

Breast cancer is a multi-faceted and diverse disease characterized by various biological features, clinical presentations, pathological features, therapeutic responses, and outcomes. Over recent decades, the rise in breast cancer incidence has been influenced by a myriad of risk factors, encompassing demographic, hormonal, hereditary, behavioral, and environmental aspects [27-31]. Accordingly, breast cancer is sometimes defined as a collection of different diseases that affect the same anatomical origin and originate from the terminal duct lobular units of the breast, modifying the normal glands into cancer.

Over the years, clinical practice has embraced various classifications of breast cancer, considering its histology, grading, tumor size, nodal status, and distant metastasis staging, all of which aid in making informed oncologic decisions

[32]. However, a molecular classification system based on the expression of estrogen receptor (ER), progesterone receptor (PR), and human epidermal growth factor receptor 2 (HER2/neu) has emerged as particularly significant in terms of prognosis and prediction [33]. Consequently, this combined histological and molecular approach has identified five intrinsic subtypes of breast cancer: luminal A, luminal B, normal breast-like, HER2-enriched, and basal-like (**Figure 1**) [34, 35]. This classification has subsequently steered breast cancer clinical management towards more biology-centered strategies. From another perspective, breast cancer can also be categorized into hormone receptor-positive breast cancers, expressing ER and/or PR, whereas triple-negative breast cancer (TNBC) lacks ER, PR, or HER2 expression, providing an additional perspective on classifying this complex disease (**Figure 1**).

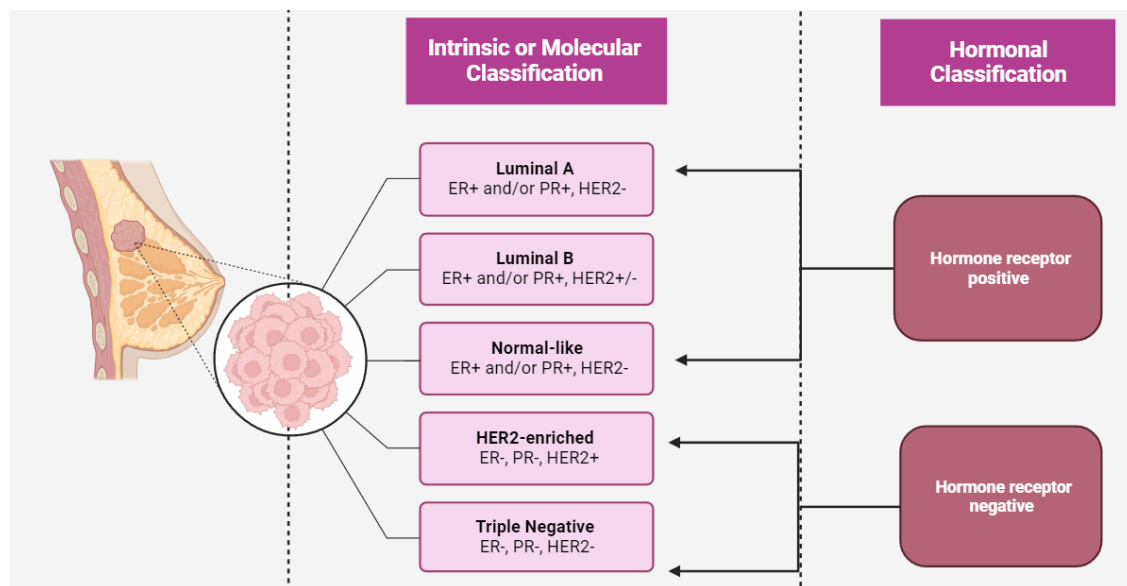


Figure 1: Classifications of Breast Cancer (created by Biorender.com)

1.3.2. Pathophysiology

Unfortunately, the complexity of breast cancer's heterogeneity has posed challenges in pinpointing the precise mechanisms of its initiation. The pathophysiology of breast cancer is believed to be a multifactorial and intricate process shaped by an interplay of genetic, hormonal, and environmental factors [36, 37]. While some risk factors are considered modifiable, like physical activity, alcohol consumption, smoking, drugs, and chemical exposure, other factors, such

as genetic mutations, family history, age, race, and sex, remain beyond our control [38, 39].

1.3.3. Management

Successful breast cancer management relies on a timely and accurate diagnosis and a well-organized, multi-approached treatment plan. Surgery, radiotherapy, and chemotherapy have remained the mainstay approaches in breast cancer treatment for nearly eight decades. While these approaches tend to focus on eradicating residual cancer tissues, preventing disease recurrence is equally crucial. In recent years, targeted therapy has emerged as a prominent focus in oncology research, particularly in the context of breast cancer. Targeted therapies specifically combat the drivers of the disease, which may include molecular abnormalities, tumor cells responsible for cancer development, or specific targets implicated in the pathogenicity of breast cancer. By directing attention to these precise targets, targeted therapies offer a promising avenue for more personalized and effective treatment strategies [40, 41].

1.4. Relevance of the investigated protein targets

In the following sections, this work delves into the detailed descriptions of the protein targets under investigation, shedding light on their physiological roles, implications in breast cancer, and comprehensive discussions on their associated significant inhibitors.

1.4.1. WEE1 and PKMYT-1 kinases

1.4.1.1. Mitotic cell cycle

The cell cycle is an orchestrated series of events aiming to reproduce two daughter cells and duplicate the genomic DNA. The cell cycle progression is divided into four major phases: gap 1 (G₁), DNA synthesis (S), gap 2 (G₂), and mitosis (M). The G₁ phase is the growth phase, where the cells produce more proteins, amplify the organelles, and grow in size [42]. Subsequently, the chromosome starts replication where the DNA amount is doubled in the S phase; then, the cell is prepared for mitosis by protein/lipid synthesis and cell growth in

the G2 phase. In another scenario, after the G1 phase, the cell decides not to go through with the cell division but to a quiescent G₀ state. While G₀, G1, S, and G2 are called interphase, the M phase comprises mitosis, where the cell's nucleus divides, followed by cytokinesis (**Figure 2**) [43-45]. For a smooth transition between the different phases, each phase must ensure the proper completion of the preceding one to prevent any accumulation or propagation of genetic errors during cell division. Therefore, there are three major cell cycle checkpoints: The G1/S checkpoint (restriction checkpoint), the G2/M DNA damage checkpoint, and the spindle assembly checkpoint (SAC) [46-48].

Progression of the cell cycle is mediated by cyclin-dependent kinases (Cdks) and their regulatory cyclin subunits. CDKs are a family of serine-threonine kinases that direct cell division through the phosphorylation of target proteins in the cell cycle. While there are almost 20 different members of the CDK family, only CDK1, CDK2, CDK4, and CDK6 play a specific role in regulating cell cycle transitions (**Figure 2**). For example, CDK1 (also known as cdc2) is a key regulator of the G2/M transition and is responsible for initiating mitosis. CDK4 and CDK6 play a role in the cell cycle's progression from G1 to S phase [49]. Activation of the CDKs is mediated through binding to the regulatory cyclin protein. Cyclins are proteins produced cyclically, with their levels peaking at specific stages of the cell cycle. Cyclins bind to the catalytic subunit of CDKs, leading to their activation, followed by the progression of the cell cycle. At different stages of the cell cycle, different CDK-Cyclin complex combinations become in charge. For instance, cyclin D binds to CDK4 and CDK6, leading to the regulation of the G1/S transition, and cyclin B binds to CDK1, leading to the regulation of the G2/M transition [50, 51].

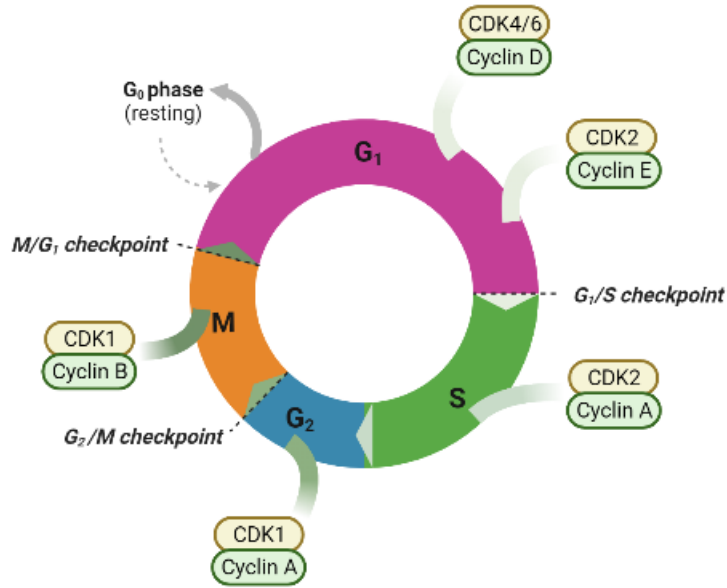


Figure 2: Eukaryote cell cycle

1.4.1.2. Physiological role WEE kinases in the cell cycle

WEE kinase is a family of protein kinases, which in humans, it constitutes three members, namely PKMYT-1 (membrane-associated tyrosine- and threonine-specific cdc2-inhibitory kinase) and two WEE1 kinases (WEE1, WEE1B). Although these kinases share similar sequences, they differ in localization, temporal expression, and regulation [52]. For instance, both WEE1 and WEE1B are known for their predominant nuclear localization as well as their ability to inactivate CDK1 via phosphorylation; still, WEE1B is considered an early expressed kinase that is replaced later by WEE1, which is more abundant in zygotes, after fertilization [53]. Therefore, only WEE1 and PKMYT-1 are known to be essential parts of the cell cycle progression, as follows. CDK1 is initially in an inactive state, maintained by the phosphorylation of two specific amino acids, threonine 14 and tyrosine 15, until the completion of DNA replication in the S phase. If DNA damage is detected, cells undergo arrest in the G₂ phase, halting the progression to mitosis. In humans, both WEE1 and PKMYT-1 are responsible for the phosphorylation of CDK1. WEE1 specifically phosphorylates tyrosine 15, while PKMYT-1 can target both threonine 14 and tyrosine 15 residues. PKMYT-1 plays a critical role in preventing cell entry into the M-phase not only by maintaining the inactivity of CDK1-cyclin B complexes but also by hindering their translocation into the nucleus. This is achieved by

stabilizing the assembly of both Golgi and endoplasmic reticulum structures in mammalian cells [54-59].

1.4.1.3. WEE Kinases and Cancer

Given that uncontrolled proliferation is a characteristic hallmark of cancer cells, it is reasonable to hypothesize that alterations in cell cycle checkpoints could contribute to an increased risk of cancer. In normal cells, recurrent defects in DNA that occur during replication are repaired at the G1/S checkpoint, preventing defective cells from entering mitosis. Additionally, the negative regulation of both WEE1 and PKMYT-1 is counteracted by CDC25 phosphatase, which removes the phosphorylation from the CDK1-cyclin B complex (**Figure 3**). This delicate balance between the WEE1/PKMYT-1 and CDC25 activity levels ultimately determines whether a cell progresses into mitosis or undergoes cell cycle arrest. Any disruptions in this balance could potentially lead to uncontrolled cell division and cancer development [56, 59, 60].

On the contrary, tumor cells are known to have abrogated G1/S checkpoint due to the mutation of the p53 suppressor gene, resulting in increased DNA damage at the G2 checkpoint compared to normal cells [61-64]. Along with the line of reasoning, cancer cells have become highly reliant on G2/M phase regulators, which play a critical role in deciding whether to allow G2/M arrest for DNA repair or undergo premature mitosis, ultimately leading to a phenomenon known as “Mitotic catastrophe“ in cancer cells. This fate-determining step is tightly controlled by WEE1 and PKMYT-1, given their inhibitory effect on CDK1. In conclusion, the role of G2/M checkpoint regulators such as WEE1 and PKMYT-1 tends to be more vital for tumor cells than normal cells [65-67].

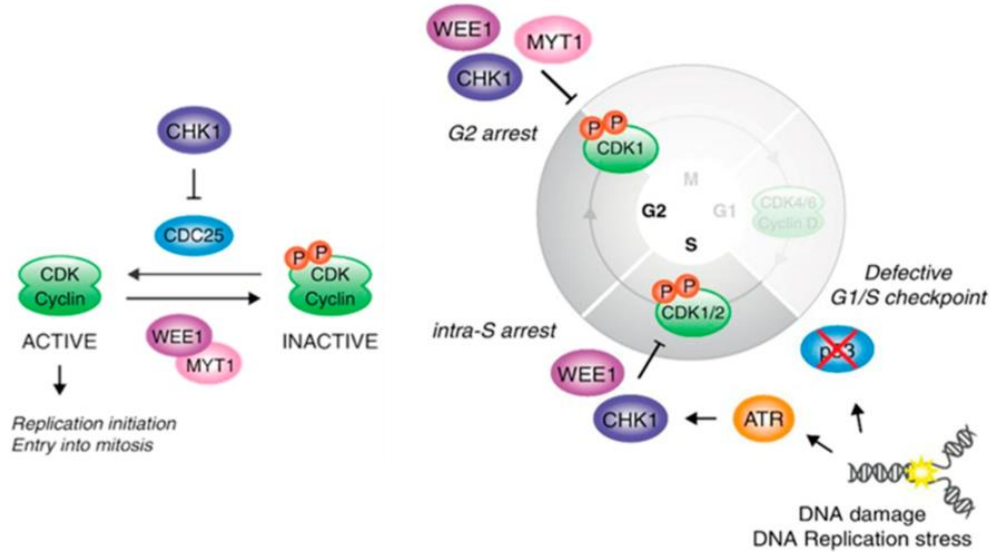


Figure 3: Cell cycle control, DNA damage checkpoint(modified from Aarts et al. [68]) Reproduced with permission from Nick Turner, Current Opinion in Pharmacology; published by Elsevier, 2013

Further studies that have been interested in correlating the genetic expression of both WEE1 and PKMYT-1 with different types of tumors found that the prevalence of mutations in WEE1 and PKMYT-1 genes among cancer patients is relatively low, with an overall mutation frequency of 1.2% and 0.2% respectively. While missense mutations cluster near the WEE1 kinase domain, PKMYT-1 mutations scatter throughout its sequence. The functional consequences of these mutations are not well understood, but transcript expression tends to be higher in mutated cases, indicating an oncogenic role [69]. On another note, elevated PKMYT-1 levels are linked to tumor progression, aggressive disease, and metastasis induction in various tumors, including hepatocellular carcinoma, colon cancer, non-small-cell lung cancer (NSCLS), and gastric cancers [70-73]. Finally, it is worth mentioning that the expression of WEE1 and PKMYT-1 is associated with activating specific cellular pathways in different cancer subtypes. For instance, WEE1 regulates melanoma cells' p38/MAPK pathway and regulates epithelial-mesenchymal transition (EMT) through beta-catenin/TCF signaling in hepatocellular carcinoma and colorectal cancers [72, 74]. PKMYT-1 controls the Notch pathway in NSCLC and stabilizes MYCN protein in neuroblastic tumors. In esophageal squamous cell carcinoma, PKMYT-1 is associated with and regulates the AKT/mTOR pathway [75, 76]. These findings suggest that WEE1 and

PKMYT-1 fulfill broader roles beyond DNA damage response, making them potential therapeutic targets.

1.4.1.4. WEE1 and PKMYT-1 Inhibition

1.4.1.4.1. Designing WEE and PKMY1 Inhibitors

As mentioned earlier, most human cancer cells are known to have defective G1 checkpoints due to p53 cancer-related mutations; therefore, there is a noticeable increase in the damaged DNA that reaches the G2 checkpoints compared to normal cells [62, 77]. With that in mind, selective targeting of the G2 checkpoint has emerged as a promising strategy to sensitize cancer cells while sparing normal cells from harmful side effects. Abrogation of the G2 checkpoint forces cells with unrepaired DNA damage into premature mitosis, leading to mitotic catastrophe and apoptosis when the extent of damage exceeds a certain bearing threshold [78-80]. Normal cells and cancer cells with an intact G1 checkpoint arrest, especially those with functional p53 signaling, demonstrate reduced reliance on the G2 checkpoint and lower sensitivity to G2 checkpoint abrogation [81]. This stream of research has highlighted the concept of “cell cycle G2 checkpoint abrogation” as a tactic for developing cancer cell-specific medicines. In 1995, original attempts to use caffeine to disrupt the G2 checkpoint against G1-defective cancer cells were reported; however, the non-specificity of caffeine towards the G2 checkpoint has led to ambiguous results [82-84]. Further studies have eventually come with a list of possible G2 abrogators such as inhibitors of CHK1 (Staurosporin, UCN-01, Go6976, SB-218078, ICP-1, LY2606368, and CEP-3891), both CHK1 and CHK2 (TAT-S216A and debromohymenialdisine), CHK2 (CEP-6367), and PP2A (okadaic acid and fostriecin), as well as the unknown checkpoint inhibitors 13-hydroxy-15-ozoapathin and the isogranulatimides [67, 78]. We herein focus on WEE1 and PKMYT-1 inhibitors since they are the main target compounds for our work.

It is essential to comprehend the structure of these kinases to develop potent and selective inhibitors targeting WEE1 and PKMYT-1. Upon structural analysis, it was observed that both WEE1 kinase and PKMYT-1 exhibit a similar architecture to other characterized kinase structures, featuring two lobes

connected by a hinge region. Moreover, the kinase's catalytic domain, which is highly conservative, is situated between two terminal lobes; the N-terminal and C-terminal lobes. The N-terminal lobe comprises five standard β -sheets and one α -helix, the α -C-helix surrounding the ATP-binding cleft. Within the N-terminal lobe exists a flexible Glycine-rich loop (P-loop or G-loop) that forms the upper surface of the ATP-binding pocket, where it alters conformations depending on the catalytic state and bound ligand. On the other hand, the C-terminal domain is a combination of α -helices and encompasses the activation loop. The catalytic cleft which also lies in the C-terminal domain is divided into a front cleft involving the ATP-binding pocket and a back cleft containing crucial residues for kinase regulation such as Asp 233 in PKMYT-1 and Asp426 in WEE1. Finally, the conserved Asp-Phe-Gly (DFG motif; WEE1: Asp463, Leu464, Gly465; PKMYT-1: Asp251, Phe252, Gly253), located at the beginning of the activation loop, plays a role in regulating the activity state of kinases and is situated within the catalytic segment (**Figure 4**) [85].



Figure 4: Superposition of crystal structures from the Protein Data Bank (PDB) of WEE1 (PDB ID: 1X8B) and PKMYT-1 (PDB ID: 3P1A). The protein ribbon is colored as following: N-Terminus: gold; C-Terminus: magenta; hinge region: dark green; activation loop: cyan; P--loop: yellow; PKMYT-1 residues: white; WEE1 residues: green

1.4.1.4.2. *WEE1 Inhibitors*

The work aimed to develop WEE1 inhibitors has surpassed that directed toward PKMYT-1 inhibitors. Recently, Du et al. provided a comprehensive summary of the structural types, structure-activity relationships (SARs), and binding modes of WEE1 inhibitors reported in scientific journals. His systemic analysis classified WEE1 inhibitors into five different chemical classes: pyridopyrimidines, pyrazolopyrimidinones, pyrrolocarbazoles, pyrimidine-based tricyclic molecules, and vanillates (**Figure 5**) [86]. Although hundreds of compounds have been reported to have inhibitory activity against WEE1 kinase, Adavosertib (AZD1775) is the only WEE1 inhibitor that has undergone more than fifty clinical trials to test its future as a potential anticancer therapy [87, 88]. Notably, Avosertib has proven active as a single therapy and in combination with others against various types of solid tumors such as neuroblastoma [89].

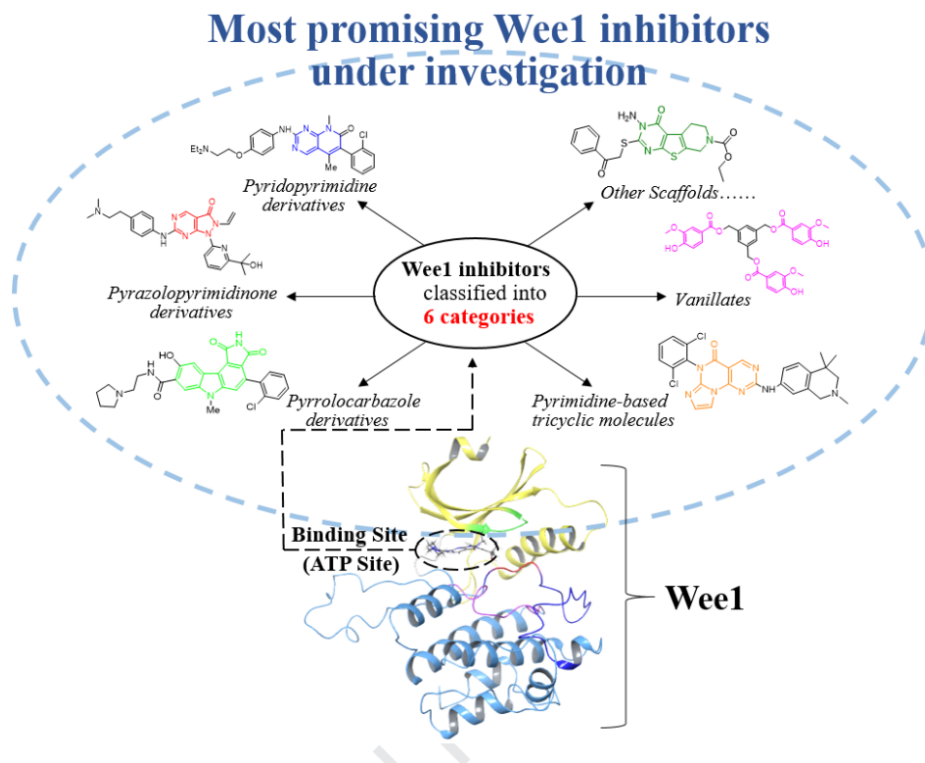


Figure 5: Most promising WEE1 inhibitors under investigation classified based on their chemical structures [86]

1.4.1.4.3. PKMYT-1 inhibitors

The discovery of PKMYT-1 dates back to 1995, but it was not until 2010 that the first crystal structure of this kinase was reported [56]. In the realm of PKMYT-1 inhibition, Zhu et al. achieved a significant milestone by successfully co-crystallizing a limited set of nine inhibitors, all demonstrating notable activity. Among these, certain drugs have emerged as noteworthy contenders, including Dasatinib and Bosutinib, both classified as tyrosine kinase inhibitors, exhibiting IC_{50} values of 130 nM and 350 nM, respectively. Furthermore, a group of pyridopyrimidine derivatives, namely PD0166285 ($IC_{50} = 7.2$ nM), PD173952, PD173955, and PD180970, have shown promising inhibitory effects (**Figure 6**). However, it is essential to mention that certain compounds, such as Pelitinib, Saracatinib, and Tyrphostin AG14784, exhibit relatively weaker inhibitory properties [90]. As a result, the abundance and potency of PKMYT-1 inhibitors appear to be more limited and challenging when compared to inhibitors targeting other kinases. This observation becomes particularly evident when considering the

selectivity score provided by Davis et al., which stands at a meager 0.0417 at an inhibitor concentration of 3 μ M. These findings accentuate the need for further research and development to improve the selectivity and efficacy of PKMYT-1 inhibitors, which could potentially lead to more effective and targeted therapeutic interventions for various diseases [91].

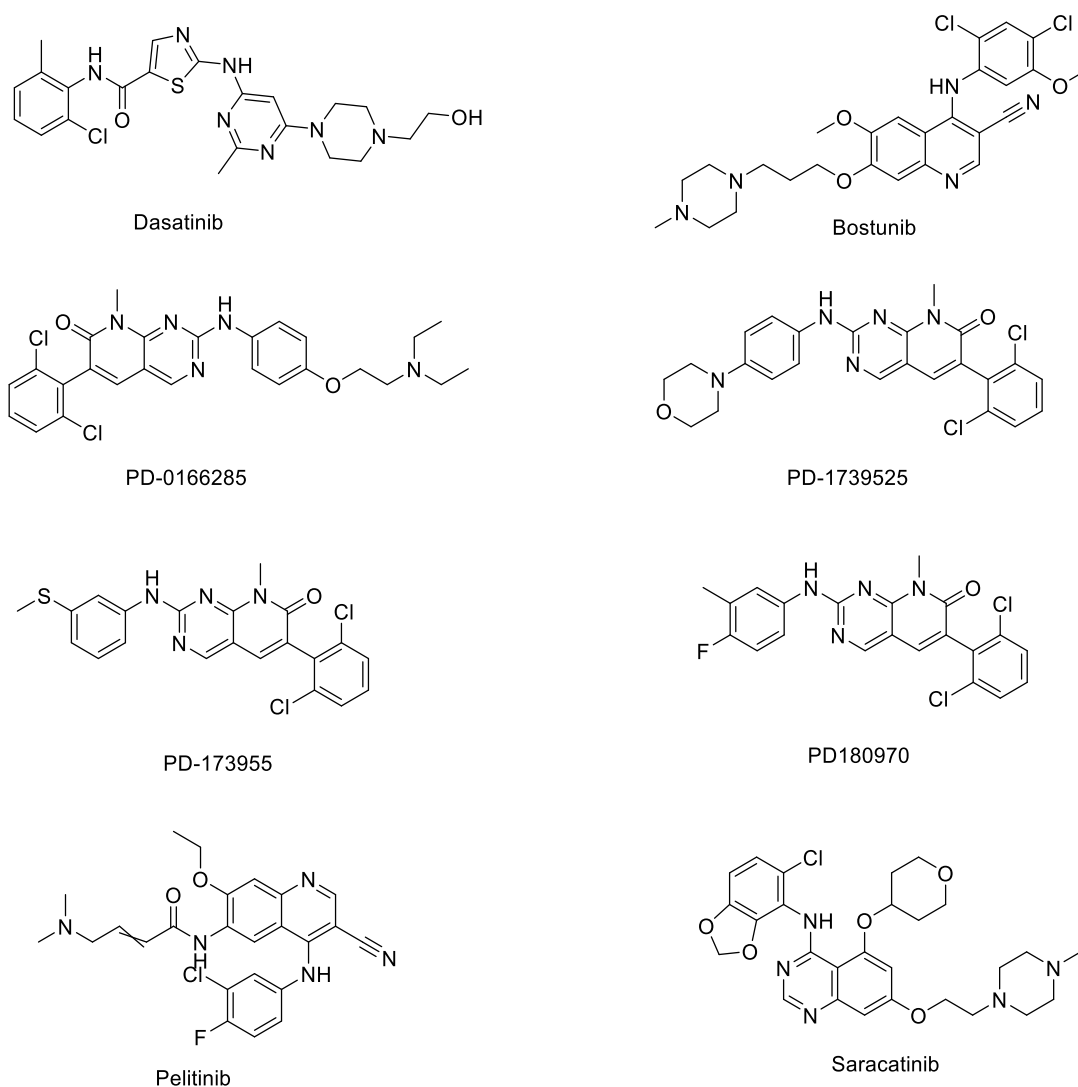


Figure 6: Chemical structures of selected PKMYT-1 inhibitor

To identify new PKMYT-1 inhibitor scaffolds and to expand the number of available inhibitors, Platzer et al. were the first to screen a compound library comprising 800 compounds against PKMYT-1. Through screening sets of protein

kinase inhibitor (PKIS) I and II published by GlaxoSmithKline, ten compounds were identified as new PKMYT-1 inhibitors with binding IC₅₀ values in a nanomolar and low micromolar range (

Table 1). Those results were obtained and validated via multiple assays, including fluorescence polarization (FP) binding assay, FP immunoblot activity assay (FPIA), and functional assays measuring the phosphorylation status [92]. The identified inhibitors would be categorized as members of three new chemical scaffolds of PKMYT-1 inhibitors, encompassing aza-stilbenes, 4-amino-quinolines, and aminopyrimidines as summarized in **Figure 7**.

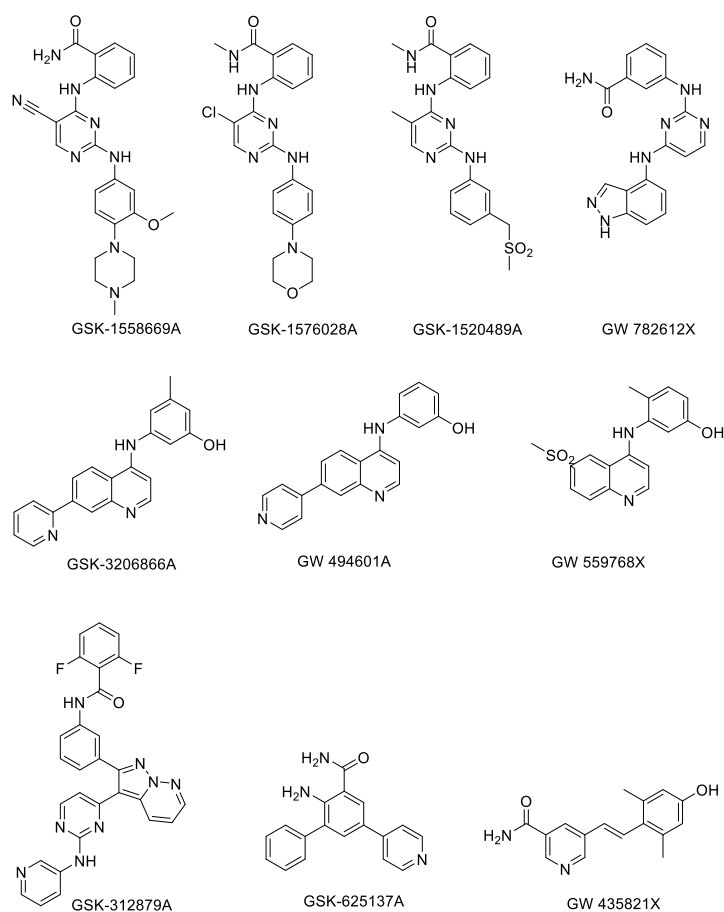


Figure 7: Structures of the ten PKMYT-1 inhibitors derived from Screening GSK PKIs and PKIIs

Table 1: Inhibition Profile of PKMYT-1

Compound	IC ₅₀ [nM] FPIA	K _i [nM] FPIA	IC ₅₀ [nM] FP binding assay	K _i [nM] FP binding assay
Bosutinib	133 ± 9	12.7 ± -0.4	704 (10)	304 (10)

Dasatinib	6 ± 1	0.5 ± 0.06	202 (10)	73 (10)
MK-1775	4940 ± 112	470 ± 14	1340 ± 26	600.9 ± 3
PD-166285	8 ± 1	0.8 ± 0.08	31.1 (10)	2.0 (10)
PD-173952	24 ± 3	2.3 ± 0.2	55 (16)	8.1 (16)
PD-180970	109 ± 32	10.4 ± 0.4	2700 (16)	13 500 (16)
Saracatinib	418 ± 54	39.8 ± 1	10 000 (16)	5200 (16)
Tyrphostin AG1478	19 600 ± 715	1870 ± 98	55 000 (10)	26 200 (10)
GSK-625137A	57 990 ± 1218	5520 ± 126	11 430 ± 778	5810 ± 96
GSK-312879A	7560 ± 298	720.2 ± 25	18 880 ± 546	14 740 ± 497
GSK-1576028A	270 ± 41	25.68 ± 0.9	352 ± 13	179.9 ± 2
GSK-3206866A	543 ± 68	51.73 ± 2	9430 ± 296	6150 ± 134
GSK-1558669A	340 ± 22	32.4 ± 1	787 ± 19	461.9 ± 10
GSK-1520489A	115 ± 11	10.94 ± 0.5	151 ± 4	104.3 ± 1
GW 559768X	177 ± 14	16.85 ± 0.4	775 ± 29	588.0 ± 51
GW 494601A	706 ± 26	67.19 ± 0.7	332 ± 6	200.9 ± 5
GW 782612X	509 ± 37	48.47 ± 0.6	2440 ± 187	1600 ± 113
GW 435821X	14 510 ± 597	1380 ± 78	876 ± 31	521.5 ± 17

Recently, Szychowski et al. reported the discovery of the first potent, selective, and orally bioavailable PKMYT-1 inhibitor, RP-6306. The journey towards the development of RP-630 commenced with a focused screen of 560 known kinase inhibitors via FP assay, where the non-specific ephrin inhibitor 1 (**Figure 8**) emerged as a potential lead structure. Guided by insights from multiple co-crystal structures, a systematic optimization process ensued, focusing on key properties such as PKMYT-1 cell-based potency, kinase selectivity, and ADME characteristics. This intensive optimization effort ultimately led to the successful creation of RP-6306, an orally bioavailable compound that exhibits remarkable selectivity for PKMYT-1.

Preclinical studies have attested to the favorable pharmacokinetic profile of RP-6306 in various species, instilling confidence in its potential therapeutic value. Notably, the compound demonstrated efficacy in a mouse xenograft model, further bolstering its prospects as a promising treatment candidate. Excitingly, RP-6306 represents a groundbreaking advancement, emerging as the first-in-class clinical candidate for the selective inhibition of PKMYT-1. As it ventures into phase 1 clinical trials (NCT04855656), scientists are now primed to research deeper into the pharmacological role of PKMYT-1 in the context of treating genetically-selected solid tumors. The clinical evaluation seeks

to unravel the compound's therapeutic potential and assess its safety and efficacy in human subjects, ultimately contributing to novel and effective treatment strategies for solid tumors. Exploring RP-6306's therapeutic efficacy marks a significant step forward in the quest for innovative solutions to combat challenging PKMYT-1-mediated malignancies [93].

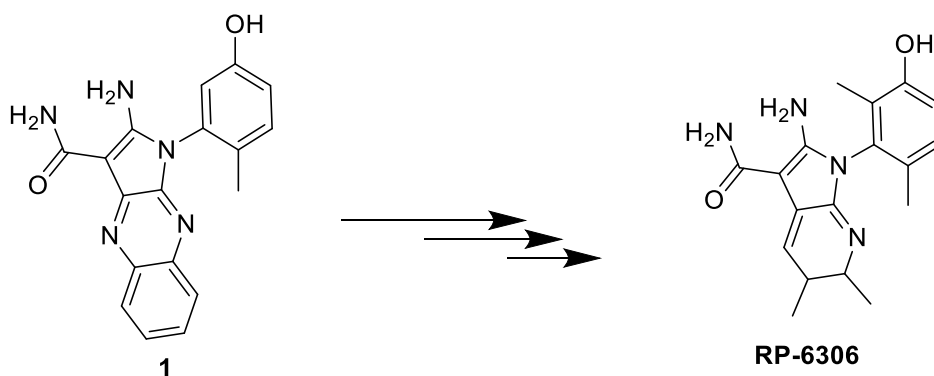


Figure 8: Rationale of design of RP-6306

1.4.2. Estrogen Receptor

1.4.2.1. Characterization and Physiological Role of Estrogen Receptor

Estrogen is a steroid hormone synthesized from cholesterol and is regarded as the key hormone that regulates the female reproductive organs. Its primary production occurs within the ovaries of females; however, the action of aromatase enzymes on androgens allows its secretion in both genders from diverse sites like adipose tissue, bone, heart, skin, and the brain. Estrogen manifests in various forms within the body, contingent upon the maturity stage of females. These distinct forms encompass estrone (E1), prevalent in postmenopausal women; estradiol (E2), the most potent variant prevailing among premenopausal women; estriol (E3), characterized as the least potent among estrogenic compounds, predominantly excreted in the urine of all women, with escalated levels during pregnancy; and estetrol (E4), abundant during pregnancy, contributing significantly to hormonal equilibrium in expectant mothers [94, 95].

The groundbreaking revelation of Estrogen Receptor (ER) by Elwood Jensen in 1958 stands as a crucial moment in the field of endocrinology, representing the first-ever identification of a hormone receptor. Cellular ERs that orchestrate estrogen functions are categorized into either the nuclear receptor family, consisting of Estrogen Receptor alpha (ER α) and Estrogen Receptor beta (ER β), or the membrane estrogen receptors (mERs), notably G protein-coupled estrogen receptor 1 (GPER1) [96-98].

As integral components of the nuclear hormone receptor superfamily, the architecture of estrogen receptors ER α and ER β encompasses a range of structural and functional domains with substantial structural overlap across various regions [99]. Those domains are the N-Terminal A/B domain (NTD), DNA binding domain (DBD; C-domain), hinge region (D-domain), ligand-binding domain (LBD; E-domain), and an additional fifth domain exclusively existent in ERs: the C-terminal domain (F-domain) (**Figure 9**). The NTD encodes a hormone-independent transcriptional activation function 1 (AF1), enabling interactions with transcription factors. In contrast, the DBD, anchored by two zinc-binding motifs and a dimerization interface, engages with the DNA estrogen response element (ERE)

while coordinating co-activator recruitment. The D domain confers flexibility to the receptor, bridging the DBD and LBD. Conversely, the LBD embodies the transcriptional activation factor 2 (AF-2) that serves as the recognition and binding site for ligands and acts synergistically with AF1 to attain maximum transcriptional activity (**Figure 9**). This domain governs the chaperonin proteins' engagement, such as heat shock protein 90 (HSP90), facilitating specific ERE interactions. Comprising 12 α -helices H1-H12, the LBD's H12, in tandem with amino acid residues in H3, H4, and H5, coordinates in forming the ligand-dependent AF-2 site. Finally, the F domain encompasses 42 amino acids essential for promoting gene transcription in the ligand's presence and contributes to receptor dimerization. While the DBD and LBD carry 96 and 60% of homology between ER α and ER β , both NTD, D-domain, and F-domain are divergent. It is worth mentioning that each ligand induces a specific conformational change to the ER, affecting the events followed after binding, including the release of inhibitory HSPs, dimerization of the receptor, recruitment of co-regulators either co-activators or co-repressors and recruitment of transcription factors [100-105].



Figure 9: Estrogen Receptor Domain Structure Landscape

1.4.2.2. Estrogen receptor signaling pathway:

Estrogen receptor (ER) dependent gene transcription is a complex network that involves diverse activation and signaling pathways. While the interaction of estrogen with different ER isoforms, ER α , ER β , and GPER1, can initiate a ligand-dependant pathway, the ligand-independent pathway is another recognized mechanism for ER gene expression [106, 107]. First, the ligand-dependent signaling mechanisms start with the estrogen binding to ER that undergoes a conformational change to recruit various co-regulators to stimulate the transcription of ER-target genes. The ligand-dependent mechanism can fall into direct genomic/classical, indirect genomic/non-classical, and non-genomic activation mechanisms. During the classical activation, Estrogen penetrates the

plasma membrane to bind to cytoplasmic ER, which undergoes conformational transformation by either homodimerization or heterodimerization. Then, ER dimers translocate into the nucleus and interface with EREs on DNA to initiate gene transcription [104, 108, 109]. Alternatively, in indirect genomic/non-classical pathways, ERs govern gene transcription of ERE-lacking genes by engaging in an indirect DNA binding process. This form of ER binding is mediated by diverse co-factors (such as SP-1, AP-1, and NF- κ B) that stimulate gene transcription by interacting with DNA [110, 111]. Finally, the non-genomic involves binding of Estrogen to membrane-associated ERs, upon which various protein kinase cascades such as RAS/RAF/MEK1/2 and ERK1/2,PI3K/Akt/mTOR are triggered (**Figure 10**). Then, those kinases phosphorylate transcription factors such as Elk-1, CREB, CCAAT-enhancer-binding protein beta (C/EBP β), and the NF- κ B complex, which function in gene expression. Notably, protein kinases, including MAPKs, can also phosphorylate ERs, implying that the non-genomic actions of estrogens could encompass self-regulation of receptor expression. In conclusion, ERs can effectively influence gene transcription by triggering non-genomic and genomic pathways through various DNA response elements beyond direct ERE binding [112-115].

The second mechanism of estrogen signaling is the ligand-independent pathway, which revolves around ER activation without Estrogen or any other ligand presence. Instead, phosphorylation of specific serine residues on the receptor is mediated by extracellular cues like epidermal growth factor, insulin-like growth factor, cytokines, neurotransmitters, and cell cycle regulators. Eventually, subsequent signaling pathways, such as PI3K and Ras/Raf/MEK/ERK, are activated [116-118].

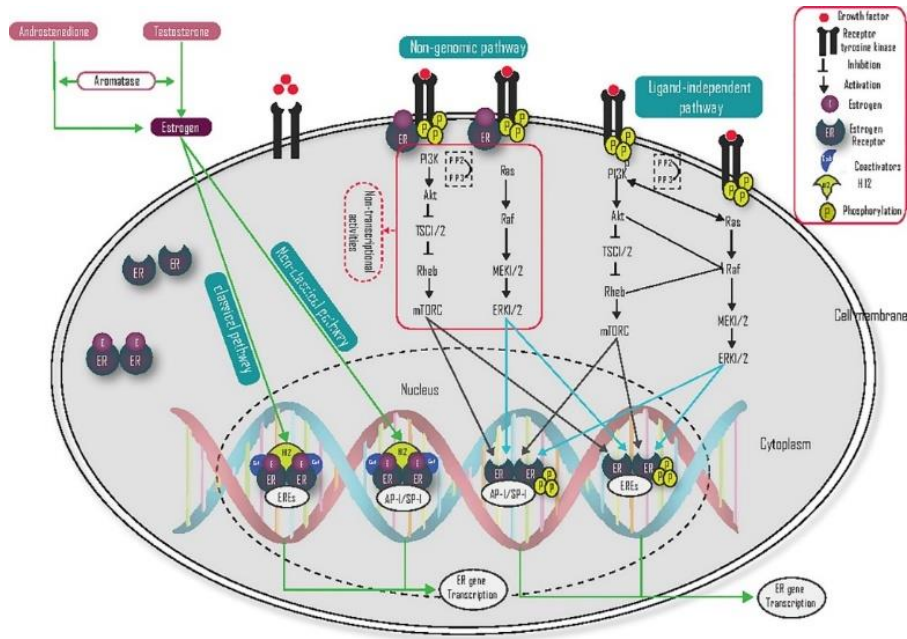


Figure 10: Ligand-dependent and ligand-independent mechanism of estrogen receptor signaling [119]

1.4.2.3. Estrogen Receptor and Breast Cancer

Estrogen receptors (ERs) play a pivotal role in normal mammary development as they operate as ligand-activated transcription factors to govern the expression of critical genes for breast tissue differentiation. Unfortunately, a growing body of evidence derived from epidemiological investigations, animal experimentation, and laboratory studies accentuated the involvement of endogenous estrogens in the complex process of breast carcinogenesis. Initial indications of hormonal influence on breast cancer emerged from the observed decrease in breast cancer risks following bilateral removal of ovaries. In addition, prolonged lifetime exposure of breast tissue to estrogen in specific conditions, such as early menarche, late menopause, and late-age childbirth, is considered an established risk factor for breast cancer [120-122]. Along with this line of reasoning, an estimated 70% of breast cancer cases exhibit a hormone-dependent nature where estrogen binding to dysregulated ER triggers uncontrolled cell proliferation, evasion of apoptosis, and angiogenesis, classifying them as ER-positive (ER+) [123-125]. Significantly, ER α emerges as the prevailing endocrine receptor in the breast, wielding a substantial impact on estrogen-driven breast

cancer. It holds the leading culprit role in approximately 65% of breast cancer cases, not solely owing to its upregulated expression and aberrant cell cycle but also in the context of diverse sequence variations. In particular, single-nucleotide polymorphisms (SNPs) within the ER α gene have been associated with elevated or reduced susceptibility to breast cancer [126, 127]. Since ER+ breast cancers rely heavily on estrogen-driven pathways, adopting strategies that modulate ER α activity has revolutionized breast cancer treatment by effectively restraining the growth of ER+ tumor cells [125, 128].

1.4.2.4. Estrogen receptor ligands for breast cancer treatment

ER-targeted therapy for breast cancer is a concept that was first reported by Beatson back in 1896. Currently, the therapeutic landscape holds a diverse array of established modalities whose objective is to inhibit the estrogen-mediated signals that fuel cancer growth. These include selective estrogen receptor modulators (SERMs) such as tamoxifen, raloxifene, and toremifene, selective estrogen receptor down-regulators (SERDs), aromatase inhibitors like anastrozole, letrozole, and exemestane, and cyclin-dependent kinases 4 and 6 inhibitors [129, 130].

1.4.2.4.1. Selective Estrogen Receptor Modulators:

Selective estrogen receptor modulators (SERMs) represent a prominent class of compounds meticulously designed for targeted therapies against various estrogen-related conditions, with a significant focus on breast cancer. With an extensive usage history spanning nearly five decades, SERMs have evolved into a form of hormone replacement therapy characterized by their controversial functionality as agonists and antagonists in different body organs. This elaborate interplay serves to optimize the benefit-to-risk ratio, a crucial consideration when tailoring breast cancer therapeutic interventions with optimum outcomes [100, 101, 131, 132]. SERMs, classified according to their developmental stages, encompass compounds segmented into three generations: first-generation like tamoxifen (**1**), second-generation as raloxifene (**2**), and third-generation featuring bazedoxifene (**3**), lasofoxifene (**4**), and ospemifene (**5**)

(Figure 11). Chemically speaking, these SERMs groups into two families, the non-steroidal compounds known as triphenylethylenes and the benzothiophenes, all of which hold characteristic features tailored for ER binding. Emerging SERM members, like naphthylenes, benzopyrans, and indoles, have been spanning both preclinical and clinical evaluations [133].

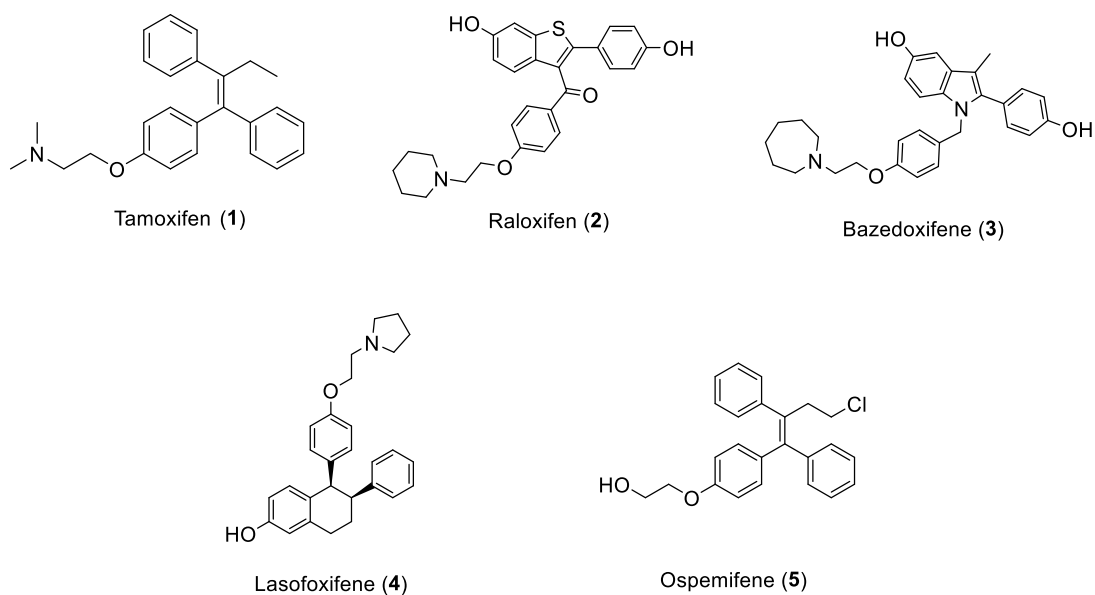


Figure 11: Structures of selected SERMs

1.4.2.4.2. *Tamoxifen*

Tamoxifen (TAM) stands as a groundbreaking medication and the first approved SERM for addressing hormone-dependent breast cancer. The journey of tamoxifen traces its origins back to the 1960s when it was first explored as a potential contraceptive. Nevertheless, the remarkable discovery that tamoxifen could stimulate ovulation and influence ER signaling marked the beginning of a new era in breast cancer therapy. Serving as a pioneering SERM endorsed for treating metastatic breast cancer, TAM showcases a paradoxical nature, acting as an agonist in the liver, uterus, and bone while concurrently exerting an antagonistic influence in breast tissue, perturbing the ER α signaling pathway [134-139]. This versatile and economically viable drug has been established as a gold standard in breast cancer treatment across all disease stages. Furthermore, TAM has revolutionized the landscape of adjuvant breast cancer trials, yielding impressive results such as a substantial 40–50% reduction in breast cancer recurrence among

early-stage breast cancer patients. These outcomes have raised interest in exploring TAM's potential for disease prevention among women without prior breast cancer history. This pursuit led to phase III breast cancer prevention trials, featuring TAM's effectiveness in women at elevated risk of developing breast cancer. Cumulatively, these studies highlight TAM's ability to limit overall breast cancer incidence by 16 to 49% and particularly ER+ breast cancer incidence by 31 to 69%, presenting a promising avenue for both the prevention and treatment of breast cancer [101, 140-144]. However, alongside the concern for the survival and proliferation of TAM-tolerant cells introducing TAM resistance, TAM therapy brings along adverse effects, including hot flashes, elevated risk of endometrial cancer, and, in rare cases, liver abnormalities [40, 145, 146].

1.4.2.4.3. Metabolism of Tamoxifen:

Tamoxifen has been recognized as a prodrug that needs to be transformed into more active forms through metabolism within the body. Pharmacological investigations into TAM metabolism have unveiled its transformation into three potent active metabolites: 1) 4-hydroxytamoxifen (4OHTAM) (**6**); 2) N-desmethyltamoxifen (**7**); and 3) 4-hydroxy-N-desmethyltamoxifen, also recognized as endoxifen (**8**) (**Figure 12**). These metabolites have a greater affinity to ER α and a much higher antiestrogenic potency in breast cancer cells than the parent drug. They are generated through the catalysis by hepatic CYP2D6 and CYP3A4/3A5 enzymes, which first induce hydroxylation followed by N-demethylation of tamoxifen. It is worth noting that patients harboring variant forms of the CYP2D6 gene experience limited therapeutic gains from tamoxifen administration or even encounter relapses due to troubled TAM metabolism to its antiestrogenic actives [147-152].

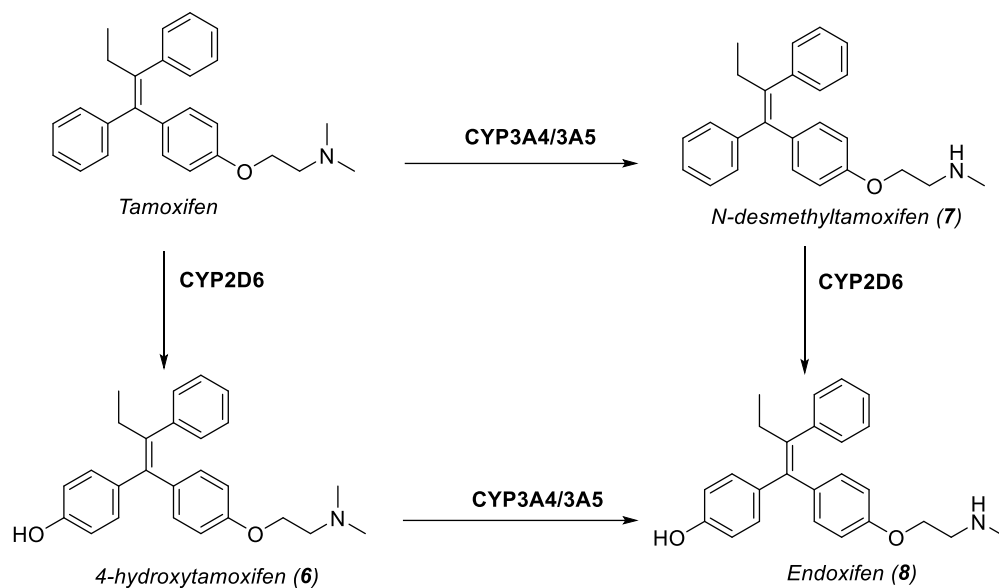


Figure 12: Tamoxifen metabolism to its active metabolites

1.4.2.4.4. Tamoxifen mechanism of action:

The effectiveness of TAM relies on the generation of clinically active metabolites, 4-OHTAM and endoxifen. The distinction between these metabolites and E2 encompasses not only their binding modes but also the orientation of specific domains and the subsequent recruitment of downstream regulators. When E2 binds to ER, H12 in the LBD is aligned precisely against helices 3, 5/6, and 11, effectively sealing the ligand binding pocket in a lid-like fashion. This arrangement enables particular amino acids within the AF-2 region to interact with coactivators, initiating the transcriptional activation of target genes. In contrast, the binding of TAM to ER shifts the positioning of H12, blocking the coactivator recognition site and thus impeding AF-2-mediated transcription, resulting in TAM's antagonistic impact (as depicted in Figure 13). However, TAM's estrogen-like effects are believed to stem from its relatively short side chain, which exposes Asp351 (D351) for interaction with AF-1, thereby leading to the expression of agonistic genes [153-156].

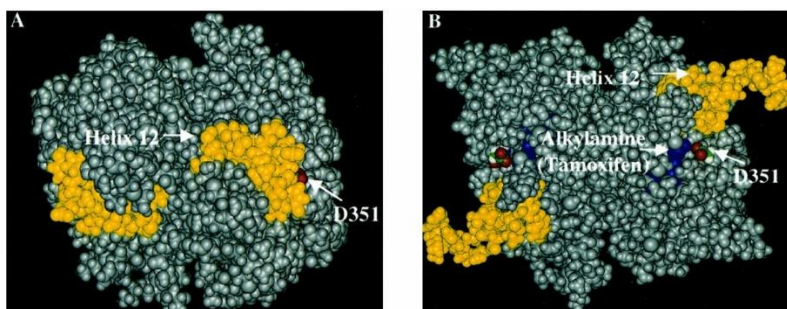


Figure 13: E2 (A) vs. 4-OHTAM (B) complex with helix 12 and exposure to D351 [157]

1.4.2.4.5. Tamoxifen Structure-Activity Relationship

The effectiveness of both 4-OHTAM and endoxifen can be attributed to specific pharmacophoric elements that play a significant role in their binding to the ER, influencing both agonistic and antagonistic properties. These essential pharmacophores include:

- Stilbene skeleton: The core structure of TAM shares a resemblance with that of the E2 molecule, with two aromatic rings arranged in a manner that they are separated by 1-3 atoms, facilitating their optimal fit within the binding pocket (Figure 14).

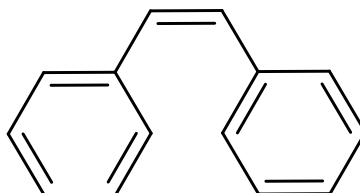


Figure 14: Stilbene skeleton

- Phenolic group: The inclusion of at least one phenolic group is generally pivotal for achieving high-affinity binding to the ER. This phenolic hydroxyl (OH) group plays a crucial role in establishing a significant contact point between the ligand and the receptor, particularly interacting with amino acids Glu 353 and Arg 394 (illustrated in Figure 15).
- 4-Substituted phenyl Group: Notably, 4-hydroxytamoxifen features an alkylaminoethoxy side chain attached to the phenyl group located between the two phenyl rings of the core structure. This side chain plays a crucial role in assuming an antagonistic conformation by displacing H12 of the ER [152, 153, 158].

The pharmacophoric features of tamoxifen provide valuable insights and guidelines for designing new tamoxifen analogues with improved properties. These features can be harnessed to create compounds that retain the beneficial aspects of tamoxifen while addressing its limitations.

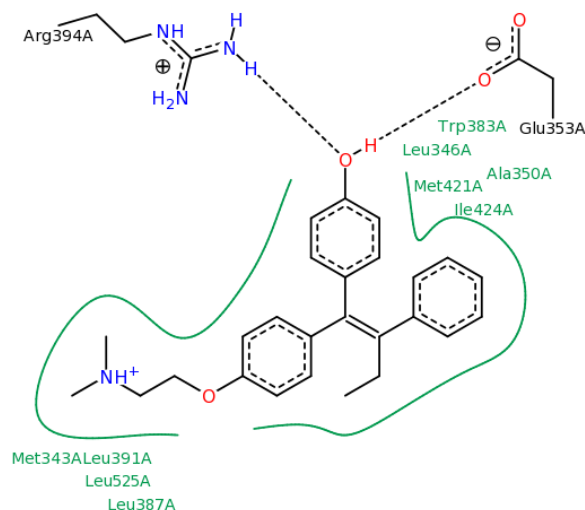


Figure 15: Hydroxytamoxifen interactions in the ER PDB ID (3ERT)

1.4.2.4.6. CYP2D6 enzyme

Human Cytochrome P450 (CYP) enzymes are heme-containing enzymes located in the inner membrane of mitochondria or the endoplasmic reticulum of cells. These enzymes play a fundamental role in the oxidative, peroxidative, and reductive transformation of diverse molecules. The human genome encompasses 57 CYP genes grouped into 18 families and 44 subfamilies according to sequence similarities. Notably, CYP2D6 is a prominent member of the CYP enzyme family II, which constitutes one-third of all CYPs and is one of the largest and best-studied isoenzyme families. The CYP2D6 isoform, recognized as debrisoquine hydroxylase, is a vital metabolizing enzyme predominantly expressed in the liver. Its significance arises from its pivotal role in human drug metabolism since it is responsible for the clearance of approximately 25% of drugs that are in current clinical use, including antiarrhythmic, antidepressants, antipsychotics, β -blockers, analgesics, and tamoxifen, among others [159-162].

Genetic polymorphisms in the CYP2D6 gene contribute to the highly variable enzymatic activity of CYP2D6. The CYP2D6 gene is located on chromosome 22q13.1, and approximately 100 variant alleles have been identified. Single nucleotide polymorphisms (SNPs) within this gene can lead to the production of inactive or reduced-activity enzymes. Noticed variability in the enzymatic activity of CYP2D6 has provided distinct CYP2D6 phenotypes, encompassing poor (PM), intermediate (IM), extensive (EM), and ultrarapid (UM) metabolizers. Those classes vary in the number of defective alleles where PM individuals carry a single defective allele, IM individuals carry two defective alleles, and EM individuals possess two alleles with regular enzyme activity. On the other hand, UM individuals harbor duplicated or multi-duplicated gene copies of the same allele [163-165]. From another perspective, there is a versatility in the prevalence of certain alleles over others among different ethnic groups. For instance, CYP2D6*4 is common in whites (about 25% frequency), CYP2D6*17 in blacks (about 25% frequency), and CYP2D6*10 in Asians (about 15% frequency). Aside from genetic influences, other factors, such as the use of CYP2D6 inhibitors such as antipsychotic drugs, selective serotonin reuptake inhibitors (SSRIs), and some cardiac medications, can impact the enzyme's activity [166-172]. Given the crucial role of CYP2D6 in tamoxifen metabolism, variations in its expression or activity have prompted concerns about the efficacy of tamoxifen therapy. Regrettably, the reduced enzymatic function of CYP2D6 contributes to the wide-ranging differences in the concentrations of tamoxifen metabolites, thus influencing its overall efficacy. This pronounced variability features the necessity for personalized treatment strategies to ensure optimal therapeutic outcomes, particularly for women harboring these genetic variations.

2. Aim of the work

As discussed in the introduction, cancer represents an escalating global public health challenge due to its versatile types, high prevalence, and mortality rates. The disease's complicated pathophysiology, driven by various biological features and risk factors, emphasizes the need for innovative approaches to tackle its complexity. Conventional methods, like surgery, radiotherapy, and chemotherapy, have been mainstays in different tumors cancer management, targeting cancerous tissues while aiming to prevent a recurrence. However, recent advancements have shifted towards targeted therapy, a promising approach that specifically targets the underlying drivers of cancer, such as receptors and kinases, some of which were the highlight of our work. In our work, we focused on two types of widespread cancers: neuroblastoma, which is the most prevalent cancer in children, and breast cancer, which is the most popular cancer type in women. The design of the projects deals with targets that have been reported to have a relation with these cancers; therefore, the search for inhibitors for these targets is the main objective of this work.

The first target discussed in our work is PKMYT-1, a less-studied member in the kinases family. Despite being overshadowed by other contributors, emerging research highlights the significant role of PKMYT-1 in cancer progression and prognosis. These findings shed light on the potential importance of PKMYT-1 as a promising target for cancer research and therapy. Therefore, we aimed to identify novel PKMYT-1 inhibitors using a combination of *in silico* and *in vitro* screening methods. The computational approach involved structural analysis, molecular docking, binding free energy calculations, and quantitative structure-activity relationship (QSAR) models. Based on the derived computational models, several derivatives were synthesized and tested *in vitro* on PKMYT-1. The study successfully identified novel inhibitors with significant activity in the sub-micromolar range, providing a foundation for further investigating PKMYT-1 as a potential target for cancer therapy.

The second target in our work was the Estrogen Receptor (ER) which has long been recognized as a key player in the development and progression of breast cancer. Since 80% of breast cancers express ERs, designing ER

antagonists that cause estrogen deprivation seems like the most logical approach for their treatment. So, our work on targeting ER has been divided into three concepts, all proposing new chemical structures, either targeting MCF-7 cells (an important representative of ER+ breast cancer / Luminal A subtype) or targeting ER. The work design always considered dodging major drawbacks witnessed with similar /approved inhibitors.

The first concept focuses on the design and synthesis of chemical derivatives of Tamoxifen (TAM), a widely used selective estrogen receptor modulator (SERM) that has been a mainstay in breast cancer treatment for years. TAM undergoes metabolism to 4-hydroxytamoxifen and endoxifen, which exhibit higher affinity and potency in breast cancer cells than the parent drug. However, genetic polymorphisms in CYP2D6, the enzyme responsible for tamoxifen metabolism, result in variable enzymatic activity and clinical outcomes among women. To address this issue, our tamoxifen analogs were designed to have similar pharmacophoric features but different metabolic activation pathways, ensuring consistent clinical benefits for all patients. These analogs were evaluated for their antiproliferative effects on MCF-7 cell lines and their binding affinity towards ER. Highly potent candidates were selected for further metabolic assays.

The second concept was to explore the therapeutic potential of isoeugenol in breast cancer treatment. Inspired by the novel trend of exploring the effect of natural and semi-synthetic active ingredients in aggressive diseases, the study aims to bridge a knowledge gap by investigating the anticancer properties of isoeugenol, a positional isomer of eugenol. Through chemical synthesis and structural validation, novel isoeugenol derivatives were generated and tested on MCF-7 cell lines. The study also investigates into the mechanistic aspects, evaluating the ability of the most active compound to induce apoptosis and abrogate the cell cycle. In vivo studies are conducted using the most promising compound on SEC-bearing mice to validate its pharmacological efficacy at the preclinical level. This research aims to contribute valuable insights into the potential of isoeugenol derivatives as a novel therapeutic strategy in breast cancer management.

The final concept was developing a series of novel compounds based on the 5,7-dibromoquinoline scaffold backbone. The design strategy adopted for the new series was to test how altering the compounds' conformational/physicochemical parameters affects the antiproliferative effect toward MCF-7 cells. This work has also explored the role of overcoming pharmacokinetic obstacles such as poor solubility and limited bioavailability for the most active compounds. Since further structural modifications may alter the desired activity of the compounds, those compounds were incorporated into pluronic nanomicelles to enhance their aqueous solubility and, consequently, their cancer cell penetrability, allowing their sustained release.

3. Results

3.1. Computer-aided design, synthesis, and biological characterization of novel inhibitors for PKMYT-1.

Abdulkarim Najjar , Charlott Platzer , Anton Lufta, Chris Alexander Aßmann , **Nehal H. Elghazawy** , Frank Erdmann , Wolfgang Sippla, Matthias Schmidt

Eur. J. Med. Chem. **2019**, *161*, 479-492. Doi:[10.1016/j.ejmech.2018.10.050](https://doi.org/10.1016/j.ejmech.2018.10.050)

Abstract

In the current work, we applied computational methods to analyze the membrane-associated inhibitory kinase PKMYT-1 and small molecule inhibitors. PKMYT-1 regulates the cell cycle at G2/M transition and phosphorylates Thr14 and Tyr15 in the Cdk1-cyclin B complex. A combination of in silico and in vitro screening was applied to identify novel PKMYT-1 inhibitors. The computational approach combined structural analysis, molecular docking, binding free energy calculations, and quantitative structure activity relationship (QSAR) models. In addition, a computational fragment growing approach was applied to a set of previously identified diaminopyrimidines. Based on the derived computational models, several derivatives were synthesized and tested in vitro on PKMYT-1. Novel inhibitors active in the sub-micromolar range were identified which provide the basis for further characterization of PKMYT-1 as putative target for cancer therapy.



Research paper

Computer-aided design, synthesis and biological characterization of novel inhibitors for PKMYT1

Abdulkarim Najjar^a, Charlott Platzer^a, Anton Luft^a, Chris Alexander Aßmann^a, Nehal H. Elghazawy^a, Frank Erdmann^b, Wolfgang Sippl^a, Matthias Schmidt^{a,*}^a Institute of Pharmacy, Department of Medicinal Chemistry, Martin-Luther-University Halle-Wittenberg, W.-Langenbeck-Str. 4, 06120, Halle, Germany^b Institute of Pharmacy, Department of Pharmacology, Martin-Luther-University Halle-Wittenberg, W.-Langenbeck-Str. 4, 06120, Halle, Germany

ARTICLE INFO

Article history:

Received 5 September 2018

Received in revised form

16 October 2018

Accepted 19 October 2018

Available online 24 October 2018

Keywords:

PKMYT1

QSAR

Docking

MD simulation

Binding free energy calculations

Fragment-based design

Diaminopyrimidines

ABSTRACT

In the current work, we applied computational methods to analyze the membrane-associated inhibitory kinase PKMYT1 and small molecule inhibitors. PKMYT1 regulates the cell cycle at G2/M transition and phosphorylates Thr14 and Tyr15 in the Cdk1-cyclin B complex. A combination of *in silico* and *in vitro* screening was applied to identify novel PKMYT1 inhibitors. The computational approach combined structural analysis, molecular docking, binding free energy calculations, and quantitative structure–activity relationship (QSAR) models. In addition, a computational fragment growing approach was applied to a set of previously identified diaminopyrimidines. Based on the derived computational models, several derivatives were synthesized and tested *in vitro* on PKMYT1. Novel inhibitors active in the sub-micromolar range were identified which provide the basis for further characterization of PKMYT1 as putative target for cancer therapy.

© 2018 Elsevier Masson SAS. All rights reserved.

1. Introduction

The membrane-associated inhibitory kinase PKMYT1 belongs to the Wee1-kinase family and regulates the cell cycle at G2/M transition [1]. PKMYT1 plays a major role in the inactivation of the second checkpoint G2 through its inhibitory phosphorylation of cyclin-dependent kinase (Cdk1) [1,2]. Functional PKMYT1 kinase phosphorylates Thr14 in the Cdk1-cyclin B complex following a phosphorylation of Tyr15 by Wee1 kinase. This double phosphorylation of Cdk1 leads to a disassociation between cyclin B and Cdk1 and consequently deactivates its function [3]. As a result, the cell cycle is restricted until DNA damage is repaired [2]. Many cancer cells lack a functional p53 signaling, which abrogates the G1 checkpoint, resulting in increased DNA damage at the G2 checkpoint compared to normal cells [4]. Thus, cancer cells rely more on the G2 checkpoint than normal cells [5]. A new strategy for cancer treatments is to keep the cell in the cell cycle with unrepaired DNA damage in premature mitosis. The abrogation of the G2 checkpoint can be induced by pharmacological manipulation, resulting in

mitotic catastrophe with a high level of unrepaired DNA damage and immediately causes apoptotic or non-apoptotic cell death [6,7]. Several PKMYT1 inhibitors including the known tyrosine kinase inhibitors dasatinib and bosutinib [8], the pyridopyrimidine derivatives PD-0166285 [9], PD-173952 [10], PD-173955 [8] and PD-180970 [9] have been identified by applying different approaches. Examples of the most active compounds from each chemotype are given in Fig. 1. In addition we recently screened the GSK kinase inhibitors sets (PKIS sets I and II) [11–13] and identified novel PKMYT1 inhibitors belonging to different chemical classes [13].

Until recently, only one crystal structure of PKMYT1 in the apo form was available. In a previous study we applied ligand docking and QM/MM based binding free energy (BFE) calculations to virtually screen several compound databases and identified active inhibitors [10]. However, we recognized that the derived hits were either highly similar to already known PKMYT1 inhibitors or showed only weak inhibitory activity. To overcome the limitations of the previously developed models and inhibitors, we were interested in developing novel computational models with increased accuracy. For this purpose we included in the current work eight new crystal structures of PKMYT1 that were released very recently by Zhu et al. [14]. The new PKMYT1 structures were

* Corresponding author.

E-mail address: matthias.schmidt@pharmazie.uni-halle.de (M. Schmidt).

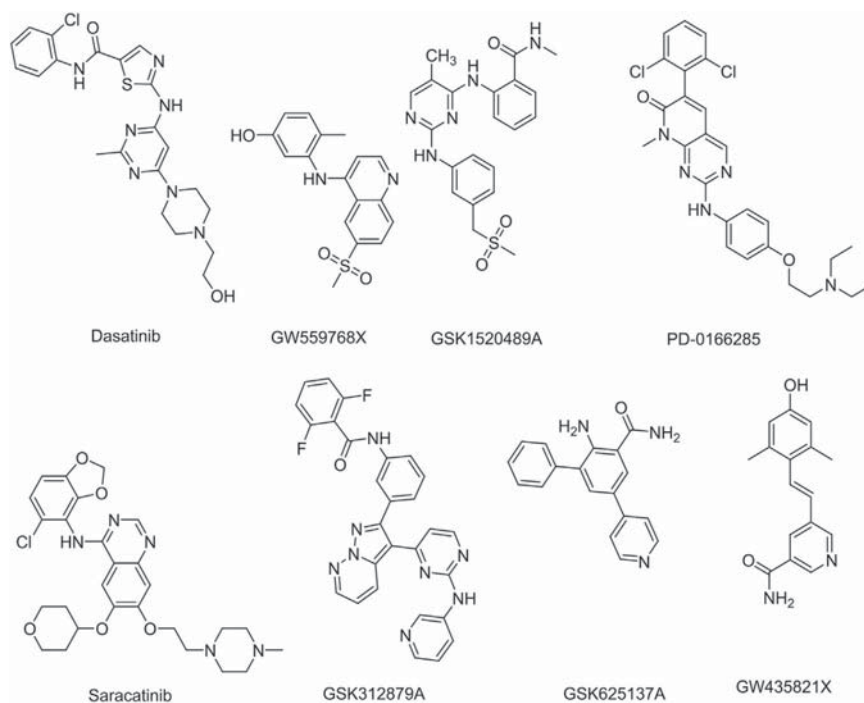


Fig. 1. Examples of active PKMYT1 inhibitors: pyridopyrimidine derivative PD-0166285, diaminopyrimidine derivative GSK1520489A, aminoquinoline derivative (GW559768X), stilbene derivative GW435821X, pyridine derivative GSK625137A, aminopyrimidine derivative GSK312879A, saracatinib and dasatinib [13].

resolved in the active form and in complex with known kinase inhibitors and thus represent more suitable starting points for generating computational models for inhibitor design.

In addition, we extended the ligand data set for establishing computational models for activity prediction. We considered all known PKMYT1 inhibitors including the ones that we identified from the GSK kinase inhibitors sets. (Supplementary data: Fig. 1S and Table 1S). Based on docking and BFE derived models, we then applied a fragment growing approach to guide the structural optimization. The most promising compounds were subsequently synthesized and their inhibitory activity on PKMYT1 was tested [15]. As a result, a set of novel diaminopyrimidines could be identified which should serve as valuable tools to further analyze the potential role of PKMYT1 inhibitors in cancer therapy.

2. Results and discussions

2.1. Structural analysis and site map of the PKMYT1 binding pocket

Totally, nine crystal structures of PKMYT1 kinase are available in the protein Data Bank (PDB), eight of which were resolved in holo form (PDB IDs: 5VCV, 5VCW, 5VCX, 5VCY, 5VCZ, 5VD0, 5VD1, and 5VD3) and one structure in apo form (PDB ID: 3P1A) [14,16]. Two structures (PDB IDs: 5VCX and 5VD3) were co-crystallized with saracatinib in different phosphorylation states of the cloned PKMYT1, where saracatinib was found to display an identical conformation.

The ATP-binding pocket of PKMYT1 and other kinases is generally divided into a back pocket behind the gatekeeper (PKMYT1: Thr187), a front pocket within the solvent-accessible area, an adenine region close to the hinge region, a ribose-binding pocket and a phosphate binding region [16,17]. The individual pockets are constructed by several amino acids which interact with ATP or other ligands occupying the pockets. Moreover,

the surrounding amino acids and the accessibility of each pocket to the solvent impart distinct properties for the individual sub-pockets. The back-pocket in PKMYT1 is characterized as a hydrophobic pocket due to the surrounding hydrophobic amino acids: Val171, Leu185, Val124, and Lys139 (Fig. 2). In addition, the back-pocket shows a limited accessibility to hydrophilic amino acids in the α C helix (His161 and Glu157). Meanwhile, the front-pocket is located in a solvent-accessible area and is surrounded by Leu116, Gly191 and Pro192 (Fig. 2). The adenine region is located close to

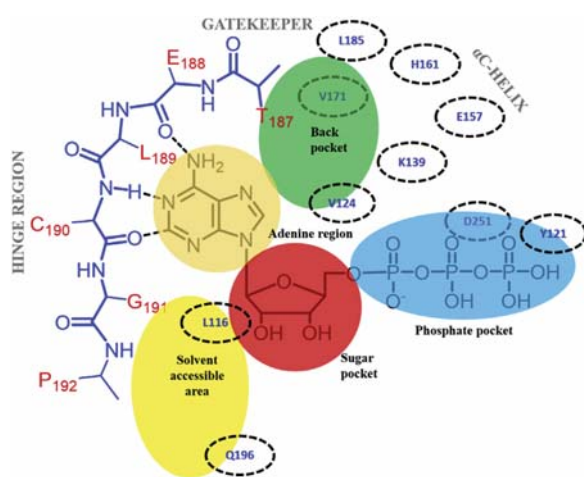


Fig. 2. Scheme of the ATP-binding pocket of PKMYT1. The backbone of the PKMYT1 key residues is colored blue, whereas the locations of the remaining key residues are estimated and depicted in circles. Colored spheres illustrate: Solvent-accessible area (yellow), ribose-binding pocket (red), phosphate region (blue), adenine region (beige), back pocket (green). (For interpretation of the references to color in this figure legend, the reader is referred to the Web version of this article.)

the hinge region to allow the embedded ligand/ATP to form conserved hydrogen bonds with the hinge region residues. The general characteristics of the sugar pocket and phosphate region are solvent-accessible and hydrophilic. The phosphate region is surrounded at the bottom by Asp251 of the DFG motif and at the top Tyr121 in the P-loop.

Analysis of protein-ligand interaction of PKMYT1 inhibitors (exemplified by MK-1775 in PKMYT1, Fig. 3) showed that the common interaction patterns include: a conserved hydrogen bond with the backbone of the hinge region residue Cys190, a π - π stacking interaction with the side chain of Phe240, targeting the back hydrophobic pocket by a substituted phenyl or a small chemical group, in addition to polar and van der Waals interactions with the front pocket residues e.g. Leu116, Pro191 and Gln196 [13]. The polar interactions with the phosphate and sugar regions residues e.g. Asp251 and Tyr121 were also observed in several inhibitors [13].

2.2. Binding free energy calculations

We found in our previous work that the docking program GOLD was performing well in redocking studies. GOLD gave the best results for all included inhibitors when the PKMYT1 structure bound to pelitinib (PDB ID: 5VCW) was taken for ligand docking [13]. Therefore, we docked all inhibitors under study into this protein conformation and used the derived poses to find a correlation between the computed and experimental affinities [13]. As training set we used 19 PKMYT1 inhibitors (whole data set shown in Supplementary data, Figure S1, Table S1) identified by us and the experimentally determined inhibitory activity from the activity assay (FPIA) and the binding assay (FPBA), respectively. Firstly, we investigated a correlation between the experimentally determined activities and several docking scores. Therefore, the obtained docking solutions were re-scored using implemented scoring functions in GOLD and Glide. Low correlation coefficients were observed using scoring function (R^2 values ranged between 0.35 and 0.38, Supplementary data, Table S2) in agreement with our previous study [10]. Further studies were performed to predict the affinities of the ligands using different BFE calculation methods (MM-PB/SA and MM-GB/SA, as well as hybrid QM/MM methods). Rescoring was performed using either a single frame after short minimization or considering ten snapshots from short molecular

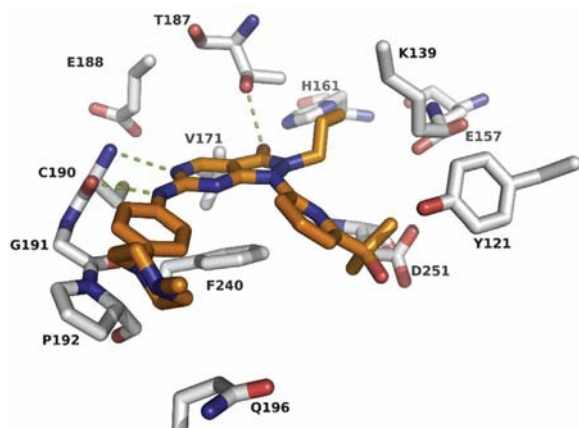


Fig. 3. Binding mode of MK-1775 (orange) in the PKMYT1 pocket (white sticks, PDB ID: 5VD0). Hydrogen bonds are shown as green dashed lines. (For interpretation of the references to color in this figure legend, the reader is referred to the Web version of this article.)

dynamics (MD) simulations (100 ps). The solvation free energy was calculated using Poisson Boltzmann (MM-PB/SA) and different models of the Generalized Born approach (MM(QM/MM)-GB/SA). These GB models were implemented in AMBERTools12 as GB^{HCT} (igb = 1), GBOC1 (igb = 2), GB^{OC2} (igb = 5) and IGB8 (igb = 8) [18–23]. The QM region of the QM/MM hybrid mechanics was firstly applied for the ligand only and later for the ligand and selected residues from the hinge region, the P-loop, the hydrophobic pocket and DFG motif of PKMYT1, surrounding the ligand. Two models for QM were used: Parameterized Model number 3 (PM3) and Austin Model 1 (AM1) [24]. The performance of the binding free energy methods was evaluated by computing the correlation coefficients between the biological activity (K_i values) and the enthalpy score (ΔH). The results are summarized in Table S3 (see Supplementary data).

The best correlation coefficient for the training set was 0.68 (RMSE was $0.59 \text{ kcal mol}^{-1}$) by applying the Poisson Boltzmann (PB) solvation model (MM-PB/SA) and using 10 snapshots from a short MD simulation (Fig. 4, Supplementary data, Table S3). The leave-one-out cross-validated q^2 was 0.60, and the RMSE $0.59 \text{ kcal mol}^{-1}$. Using only one frame after minimization the model showed slightly weaker correlation ($R^2 = 0.62$, RMSE = $0.65 \text{ kcal mol}^{-1}$ and cross-validated $q^2 = 0.51$). Using the GB solvation models resulted in poor correlation coefficients in all applied settings. Also the hybrid QM/MM-GB/SA models failed to correctly predict the experimental activity (Supplementary data, Table S3).

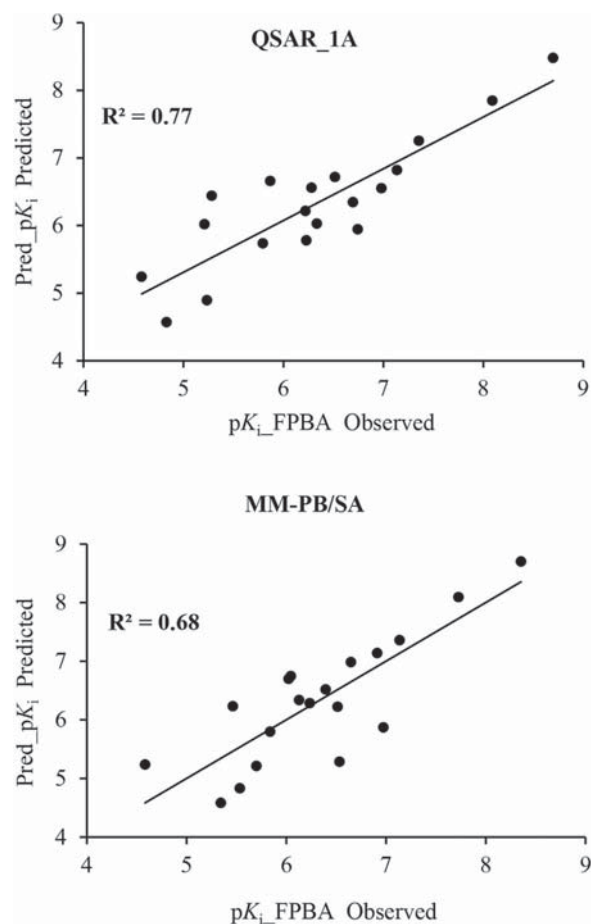


Fig. 4. Correlation plots between calculated pK_i (Model QSAR_1A from Eq. (1) and MM-PB/SA) and observed pK_i for the training set.

2.3. QSAR models

Table 1 displays ΔH values using (MM-PB/SA method) for the inhibitors under study. MM-PB/SA gave the lowest (favourable) value for PD-0166285 among the inhibitors $-49.80 \text{ kcal mol}^{-1}$ with very low Z-score (Z score = 0.58). Meanwhile, for weakly active compounds e.g. tyrphostin and GSK3206866A unfavourable values were obtained (-24.12 and $-27.17 \text{ kcal mol}^{-1}$, respectively). Thus, the applied MM-PB/SA model is able to accurately identify the high and weakly active compounds. The comparison between pyridopyrimidine derivatives (PD-series) emphasizes the latter observation. Furthermore, Z-scores for all inhibitors were less than 2 with the exception of saracatinib (Z-score of 2.11).

Based on the MM-PB/SA-derived model, which showed a significant correlation with the experimentally determined data, further improvement of this correlation was analyzed by including two-dimensional (2D) molecular descriptors. The available 2D molecular descriptors implemented in Molecular Operation Environment System (MOE; Chemical Computing Group Inc., Montreal, QC, Canada) were tested. As a result, incorporating the 2D descriptor PEOE_VSA-4 improved the correlation and increased R^2 of the MM-PB/SA model to 0.77 and cross-validated q^2 to 0.70 (RMSE decreased to 0.50 and 0.58 kcal mol^{-1} , respectively) (Fig. 4). PEOE_VSA-4 indicates electro-negative parts of an approximated accessible van der Waals surface area (in \AA^2) [25]. The following equation (Eq. (1)) shows the generated QSAR model (named QSAR_1A) that includes two descriptors (MM-PB/SA enthalpy score ΔH and PEOE_VSA-4) to predict K_i values of PKMYT1 inhibitors.

$$\text{QSAR_1A: Pred_}K_i = -0.11803 * (\text{MM-PB/SA}) - 0.03631 * (\text{PEOE_VSA-4}) + 2.81241 \quad (1)$$

2.4. Computational fragment growing using the diaminopyrimidine scaffold

In order to design novel inhibitors for PKMYT1, two different approaches were employed in the current work. The hybrid approach, fragment growing and single point modification, was used to design diphenyldiaminopyrimidine derivatives. In the previous work, the conserved interactions and the relevant

interactions of the PKMYT1 binding site have been discussed [13]. In the current work we used this information and the derived BFE/QSAR models to optimize selected hits.

First, ligand efficiency (LE) and ligand lipophilicity efficiency (LLE) were calculated for the starting fragments (Fig. 5). LLE does not take into account the size of the ligand, therefore, it can be used in the optimization process for the diaminopyrimidine series (LLE = 1.41) in order to improve the potency without solely increasing the lipophilicity [26–28]. The diphenyldiaminopyrimidine scaffold was substituted to improve the potency from a predicted K_i value of $33.25 \mu\text{M}$ for the starting fragment to design selective compounds with predicted K_i in the nanomolar range. The visualization of the putative binding mode, structural analysis of the PKMYT1 binding site, and structure-activity relationship study of the diaminopyrimidine derivatives revealed that three vectors on the diaminopyrimidine scaffold could be expanded to target the adjacent pockets (Fig. 5). Based on the derived QSAR_1A model, the biological activities of the designed compounds were predicted.

Modifications interacting at the front-pocket/solvent-accessible area: First, the diaminopyrimidine core was expanded at the front-pocket following a single point modification approach in order to boost the affinity by providing polar substituents based

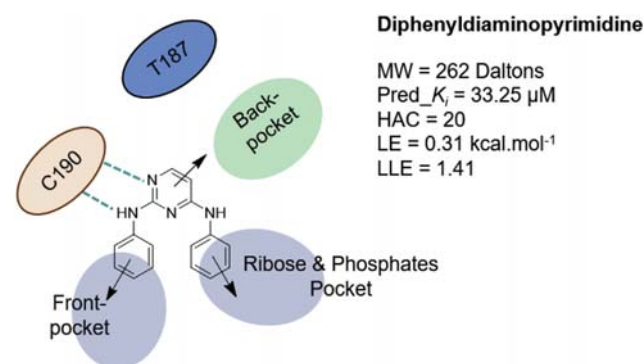


Fig. 5. Diphenyldiaminopyrimidine scaffold and three possible vectors to start a fragment growing process. (MW: molecular weight; Pred K_i : predicted affinity using the QSAR model; HAN: heavy atoms number; LE: ligand efficiency; LLE: ligand lipophilicity efficiency). Blue spheres refer to hydrophilic pockets and the green sphere to hydrophobic pocket. (For interpretation of the references to color in this figure legend, the reader is referred to the Web version of this article.)

Table 1

Experimentally determined K_i (nM) from the binding assay (K_i (FPBA)) and predicted pK_i using the derived MM-PB/SA (10 frames of MD simulation) and the QSAR_1A model.

Name	K_i (FPBA)	pK_i (FPBA)	MM-PB/SA	Predicted pK_i		Z-Score
				MM-PB/SA	QSAR_1A	
Bosutinib	304	6.52	-33.09	6.40	6.72	0.21
Dasatinib	73	7.14	-37.50	6.91	6.82	0.38
GSK1520489A	104.3	6.98	-35.25	6.65	6.55	0.56
GSK1558669A	461.9	6.34	-30.83	6.13	6.03	0.35
GSK1576028A	179.9	6.74	-30.12	6.05	5.94	1.18
GSK312879A	14740	4.83	-25.76	5.54	4.57	1.19
GSK3206866A	6150	5.21	-27.17	5.70	6.02	0.83
GSK625137A	5810	5.24	-17.64	4.58	4.90	1.10
GW435821X	521.5	6.28	-31.74	6.24	6.56	0.08
GW494601A	200.9	6.70	-29.93	6.03	6.35	1.13
GW559768X	588	6.23	-25.15	5.46	5.78	1.29
GW782612X	1600	5.80	-28.35	5.84	5.74	0.07
MK-1775	600	6.22	-34.11	6.51	6.21	0.50
PD-0166285	2	8.70	-49.80	8.35	8.48	0.58
PD-173952	8.1	8.09	-44.45	7.73	7.85	0.62
PD-173955	44	7.36	-39.42	7.14	7.25	0.37
PD-180970	1350	5.87	-38.04	6.97	6.66	1.87
Saracatinib	5200	5.28	-34.28	6.53	6.44	2.11
Tyrphostin	26200	4.58	-24.12	5.34	5.24	1.29

on other known active compounds. The added group should form interactions as planned with Leu116, Pro192 and Gln196. Morpholine, piperazine or sulfone groups were suggested to occupy the front-pocket and to interact with Leu116 and Gln196 (Fig. 6). Based on the structure of known active compounds, it was known that a morpholine moiety has the ability to enhance the affinity more than methylpiperazine and sulfone groups. Adding a morpholine ring improved the predicted potency of the new derivatives (Pred_ K_i = 2.13 μ M), while the LE was maintained near the original value of 0.31 and LLE was increased to 3.12. Meanwhile, the methylpiperazine group was predicted to improve the potency (Pred_ K_i = 6.48 μ M, LE = 0.27, LLE = 2.68). A similar observation was found through using methyl sulfone, which was predicted to improve the ligand metrics and the potency (Pred_ K_i = 2.43 μ M, LE = 0.33, LLE = 3.35). The enhanced potency could be explained by the interactions with Gln196, Pro192 and Leu116 (Fig. 6).

Targeting the hydrophobic back-pocket: The structure-activity relationship study shows the importance of the back hydrophobic pocket for the PKMYT1 inhibitory activity. Therefore, the same approach was established to target the back-pocket by adding a phenyl amide that mimic the highly active PKMYT1 inhibitors (PD-series and dasatinib, Supplementary; Figure S1). The amide group serves as a linker to reach that pocket. This expansion led to an improvement in the predicted potency (Pred_ K_i = 1.30 μ M) with respect the starting fragment. However, this led to a reduction of the LE/LLE values (LE = 0.29, LLE = 1.08), respectively (Fig. 7, Table 2).

The residues at the hydrophobic back-pocket, which are located on the α C helix of PKMYT1, were targeted to improve the activity of the designed compounds. Since the remaining place is quite small after attaching a phenyl ring, small substituents e.g. hydroxyl, or halogens on the phenyl ring were tested. The main residues that are targeted here are Glu157 and Glu251. The hydroxyl groups at *p*- or *m*-position were predicted to cause an increase of the ligand affinity. The *m*-position for the hydroxyl group was preferred compared to the *p*-position (Pred_ K_i = 0.22 μ M and Pred_ K_i = 0.51 μ M, respectively; Table 2). Thus, an additional small group, e.g. hydroxyl has shown the ability to strongly boost the potency.

A good improvement of the predicted potency was obtained by using primary amine or methyl group attached at the position R₀ (Fig. 7 and Table 3). The chloro substituent was predicted to improve the activity but it also increased the lipophilicity (LLE value 0.98, Table 3). Meanwhile, a fluoro group did not show a significant

increase in the predicted activity. Using more bulky substituents at position R₀ gave worse predicted affinities (data not shown).

Modification of residues interacting in the ribose and phosphates pocket: The polar interactions nearby the DFG-motif notably contribute to the inhibitory activity. The most favourable substituent was predicted to be a methyl amide group, which showed the ability to improve the predicted activity and the LE and LLE values (Pred_ K_i = 2.77 μ M, LE = 0.32, LLE = 3.20; Table 4 and Fig. 8). Moreover, a hydroxyl group was predicted to improve the potency as much as the amide group. However, the methyl amide group was useful to decrease the lipophilicity resulting in increasing the LLE value (Table 4, Fig. 8).

2.5. Optimization of the derived hits for PKMYT1

The obtained results of the fragment-based growing approach on the diaminopyrimidine scaffold helped to select useful substituents to optimize the compounds. All synthesized compounds were first tested *in vitro* and IC₅₀ values were determined (Table 5). Since our QSAR model is based on K_i values, we used the Cheng-Prusoff equation [29] to calculate the corresponding IC₅₀ values for the identified actives based on the predicted K_i values.

Synthesis of the diaminopyrimidine derivatives was realized according to a protocol previously reported for the synthesis of potential aurora kinase-inhibitors [30] and an adapted protocol for microwave synthesis conditions [31]. Fig. 9 shows the general synthetic scheme. The two step synthesis started with the reaction of the respective 5-substituted-2,4-dichloropyrimidine derivatives **1** with the respective aniline derivatives **2** (substituted R₂₋₅) in ethanol in the presence of DIPEA to quench the released HCl. In the second synthesis step, the obtained intermediates, which were used without further purification, were reacted with morpholino-aniline **4** using HCl as catalyst in 1-butanol. Purification of the final compounds was performed via preparative HPLC.

Based on our *in silico* results, we predicted that a morpholine moiety is most suitable to address the front-pocket. Meanwhile, various substituents at the phenyl group occupying the ribose/phosphate-binding pocket were assessed, which encompassed chloro, hydroxyl, and methyl amide groups at different positions.

First, a compound was synthesized to check whether the back-pocket is able to accommodate large groups. A benzyloxy moiety at position R₁ was chosen to target the back-pocket, while using a 3-hydroxy-4-methylphenyl group and a morpholine ring to target

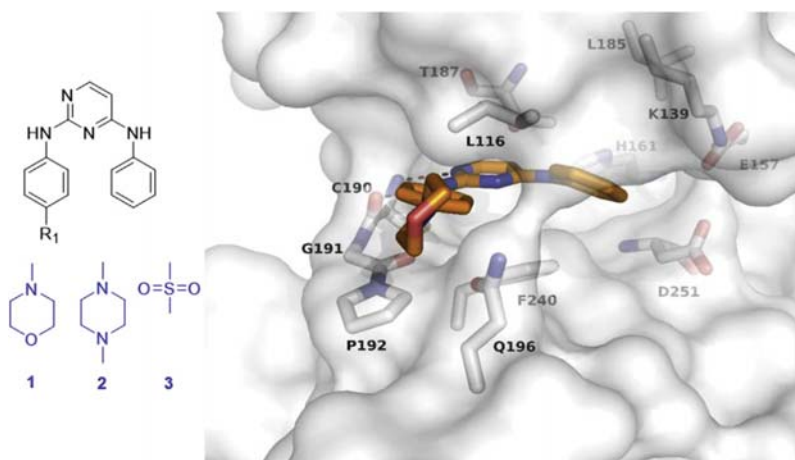


Fig. 6. Extension site of the diaminopyrimidine scaffold at the front pocket/solvent-accessible area of PKMYT1 and the putative binding mode of the attached morpholine derivative (orange). (For interpretation of the references to color in this figure legend, the reader is referred to the Web version of this article.)

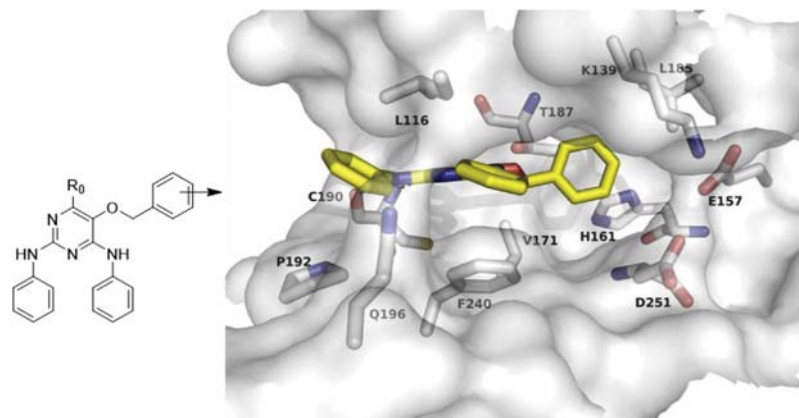


Fig. 7. Suggested modifications on the diaminopyrimidine scaffold and the predicted binding mode of a compound with benzyloxy group interacting at the back-pocket of PKMYT1. Position R_0 contains a hydrogen.

Table 2
Substitutions at the phenyl occupied the hydrophobic back-pocket.

	R-Group	Pred_KE (μM)	LE	LLE
DAP		33.25	0.31	1.41
Benzyloxy	H	1.30	0.29	1.08
Benzyloxy	<i>o</i> -OH	0.34	0.31	1.97
Benzyloxy	<i>m</i> -OH	0.22	0.32	2.13
Benzyloxy	<i>p</i> -OH	0.51	0.31	1.80
Benzyloxy	<i>o</i> -Cl	7.02	0.25	-0.25
Benzyloxy	<i>o</i> -F	23.61	0.22	-0.33

Table 3
Substitutions at position R_0 of the pyrimidine of diaminopyrimidine.

R_0	Pred_KE (μM)	LE	LLE
Diaminopyrimidine	33.25	0.31	1.41
CH ₃	17.71	0.32	1.39
Cl	8.42	0.34	0.98
F	13.73	0.32	1.2
NH ₂	8.42	0.34	2.24

Table 4
Substitutions at the phenyl of diphenyldiaminopyrimidine located in the ribose and phosphates pocket.

R-Group	Pred_KE (μM)	LE	LLE
Diaminopyrimidine	33.25	0.31	1.41
CONH ₂	4.73	0.32	3.32
CONHCH ₃	2.77	0.32	3.20
OH	6.36	0.35	2.44
OCH ₃	6.79	0.33	2.15
CH ₂ OH	11.4	0.32	2.4

the ribose/phosphate- and front-pocket, respectively. Therefore, compound **5a** was synthesized and biologically tested, where it did not show any activity against PKMYT1 (displacement percentage less than 10%, Table 5). We hypothesized, that the back-pocket might not be suitable to accommodate large groups. Hence, the analogous compound **5l**, which contains a methoxy group instead of the benzyloxy moiety, was synthesized and tested. It noteworthy, that compound **5l** showed a high displacement percentage 100%. We thus decided to only use small hydrophobic groups at position R_1 of the pyrimidine ring to target the back-pocket.

The chosen substitutions at position R_1 tried to mimic those

found in active compounds and included chloro, bromo, methyl, methoxy and methylsulfanyl substituents. Methyl amide was proposed for position R_2 , whereas a hydroxyl group was introduced at position R_3 . Position R_4 was substituted by either methoxy or methyl groups. Finally, a chloro substituent was used at position R_5 . So, novel hits presented in Table 5 were synthesized and biologically evaluated.

The first set of compounds was substituted at position R_1 by several small groups and position R_3 by a hydroxyl group, whereas the remaining positions at the pyrimidine were unsubstituted. As a result, five compounds containing chloro, bromo, methyl, methylsulfanyl, methoxy groups (compounds **5f**, **5h**, **5b**, **5d**, and **5k**) were biologically evaluated at 20 μM in order to determine the displacement percentage and assess their activities. Their displacement percentages ranged from 21.11% till 100% (Table 5). One exception is derivative **5b**, containing a methyl group at the position R_1 , which could not displace ATP in PKMYT1 showing a displacement percentage less than 10% (Table 5).

The substituents at position R_5 were evaluated: derivatives **5e** and **5g** contain a chloro substituent at position R_5 and a hydroxyl or methyl group at position R_3 , whereas position R_1 contains either chloro or methylsulfanyl moieties (Table 5). Compounds **5f**, and **5d**, containing chloro and methylsulfanyl groups at R_1 position, showed high displacement percentages 75% and 100%, respectively. It was observed that the chloro group at position R_5 has a negative impact on the activity, where compound **5g** showed a significant loss of activity (the displacement percentage is less than 10%). Compound **5e** is also very weakly active (the displacement percentage is 13%) (Table 5). This can be due to the interfering of the substituent e.g. chloro at position R_5 with the molecular surfaces of Gln196 and Leu116 (Fig. 8). Thus, position R_5 cannot be substituted due to the restricted space available nearby.

The importance of position R_4 was evaluated by using different small groups, which led in most cases to an enhancement of the inhibitory activity. Compound **5l**, which contains an additional methyl group at R_4 compared to compound **5k**, showed a comparable activity (100% displacement compared to **5k**). Meanwhile, using a methoxy at R_4 had a negative impact e.g. **5m** showing a displacement of 39.67% (Table 5).

Further, compound **6** containing a methyl group as part of thiolane ring, was employed to assess the influence of a methylene group at position R_0 (Fig. 10). Compared to **5d** the modified compound **6** showed loss of activity exhibiting a displacement percentage less than 10%. This confirms the negative impact of

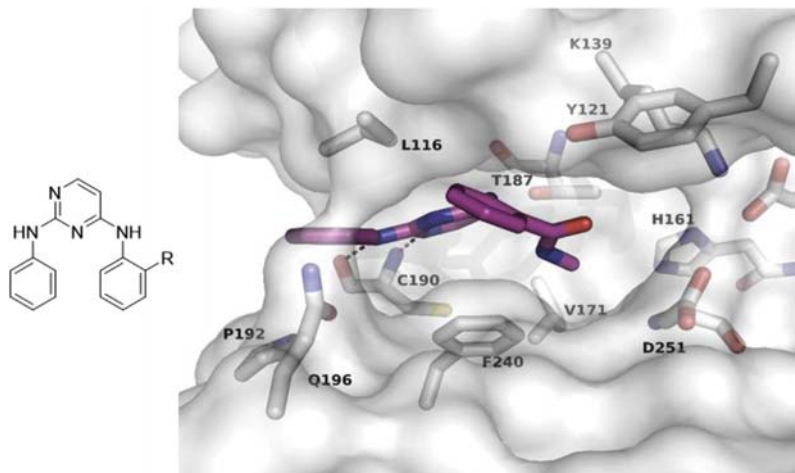
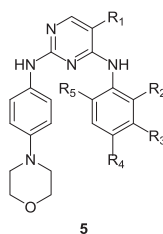


Fig. 8. Suggested modification site on diaminopyrimidine scaffold and the putative binding mode of the added methyl-amide group (purple) at the ribose and phosphates binding pocket of PKMYT1. (For interpretation of the references to color in this figure legend, the reader is referred to the Web version of this article.)

Table 5
Novel diaminopyrimidine derivatives and their activities against PKMYT1.



Name	R_1	R_2	R_3	R_4	R_5	Predicted pIC_{50}		Displacement [%] @ 20 μ M	pIC_{50} FPBA	pIC_{50} FPIA
						MM-PB/SA	QSAR1A			
5a	benzyloxy	H	OH	CH ₃	H	6.97	6.89	<10	n.t.	n.t.
5b	CH ₃	H	OH	H	H	5.63	5.44	<10	n.t.	n.t.
5c	CH ₃	H	OH	H	Cl	5.30	5.21	<10	n.t.	n.t.
5d	SCH ₃	H	OH	H	H	6.07	5.99	100	5.22	5.81
5e	SCH ₃	H	CH ₃	H	Cl	5.25	5.16	13	n.t.	n.t.
5f	Cl	H	OH	H	H	5.87	5.79	75	5.22	6.21
5g	Cl	H	OH	H	Cl	5.22	5.13	<10	n.t.	n.t.
5h	Br	H	OH	H	H	5.93	5.85	21.1	n.t.	n.t.
5i	Br	H	OH	CH ₃	H	6.18	6.01	26.7	n.t.	n.t.
5j	Br	H	OH	OCH ₃	H	6.28	6.20	27.0	n.t.	n.t.
5k	OCH ₃	H	OH	H	H	6.24	6.19	74.8	n.t.	n.t.
5l	OCH ₃	H	OH	CH ₃	H	6.38	6.30	100	5.03	6.51
5m	OCH ₃	H	OH	OCH ₃	H	5.68	5.60	39.7	n.t.	n.t.
5n	OCH ₃	CONHCH ₃	H	H	H	5.92	5.84	100	5.20	6.02

introducing a second substituent at position R_0 of the pyrimidine ring.

The IC_{50} values of the compounds, which showed high displacements, were measured using both an activity (FPIA) and binding (FPBA) assay. The tested compounds showed an inhibitory activity in the low-micromolar and sub-micromolar range (Table 5). Then we tested whether the BFE and the derived QSAR model were able to predict the biological activities. Both models did not show a significant ability to predict the affinities of the novel compounds. However, some of the compounds predicted to be highly active (e.g. **5l** and **5n**) were experimentally confirmed to be sub-micromolar inhibitors of PKMYT1. Furthermore, both models predicted the negative impact of the chloro group at position R_5 , where the

predicted pIC_{50} was decreased compared to their parent molecules (**5d** and **5e**: predicted pIC_{50} = 5.99 and 5.16, **5f** and **5g**: 5.79 and 5.13, respectively, Table 5). Generally, the MM-PBSA model overestimated the affinity of the novel compounds compared to QSAR model 1A.

In order to evaluate the predicted binding mode of the diaminopyrimidines (e.g. compound **5l**), we searched for analogues that have been co-crystallized with other kinases. Thus, the database of ligands deposited in the PDB was screened using Swissimilarity [32]. This resulted in 23 similar compounds showing a similarity score between 0.56 and 0.79. We found that diaminopyrimidine derivatives are found as inhibitors of the following kinases: Aurora A [33], Ephb4 [34], EGFR [35] and CDK2 [36]. A

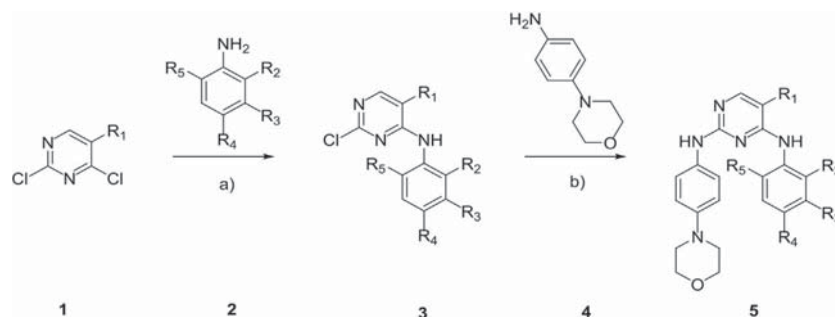


Fig. 9. Scheme of synthesis of novel diaminopyrimidine derivatives as PKMYT1 inhibitors (conditions a: EtOH/DIPEA/50 min at 150 °C microwave; b: 1-BuOH/1 M HCl/20 min at 160 °C microwave).

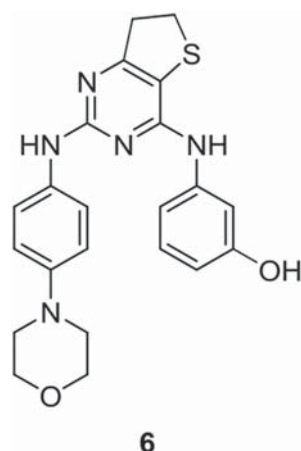


Fig. 10. Chemical structure of a further synthesized diaminopyrimidine derivative.

series of diaminopyrimidine analogues have been co-crystallized with Aurora A kinase (PDB IDs 3UNZ, 3UO5, 3UO6, 3UOD, 3UOH, 3UOJ, 3UOK, 3UOL, 3UP2, 3UP7, 4DEB, 4DED, 4DEE) [37,38]. In addition, other analogues were co-crystallized with CDK2 (PDB IDs 3UNJ, 3UNK [33,37] and 1H08 [36]) and EGFR (PDB ID 5UWD [35]). In Aurora A, the diaminopyrimidine compounds show the same binding mode as predicted for PKMYT1. This binding mode is characterized by a horseshoe shape conformation and two hydrogen bonds to the hinge region of the ATP pocket, whereas the phenyl ring occupies the ATP-ribose binding site (Fig. 11A). Meanwhile, diaminopyrimidine compounds display two distinct conformations co-crystallized with CDK2; a horseshoe shape (PDB ID 1H08 [36]) and a conformation (PDB ID 3UNJ [33]) where the phenyl ring flips towards the back-pocket (Fig. 11B). Also the analogues co-crystallized with EGFR (PDB ID 5UWD [35]) show a horseshoe shape binding mode at the ATP pocket.

The diaminopyrimidine derivatives containing a substituent on the pyrimidine at position R₁ show in the X-ray structures a horseshoe shape binding mode. The diaminopyrimidine analogue co-crystallized with CDK2 (PDB ID 1H08 [36]) contains a bromo group at position R₁ and shows the horseshoe-shape binding mode (Fig. 12). A second example is the crystal structure of EGFR (PDB ID 5UWD [35]), which contains an analogue with a trifluoromethyl attached at position R₁ (Fig. 12). Thus, substituting R₁ with e.g. halogens, methoxy or sulfur are only found in the horseshoe shape binding mode, which was also predicted for compound **5l** that contains a methoxy group at position R₁.

The binding mode of compound **5l** displays the conserved hydrogen bonds with the hinge region residue Cys190 [13], which are critical for the inhibitory activity of the ATP-competitive inhibitors. The interactions with Tyr121 and Asp251 in addition with the P-loop residue Gly117 (Fig. 11C) might be the reason for the increase in potency as proposed by the computational fragment growing approach. The methyl group at R₄ of compound **5l** forms additional interactions with the P-loop residues. Substitution at position R₅ by a chloro group decreases the activity of the diaminopyrimidine compounds **5e** and **5g**. This is due to the interference of the chloro group with Asn196 and Leu116, which is predicted to be unfavourable. Compound **5n** containing a methyl amide at the position R₂ showed decreased activity compared to **5l**. This shows the importance of the interactions with the P-loop residues to boost the inhibitory activity. Substituting R₁ using small groups (methoxy group in case of **5l**) has a big impact on the inhibitory activity of the diaminopyrimidine derivatives. The substitution is favouring a horse shoe shape binding conformation that fits into the ATP-binding pocket of PKMYT1 (Fig. 11C). On the other hand, using more bulky groups (benzyloxy group in **5a**) results in loss of inhibitory activity due to the limited space in the back-pocket. Furthermore, a combination of the methyl group at R₁ and the hydroxyl group at R₃ might destroy the bioactive conformation (horse shoe shape), thus, compound **5b** and **5c** lose their activities (Table 5). The methylsulfanyl and methoxy groups of compounds **5d** and **5l** fit perfectly in the PKMYT1 back-pocket and interact with the gatekeeper Thr187. We found also that adding a second substituent on the pyrimidine ring e.g. compound **6** decreases the activity dramatically.

3. Conclusion

In the current study, we generated several computational models in order to predict the biological activity of novel PKMYT1 inhibitors. We extended our previously developed models by including novel X-ray structures of PKMYT1 and by increasing the ligand data set. We observed a good reproduction of the binding mode of recently reported PKMYT1 inhibitors. However, the docking and scoring failed to correctly predict the affinity of the ligands, where only a weak correlation was obtained between computed and experimental affinities. We were able to show that binding free energy calculations (especially the MM-PB/SA solvation model) were better to predict the activities of the compounds. Moreover, including 2D molecular descriptors based on the partial charges of the ligands slightly improved the quality of the

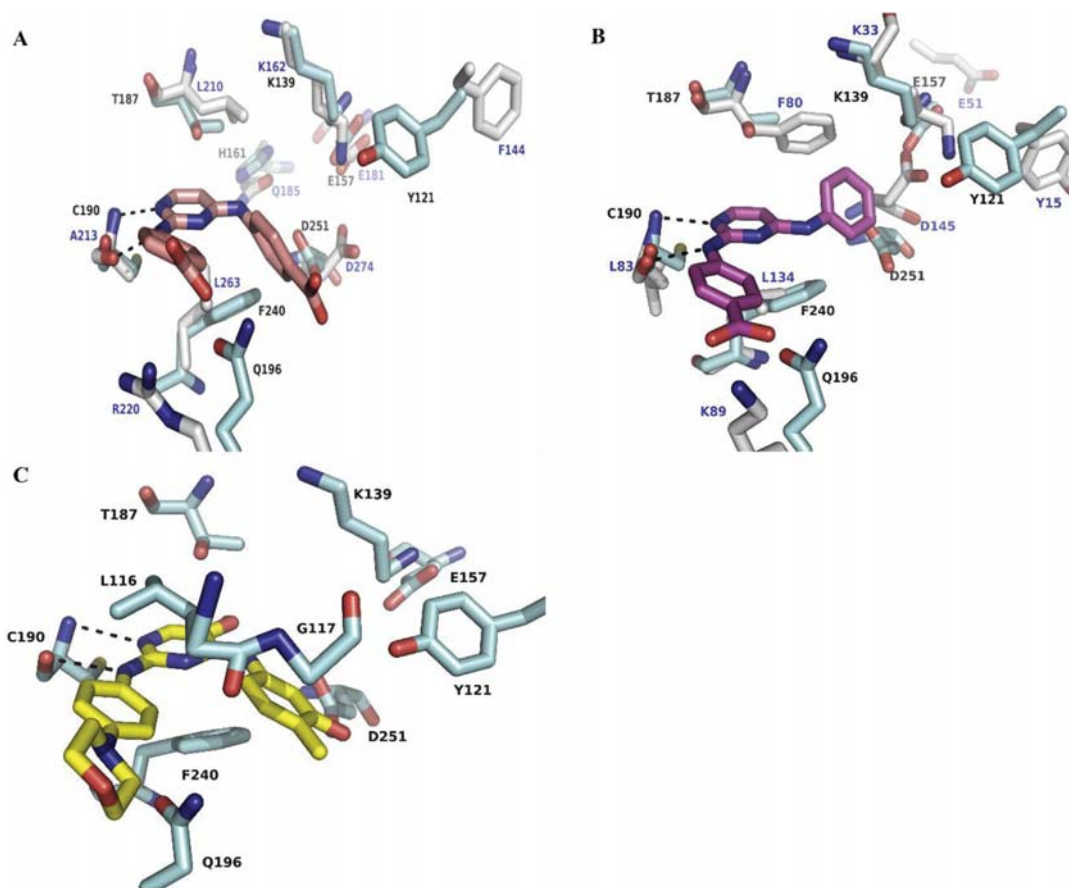


Fig. 11. A) Superimposition of the ATP binding pocket of PKMYT1 (PDB ID 5VCW [14], colored cyan and labeled in black) and aurora A kinase (PDB ID 4DEA [38]). B) Superimposition of PKMYT1 and CDK2 kinase (PDB ID 3UNJ [33]), colored white and labeled in blue. The co-crystallized diaminopyrimidine analogue is colored pink in Aurora A (A) and violet in CDK2 (B). C) Binding mode of compound **51** (yellow) within the PKMYT1 binding pocket (cyan colored residues). (For interpretation of the references to color in this figure legend, the reader is referred to the Web version of this article.)

prediction. The applied fragment growing allowed to design a first set of diaminopyrimidine derivatives, which are active in the sub-micromolar range (e.g. compound **51**). As a consequence, we were able to generate several active analogues and to assess first structure-activity relationships of the diaminopyrimidine derivatives. The derived results provide now the basis for further chemical modifications to design more potent PKMYT1 inhibitors.

4. Materials and methods

4.1. Molecular docking

4.1.1. Preparation of the inhibitors databases

The inhibitors dataset was prepared using the LigPrep module in Schrödinger (LigPrep, Schrödinger, LLC, New York, NY, 2017-1). The preparation involved 3D protonation at pH = 7.4 using Epik module [39,40], minimization using the integrated Optimized Potentials for

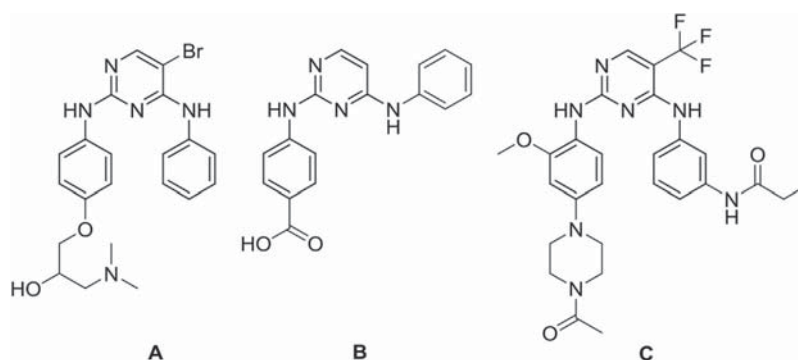


Fig. 12. Co-crystallized diaminopyrimidine derivatives in CDK2 (A PDB ID 1H08 [36]; B: PDB ID 3UNJ [33]) and EGFR (C: PDB ID 5UWD [35]).

Liquid Simulations (OPLS_2005) force field [41] and generation of ten low energy conformations per ligand. Further preparation comprised conformer generation with OMEGA in OpenEye Scientific Software [42], where a maximum of twenty conformers for each compound were generated.

4.1.2. Preparation of PKMYT1 X-ray structures

Nine crystal structures of PKMYT1 are stored in the Protein Data Bank (PDB; www.rcsb.org) [43] (PDB IDs: 3P1A (no associated citation), 5VCV, 5VCW, 5VCX, 5VCY, 5VCZ, 5VD0, 5VD1 and 5VD3) [14]. In our previous work, we found that the structure of PKMYT1 co-crystallized with Pelitinib (PDB ID: 5VCW) was able to reproduce and predict the binding mode of native and non-native ligands [13]. Thus, it was used in the current work to dock the newly designed compounds. Preparation module in Molecular Operation Environment System (MOE) (Chemical Computing Group Inc., Montreal, QC, Canada) was used for preparing the PKMYT1 structures. The process encompassed 3D protonation, followed by energy minimization employing Amber10: Extended Huckel Theory (EHT) force field implemented in MOE [23,44] with a tethering (0.5) Å and a gradient of 0.1 kcal mol⁻¹ Å⁻² for all atoms during the minimization.

4.1.3. Molecular docking

The inhibitors were docked into the prepared PKMYT1 structures using GOLD v5.2 [45]. The co-crystallized ligand (Pelitinib) within the PKMYT1 structures was defined as a center of the binding site. One hydrogen bond formed with the backbone-NH of Cys190 was used as hydrogen bond constraints. In addition, one conserved water molecule, which forms a water bridge with His161 and Glu157, was considered during the docking procedure. Generally, ten poses were generated for each docked ligand. Other docking options were kept as default. The obtained top-ranked docking poses were subjected to re-scoring by different docking scores implemented GOLD and Glide (Schrödinger 2017u1) [46–48].

4.2. Molecular dynamics (MD) simulations

Molecular dynamics (MD) simulations were performed prior the calculation of the binding free energy. MD simulations were carried out using AMBER 12 [24] and employing AMBER03 force field [49–51]. Antechamber module was used to generate parameters for atom type and AM1-BCC [52] atomic charges for each ligand in general AMBER force field GAFF [53]. The preparation of the protein-ligand complexes was performed using LEaP module in AMBER. Water model TIP3BOX was used to solvate the system (protein-ligand complex and ions) in a box size of 10 Å [54] and counter ions were added to neutralize the system. Several steps were performed to prepare the system for MD simulations, starting with two consecutive steps of energy minimization. Firstly, minimization was carried out for water and ion molecules while keeping the ligand-protein complexes restrained to their initial coordinates with a force constant of 500 kcal mol⁻¹ Å⁻². The procedure helped to reduce unreal van der Waals interactions with the surrounding solvent molecules and rearrange of the inserted water and ions molecules. In this step 2000 iterations (beginning with 1000 steepest descent and followed by 1000 conjugate gradient) were performed. The second minimization step was applied for the whole system through 10000 iterations (first 5000 steepest descent and then 5000 conjugate gradients). The next step involved heating. The temperature was equilibrated from 0 to 300 K and occurred gradually over a timescale 2 fs of 100 ps to avoid problems with the hot solvent cold solute. Langevin dynamics was set for temperature control using a collision frequency of 1 ps⁻¹ during the

temperature equilibration [55]. The cutoff force constant of the restrained system was set at 10 kcal mol⁻¹ Å⁻². The output coordinates after the heating were inserted in a pressure equilibration routine. The third step was called density, which was used to set the constant pressure periodic boundary. The constant pressure periodic boundary was converted from 1 bar to 2 bar during 100 ps with a timescale of 2 fs at 300 K for the temperature and applying the same cutoff of force constant at 10 kcal mol⁻¹ Å⁻². During the MD simulation, a cutoff of 10 Å for non-bonded atoms was applied using Particle Mesh Ewald methods [56]. Moreover, all simulation were run using SHAKE to constrain hydrogen bonds [57]. Finally, 100 ps MD simulation was performed.

4.3. Binding free energy (BFE) calculations

The binding free energy calculations were performed for the putative binding modes described in the previous work [13]. AMBERTools12 [24] and MOE (Chemical Computing Group Inc., Montreal, QC, Canada) were used to calculate the binding free energies. The calculation was first carried out using one snapshot after a short energy minimization of the whole system in explicit water. Later, ten snapshots (frames) of ligand-protein complexes from MD simulation were considered for calculating the binding free energy. Different theories were applied using Generalized Born (GB) [58,59] and Poisson Boltzmann (PB) solvation models [60]. The molecular mechanics (MM) and quantum mechanics/molecular mechanics (QM/MM) hybrid were considered too [61,62]. The QM region of the QM/MM hybrid mechanics was firstly applied for the ligand only and later for the ligand and selected residues from the PKMYT1 binding pocket, surrounding the ligand (In total 10 residues were considered: Leu116, Lys139, His161, Val171, Leu185, Thr187, Leu189, Cys190, Gln196, Asp251). Two models for QM were used: Parameterized Model number 3 (PM3) and Austin Model 1 (AM1) [24]. Finally, the binding free energy calculation of MM-PB(GB)/SA and MM/QM-GB/SA models were computed using MMPBSA.py [63] module in AMBERTools12 [64–69]. In addition, the implemented MM-GB/SA model in MOE was used to estimate the binding free energy.

The computed affinity of a ligand to a protein can be estimated by differences between the free energy of complex and the sum of the free energies of ligand and protein separately, eq. (2) [70]:

$$\Delta G_{\text{binding}} = G_{\text{protein/ligand}} - (G_{\text{protein}} + G_{\text{ligand}}) \quad (2)$$

The absolute free energy for each part can be computed as a sum of the gas-phase free energy E_{MM} plus the changing of the free energy because of solvation $\Delta G_{\text{solvation}}$ and the entropic contributions $-T\Delta S$, eq. (3) [71]:

$$G_{\text{molecule}} = E_{MM} + \Delta G_{\text{solvation}} - T\Delta S \quad (3)$$

The conformational entropy value $-T\Delta S$ was not considered. Thus, the change of enthalpy (ΔH) was considered to calculate the binding free energy and it will indicate to the binding free energy, eq. (4).

$$\Delta H = E_{MM} + \Delta G_{\text{solvation}} \quad (4)$$

4.4. Fragment-based drug design

Fragment-based drug design (FBDD) shows a high ability to sample the chemical space rather than other techniques [72]. Fragments are defined by Astex through 'rule-of-3' [73]. Fragment

growing approach provides useful tools for the hit and lead optimization, which aims to build additional interactions with the adjacent pockets [74,75]. Two metrics, namely ligand efficiency (LE) and ligand lipophilicity efficiency (LLE), are available to aid in the fragment hit selection and optimization. The ligand efficiency (LE) is used to rank fragments and to monitor the progress of optimization, whereas ligand lipophilicity efficiency (LLE) is a metric used to monitor the lipophilicity with respect to *in vitro* potency of a molecule [26,27,76]. Moreover, the ligand lipophilicity efficiency does not consider the size of the ligand. During the optimization studies, the goal is to improve potency without increasing lipophilicity. However, the ideal values of LLE are located in the range of 5–7 or greater [28,77,78]. The following equations were used to estimate the ligand efficiency and ligand lipophilicity efficiency:

$$LE = 1.4(-\log K_i)/HAC, HAC \text{ is heavy atoms count.}$$

$$LLE = pK_i - cLogP, cLogP \text{ was calculated using MOE.}$$

4.5. Biological screening of the compound collection

Aside from kinase inhibitors, all chemicals used were purchased from Sigma (Schnelldorf, Germany) unless stated otherwise. PD-0166285 was from Santa Cruz Biotechnology (Santa Cruz, CA, USA), PD-173952 and PD-180970 from Sigma (Schnelldorf, Germany) and MK-1775 from Selleckchem (Houston, TX, USA). All other tested kinase inhibitors were purchased from LC Laboratories (Woburn, MA, USA). The GSK published kinase inhibitor set (PKIS) I and II was kindly provided by Glaxo Smith Kline LCC (Research Triangle Park, NC USA). The monoclonal *p*-Tyr P-100 antibody was from Cell Signaling (#9411, Danvers, MA, USA).

PKMYT1 full-length (FL) and PKMYT1 kinase domain (KD) were expressed and purified as described before [79]. (6-FAM)KI(pY)VV was from IKFZ (Leipzig, Germany). EFS247-259 and pY-EFS247-259 were synthesized via solid-phase peptide synthesis on Fmoc-Rink MBHA as basically described in the work of Rohe et al. [80] following a standard Fmoc/*t*Bu based strategy. Processing and purification was performed as described in Rohe et al.

To test the activities of the compounds as PKMYT1 inhibitors, the synthesized compounds were screened with a fluorescence anisotropy-based binding assay, using the PKMYT1 domain (KD) and a fluorescently labeled ATP-competitive compound [15]. The initial screening was performed at 20 μ M inhibitor concentration as triple measurement of each compound. Dasatinib (10 μ M) was used as inhibitory control and 1% DMSO as vehicle control. Compounds with a tracer displacement >60% were retested at 20 μ M and 5 μ M concentrations in triple measurement. The IC₅₀ and K_i values were determined for confirmed hits using the FP binding assay. To confirm the inhibitory activities of the hit compounds, we further used the newly developed activity assay (FPIA) [81], and determined the IC₅₀ and K_i values for PKMYT1 (FL) inhibition. Similar to the FP-binding assay, 10 μ M dasatinib and 1% DMSO were used as controls.

The data processing was performed as described before. Because the FP does not behave additively, anisotropy (*r*) was calculated according to Rohe et al. [79,80]. The Δr was calculated as the difference between *r* of positive control (PKMYT1 reaction) and negative control (reaction without PKMYT1). Data is represented as means \pm SEM. Kinetics, binding and inhibition curves as well as linear and nonlinear regression were generated using GraphPad Prism 5 (GraphPad Software, Inc., La Jolla, CA, USA).

4.6. Synthesis and characterization of novel compounds

General: All materials and reagents were purchased from

Sigma–Aldrich Co. Ltd., abcr GmbH, ChemPUR Feinchemikalien und Forschungsbedarf GmbH, and Carbolution Chemicals. All solvents were analytically pure and dried before use. Synthesis was carried out under microwave conditions using Monowave 450 (Anton Paar, Graz, Austria). Thin-layer chromatography (TLC) was carried out on aluminum sheets coated with silica gel 60 F254 (Merck, Darmstadt, Germany). Purification of the final compounds was carried out with preparative HPLC (Shimadzu, Kyoto, Japan; LC-10AD, SIL-HAT auto sampler). Therefore a 7.8 \times 300 mm XTerra RP-18 column (7 μ M), Waters (Milford, MA, USA) with a UV-Vis-detector SPD-M10A VP PDA was used. Separation was achieved with a gradient of MeOH/H₂O (starting at 95% H₂O going to 5% H₂O). Final compounds were confirmed to be of >95% purity based on HPLC. Purity was measured by UV absorbance at 254 nm. HPLC instrumentation consisted of an XTerra RP18 column (3.5 mm 3.9_100 mm; Waters, Milford, MA, USA) two LC-10AD pumps, an SPD-M10A VP PDA detector, and an SIL-HT auto sampler all from the manufacturer Shimadzu (Kyoto, Japan). The mobile phase was in all cases a gradient of MeOH/H₂O (starting at 95% H₂O going to 5% H₂O). Mass spectrometry analyses were performed with a Finnigan MAT 710C (Thermo Separation Products, San Jose, CA, USA) for ESI-MS spectra, and with a LTQ (linear ion trap)–Orbitrap XL hybrid mass spectrometer (Thermo Fisher Scientific, Bremen, Germany) for HRMS-ESI (high-resolution mass spectrometry) spectra. For HRMS analyses, the signal for the isotopes with the highest prevalence was given and calculated for ³⁵Cl and ⁷⁹Br. ¹H NMR spectra were taken on a Varian Gemini 2000 and a Varian Inova 500 using CDCl₃ and [D₆] DMSO as solvents. Chemical shifts (δ , ppm) are referenced to the residual solvent signals.

General procedure for the conversion of the 2,4-dichloropyrimidine derivatives **1** with corresponding aniline derivatives **2**:

The 2,4-dichloropyrimidine derivative **1** was dissolved in EtOH and 1.1 equiv. of the aniline derivative **2** and 1.1 equiv. of DIPEA were added. The reaction was carried out for 50 min at 150 °C under microwave conditions. The reaction mixture was diluted with ethyl acetate and washed with water. The organic phase was evaporated and the crude intermediate was used for the following reaction step without purification.

General procedure for conversion of the 2-chloro-4-anilinoypyrimidine derivatives **3** with 4-morpholinoaniline **4**:

The crude 2-chloro-4-anilinoypyrimidine derivative **3** was dissolved in 1-BuOH and 1.1 equiv. of 4-morpholinoaniline **4** and 1.1 equiv. of 1 M HCl were added. The reaction was carried out for 20 min at 160 °C under microwave conditions. The reaction mixture was diluted with ethyl acetate and washed with 1 M aqueous NaOH. The mixture was evaporated and purified with preparative HPLC.

4.6.1. 5-[5-Benzyloxy-2-[4-(1-morpholinyl)phenyl]aminopyrimidin-4-yl]amino-2-methylphenol (**5a**)

¹H NMR (400 MHz, DMSO) δ 10.08 (d, *J* = 6.0 Hz, 1H, –NH), 10.02 (d, *J* = 9.7 Hz, 1H, –NH), 9.43 (s, 1H, –OH), 7.62 (s, 1H, Ar–H), 7.54 (d, *J* = 7.1 Hz, 2H, Ar–H), 7.41 (dd, *J* = 7.0, 5.5 Hz, 2H, Ar–H), 7.36 (dd, *J* = 6.2, 3.8 Hz, 1H, Ar–H), 7.24 (d, *J* = 9.0 Hz, 2H, Ar–H), 7.03 (d, *J* = 8.2 Hz, 1H, Ar–H), 6.95–6.92 (m, 1H, Ar–H), 6.90 (d, *J* = 1.7 Hz, 1H, Ar–H), 6.86 (d, *J* = 9.0 Hz, 2H, Ar–H), 5.20 (s, 2H, Ar–CH₂–), 3.74–3.71 (m, 4H, –OCH₂), 3.08–3.03 (m, 4H, –NCH₂), 2.09 (d, *J* = 17.8 Hz, 3H, –CH₃). HRMS-ESI *m/z* [M+H]⁺ calcd for C₂₈H₃₀N₅O₃: 484.5697, found: 484.5688.

4.6.2. 3-[5-Methyl-2-[4-(1-morpholinyl)phenyl]aminopyrimidin-4-yl]aminophenol (**5b**)

¹H NMR (400 MHz, DMSO) δ 9.90 (s, 1H, –NH), 9.51 (s, 1H, –NH), 8.30 (s, 1H, –OH), 7.72 (s, 1H, Ar–H), 7.36–6.43 (m, 8H, Ar–H),

3.85–3.63 (m, 4H, $-\text{OCH}_2$), 3.24–2.91 (m, 4H, $-\text{NCH}_2$), 2.12 (m, 3H, $-\text{CH}_3$). HRMS-ESI m/z $[\text{M}+\text{H}]^+$ calcd for $\text{C}_{21}\text{H}_{24}\text{N}_5\text{O}_2^+$: 378.4478, found: 378.4486.

4.6.3. 4-Chloro-3-[5-methyl-2-[4-(1-morpholinyl)phenyl]aminopyrimidin-4-yl]aminophenol (**5c**)

^1H NMR (400 MHz, CDCl_3) δ 8.03 (s, 1H, $-\text{NH}$), 7.40–7.14 (m, 5H, $-\text{NH}$, $-\text{OH}$, Ar–H), 6.99 (s, 1H, Ar–H), 6.75 (d, $J = 9.0$ Hz, 2H, Ar–H), 6.61 (d, $J = 2.6$ Hz, 1H, Ar–H), 6.51 (dd, $J = 8.6, 2.6$ Hz, 1H, Ar–H), 3.99–3.66 (m, 4H, $-\text{OCH}_2$), 3.19–2.93 (m, 4H, $-\text{NH}_2$), 2.17 (m, 3H, $-\text{CH}_3$). HRMS-ESI m/z $[\text{M}+\text{H}]^+$ calcd for $\text{C}_{21}\text{H}_{22}\text{ClN}_5\text{O}_2^+$: 411.8846, found: 411.8856.

4.6.4. 3-[5-Methylthio-2-[4-(1-morpholinyl)phenyl]aminopyrimidin-4-yl]aminophenol (**5d**)

^1H NMR (400 MHz, DMSO) δ 9.30 (s, 1H, $-\text{NH}$), 9.08 (s, 1H, $-\text{NH}$), 8.41 (s, 1H, $-\text{OH}$), 8.14 (s, 1H, Ar–H), 7.51 (d, $J = 9.1$ Hz, 2H, Ar–H), 7.22–6.97 (m, 3H, Ar–H), 6.80 (d, $J = 9.1$ Hz, 2H, Ar–H), 6.55–6.46 (m, 1H, Ar–H), 3.86–3.57 (m, 4H, $-\text{OCH}_2$), 3.12–2.83 (m, 4H, $-\text{NCH}_2$), 2.28 (d, $J = 21.2$ Hz, 3H, $-\text{SCH}_3$). HRMS-ESI m/z $[\text{M}+\text{H}]^+$ calcd for $\text{C}_{21}\text{H}_{24}\text{N}_5\text{O}_2\text{S}^+$: 410.5138, found: 410.5129.

4.6.5. N^4 -(2-Chloro-5-methylphenyl)-5-(methylthio)- N^2 -[4-(1-morpholinyl)phenyl]pyrimidine-2,4-diamine (**5e**)

^1H NMR (400 MHz, CDCl_3) δ 8.72 (s, 1H, $-\text{NH}$), 8.27 (s, 1H, $-\text{NH}$), 8.22 (s, 1H, Ar–H), 7.45–7.39 (m, 2H, Ar–H), 7.32–7.26 (m, 2H, Ar–H), 6.93–6.80 (m, 3H, Ar–H), 3.91–3.82 (m, 4H, $-\text{OCH}_2$), 3.17–3.02 (m, 4H, $-\text{NH}_2$), 2.35 (d, $J = 17.5$ Hz, 3H, $-\text{CH}_3$), 2.28 (d, $J = 13.9$ Hz, 3H, $-\text{SCH}_3$). HRMS-ESI m/z $[\text{M}+\text{H}]^+$ calcd for $\text{C}_{23}\text{H}_{27}\text{N}_6\text{O}_2\text{S}^+$: 451.5657, found: 451.5668.

4.6.6. 3-[5-Chloro-2-[4-(1-morpholinyl)phenyl]aminopyrimidin-4-yl]aminophenol (**5f**)

^1H NMR (400 MHz, DMSO) δ 9.32 (s, 1H, $-\text{NH}$), 9.02 (s, 1H, $-\text{NH}$), 8.56 (s, 1H, $-\text{OH}$), 8.04 (s, 1H, Ar–H), 7.47 (d, $J = 9.0$ Hz, 2H, Ar–H), 7.09 (d, $J = 5.1$ Hz, 2H, Ar–H), 7.01 (s, 1H, Ar–H), 6.77 (d, $J = 9.0$ Hz, 2H, Ar–H), 6.59–6.46 (m, 1H, Ar–H), 3.84–3.56 (m, 4H, $-\text{OCH}_2$), 3.06–2.85 (m, 3H, $-\text{NH}_2$). HRMS-ESI m/z $[\text{M}+\text{H}]^+$ calcd for $\text{C}_{20}\text{H}_{21}\text{ClN}_5\text{O}_2^+$: 398.8659, found: 398.8650.

4.6.7. 4-Chloro-3-[5-chloro-2-[4-(1-morpholinyl)phenyl]aminopyrimidin-4-yl]aminophenol (**5g**)

^1H NMR (400 MHz, CDCl_3) δ 10.95 (s, 2H; $-\text{NH}$), 8.19 (s, 1H, $-\text{OH}$), 7.37 (m, 4H, Ar–H), 7.16 (d, $J = 9.1$ Hz, 2H, Ar–H), 6.61 (d, $J = 2.6$ Hz, 1H, Ar–H), 6.49 (dd, $J = 8.6, 2.7$ Hz, 1H, Ar–H), 4.11–4.00 (m, 4H, $-\text{OCH}_2$), 3.47–3.34 (m, 4H, $-\text{NH}_2$). HRMS-ESI m/z $[\text{M}+\text{H}]^+$ calcd for $\text{C}_{20}\text{H}_{20}\text{Cl}_2\text{N}_5\text{O}_2^+$: 433.3107, found: 433.3115.

4.6.8. 3-[5-Bromo-2-[4-(1-morpholinyl)phenyl]aminopyrimidin-4-yl]aminophenol (**5h**)

^1H NMR (400 MHz, DMSO) δ 9.07 (s, 1H, $-\text{NH}$), 8.50 (s, 1H, $-\text{NH}$), 8.29 (s, 1H, $-\text{OH}$), 8.12 (s, 1H, Ar–H), 7.46 (d, $J = 9.1$ Hz, 2H, Ar–H), 7.12–7.02 (m, 3H, Ar–H), 6.77 (d, $J = 9.0$ Hz, 2H, Ar–H), 6.54 (d, $J = 8.0$ Hz, 1H, Ar–H), 3.76–3.66 (m, 4H, $-\text{OCH}_2$), 3.03–2.92 (m, 4H, $-\text{NCH}_2$). HRMS-ESI m/z $[\text{M}+\text{H}]^+$ calcd for $\text{C}_{20}\text{H}_{21}\text{BrN}_5\text{O}_2^+$: 443.3172, found: 443.3165.

4.6.9. 5-[5-Bromo-2-[4-(1-morpholinyl)phenyl]aminopyrimidin-4-yl]amino-2-methylphenol (**5i**)

^1H NMR (400 MHz, DMSO) δ 9.52 (s, 1H, $-\text{NH}$), 8.93 (s, 1H, $-\text{NH}$), 8.17 (s, 1H, $-\text{OH}$), 7.40–7.33 (m, 2H, Ar–H), 7.08–6.91 (m, 2H, Ar–H), 6.89–6.77 (m, 4H, Ar–H), 3.73 (s, 4H, $-\text{OCH}_3$), 3.11–3.00 (m, 4H, $-\text{NCH}_3$), 2.11 (d, $J = 12.6$ Hz, 3H, $-\text{CH}_3$). HRMS-ESI m/z $[\text{M}+\text{H}]^+$ calcd for $\text{C}_{21}\text{H}_{23}\text{BrN}_5\text{O}_2^+$: 457.3438, found: 457.3445.

4.6.10. 5-[5-Bromo-2-[4-(1-morpholinyl)phenyl]aminopyrimidin-4-yl]amino-2-methoxyphenol (**5j**)

^1H NMR (400 MHz, DMSO) δ 8.96 (s, $J = 7.8$ Hz, 2H, $-\text{NH}$), 8.28 (d, $J = 6.9$ Hz, 1H, $-\text{OH}$), 8.07 (s, 1H, Ar–H), 7.43 (d, $J = 9.0$ Hz, 2H, Ar–H), 6.96 (d, $J = 2.1$ Hz, 1H, Ar–H), 6.92–6.85 (m, 2H, Ar–H), 6.74 (d, $J = 9.0$ Hz, 2H, Ar–H), 3.77 (s, 3H, $-\text{OCH}_3$), 3.73–3.67 (m, 4H, $-\text{OCH}_2$), 3.01–2.93 (m, 4H, $-\text{NCH}_2$). HRMS-ESI m/z $[\text{M}+\text{H}]^+$ calcd for $\text{C}_{21}\text{H}_{23}\text{BrN}_5\text{O}_3^+$: 473.3432, found: 473.3442.

4.6.11. 3-[5-Methoxy-2-[4-(1-morpholinyl)phenyl]aminopyrimidin-4-yl]aminophenol (**5k**)

^1H NMR (400 MHz, DMSO) δ 10.14 (s, 1H, $-\text{NH}$), 10.03 (s, 1H, $-\text{NH}$), 9.63–9.35 (m, 1H, $-\text{OH}$), 7.60 (s, 1H, Ar–H), 7.28 (d, $J = 9.0$ Hz, 2H, Ar–H), 7.16–7.08 (m, 2H, Ar–H), 7.03 (d, $J = 1.9$ Hz, 1H, Ar–H), 6.91 (d, $J = 9.0$ Hz, 2H, Ar–H), 6.63 (dt, $J = 6.8, 2.4$ Hz, 1H, Ar–H), 3.87 (d, $J = 4.8$ Hz, 3H, $-\text{OCH}_3$), 3.72 (dd, $J = 15.4, 10.5$ Hz, 4H, $-\text{OCH}_2$), 3.13–2.98 (m, 4H, $-\text{NCH}_2$). HRMS-ESI m/z $[\text{M}+\text{H}]^+$ calcd for $\text{C}_{21}\text{H}_{24}\text{N}_5\text{O}_3^+$: 394.4472, found: 394.4465.

4.6.12. 5-[5-Methoxy-2-[4-(1-morpholinyl)phenyl]aminopyrimidin-4-yl]amino-2-methylphenol (**5l**)

^1H NMR (400 MHz, DMSO) δ 9.08 (s, 1H, $-\text{NH}$), 8.49 (s, 1H, $-\text{NH}$), 8.36 (d, $J = 48.9$ Hz, 2H, $-\text{OH}$), 7.73 (s, 1H, Ar–H), 7.53 (d, $J = 7.6$ Hz, 2H, Ar–H), 7.21–7.14 (m, 1H, Ar–H), 7.11 (s, 1H, Ar–H), 6.94 (d, $J = 8.1$ Hz, 1H, Ar–H), 6.79 (d, $J = 7.2$ Hz, 2H, Ar–H), 3.78 (d, $J = 19.4$ Hz, 3H, $-\text{OCH}_3$), 3.71 (d, $J = 4.3$ Hz, 4H, $-\text{OCH}_2$), 2.97 (s, 4H, $-\text{NCH}_2$), 2.08 (s, 3H, $-\text{CH}_3$). HRMS-ESI m/z $[\text{M}+\text{H}]^+$ calcd for $\text{C}_{22}\text{H}_{26}\text{N}_5\text{O}_3^+$: 408.4737, found: 408.4746.

4.6.13. 5-[5-Methoxy-2-[4-(1-morpholinyl)phenyl]aminopyrimidin-4-yl]amino-2-methoxyphenol (**5m**)

^1H NMR (400 MHz, DMSO) δ 8.81 (s, 1H, $-\text{NH}$), 8.51 (s, 1H, $-\text{NH}$), 8.36 (s, 1H, $-\text{OH}$), 7.71 (s, 1H, Ar–H), 7.53 (d, $J = 8.9$ Hz, 2H, Ar–H), 7.17 (dt, $J = 8.6, 2.4$ Hz, 2H, Ar–H), 6.81 (dd, $J = 10.9, 8.9$ Hz, 3H, Ar–H), 3.80 (s, 3H, $-\text{OCH}_3$), 3.74 (s, 3H, $-\text{OCH}_3$), 3.73–3.67 (m, 4H, $-\text{OCH}_2$), 3.00–2.94 (m, 4H, $-\text{NCH}_2$). HRMS-ESI m/z $[\text{M}+\text{H}]^+$ calcd for $\text{C}_{22}\text{H}_{26}\text{N}_5\text{O}_4^+$: 424.4731, found: 424.4739.

4.6.14. 2-[6-Methoxy-2-[4-(1-morpholinyl)phenyl]aminopyrimidin-4-yl]amino- N -methylbenzamide (**5n**)

^1H NMR (400 MHz, DMSO) δ 12.32 (s, 1H, $-\text{CONH}$), 10.15 (s, 1H, $-\text{NH}$), 8.82 (d, $J = 4.5$ Hz, 1H, $-\text{NH}$), 8.58 (d, $J = 8.3$ Hz, 1H, $-\text{OH}$), 7.78 (dd, $J = 7.9, 1.4$ Hz, 1H, Ar–H), 7.69 (s, 1H, Ar–H), 7.42 (t, $J = 7.8$ Hz, 1H, Ar–H), 7.30 (t, $J = 8.8$ Hz, 2H, Ar–H), 7.25–7.20 (m, 1H, Ar–H), 6.99 (t, $J = 9.5$ Hz, 2H, Ar–H), 3.88 (d, $J = 14.7$ Hz, 3H, $-\text{OCH}_3$), 3.78–3.73 (m, 4H, $-\text{OCH}_2$), 3.13 (dd, $J = 10.6, 5.8$ Hz, 4H, $-\text{NCH}_2$), 2.79 (d, $J = 4.5$ Hz, 3H, $-\text{NCH}_3$). HRMS-ESI m/z $[\text{M}+\text{H}]^+$ calcd for $\text{C}_{23}\text{H}_{27}\text{N}_6\text{O}_3^+$: 435.4991, found: 435.4983.

4.6.15. 3-[2-[(4-(1-Morpholinyl)phenyl)amino]thieno[3,2- d]pyrimidin-4-yl]aminophenol (**6**)

^1H NMR (400 MHz, DMSO) δ 9.31 (s, 1H, $-\text{NH}$), 9.23 (s, 1H), 8.77 (s, 1H, $-\text{NH}$), 8.00 (dd, $J = 7.0, 3.9$ Hz, 1H, $-\text{OH}$), 7.63 (d, $J = 9.0$ Hz, 2H, $-\text{SCH}=\text{CH}$), 7.28 (d, $J = 8.0$ Hz, 1H, Ar–H), 7.16–7.07 (m, 3H, Ar–H), 6.83 (d, $J = 9.1$ Hz, 2H, Ar–H), 6.51 (dd, $J = 8.0, 1.5$ Hz, 1H, Ar–H), 3.75–3.69 (m, 4H, $-\text{OCH}_2$), 3.05–2.96 (m, 4H, $-\text{NCH}_2$). HRMS-ESI m/z $[\text{M}+\text{H}]^+$ calcd for $\text{C}_{22}\text{H}_{22}\text{N}_5\text{O}_2\text{S}^+$: 420.5086, found: 420.5073.

Acknowledgments

This work was supported by the “Kultusministerium des Landes Sachsen-Anhalt” and the European Regional Development Fund of the European Commission. We are truly grateful for the kinase inhibitor libraries PKIS I and II that were kindly provided by Glaxo Smith Kline LCC.

Appendix A. Supplementary data

Supplementary data to this article can be found online at <https://doi.org/10.1016/j.ejmech.2018.10.050>.

References

- [1] P.R. Mueller, T.R. Coleman, A. Kumagai, W.G. Dunphy, Myt1: a Membrane-associated Inhibitory Kinase that Phosphorylates Cdc2, 1995, p. 270.
- [2] R.N. Booher, P.S. Holman, A. Fattaey, Human Myt1 is a cell cycle-regulated kinase that inhibits Cdc2 but not Cdk2 activity, *J. Biol. Chem.* 272 (1997) 22300–22306.
- [3] S. Larochelle, K.A. Merrick, M.E. Terret, L. Wohlbold, N.M. Barboza, C. Zhang, K.M. Shokat, P.V. Jallepalli, R.P. Fisher, Requirements for Cdk7 in the assembly of Cdk1/cyclin B and activation of Cdk2 revealed by chemical genetics in human cells, *Mol. Cell* 25 (2007) 839–850.
- [4] H. Dixon, C.J. Norbury, Therapeutic exploitation of checkpoint defects in cancer cells lacking p53 function, *Cell cycle (Georgetown, Tex.)* 1 (2002) 362–368.
- [5] M. Suganuma, T. Kawabe, H. Hori, T. Funabiki, T. Okamoto, Sensitization of cancer cells to DNA damage-induced cell death by specific cell cycle G2 checkpoint abrogation, *Cancer Res.* 59 (1999) 5887–5891.
- [6] P.C. De Witt Hamer, S.E. Mir, D. Noske, C.J.F. Van Noorden, T. Würdinger, WEE1 kinase targeting combined with DNA-damaging cancer therapy catalyzes mitotic catastrophe, *Clin. Canc. Res.* 17 (2011) 4200–4207.
- [7] M.V. Blagosklonny, Mitotic arrest and cell fate: why and how mitotic inhibition of transcription drives mutually exclusive events, *Cell cycle (Georgetown, Tex.)* 6 (2007) 70–74.
- [8] M.I. Davis, J.P. Hunt, S. Herrgard, P. Ciceri, L.M. Wodicka, G. Pallares, M. Hocker, D.K. Treiber, P.P. Zarrinkar, Comprehensive analysis of kinase inhibitor selectivity, *Nat. Biotechnol.* 29 (2011) 1046–1051.
- [9] A. Rohe, C. Göllner, K. Wichapong, F. Erdmann, G.M.A. Al-Mazaideh, W. Sippl, M. Schmidt, Evaluation of potential Myt1 kinase inhibitors by TR-FRET based binding assay, *Eur. J. Med. Chem.* 61 (2013) 41–48.
- [10] K. Wichapong, A. Rohe, C. Platzer, I. Slynko, F. Erdmann, M. Schmidt, W. Sippl, Application of docking and QM/MM-GBSA rescoring to screen for novel Myt1 kinase inhibitors, *J. Chem. Inf. Model.* 54 (2014) 881–893.
- [11] P. Dranchak, R. MacArthur, R. Guha, W.J. Zuercher, D.H. Drewry, D.S. Auld, J. Ingles, Profile of the GSK published protein kinase inhibitor set across ATP-dependent and -independent luciferases: implications for reporter-gene assays, *PLoS One* 8 (2013) 1–9.
- [12] D.H. Drewry, W.J. Zuercher, The Published Kinase Inhibitor Set: a Resource to Develop Probes for the Untargeted Kinome, Symposium, R S C Biology, Chemical March, Drug Discovery, 2012.
- [13] C. Platzer, A. Najjar, A. Rohe, F. Erdmann, W. Sippl, M. Schmidt, Identification of PKMYT1 inhibitors by screening the GSK published protein kinase inhibitor set I and II, *Bioorg. Med. Chem.* 26 (2018) 4014–4024.
- [14] J.-Y. Zhu, R.A.D. Cuellar, N. Berndt, H.E. Lee, S.H. Olesen, M.P. Martin, J.T. Jensen, G.I. Georg, E. Schönbrunn, Structural basis of Wee kinases functionality and inactivation by diverse small molecule inhibitors, *J. Med. Chem.* 60 (2017) 7863–7875.
- [15] A. Rohe, C. Henze, F. Erdmann, W. Sippl, M. Schmidt, A fluorescence anisotropy-based Myt1 kinase binding assay, *Assay Drug Dev. Technol.* 12 (2014) 136–144.
- [16] M. Schmidt, A. Rohe, C. Platzer, A. Najjar, F. Erdmann, W. Sippl, Regulation of G2/M transition by inhibition of WEE1 and PKMYT1 kinases, *Molecules* 22 (2017).
- [17] F. Zuccotto, E. Ardini, E. Casale, M. Angiolini, Through the "gatekeeper door": exploiting the active kinase conformation, *J. Med. Chem.* 53 (2010) 2681–2694.
- [18] G.D. Hawkins, C.J. Cramer, D.G. Truhlar, Pairwise solute descreening of solute charges from a dielectric medium, *Chem. Phys. Lett.* 246 (1995) 122–129.
- [19] G.D. Hawkins, C.J. Cramer, D.G. Truhlar, Parametrized models of aqueous free energies of solvation based on pairwise descreening of solute atomic charges from a dielectric medium, *J. Phys. Chem.* 100 (1996) 19824–19839.
- [20] V. Tsui, D.A. Case, Theory and applications of the Generalized Born solvation model in macromolecular simulations, *Biopolymers* 56 (2000) 275–291.
- [21] A. Onufriev, D. Bashford, D.A. Case, Exploring protein native states and large-scale conformational changes with a modified generalized Born model, *Protein Struct. Funct. Genet.* 55 (2004) 383–394.
- [22] J. Mongan, C. Simmerling, J.A. McCammon, D.A. Case, A. Onufriev, Generalized Born model with simple, robust molecular volume correction, *NIH Publ. Access* 3 (2010) 156–169.
- [23] D.A. Case, T.E. Cheatham 3rd, T. Darden, H. Gohlke, R. Luo, K.M. Merz Jr., A. Onufriev, C. Simmerling, B. Wang, R.J. Woods, The Amber biomolecular simulation programs, *J. Comput. Chem.* 26 (2005) 1668–1688.
- [24] T.A.D.D.A. Case, T.E. Cheatham III, C.L. Simmerling, J. Wang, R.E. Duke, R.R.C.W. Luo, W. Zhang, K.M. Merz, B. Roberts, S. Hayik, A. Roitberg, G. Seabra, A.W.G.J. Swails, I. Kolossváry, K.F. Wong, F. Paesani, J. Vanicek, R.M. Wolf, J. Liu, S.R.B.X. Wu, T. Steinbrecher, H. Gohlke, Q. Cai, X. Ye, J. Wang, M.-J. Hsieh, G.D.R.R. Cui, D.H. Mathews, M.G. Seetin, R. Salomon-Ferrer, C. Sagui, V. Babin, T.S.G. Luchko, A. Kovalenko, P.A. Kollman, AMBER 12, University of California, San Francisco, 2012.
- [25] J. Gasteiger, M. Marsili, Iterative partial equalization of orbital electro-negativity—a rapid access to atomic charges, *Tetrahedron* 36 (1980) 3219–3228.
- [26] S.D. Bembek, B.A. Tounge, C.H. Reynolds, Ligand efficiency and fragment-based drug discovery, *Drug Discov. Today* 14 (2009) 278–283.
- [27] S. Schultes, C. De Graaf, E.E.J. Haaksma, I.J.P. De Esch, R. Leurs, O. Krämer, Ligand efficiency as a guide in fragment hit selection and optimization, *Drug Discov. Today Technol.* 7 (2010) 157–162.
- [28] C.W. Murray, M.L. Verdonk, D.C. Rees, Experiences in fragment-based drug discovery, *Trends Pharmacol. Sci.* 33 (2012) 224–232.
- [29] Y. Cheng, W.H. Prusoff, Relationship between the inhibition constant (K₁) and the concentration of inhibitor which causes 50 per cent inhibition (I₅₀) of an enzymatic reaction, *Biochem. Pharmacol.* 22 (1973) 3099–3108.
- [30] M.e.a. Jeffrey, Anthranilamide Inhibitors of Aurora Kinase and Their Preparation, *Pharmaceutical Compositions and Use in the Treatment of Cancer*, 2008.
- [31] C. Russell, A.J.S. Lin, P. Hains, M.I. Simone, P.J. Robinson, A. McCluskey, An integrated flow and microwave approach to a broad spectrum protein kinase inhibitor, *RSC Adv.* 5 (2015) 93433–93437.
- [32] V. Zoete, A. Daina, C. Bovigny, O. Michielin, SwissSimilarity: a web tool for low to ultra high throughput ligand-based virtual screening, *J. Chem. Inf. Model.* 56 (2016) 1399–1404.
- [33] M.P. Martin, J.-Y. Zhu, H.R. Lawrence, R. Pireddu, Y. Luo, R. Alam, S. Ozcan, S.M. Sebt, N.J. Lawrence, E. Schönbrunn, A novel mechanism by which small molecule inhibitors induce the DFG flip in aurora A, *ACS Chem. Biol.* 7 (2012) 698–706.
- [34] C. Bardelle, B. Barlaam, N. Brooks, T. Coleman, D. Cross, R. Ducray, I. Green, C.L. Brempt, A. Olivier, J. Read, Inhibitors of the tyrosine kinase EphB4. Part 3: identification of non-benzodioxole-based kinase inhibitors, *Bioorg. Med. Chem. Lett* 20 (2010) 6242–6245.
- [35] S. Niessen, M.M. Dix, S. Barbas, Z.E. Potter, S. Lu, O. Brodsky, S. Planken, D. Behenna, C. Almaden, K.S. Gajiwala, K. Ryan, R. Ferre, M.R. Lazear, M.M. Hayward, J.C. Kath, B.F. Cravatt, Proteome-wide map of targets of T790M-EGFR-directed covalent inhibitors, *Cell Chem. Biol.* 24 (2017) 1388–1400, e1387.
- [36] J.F. Beattie, G.A. Breault, R.P. Ellston, S. Green, P.J. Jewsbury, C.J. Midgley, R.T. Naven, C.A. Minshull, R.A. Paupit, J.A. Tucker, J.E. Pease, Cyclin-dependent kinase 4 inhibitors as a treatment for cancer. Part 1: identification and optimisation of substituted 4,6-bis anilino pyrimidines, *Bioorg. Med. Chem. Lett* 13 (2003) 2955–2960.
- [37] M.P. Martin, J.Y. Zhu, H.R. Lawrence, R. Pireddu, Y. Luo, R. Alam, S. Ozcan, S.M. Sebt, N.J. Lawrence, E. Schönbrunn, A novel mechanism by which small molecule inhibitors induce the DFG flip in Aurora A, *ACS Chem. Biol.* 7 (2012) 698–706.
- [38] H.R. Lawrence, M.P. Martin, Y. Luo, R. Pireddu, H. Yang, H. Gevariya, S. Ozcan, J.Y. Zhu, R. Kendig, M. Rodriguez, R. Elias, J.Q. Cheng, S.M. Sebt, E. Schönbrunn, N.J. Lawrence, Development of o-chlorophenyl substituted pyrimidines as exceptionally potent aurora kinase inhibitors, *J. Med. Chem.* 55 (2012) 7392–7416.
- [39] J.R. Greenwood, D. Calkins, A.P. Sullivan, J.C. Shelley, Towards the comprehensive, rapid, and accurate prediction of the favorable tautomeric states of drug-like molecules in aqueous solution, *J. Comput. Aided Mol. Des.* 24 (2010) 591–604.
- [40] J.C. Shelley, A. Cholleti, L.L. Frye, J.R. Greenwood, M.R. Timlin, M. Uchimaya, Epik: a software program for pK_a prediction and protonation state generation for drug-like molecules, *J. Comput. Aided Mol. Des.* 21 (2007) 681–691.
- [41] J.L. Banks, H.S. Beard, Y. Cao, A.E. Cho, W. Damm, R. Farid, A.K. Felts, T.A. Halgren, D.T. Mainz, J.R. Maple, R. Murphy, D.M. Philipp, M.P. Repasky, L.Y. Zhang, B.J. Berne, R.A. Friesner, E. Gallicchio, R.M. Levy, Integrated modeling program, applied chemical theory (IMPACT), *J. Comput. Chem.* 26 (2005) 1752–1780.
- [42] P.C. Hawkins, A.G. Skillman, G.L. Warren, B.A. Ellingson, M.T. Stahl, Conformer generation with OMEGA: algorithm and validation using high quality structures from the Protein Databank and Cambridge Structural Database, *J. Chem. Inf. Model.* 50 (2010) 572–584.
- [43] S.K. Burley, H.M. Berman, C. Christie, J.M. Duarte, Z. Feng, J. Westbrook, J. Young, C. Zardecki, RCSB Protein Data Bank: sustaining a living digital data resource that enables breakthroughs in scientific research and biomedical education, *Protein Sci.* 27 (2018) 316–330.
- [44] P.R. Gerber, K. Müller, MAB, a generally applicable molecular force field for structure modelling in medicinal chemistry, *J. Comput. Aided Mol. Des.* 9 (1995) 251–268.
- [45] G. Jones, P. Willett, R.C. Glen, A.R. Leach, R. Taylor, Development and validation of a genetic algorithm for flexible docking, in: F.E. Cohen (Ed.), *J. Mol. Biol.* 267 (1997) 727–748.
- [46] R.A. Friesner, J.L. Banks, R.B. Murphy, T.A. Halgren, J.J. Klicic, D.T. Mainz, M.P. Repasky, E.H. Knoll, M. Shelley, J.K. Perry, D.E. Shaw, P. Francis, P.S. Shenkin, Glide: a new approach for rapid, accurate docking and scoring. 1. Method and assessment of docking accuracy, *J. Med. Chem.* 47 (2004) 1739–1749.
- [47] R.A. Friesner, R.B. Murphy, M.P. Repasky, L.L. Frye, J.R. Greenwood, T.A. Halgren, P.C. Sanschagrin, D.T. Mainz, Extra precision glide: docking and scoring incorporating a model of hydrophobic enclosure for protein-ligand complexes, *J. Med. Chem.* 49 (2006) 6177–6196.
- [48] R.A. Friesner, et al., Glide: a new approach for rapid, accurate docking and

- scoring. 1. Method and assessment of docking accuracy, *J. Med. Chem.* 47 (2004) 1739–1749.
- [49] Y. Duan, C. Wu, S. Chowdhury, M.C. Lee, G. Xiong, W. Zhang, R. Yang, P. Cieplak, R. Luo, T. Lee, J. Caldwell, J. Wang, P. Kollman, A point-charge force field for molecular mechanics simulations of proteins based on condensed-phase quantum mechanical calculations, *J. Comput. Chem.* 24 (2003) 1999–2012.
- [50] M.C. Lee, Y. Duan, Distinguish protein decoys by using a scoring function based on a new AMBER force field, short molecular dynamics simulations, and the generalized Born solvent model, *Protein Struct. Funct. Genet.* 55 (2004) 620–634.
- [51] D.A. Case, T. Darden, T.E. Cheatham, C. Simmerling, J. Wang, R.E. Duke, R. Luo, R.C. Walker, W. Zhang, K.M. Merz, B.P. Roberts, S. Hayik, A. Roitberg, G. Seabra, J. Swails, A.W. Götz, I. Kolossvary, K.F. Wong, P. Paesani, J. Vanicek, R.M. Wolf, J. Liu, X. Wu, S.R. Brozell, T. Steinbrecher, H. Gohlke, Q. Cai, X. Ye, J. Wang, M.-J. Hsieh, G. Cui, D.R. Roe, D.H. Mathews, M.G. Seetin, R. Salomon-Ferrer, C. Sagui, V. Babin, T. Luchko, S. Gusarow, A. Kovalenko, P.A. Kollman, *Amber 12 Reference Manual*, University of California, San Francisco, 2012, 350–350.
- [52] A. Jakalian, D.B. Jack, C.I. Bayly, Fast, efficient generation of high-quality atomic charges. AM1-BCC model: II. Parameterization and validation, *J. Comput. Chem.* 23 (2002) 1623–1641.
- [53] J.M. Wang, R.M. Wolf, J.W. Caldwell, P.A. Kollman, D.A. Case, Development and testing of a general amber force field, *J. Comput. Chem.* 25 (2004) 1157–1174.
- [54] W.L. Jorgensen, J. Chandrasekhar, J.D. Madura, R.W. Impey, M.L. Klein, Comparison of simple potential functions for simulating liquid water, *J. Chem. Phys.* 79 (1983), 926–926.
- [55] R.W. Pastor, B.R. Brooks, A. Szabo, An analysis of the accuracy of Langevin and molecular dynamics algorithms, *Mol. Phys.* 65 (1988) 1409–1419.
- [56] T. Darden, D. York, L. Pedersen, Particle mesh Ewald: an N-log(N) method for Ewald sums in large systems, *J. Chem. Phys.* 98 (1993), 10089–10089.
- [57] J.P. Ryckaert, G. Ciccotti, H.J.C. Berendsen, Numerical integration of the cartesian equations of motion of a system with constraints: molecular dynamics of n-alkanes, *J. Comput. Phys.* 23 (1977) 327–341.
- [58] W.C. Still, A. Tempczyk, R.C. Hawley, T. Hendrickson, Semianalytical treatment of solvation for molecular mechanics and dynamics, *J. Am. Chem. Soc.* 112 (1990) 6127–6129.
- [59] J. Srinivasan, M.W. Trevathan, P. Beroza, D.A. Case, Application of a pairwise generalized Born model to proteins and nucleic acids: inclusion of salt effects, *Theor. Chem. Accounts* 101 (1999) 426–434.
- [60] R. Luo, L. David, M.K. Gilson, Accelerated Poisson-Boltzmann calculations for static and dynamic systems, *J. Comput. Chem.* 23 (2002) 1244–1253.
- [61] M.P. Gleeson, D. Gleeson, QM/MM as a tool in fragment based drug discovery. A cross-docking, rescoring study of kinase inhibitors, *J. Chem. Inf. Model.* 49 (2009) 1437–1448.
- [62] S.A. Hayik, R. Dunbrack, K.M. Merz, A mixed QM/MM scoring function to predict protein-ligand binding affinity, *J. Chem. Theor. Comput.* 6 (2010) 3079–3091.
- [63] B.R. Miller, T.D. McGee, J.M. Swails, N. Homeyer, H. Gohlke, A.E. Roitberg, MMPBSA.py: an efficient program for end-state free energy calculations, *J. Chem. Theor. Comput.* 8 (2012) 3314–3321.
- [64] A.M. Ferrari, G. Degliesposti, M. Sgobba, G. Rastelli, Validation of an automated procedure for the prediction of relative free energies of binding on a set of aldose reductase inhibitors, *Bioorg. Med. Chem.* 15 (2007) 7865–7877.
- [65] T. Hou, J. Wang, Y. Li, W. Wang, Assessing the performance of the MM/PBSA and MM/GBSA methods. I. The accuracy of binding free energy calculations based on molecular dynamics simulations, *J. Chem. Inf. Model.* 51 (2010) 69–82.
- [66] K. Wichapong, M. Lawson, S. Pianwanit, S. Kokpol, W. Sippl, Postprocessing of protein-ligand docking poses using linear response MM-PB/SA: application to Wee1 kinase inhibitors, *J. Chem. Inf. Model.* 50 (2010) 1574–1588.
- [67] U. Uciechowska, J. Schemies, M. Scharfe, M. Lawson, K. Wichapong, M. Jung, W. Sippl, Binding free energy calculations and biological testing of novel thiobarbiturates as inhibitors of the human NAD⁺ dependent histone deacetylase Sirt2, *MedChemComm* 3 (2012), 167–167.
- [68] S. Genheden, U. Ryde, The MM/PBSA and MM/GBSA methods to estimate ligand-binding affinities, *Expert Opin. Drug Discov.* 0441 (2015) 1–13.
- [69] I. Slynko, K. Schmidtkunz, T. Rumpf, S. Klaeger, S. Heinzlmeir, A. Najjar, E. Metzger, B. Kuster, R. Schule, M. Jung, W. Sippl, Identification of highly potent protein KinaseC-related Kinase1 inhibitors by virtual screening, binding free energy rescoring, and in vitro testing, *ChemMedChem* 11 (2016) 2084–2094.
- [70] B. Karaman, W. Sippl, Docking and binding free energy calculations of sirtuin inhibitors, *Eur. J. Med. Chem.* 93 (2015) 584–598.
- [71] P.A. Kollman, I. Massova, C. Reyes, B. Kuhn, S. Huo, L. Chong, M. Lee, T. Lee, Y. Duan, W. Wang, O. Donini, P. Cieplak, J. Srinivasan, D.A. Case, T.E. Cheatham, Calculating structures and free energies of complex molecules: combining molecular mechanics and continuum models, *Acc. Chem. Res.* 33 (2000) 889–897.
- [72] P.J. Hajduk, J. Greer, A decade of fragment-based drug design: strategic advances and lessons learned, *Nat. Rev. Drug Discov.* 6 (2007) 211.
- [73] M. Congreve, R. Carr, C. Murray, H. Jhoti, A 'Rule of Three' for fragment-based lead discovery? *Drug Discov. Today* 8 (2003) 876–877.
- [74] G. Chessari, A.J. Woodhead, From fragment to clinical candidate—a historical perspective, *Drug Discov. Today* 14 (2009) 668–675.
- [75] G.E. de Kloe, D. Bailey, R. Leurs, I.J.P. de Esch, Transforming fragments into candidates: small becomes big in medicinal chemistry, *Drug Discov. Today* 14 (2009) 630–646.
- [76] A.L. Hopkins, C.R. Groom, A. Alex, Ligand efficiency: a useful metric for lead selection, *Drug Discov. Today* 9 (2004) 430–431.
- [77] P.D. Leeson, B. Springthorpe, The influence of drug-like concepts on decision-making in medicinal chemistry, *Nat. Rev. Drug Discov.* 6 (2007) 881–890.
- [78] R.E. Hubbard, J.B. Murray, Experiences in fragment-based lead discovery, *Methods Enzymol.* 493 (2011) 509–531.
- [79] A. Rohe, F. Erdmann, C.B. Bäßler, K. Wichapong, W. Sippl, M. Schmidt, In vitro and in silico studies on substrate recognition and acceptance of human PKMYT1, a Cdk1 inhibitory kinase, *Bioorg. Med. Chem. Lett* 22 (2012) 1219–1223.
- [80] A. Rohe, C. Platzer, A. Masch, S. Greiner, C. Henze, C. Ihling, F. Erdmann, M. Schutkowski, W. Sippl, M. Schmidt, Identification of peptidic substrates for the human kinase Myt1 using peptide microarrays, *Bioorg. Med. Chem.* 23 (2015) 4936–4942.
- [81] A. Rohe, C. Platzer, A. Masch, S. Greiner, C. Henze, C. Ihling, F. Erdmann, M. Schutkowski, W. Sippl, M. Schmidt, Identification of peptidic substrates for the human kinase Myt1 using peptide microarrays, *Bioorg. Med. Chem.* 23 (2015) 4936–4942.

3.2. (Manuscript to be submitted)

Computer-aided design and Synthesis of novel anticancer agents: Introducing diaminopyrimidine derivatives with potential PKMYT-1 kinases inhibition

**Nehal H. Elghazawy ^a, Sven Hagemann ^b, Frank Erdmann ^a, Stefan Hüttelmaier ^b,
Matthias Schmidt ^a, Wolfgang Sippl ^a**

^a Institute of Pharmacy, Department of Medicinal Chemistry, Martin-Luther-University Halle-Wittenberg, W.-Langenbeck-Str. 4, 06120 Halle, Germany

^b Institute of Molecular Medicine, Charles-Tandford Protein Centre, Martin-Luther-University Halle-Wittenberg, Kurt-Mothes-Str. 3a, 06120 Halle, Germany

Abstract

In order to develop novel inhibitors against the membrane-associated inhibitory kinase PKMYT-1, a series of diaminopyrimidines with a variety of substituents at positions 2 and 4 were synthesized. After purification and structure elucidation of the synthesized compounds, they were tested for their anticancer activity towards different cancer cell lines, including hepatoma, and neuroblastoma cell lines. Some of the compounds showed good antiproliferative activity toward those cell lines. In vitro studies of the compounds have extended to analyze their ability to bind and inhibit PKMYT-1, where half of the synthesized compounds have shown remarkable binding and inhibitory activity towards PKMYT-1. Since there is no direct correlation between the compounds' anticancer activity and PKMYT-1 inhibition, docking studies were performed on several related kinases that are overexpressed in the cancer cell lines studied. The docking results indicate that the aminopyrimidines that are most active in the cancer cell lines have a higher preference for the WEE1 and Aurora kinases. Further in vitro studies need to be performed to confirm the results of the present study.

Keywords

- PKMYT-1
- WEE1
- Docking
- Diaminopyrimidines

1. Introduction:

The cell cycle is an orchestrated series of events in which the cell undergoes to duplicate the genomic DNA, amplify the organelles, grow in size, and produce daughter cells. It is divided into four major phases: gap 1 (G_1), DNA synthesis (S), gap 2 (G_2), and Mitosis (M) [42-45]. Throughout the cell cycle, three significant checkpoints ensure the smooth transition between different phases, namely G_1/S checkpoint (restriction checkpoint), the G_2/M DNA damage checkpoint, and the spindle assembly checkpoint (SAC) [46-48]. The WEE kinase family holds prominence among the families of kinases involved in the cell cycle, comprising two significant members: WEE1 and PKMYT-1. While both kinases share similar biological functions, they diverge in cellular localization. WEE1 primarily resides within the nucleus, phosphorylating Tyr15 of its natural substrate, cyclin-dependent kinase 1 (Cdk1). In contrast, PKMYT-1 is membrane-associated, specifically located in the endoplasmic reticulum, and possesses the unique capability to dual-specifically phosphorylate Thr14 and Tyr15 of Cdk1. These phosphorylation events are pivotal in inhibiting the Cdk1/cyclin B-complex, a critical determinant in the cellular decision to enter the M phase. [54-59]

When it comes to DNA repair, a significant number of cancer cells rely heavily on the G_2 checkpoint, primarily due to a malfunctioning G_1 checkpoint mechanism often attributed to p53 mutations. This dependency on the G_2 checkpoint makes cancer cells particularly susceptible to interventions targeting this stage, such as WEE1 and PKMYT-1 inhibition. This strategic approach aims to selectively induce harm to cancer cells while preserving the integrity of noncancerous cells. Although hundreds of compounds have been reported to have inhibitory activity against WEE1 kinase, Adavosertib (AZD1775) is the only WEE1 inhibitor that has undergone more than fifty clinical trials to test its future as a potential anticancer therapy [87, 88]. Conversely, pursuing PKMYT-1 as a

therapeutic target has proven to be significantly more challenging than WEE1. This complexity arises from the membrane-associated nature of PKMYT-1, which interferes with its handling for assay purposes. Intensifying this challenge is the absence of a reference compound for conducting in vitro studies specifically designed to target PKMYT-1. To overcome such hurdles, Platzer et al. screened a compound library comprising 800 compounds against PKMYT-1. Utilizing the protein kinase inhibitor sets (PKIS) I and II originally developed by GlaxoSmithKline, this screening effort led to the discovery of ten novel PKMYT-1 inhibitors characterized by their binding IC_{50} values within the nanomolar and low micromolar range, as depicted in **Figure 16**. Those results were obtained and validated via multiple assays, including fluorescence polarization (FP) binding assay, FP immunoblot activity assay (FPIA), and functional assays measuring the phosphorylation status, all developed before in our group [85, 92, 173]. These newly identified compounds are categorized under three distinct chemical scaffolds of PKMYT-1 inhibitors, including aza-stilbenes, 4-amino-quinolines, and aminopyrimidines [92]. Those PKMYT-1 inhibitors along with other reported [90] have been used by our group to come up with computational models used for PKMYT-1 activity prediction. Guided by those models, we used a fragment-growing strategy to identify a novel set of diaminopyrimidines, which hold promise as potential valuable PKMYT-1 inhibitors in cancer therapy [174]. In continuation of our work, we here report the synthesis of novel diaminopyrimidines where the approach of single-point modification was adopted. The synthetic protocol ensured that the added substituents were able to extend the structure in the corresponding pockets within the ATP-binding pocket of PKMYT-1. All the compounds were designed in a way to ensure the presence of all important interactions with the essential amino acids in the PKMYT-1 binding pocket. Further molecular docking study was performed in order to visualize the interactions between the proposed ligands and the binding pocket. Finally, those compounds were tested against various cancer cell lines to test their activity as anticancer agents.

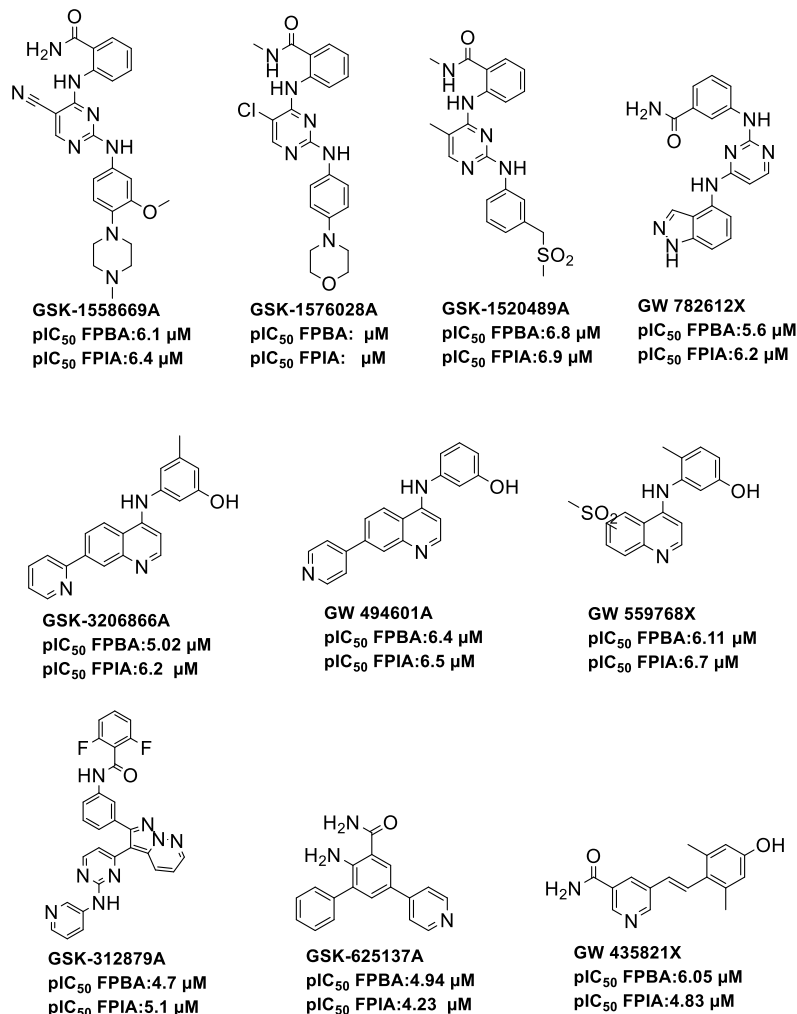


Figure 16: Structures for ten PKMYT-1 inhibitors derived from Screening GSK PKIs and PKIIs

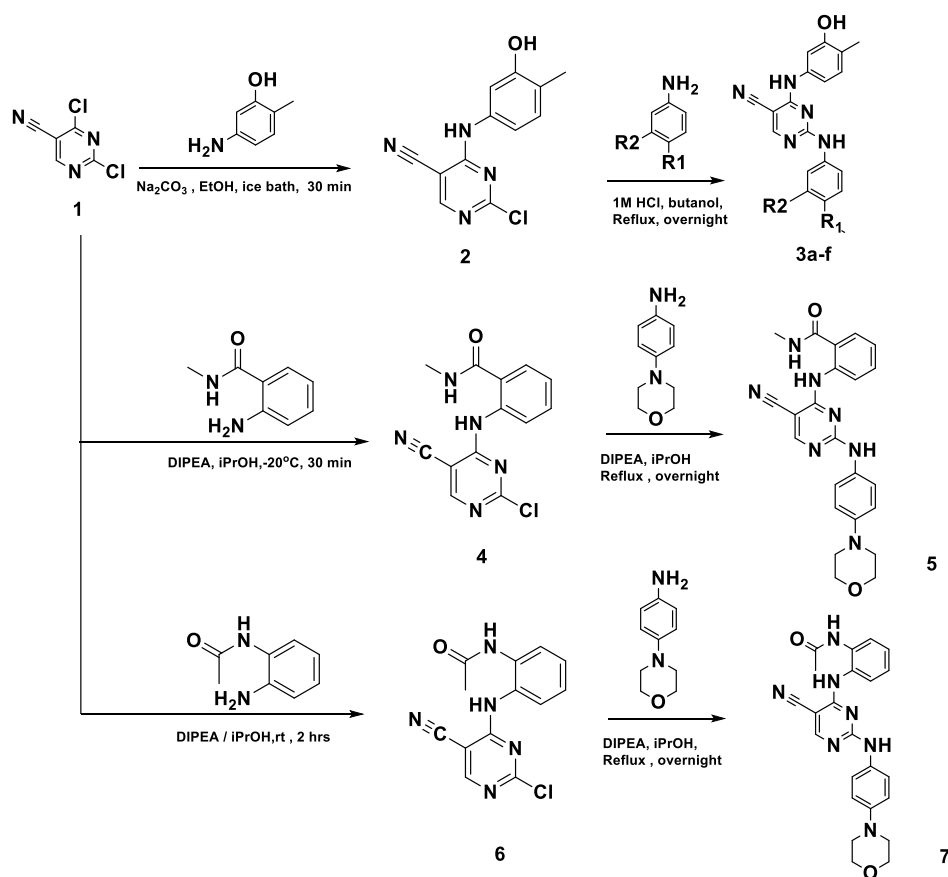
2. Results and Discussion:

2.1. Chemistry:

The synthetic route followed for the preparation of the target compounds is depicted in Schemes 1, 2, and 3.

First, for the synthesis of compounds **3a-f**, the starting material 2,4-dichloropyrimidine-5-carbonitrile (**1**) was stirred with 5-amino-2-methylphenol in ethanol with the presence of Na₂CO₃ in an ice bath to obtain 2-chloro-4-((3-hydroxy-4-methylphenyl)amino)pyrimidine-5-carbonitrile (**2**). After the evaporation of ethanol, the residue of intermediate (**2**) was transferred to the subsequent reaction without further purification. Then, Intermediate **2** was allowed to reflux overnight in butanol with the corresponding aniline in the presence of 1M HCL to

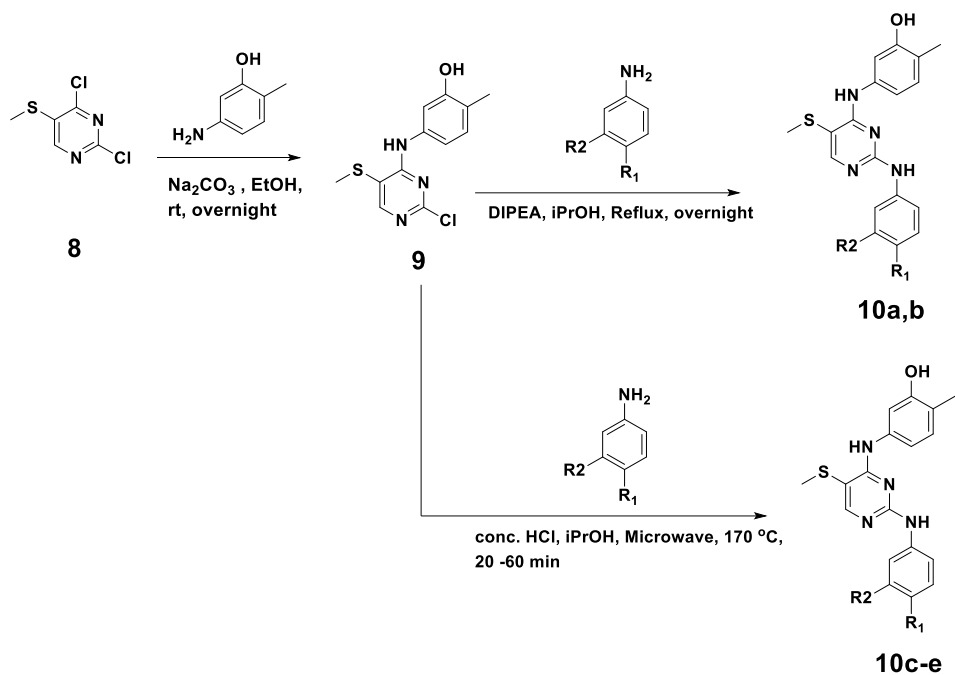
obtain compounds **3a-f**. On the other hand, stirring of (**1**) with 2-amino-N-methylbenzamide in iPrOH at a temperature of -20 °C in the presence of DIPEA yielded intermediate **4** which was then allowed to react with 4-morpholinoaniline to yield compound **5**. Finally, Scheme 1 has shown the conversion of compound **1** to intermediate **6** through its reaction with N-(2-aminophenyl)acetamide through a 2-hour reaction in iPrOH and in the presence of DIPEA. Intermediate **6** was also allowed to react with 4-morpholinoaniline to give compound **7**.



Scheme 1: synthesis of the target compounds 3a-f, 5 and 7

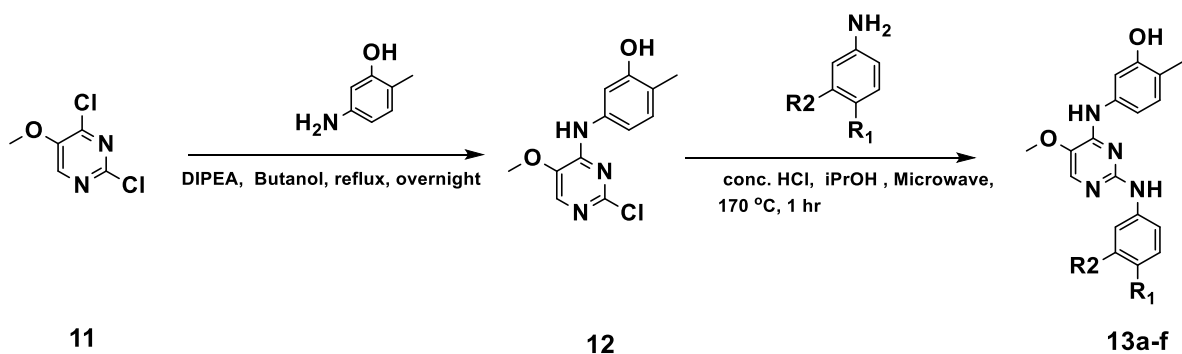
In Scheme 2, all compounds **10a-e** were synthesized via a two-step reaction. The first step included the conversion of 2,4-dichloro-5-(methylthio)pyrimidine (**8**) to intermediate (**9**) through an overnight reaction with 2-methyl-5-aminophenol in ethanol and in the presence of Na_2CO_3 . The conditions of the second step varied based on the subsequent used aniline. For example, during the synthesis of compounds **10 a,b**, an overnight reflux reaction in the presence of DIPEA and

using *i*PrOH as solvent was able to convert the intermediate 5-((2-chloro-5-(methylthio)pyrimidin-4-yl)amino)-2-methylphenol (**9**) to its corresponding final compounds. On the contrary, compounds **10c-e** were synthesized via microwave conditions.



Scheme 2. Synthesis of the target compounds 10a-e

Finally, Scheme 3 illustrates the synthesis of compounds **13a-e**, where 5-((2-chloro-5-methoxypyrimidin-4-yl)amino)-2-methylphenol **12** were obtained via reaction of 2,4-dichloro-5-thiomethylpyrimidine (**11**) and 5-amino-2-methylphenol. Without further purification, intermediate **12** was converted to the final compounds **13a-f** by reacting under microwave conditions.



Scheme 3. Synthesis of the target compounds 13a-f

2.2. Biological evaluation:

2.2.1. Cellular assay

To evaluate the antiproliferative properties of the synthesized compounds a cell viability assay was performed. In this assay, several cancer cell lines, including hepatoma cancer cells (Huh7) and neuroblastoma cell lines (BE(2)-C and NBL-S) were tested. The obtained results show a promising anticancer effect for some of the synthesized compounds. For instance, in the series of compounds **3a-3f**, compounds **3a** and **3f** were the only two compounds to show high inhibitory activity against the cancer cell lines. Compound **3a** has given EC_{50} values in the submicromolar range of 0.428 μM , 0.227 μM , and 0.296 μM for the cell lines Huh7, BE(2)-C, and NBL-S, respectively. On the other hand, Compound **3f** was considered slightly less active towards the three cell lines with EC_{50} values towards Huh7, BE(2)-C, and NBL-S of 1.185 μM , 0.433 μM and 0.323 μM respectively. Unfortunately, the other two series of synthesized compounds, **10a-e** and **13a-13f**, didn't show any remarkable activity against Huh7 cell lines. It is planned to be tested for their antiproliferative effect against both neuroblastoma cell lines BE(2)-C and NBL-S (**Table 1**).

Concerning compound **5**, it has shown promising activity as it is considered the second most potent compound against the neuroblastoma cell lines with EC_{50} values of 0.129 μM and 0.156 μM against BE(2)-C, and NBL-S, respectively. Compound **7** was considered the most interesting compound in the series of synthesized compounds since it showed an EC_{50} in the submicromolar range of

0.722 μM against Huh7 cell lines. Most importantly, compound **7**'s activity towards the neuroblastoma cells was remarkable since it falls in the nanomolar range with EC_{50} values of 16.5 nM and 17.9 nM against BE(2)-C, and NBL-S, respectively.

Table 1: EC_{50} s of all the synthesized compounds against various cancer cell lines: Huh7, BE(2)-C, NBL-S, and MCF-7.

ND: Not Determined

Compound	Huh7 EC_{50} (μM)	BE(2)-C EC_{50} (μM)	NBL-S EC_{50} (μM)
3a	0.428	0.227	0.296
3b	ND	> 0.1	ND
3c	ND	> 0.1	ND
3d	ND	ND	ND
3e	ND	> 0.1	ND
3f	1.185	0.433	0.323
5	ND	0.129	0.156
7	0.722	0.0165	0.0179
10a	ND	> 0.1	ND
10b	ND	> 0.1	ND
10c	ND	> 1.0	ND
10d	ND	> 0.1	ND
10e	ND	> 1.0	ND
13a	ND	> 0.1	ND
13b	ND	> 0.1	ND
13c	ND	> 0.1	ND
13d	ND	ND	ND
13e	ND	> 0.1	ND
13f	ND	4.53	ND

2.2.2. Kinases Binding Assay

Preliminary testing for the ability of the synthesized compounds to bind to the PKMYT-1 was performed to explore the possible mechanism of action through which the compounds show their anticancer activity. Accordingly, all the compounds were tested at two concentrations of 20 μM and 5 μM . Out of all 19 compounds, only nine compounds show more than 40% binding displacement at 20 μM . Those compounds are in a descending order: **13a**, **13b**, **13f**, **10b**, **13c**, **10a**, **13d**, **7** and **3b**. These compounds have been retested at 5 μM where only **13a**,

13b, 13c, 13d, 10b, and 3b have shown more than 25% displacement percentages. (**Table 2**)

Table 2: Percentage inhibition of the synthesized compounds' binding at 20 μM and 5 μM

ND: Not Determined

Compound	% Inhibition @ 20 μM	% Inhibition @ 5 μM
3a	27.9	<25
3b	42.5	35.2
3c	ND	ND
3d	ND	ND
3e	ND	ND
3f	<25	<25
5	<25	<25
7	43.4	<25
10a	50.2	<25
10b	71.8	26.5
10c	ND	ND
10d	ND	ND
10e	ND	ND
13a	>95	87.5
13b	>95	75.7
13c	70.8	54.0
13d	48.1	52.4
13e	<25	<25
13f	>95	80.3

2.2.3. Kinase Inhibitory Activity Assay:

All the compounds that have shown a displacement percentage of more than 20% in the binding assay were chosen to be tested for their activity assays, where only 8 out of 9 compounds have shown activity displacement of more than 25% at 20 μ M . However, there has not been a direct correlation between binding and activity assay results. For example, compounds **3b**, **7**, **10a**, and **10b** have shown binding displacement of 42.5%, 43.4%, 50.2%, and 71.8%, respectively; still, all have shown the highest percentage inhibition between 73.8 % and 94.2 %. Retesting those compounds at 5 μ M, has shown their activity to exceed 40%, which can be a promising indication for the IC₅₀s for those compounds. The rest of the compounds **3a**, **10b**, **13a**, **13c**, **13d**, **13f** were less active but with higher percentage inhibition than the cutoff value of 25% for both concentrations of 20 μ M and 5 μ M (**Table 3**).

Table 3: Percentage inhibition of the synthesized compounds' activity binding at 20 μ M and 5 μ M.

ND: Not Determined

Compound	% Inhibition @ 20 μ M	% Inhibition @ 5 μ M
3a	61.1	62.3
3b	89.0	50.8
3c	ND	ND
3d	ND	ND
3e	ND	ND
3f	ND	ND
5	ND	ND
7	73.8	41.0
10a	75.1	72.6
10b	50.1	38.3
10c	ND	ND
10d	ND	ND
10e	ND	ND
10f	ND	ND

13a	48.0	25.5
13b	94.2	86.6
13c	47.4	37.4
13d	64.7	52.7
13e	ND	ND
13f	<25	<25

2.3. Docking studies:

The most active PKMYT-1 inhibiting compounds were docked into the available crystal structure of PKMYT-1 to study their key interactions. The binding mode involves two essential hydrogen-bonds between the aminopyrimidine fragment and the hinge region of the kinase (hydrogen-bond to the NH backbone group of Cys190 and CO backbone group of Gly189). **13a**, **13b**, and **13f** all have a methoxy group on the pyrimidine ring, forming van-der-Waals interactions with the gatekeeper residue Thr189 (**Figure 17**). The 3-hydroxy,4-methylphenyl ring, also present in all three most active inhibitors, forms a hydrogen-bond to Lys139 and the conserved water molecule in PKMYT-1. **13a** shows another hydrogen-bond between the morpholine oxygen and Lys125 (**Figure 17A**). Interestingly the compounds most active in the cancer cell lines (**3a**, **5**, **7**), all with a cyano substituent at the pyrimidine ring, showed less favorable docking scores. This might be due to a weaker interaction between the cyano group and the gatekeeper residue Thr189.

Since the docking results on PKMYT-1 showed no agreement with the cellular results on the cancer cells, the compounds were also docked into the related kinases WEE1 and Aurora A kinase. In the case of the most active compounds in the cancer cells, a more favorable docking score on WEE1 was observed than on PKMYT-1. In WEE1, the binding mode again shows the classical hydrogen bond pattern to the hinge region (NH backbone Cys379 and CO backbone Asn380 (**Figure 18**)). The reason for the better docking scores could be the hydrogen-bond network of the cyano group of **3a**, **5**, and **7** with the gatekeeper residue Asn376 and the conserved water molecule, which is not possible with PKMYT-1 due to the

different gatekeeper residue (Thr187). **3a** and **7** make a further hydrogen bond to Lys328 with their polar substituents of the terminal phenyl ring, whereas the phenyl ring of all actives makes van-der-Waals interactions with the Lys328 side chain.

In the docking results for Aurora A Kinase, more favorable docking scores were obtained compared to that of PKMYT-1. The aminopyrimidine ring of the most active compounds (**3a**, **5** and **7**) is involved in two hydrogen bonds with the hinge backbone (CO Pro214, NH Ala213), and the cyano group shows a hydrogen-bond to Lys162 (**Figure 19**). Moreover, additional hydrogen bonds are made by the polar substituents of the terminal phenyl ring. For instance, the phenol group of **3a** donates a further hydrogen bond to the backbone CO of Glu260, whereas the carbonyl groups of **5** and **7** undergo hydrogen bonds with Lys162 and Lys141. The amide nitrogen atom is involved in a further hydrogen bond with the backbone CO of Glu260, as observed for **5** and **7**. All three most active compounds from the cancer cell testing possess a morpholine ring in the para position of the aniline ring that can make hydrogen bonds to Arg220 (or alternatively to Arg137).

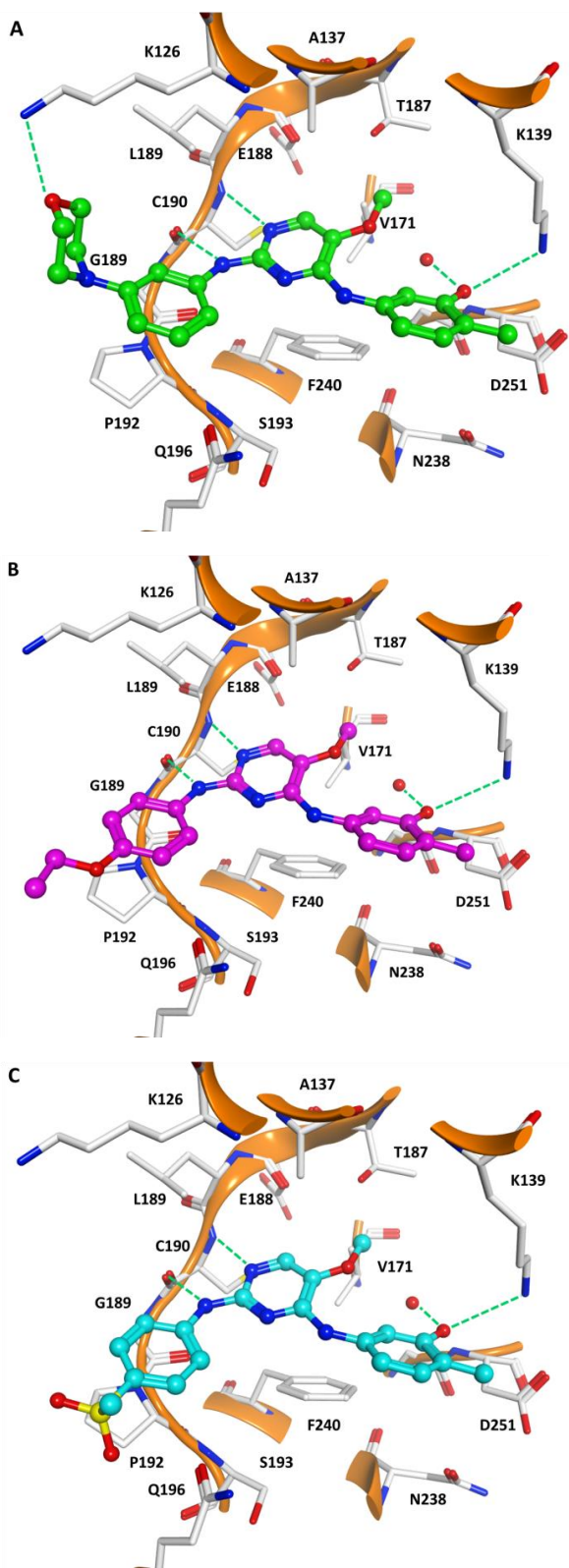


Figure 17: Docking results of the three most potent inhibitors found for PKMYT-1 (PDB ID 5VD1). **A)** 13a (colored green), **B)** 13b (colored magenta), and **C)** 13f (colored cyan). Hydrogen-bonds are shown as green colored dashed lines. Only the residues of the binding pocket are shown for clarity.

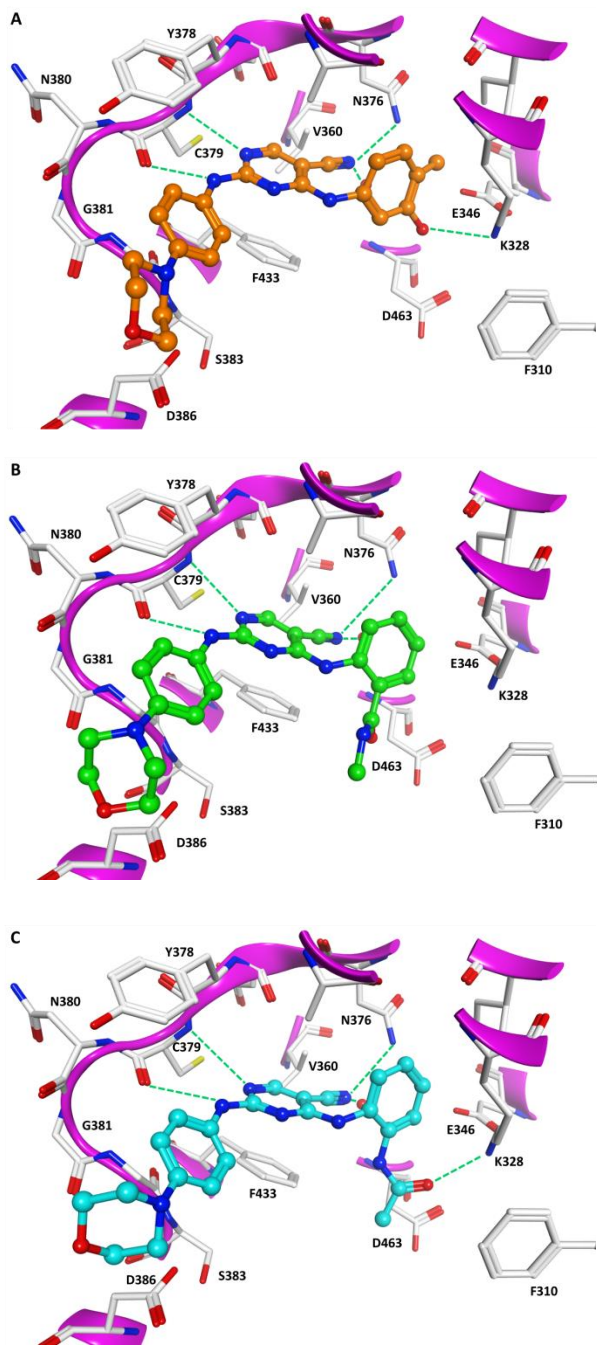


Figure 18: . Docking results of the three most potent inhibitors from the cancer cell testing for WEE1 (PDB ID 5Y5V). **A)** 3a (colored orange), **B)** 5 (colored green), and **C)** 7 (colored cyan). Hydrogen-bonds are shown as green colored dashed lines. Only the residues of the binding pocket are shown for clarity.

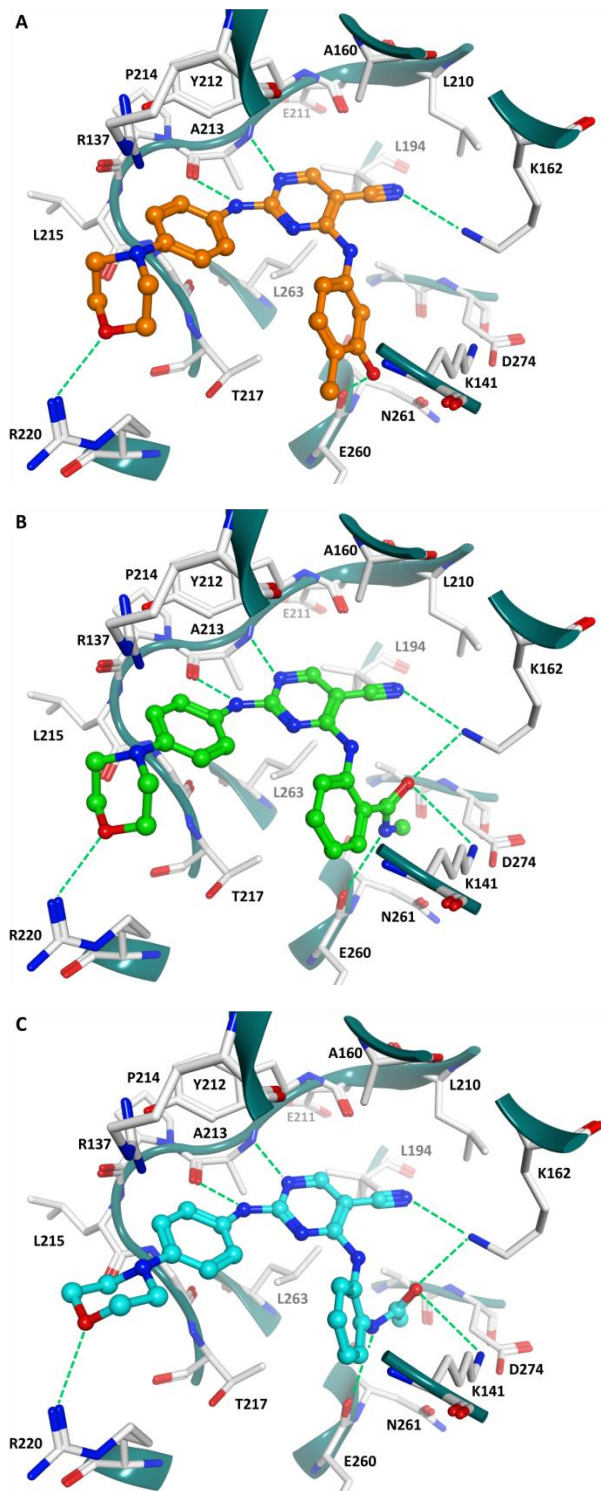


Figure 19: Docking results of the three most potent inhibitors from the cancer cell testing for Aurora A kinase (PDB ID 4DEB). **A)** 3a (colored orange), **B)** 5 (colored green), and **C)** 7 (colored cyan). Hydrogen-bonds are shown as green colored dashed lines. Only the residues of the binding pocket are shown for clarity.

3. Conclusion:

The aminopyrimidines developed in the current study could be modified to potent kinase inhibitors for PKMYT-1 by appropriate substitutions. This was achieved primarily through a terminal 3-methyl,4-hydroxyphenyl ring. The solvent-exposed side of the compounds tolerated more changes in the case of PKMYT-1. Interestingly, cellular testing in neuroblastoma cells resulted in extremely potent inhibitors, i.e. **3a**, **5** and **7**. Analysis of the docking results showed that this is probably not due to potent PKMYT-1 inhibition. Docking studies on the closely related WEE1 and Aurora A kinases showed a better interaction and more formed hydrogen-bonds than in the case of PKMYT-1 binding. Experimental confirmation by in vitro testing is still pending and will demonstrate the accuracy of the in silico data. In summary, we have developed a novel class of kinase inhibitors with high potency in neuroblastoma cells that represent promising compounds for future biological studies.

4. Experimental Section:

4.1. Chemistry:

General

All materials and reagents were purchased from Sigma Aldrich Co. Ltd., abcr GmbH, ChemPUR Feinchemikalien und Forschungsbedarf GmbH, and Carbolution Chemicals. All solvents were analytically pure and dried before use. Microwave reactions were carried out using Monowave 450 (Anton Paar, Graz, Austria). Thin-layer chromatography (TLC) was carried out on aluminum sheets coated with silica gel 60 F254 (Merck, Darmstadt, Germany). Final compounds were confirmed to be of >95% purity based on HPLC. Purity was measured by UV absorbance at 254 nm. HPLC instrumentation consisted of an XTerra RP18 column (3.5mm 3.9_100 mm; Waters, Milford, MA, USA) two LC-10AD pumps, an SPD-M10AVP PDA detector, and an SIL-HT auto sampler all from the manufacturer Shimadzu (Kyoto, Japan). The mobile phase was in all cases a gradient of MeOH/H₂O (starting at 95% H₂O going to 5% H₂O). High resolution Mass spectrometry analyses were performed with a LTQ (linear ion trap)-Orbitrap XL hybrid mass spectrometer (Thermo Fisher Scientific, Bremen, Germany) for obtaining HRMS-ESI (high-resolution mass spectrometry) spectra. For HRMS analyses, the signal for the isotopes with the highest prevalence was given and calculated for ³⁵Cl and ⁷⁹Br. ¹H NMR and ¹³C spectra were taken on a Varian Gemini 2000 and a Varian Inova 500 using [D₆] DMSO as solvent. Chemical shifts (δ, ppm) are referenced to the residual solvent signals.

4.2. Synthetic Procedure:

4.2.1. Procedure for synthesis 2:

The 2,4-dichloropyrimidine derivative **1** was dissolved in EtOH and 1.1 equiv. of 5-amino-2-methylphenol and 1.5 equiv. of Na₂CO₃ were added. The reaction was carried out for 30 minutes in an ice bath after which the reaction was stopped by the addition of water and dilution with ethyl acetate. The organic phase was evaporated, and the crude intermediate was used for the following reaction step without purification.

4.2.2. Procedure for synthesis of 4

The 2,4-dichloropyrimidine derivative **1** was dissolved in iPrOH and 1.1 equiv. of 2-amino-N-methylbenzamide and 1.1 equiv. of DIPEA were added. The reaction was carried out for 30 minutes in -20°C after which the reaction was stopped by the addition of water and dilution with ethyl acetate. The organic phase was evaporated and the crude intermediate was used for the following reaction step without purification.

4.2.3. Procedure for synthesis of 6

The 2,4-dichloropyrimidine derivative **1** was dissolved in iPrOH and 1.1 equiv. of N-(2-aminophenyl)acetamide and 1.1 equiv. of DIPEA were added. The reaction was carried out for 2h at rt after which the reaction was stopped by the addition of water and dilution with ethyl acetate. The organic phase was evaporated and the crude intermediate was used for the following reaction step without purification

4.2.4. Procedure for synthesis of 9

The 2,4-dichloropyrimidine derivative **8** was dissolved in EtOH and 1.1 equiv. of 5-amino-2-methylphenol and 1.5 equiv. of Na₂CO₃ were added. The reaction was allowed to stir overnight at room temperature, after which it was stopped by the addition of water and dilution with ethyl acetate. The organic phase was evaporated and the crude intermediate was used for the following reaction step without purification.

4.2.5. Procedure for synthesis of 12

The 2,4-dichloropyrimidine derivative **11** was dissolved in butanol and 1.1 equiv. of 5-amino-2-methylphenol and 1.1 equiv. of DIPEA were added. The reaction was left to reflux overnight. After cooling, the reaction was stopped by the addition of water and dilution with ethyl acetate. The organic phase was evaporated, and the crude intermediate was used for the following reaction step without purification.

4.2.6. General procedure for synthesis of 3a-f:

The crude of 2-chloro-4-((3-hydroxy-4-methylphenyl)amino)pyrimidine-5-carbonitrile **2** was dissolved in butanol and 1.1 Equiv. of corresponding aniline and 1 equiv. of 1M HCl were added. The reaction was left to reflux overnight. After cooling, the reaction mixture was poured on water and extracted using ethylacetate. After evaporation of the organic solvent, the crude was suspended in iPrOH, which was later filtered, and the precipitate was allowed to dry to give the final compounds **3a-f**.

4-((3-hydroxy-4-methylphenyl)amino)-2-((4-morpholinophenyl)amino) pyrimidine-5-carbonitrile (3a)

Grey powder (15% yield). ¹H NMR (400 MHz, DMSO-*d*₆) δ 9.69 (s, 1H), 9.30 (s, 2H), 8.41 (d, *J* = 3.7 Hz, 1H), 7.50 – 7.42 (m, 2H), 7.04 – 6.99 (m, 1H), 6.90 – 6.81 (m, 2H), 6.81 – 6.68 (m, 2H), 3.76 – 3.71 (m, 4H), 3.05 – 2.97 (m, 4H), 2.13 (s, 3H); ¹³C NMR (101 MHz, DMSO-*d*₆) δ 162.38, 159.71, 155.15, 154.98, 146.79, 136.41, 131.43, 129.93, 124.85, 118.46, 116.89, 115.20, 114.96, 111.55, 107.42, 66.09, 49.02, 15.62. HRMS calcd for C₂₂H₂₂N₆O₂[M+H]⁺ 403.1882, found 403.1868.

4-(3-hydroxy-4-methylphenylamino)-2-(3-morpholinophenylamino)pyrimidine-5-carbonitrile (3b) White powder (28.2% yield). ¹H NMR (400 MHz, DMSO-*d*₆) δ 9.67 (s, 1H), 9.31 (s, 1H), 9.28 (s, 1H), 8.46 (s, 1H), 7.25 – 7.18 (m, 1H), 7.15 – 7.07 (m, 1H), 7.05 – 6.94 (m, 2H), 6.92 – 6.80 (m, 2H), 6.62 – 6.52 (m, 1H), 3.71 – 3.55 (m, 4H), 2.95 – 2.76 (m, 4H), 2.11 (s, 3H). HRMS calcd for C₂₂H₂₂N₆O₂ [M+H]⁺ 403.1882, found, 403.1888.

2-((4-ethoxyphenyl)amino)-4-((3-hydroxy-4-methylphenyl)amino)pyrimidine-5-carbonitrile (3c) White powder (55% yield) ¹H NMR (400 MHz, DMSO-*d*₆) δ 9.73 (s, 1H), 9.30 (s, 2H), 8.41 (s, 1H), 7.52 – 7.46 (m, 2H), 7.04 – 7.00 (m, 1H), 6.91 – 6.82 (m, 2H), 6.78 – 6.64 (m, 2H), 3.95 (q, *J* = 7.0 Hz, 2H), 2.13 (s, 3H), 1.30 (t, *J* = 7.0 Hz, 3H). HRMS calcd for C₂₀H₁₉N₅O₂ [M+H]⁺ 362.1617, found 362.1611.

2-((3-ethoxyphenyl)amino)-4-((3-hydroxy-4-methylphenyl)amino)pyrimidine-5-carbonitrile (3d) White powder (7% yield) ¹H NMR (400 MHz, DMSO-*d*₆) δ 9.90 (s, 1H), 9.46 (s, 1H), 8.50 (s, 1H), 7.30 – 7.24 (m, 1H), 7.21 – 7.17 (m, 1H), 7.07 – 6.99 (m, 2H), 6.98 – 6.79 (m, 3H), 6.56 – 6.50 (m, 1H), 3.87 – 3.72 (m, 2H), 2.12 (s, 3H), 1.26 (t, *J* = 7.0 Hz, 3H). HRMS calcd for C₂₀H₁₉N₅O₂ [M+H]⁺ 362.1617, found 362.1613.

2-((4-acetylphenyl)amino)-4-((3-hydroxy-4-methylphenyl)amino)pyrimidine-5-carbonitrile (3e) White powder (25% yield). ¹H NMR (400 MHz, DMSO-*d*₆) δ 10.32 (s, 1H), 9.57 (s, 1H), 8.55 (s, 1H), 7.82 – 7.70 (m, 4H), 7.16 – 7.03 (m, 2H), 7.00 – 6.88 (m, 1H), 6.86 – 6.78 (m, 1H), 2.49 (s, 3H), 2.16 (s, 3H). HRMS calcd for C₂₀H₁₇N₅O₂ [M+H]⁺: 360.1460, found 360.1455.

4-((3-hydroxy-4-methylphenyl)amino)-2-((4-(methylsulfonyl)phenyl)amino)pyrimidine-5-carbonitrile (3f) White powder (16.7 % yield). ¹H NMR (400 MHz, DMSO-*d*₆) δ 10.37 (s, 1H), 10.06 – 9.72 (m, 1H), 9.62 (s, 1H), 8.56 (s, 1H), 7.91 – 7.83 (m, 2H), 7.71 – 7.60 (m, 2H), 7.08 (d, *J* = 8.0 Hz, 1H), 7.00 (s, 1H), 6.84 – 6.79 (m, 1H), 3.12 (s, 3H), 2.16 (s, 3H); ¹³C NMR (101 MHz, DMSO-*d*₆) δ 162.42, 160.38, 158.95, 155.40, 144.00, 136.10, 133.38, 130.08, 127.66, 127.48, 121.12, 119.21, 116.15, 115.46, 111.58, 43.95, 15.64.; HRMS calcd for C₁₉H₁₇N₅O₃S [M+H]⁺: 396.1130, found 396.1115.

4.2.7. General procedure for synthesis of 5, 7

The crude 2-chloro-4-anilinopyrimidine derivatives **4** and **6** were dissolved in iPrOH and 1.1Equiv. of corresponding aniline and 1.1 equiv. of DIPEA were added. The reaction allowed to reflux overnight where the products **5** and **7** were obtained, respectively as white precipitate that was filtered off and allowed to dry.

2-((5-cyano-2-((4-morpholinophenyl) amino) pyrimidin-4-yl) amino)-N-methyl benzamide (5) White powder (17.2 % yield). ¹H NMR (400 MHz, DMSO-*d*₆) δ 11.30 (s, 1H), 9.49 (s, 1H), 8.69 – 8.62 (m, 1H), 8.47 (s, 1H), 8.40 – 8.31 (m, 1H), 7.65 (dd, *J* = 7.9, 1.6 Hz, 1H), 7.40 – 7.30 (m, 2H), 7.29 – 7.21 (m, 1H), 7.04 (td, *J* = 7.6, 1.2 Hz, 1H), 7.00 – 6.94 (m, 2H), 3.81 – 3.73 (m, 4H), 3.18 – 3.09 (m, 4H), 2.78 (d, *J* = 4.5 Hz, 3H); ¹³C NMR (101 MHz, DMSO-*d*₆) δ 168.80, 162.63, 160.43,

159.00, 148.70, 139.13, 131.28, 129.35, 127.81, 125.68, 121.46, 120.40, 120.22, 116.43, 114.87, 82.10, 66.10, 48.69, 26.21. HRMS calcd for C₂₃H₂₃N₇O₂ [M+H]⁺ 430.1976, found 430.1991.

N-(2-((5-cyano-2-((4-morpholinophenyl)amino)pyrimidin-4-yl)amino)phenyl)acetamide (**7**) White powder (71% yield). ¹H NMR (500 MHz, DMSO-*d*₆) δ 9.84 (s, 1H), 9.75 (s, 1H), 8.82 – 8.64 (m, 1H), 8.44 (s, 1H), 7.68 – 7.49 (m, 2H), 7.44 – 7.31 (m, 2H), 7.30 – 7.17 (m, 2H), 6.84 – 6.62 (m, 2H), 3.76 – 3.67 (m, 4H), 3.06 – 2.93 (m, 4H), 2.08 (s, 3H); ¹³C NMR (126 MHz, DMSO-*d*₆) δ 169.27, 161.92, 159.31, 146.74, 132.41, 131.36, 130.25, 128.01, 125.94, 124.87, 124.01, 120.83, 120.72, 116.53, 115.12, 82.67, 66.09, 48.98, 23.28. HRMS calcd for C₂₃H₂₃N₇O₂ [M+H]⁺: 430.1991, found 430.1983.

4.2.8. General procedure for synthesis of 10a, b:

The crude 5-((2-chloro-5-(methylthio)pyrimidin-4-yl)amino)-2-methylphenol **9** was dissolved in iPrOH and 1.1 Equiv. of corresponding aniline and 1 equiv. of DIPEA were added. The reaction was left to reflux overnight. After cooling the reaction mixture was filtered and the precipitate was washed with iPrOH and allowed to dry to give the final compounds **10a, b**.

2-methyl-5-(5-(methylthio)-2-(4-morpholinophenylamino)pyrimidin-4-ylamino)phenol (10a) Brown powder (30% yield). ¹H NMR (400 MHz, DMSO-*d*₆) δ 9.19 (s, 1H), 9.00 (s, 1H), 8.39 (s, 1H), 8.13 (s, 1H), 7.57 – 7.45 (m, 2H), 7.09 – 6.93 (m, 3H), 6.84 – 6.74 (m, 2H), 3.78 – 3.69 (m, 4H), 3.06 – 2.95 (m, 4H), 2.27 (s, 3H), 2.13 (s, 3H); ¹³C NMR (101 MHz, DMSO-*d*₆) δ 161.80, 160.53, 159.32, 155.11, 145.95, 137.32, 132.89, 129.92, 120.43, 119.48, 115.47, 114.08, 110.19, 102.04, 66.15, 49.32, 19.44, 15.60. HRMS calcd for C₂₂H₂₅N₅O₂S [M+H]⁺ 424.1807, found 424.1802.

2-methyl-5-(5-(methylthio)-2-(3-morpholinophenylamino)pyrimidin-4-ylamino)phenol (10b) Brownish white powder (71.4% yield). ¹H NMR (400 MHz, DMSO-*d*₆) δ 10.59 (s, 1H), 9.76 (s, 1H), 9.51 (s, 1H), 8.25 (s, 1H), 7.14 – 7.01 (m, 3H), 6.97 – 6.85 (m, 3H), 6.72 (dd, *J* = 8.4, 2.4 Hz, 1H), 3.66 (d, *J* = 9.6 Hz, 4H),

2.90 (t, $J = 4.8$ Hz, 4H), 2.38 (s, 3H), 2.14 (s, 3H). ^{13}C NMR (101 MHz, DMSO- d_6) δ 160.86, 155.35, 151.89, 151.33, 148.46, 137.75, 135.23, 130.08, 129.22, 121.95, 115.56, 112.12, 111.62, 111.50, 107.31, 105.03, 65.92, 48.29, 18.56, 15.69. HRMS calcd for $\text{C}_{22}\text{H}_{25}\text{N}_5\text{O}_2\text{S}$ $[\text{M}+\text{H}]^+$ 424.1807, found 424.1811.

4.2.9. General procedure for synthesis of 10c-e:

The crude 5-((2-chloro-5-(methylthio)pyrimidin-4-yl)amino)-2-methylphenol **9** was dissolved in iPrOH and 1.1 Equiv. of corresponding aniline and 1 equiv. of conc. HCl were added. The reaction was carried out for 20 to 60 min based on the aniline derivative at 170°C under microwave conditions. After cooling the reaction mixture was filtered and the precipitate was washed with iPrOH and allowed to dry to give the final compounds **10c-e**

5-((2-((4-ethoxyphenyl)amino)-5-(methylthio)pyrimidin-4-yl)amino)-2-methylphenol (10c) White powder (17% yield) ^1H NMR (400 MHz, DMSO- d_6) δ 9.20 (s, 1H), 9.05 (s, 1H), 8.41 (s, 1H), 8.13 (s, 1H), 7.57 – 7.49 (m, 2H), 7.01 (s, 2H), 6.98 – 6.87 (m, 1H), 6.77 – 6.69 (m, 2H), 3.95 (q, $J = 7.0$ Hz, 2H), 2.27 (s, 3H), 2.13 (s, 3H), 1.30 (t, $J = 7.0$ Hz, 3H). HRMS calcd for $\text{C}_{20}\text{H}_{22}\text{N}_4\text{O}_2\text{S}$ $[\text{M}+\text{H}]^+$ 383.1541, found 383.1539.

5-((2-((3-ethoxyphenyl)amino)-5-(methylthio)pyrimidin-4-yl)amino)-2-methylphenol (10d) White powder (6% yield). ^1H NMR (400 MHz, DMSO- d_6) δ 10.48 (s, 1H), 9.71 (s, 1H), 9.48 (s, 1H), 8.24 (s, 1H), 7.14 – 7.09 (m, 2H), 7.09 – 7.04 (m, 1H), 7.03 – 6.99 (m, 1H), 6.93 – 6.88 (m, 2H), 6.63 (dd, $J = 8.3, 2.5, 0.9$ Hz, 1H), 3.79 (q, $J = 6.9$ Hz, 2H), 2.38 (s, 3H), 2.14 (s, 3H), 1.27 (t, $J = 6.9$ Hz, 3H). HRMS calcd for $\text{C}_{20}\text{H}_{22}\text{N}_4\text{O}_2\text{S}$ $[\text{M}+\text{H}]^+$ 383.1541, found 383.1536.

1-(4-((4-((3-hydroxy-4-methylphenyl)amino)-5-(methylthio)pyrimidin-2-yl)amino)phenyl)ethan-1-one (10e) White powder (55% yield). ^1H NMR (400 MHz, DMSO- d_6) δ 10.89 – 10.74 (m, 1H), 9.78 (s, 1H), 9.54 (s, 1H), 8.29 (s, 1H), 7.80 – 7.73 (m, 2H), 7.66 – 7.59 (m, 2H), 7.17 – 7.10 (m, 1H), 6.96 (d, $J = 2.0$ Hz, 1H), 6.84 (dd, $J = 7.9, 2.1$ Hz, 1H), 2.50 (s, 3H), 2.40 (s, 3H), 2.19 (s, 3H). HRMS calcd for $\text{C}_{20}\text{H}_{20}\text{N}_4\text{O}_2\text{S}$ $[\text{M}+\text{H}]^+$ 381.13852, found 381.1376

4.2.10. General procedure for synthesis of 13a-f:

The crude 5-((2-chloro-5-methoxypyrimidin-4-yl)amino)-2-methylphenol **12** was dissolved in iPrOH and 1.1 Equiv. of corresponding aniline and 1 equiv. of conc. HCl were added. The reaction was carried out for 1 h at 170°C under microwave conditions. After cooling the reaction mixture was filtered and the precipitate was washed with iPrOH and allowed to dry to give the final compounds **13a-f**.

5-((5-methoxy-2-((3-morpholinophenyl)amino)pyrimidin-4-yl)amino)-2-methylphenol (13a) Brownish powder (66% yield) ¹H NMR (400 MHz, DMSO-*d*₆) δ 9.11 (s, 1H), 8.58 (s, 1H), 8.45 (s, 1H), 7.80 (s, 1H), 7.39 – 7.36 (m, 1H), 7.20 – 7.14 (m, 2H), 7.10 (d, *J* = 2.1 Hz, 1H), 7.01 (t, *J* = 8.1 Hz, 1H), 6.97 – 6.93 (m, 1H), 6.43 (ddd, *J* = 8.2, 2.4, 0.9 Hz, 1H), 3.83 (s, 3H), 3.69 – 3.64 (m, 4H), 2.98 – 2.92 (m, 4H), 2.09 (s, 3H); ¹³C NMR (101 MHz, DMSO-*d*₆) δ 155.32, 154.28, 151.61, 148.83, 138.16, 135.03, 133.99, 130.08, 129.25, 121.60, 114.57, 111.63, 111.08, 110.57, 106.90, 65.99, 57.04, 48.20, 15.67. HRMS calcd for C₂₂H₂₅N₅O₃ [M+H]⁺ 408.2035, found 408.2033.

5-((2-((4-ethoxyphenyl)amino)-5-methoxypyrimidin-4-yl)amino)-2-methylphenol (13b) Greenish white powder (57% yield). ¹H NMR (400 MHz, DMSO-*d*₆) δ 10.39 (s, 1H), 10.02 (s, 1H), 9.63 (s, 1H), 7.76 (s, 1H), 7.40 – 7.31 (m, 2H), 7.17 (s, 1H), 7.04 – 6.98 (m, 1H), 6.93 (dd, *J* = 8.1, 2.1 Hz, 1H), 6.86 – 6.78 (m, 2H), 3.98 (q, *J* = 6.9 Hz, 2H), 3.86 (s, 3H), 2.11 (s, 3H), 1.31 (t, *J* = 7.0 Hz, 3H); ¹³C NMR (101 MHz, DMSO-*d*₆) δ 155.42, 155.26, 154.52, 148.90, 134.94, 133.79, 129.95, 129.71, 123.17, 121.74, 120.75, 114.73, 114.58, 110.86, 63.16, 57.04, 15.63, 14.61. HRMS calcd for C₂₀H₂₂N₄O₃ [M+H]⁺ 367.1770, found 367.1770.

5-((2-((3-ethoxyphenyl)amino)-5-methoxypyrimidin-4-yl)amino)-2-methylphenol (13c) Whitish yellow powder (28.1 % yield) ¹H NMR (400 MHz, DMSO-*d*₆) δ 10.44 (s, 1H), 10.15 (s, 1H), 9.50 (s, 1H), 7.78 (s, 1H), 7.16 (t, *J* = 8.2 Hz, 1H), 7.12 (t, *J* = 2.3 Hz, 1H), 7.06 – 6.98 (m, 3H), 6.96 (ddd, *J* = 8.1, 2.1, 0.9 Hz, 1H), 6.64 (ddd, *J* = 8.3, 2.5, 0.9 Hz, 1H), 3.88 (s, 3H), 3.84 – 3.78 (m, 2H), 2.13 (s, 3H), 1.27 (t, *J* = 6.9 Hz, 3H); ¹³C NMR (101 MHz, DMSO-*d*₆) δ 159.00, 155.39, 154.45, 148.51,

138.48, 134.87, 134.02, 130.12, 129.60, 121.78, 121.12, 114.84, 112.47, 110.72, 109.80, 106.38, 62.83, 57.04, 15.67, 14.60. HRMS calcd for C₂₀H₂₂N₄O₃ [M+H]⁺ 367.1770 , found 367.1774 .

1-(4-((4-((3-hydroxy-4-methylphenyl)amino)-5-methoxypyrimidin-2-yl)amino)phenyl)ethenone (13d) Light brown powder(21.5% yield). ¹H NMR (400 MHz, DMSO-*d*₆) δ 10.75 (s, 1H), 10.19 (s, 1H), 9.54 (s, 1H), 7.86 (s, 1H), 7.83 – 7.80 (m, 2H), 7.64 – 7.60 (m, 2H), 7.13 – 7.09 (m, 1H), 7.04 (d, *J* = 2.1 Hz, 1H), 6.93 (dd, *J* = 8.0, 2.1 Hz, 1H), 3.90 (s, 3H), 2.51 (s, 3H), 2.17 (s, 3H); ¹³C NMR (101 MHz, DMSO-*d*₆) δ 196.28, 155.45, 154.44, 148.35, 142.33, 142.32, 135.03, 134.54, 131.40, 130.11, 129.29, 121.95, 118.74, 115.09, 111.18, 57.01, 26.35, 15.67. HRMS calcd for C₂₀H₂₀N₄O₃ [M+Cl]⁻ 399.1223 , found 399.1231.

1-(3-((4-((3-hydroxy-4-methylphenyl)amino)-5-methoxypyrimidin-2-yl)amino)phenyl)ethenone (13e) Greenish white powder (48.4% yield). ¹H NMR (400 MHz, DMSO-*d*₆) δ 10.56 (s, 1H), 10.15 (s, 1H), 9.46 (s, 1H), 7.90 (t, *J* = 1.9 Hz, 1H), 7.82 – 7.77 (m, 2H), 7.67 (dt, *J* = 7.8, 1.3 Hz, 1H), 7.40 (t, *J* = 7.9 Hz, 1H), 7.03 – 6.92 (m, 3H), 3.90 (s, 3H), 2.43 (s, 3H), 2.09 (d, *J* = 8.5 Hz, 3H); ¹³C NMR (101 MHz, dmsO) δ 197.41, 155.29, 154.38, 148.66, 137.88, 137.42, 134.87, 134.33, 129.95, 129.14, 125.27, 123.49, 121.81, 121.49, 120.07, 114.76, 110.74, 57.07, 26.50, 15.62. HRMS calcd for C₂₀H₂₀N₄O₃ [M+H]⁺ 365.1613 , found 365.1608.

5-((5-methoxy-2-((4-(methylsulfonyl)phenyl)amino)pyrimidin-4-yl)amino)-2-methylphenol (13f). Brownish white powder (13.7% yield). ¹H NMR (400 MHz, DMSO-*d*₆) δ 10.91 (s, 1H), 10.24 (s, 1H), 9.56 (s, 1H), 7.87 (s, 1H), 7.77 – 7.70 (m, 4H), 7.14 – 7.08 (m, 1H), 7.04 (d, *J* = 2.1 Hz, 1H), 6.91 (dd, *J* = 8.0, 2.1 Hz, 1H), 3.91 (s, 3H), 3.15 (s, 3H), 2.16 (s, 3H).HRMS calcd for C₁₉H₂₀N₄O₄S [M+H]⁺ 401.1283, found 401.1282 .

4.3. Biological evaluation:

4.3.1. Cellular assay

BE(2)-C (ATCC, CRL-2268) cells were cultured in a 1:1 mixture of DMEM/F12 (with HEPES, Gibco) and EMEM (ATCC); Huh7 and NBL-S (DSMZ, ACC-656) cells

were cultured in IMDM (Gibco) all supplemented with 10% FBS. Cells were grown at 37°C and 5% CO₂. For determining the EC₅₀ values 5 x 10³ BE(2)-C, 1 x 10⁴ NBL-S or 1.25 x 10⁴ Huh7 cells were seeded per well of a 96-well plate. A serial dilution of the drugs was performed and added to the cells at the indicated concentrations. DMSO served as control condition. After 72 h of treatment, an image was acquired using IncuCyte S3 (Sartorius). Confluence was determined using the IncuCyte software. Confluence values were normalized to DMSO control. Cell viability was determined 72 h upon drug exposure using CellTiter GLO (Promega) in a drug matrix screen.

4.3.2. Kinases Binding Assay

The FP binding assay with PKMYT-1 and data processing were performed exactly as previously described [175]. 10 Serial dilutions starting from 20mM ATP were tested. Plates were read repeatedly within a time frame of 15 min to 4 h. In these experiments, ATP and fluorescent kinase tracer were premixed to prevent time-dependent discrimination.

4.3.3. Kinase Activity Assay:

To test the activities of the compounds as PKMYT-1 inhibitors, the synthesized compounds were screened with a fluorescence anisotropy-based binding assay, using the PKMYT-1 domain (KD) and a fluorescently labeled ATP-competitive compound [175]. The initial screening was performed at 20 mM inhibitor concentration as a triple measurement of each compound. Dasatinib (10 mM) was used as inhibitory control and 1% DMSO as vehicle control. Compounds were then retested at 20 mM and 5 mM concentrations in triple measurement.

4.4. Computational Methods:

Molecular docking

The crystal structure of PKMYT-1 (PDB ID 5VD1), WEE1 (PDB ID 5V5Y), and Aurora A Kinase (PDB ID 4DEB) were downloaded from the Protein Data Bank. The protein structures were prepared using Protein Preparation Wizard by adding the hydrogen atoms and missing side chains in Schrödinger suite. [Schrödinger

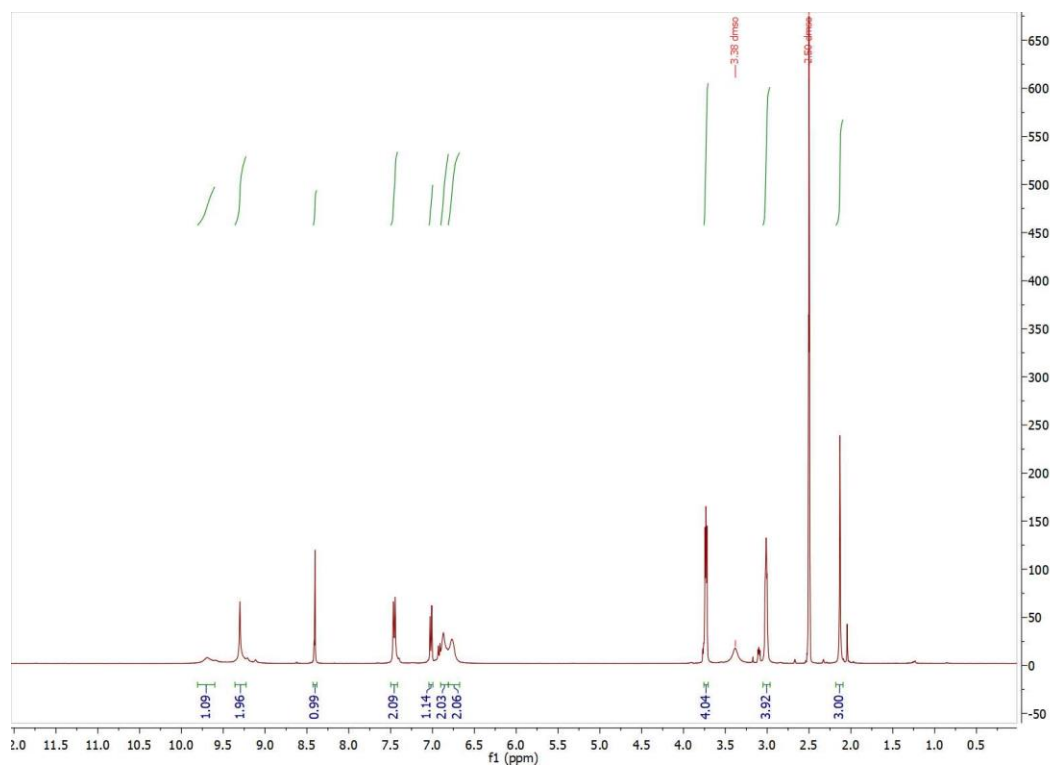
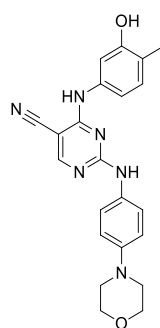
Release 2021-1: Maestro, Protein Preparation Wizard, Prime, Epik, Ligprep, Confgen, Glide; Schrödinger LLC, New York, NY (USA), 2021.] Solvent molecules were removed. Tautomeric states and protonation states of the amino acids were adjusted with PROPKA tool at pH 7.0. OPLS3e force field was applied to minimize the complex to remove the steric clashes, bad contacts and unsuitable torsional angles. The inhibitor structures were prepared using the Ligprep tool by applying the OPLS3e force field. Subsequently, 64 conformers per ligand were generated using the Confgen tool with force field minimization on output conformers. Molecular docking studies were performed in Glide from Schrödinger suite. Grid files were prepared with default settings by applying box-size as 15 Å * 15 Å * 15 Å. Standard Precision (SP) mode with flexible ligand sampling and enhanced planarity of conjugated π groups were used for docking studies. The validation of the docking protocol was done by re-docking. The root mean square deviation (RMSD) value of the re-docked inhibitors from the three X-ray structures compared to the observed binding mode in the crystal structure were all below 1.0 Å.

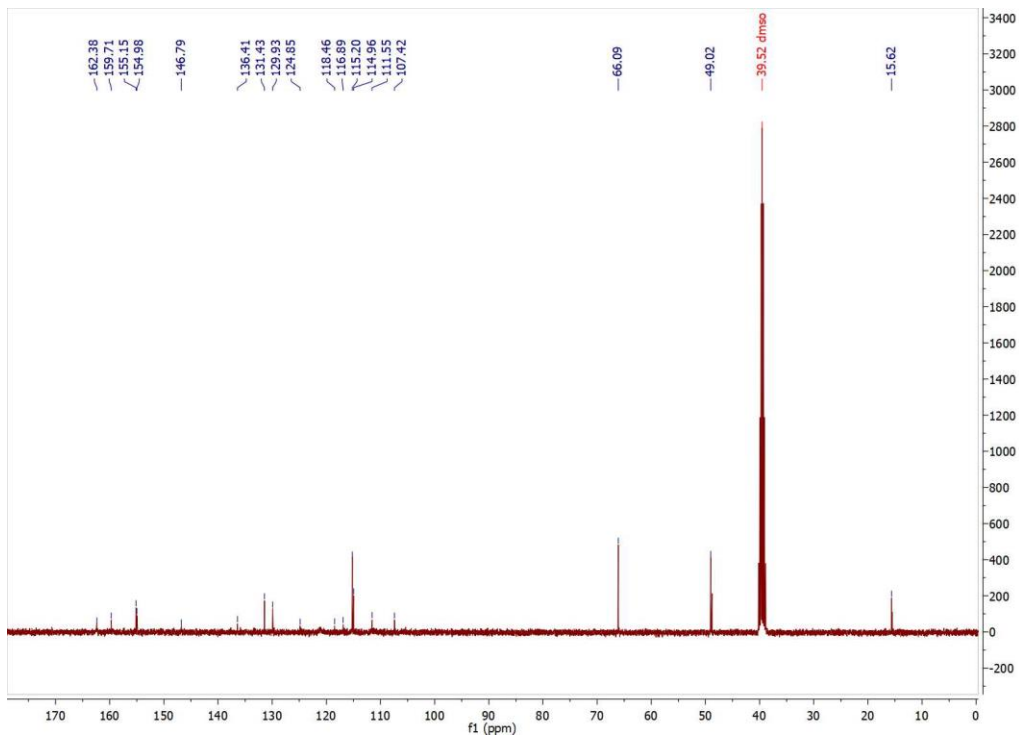
Supplementary information

Contents

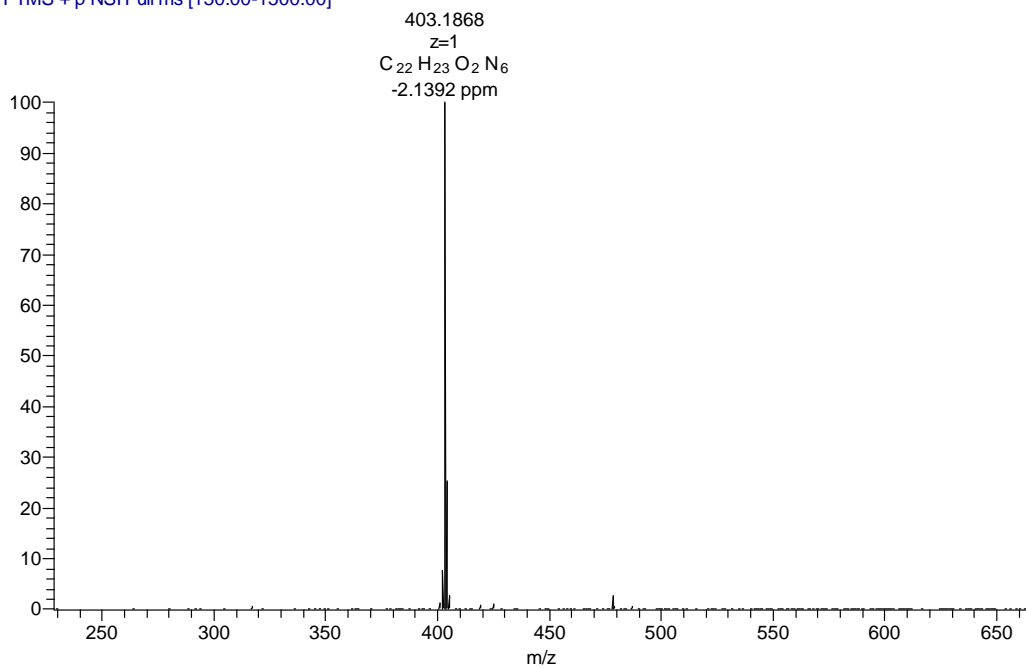
Representative ^1H , ^{13}C NMR ,and HRMS Spectra

Compound 3a

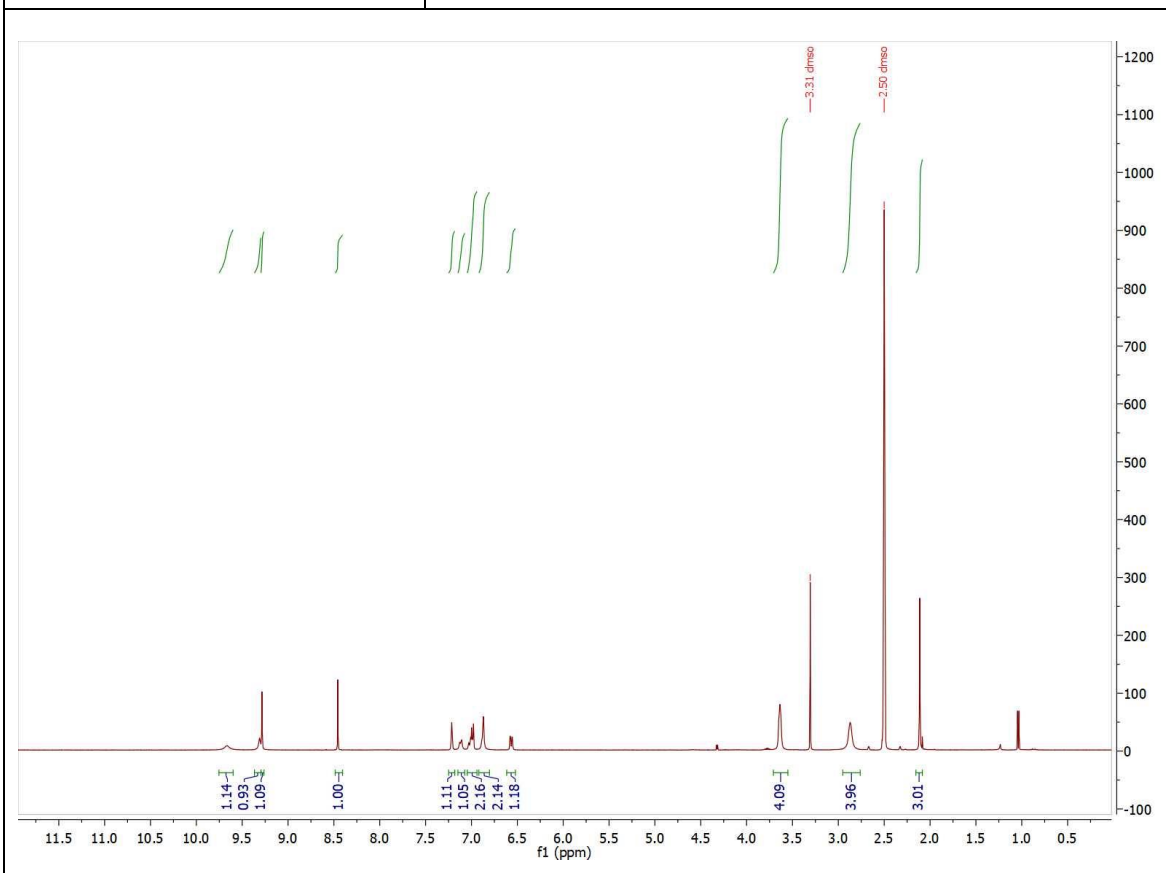
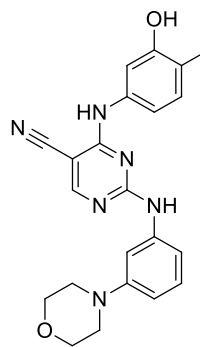




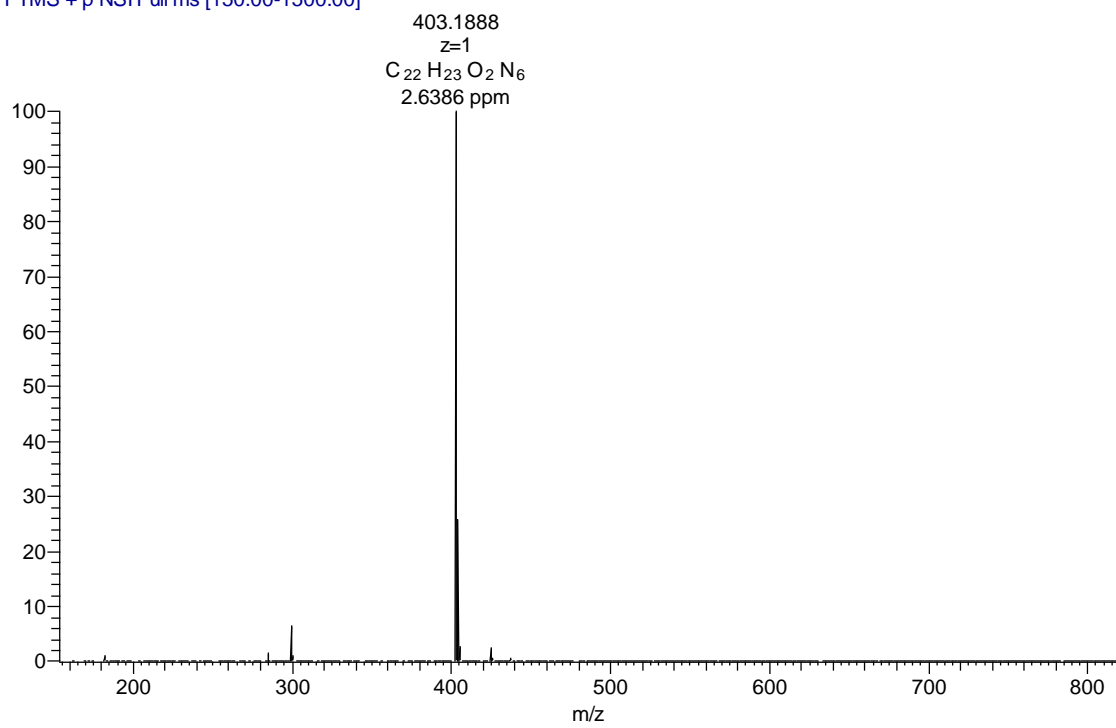
NE36pos #3-11 RT: 0.05-0.28 AV: 9 NL: 1.62E8
 T: FTMS + p NSI Full ms [150.00-1500.00]



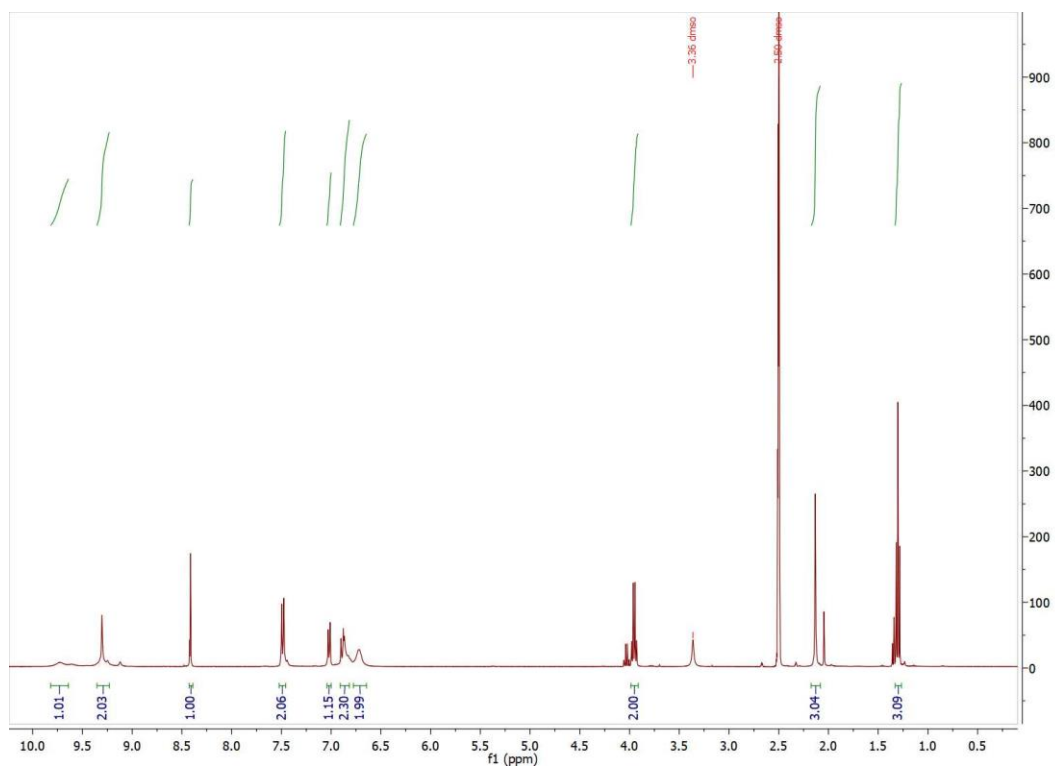
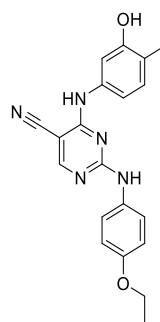
Compound 3b



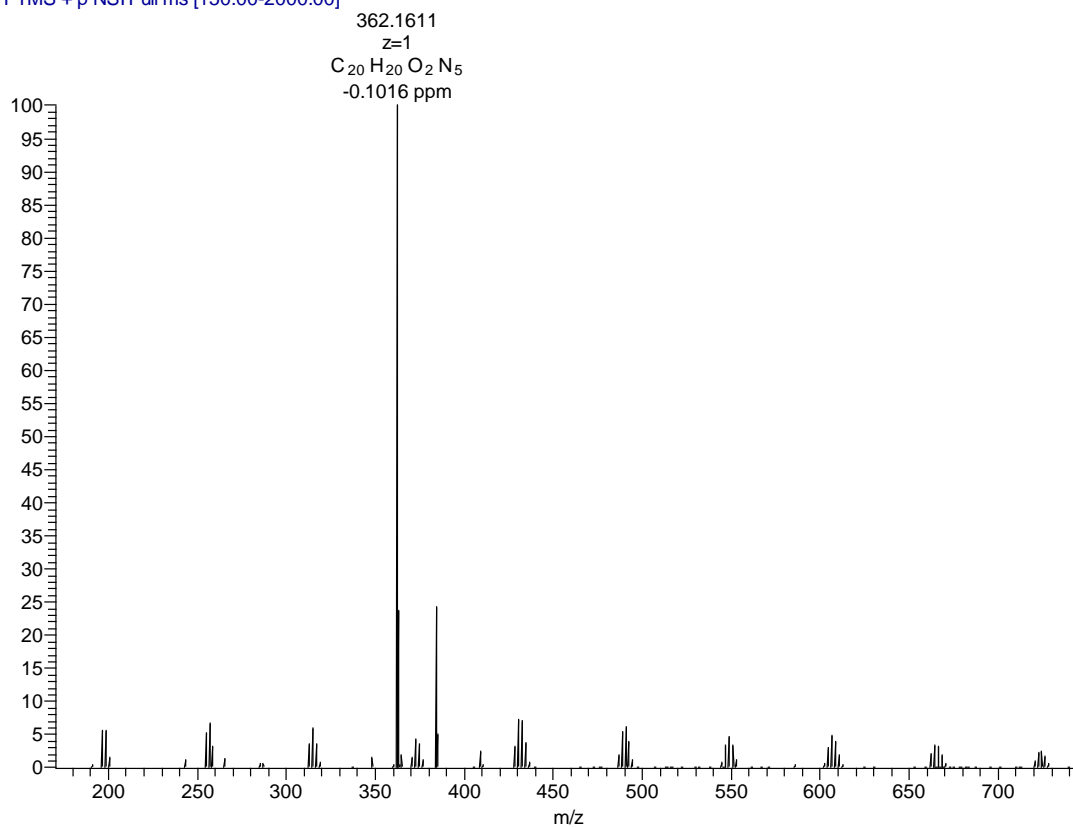
NE35pos #10 RT: 0.28 AV: 1 NL: 2.57E8
T: FTMS + p NSI Full ms [150.00-1500.00]



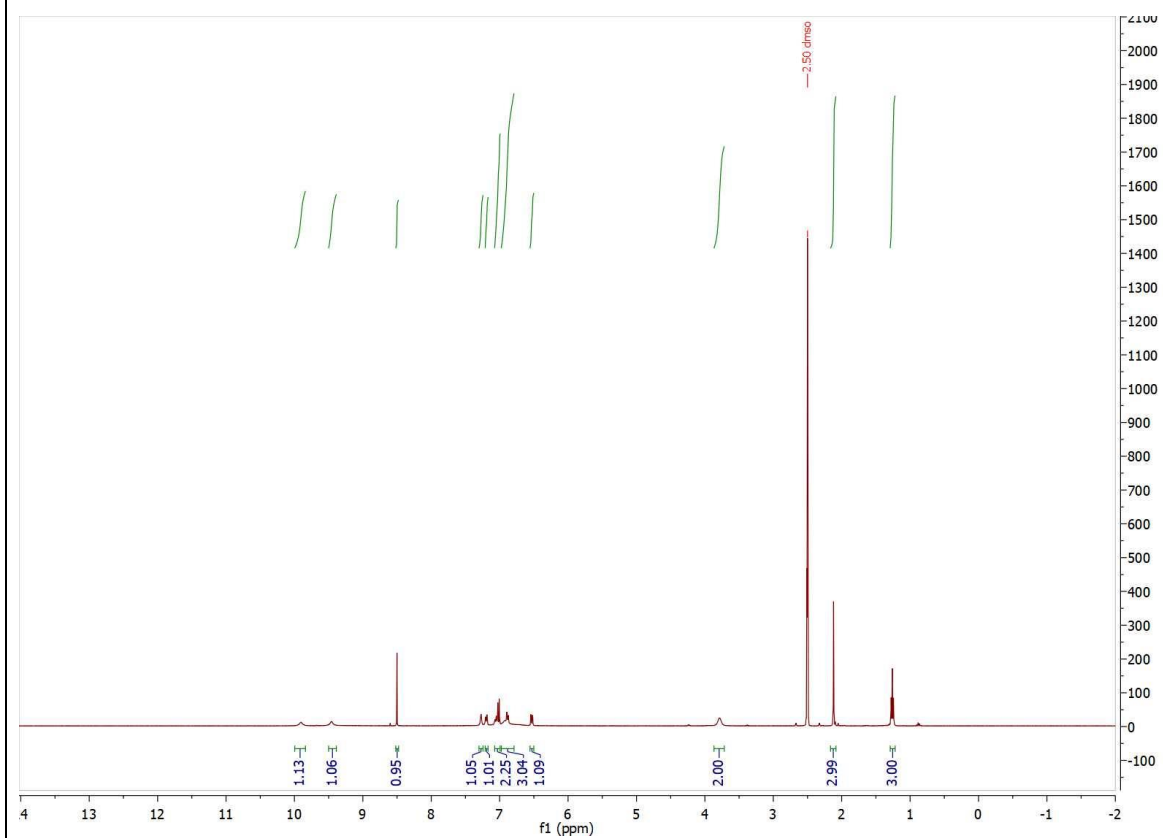
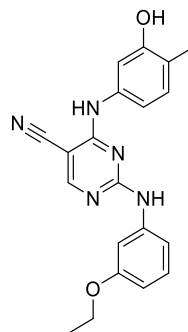
Compound 3c



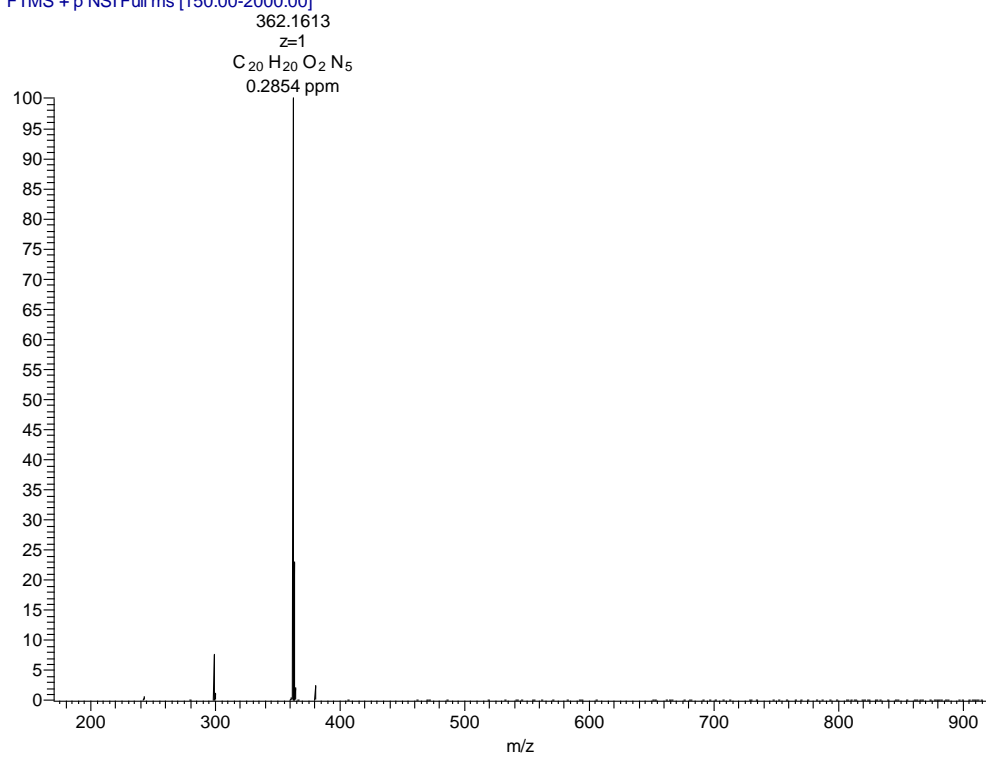
NE64_#1-13 RT: 0.02-0.46 AV: 13 NL: 1.25E6
T: FTMS + p NSI Full ms [150.00-2000.00]



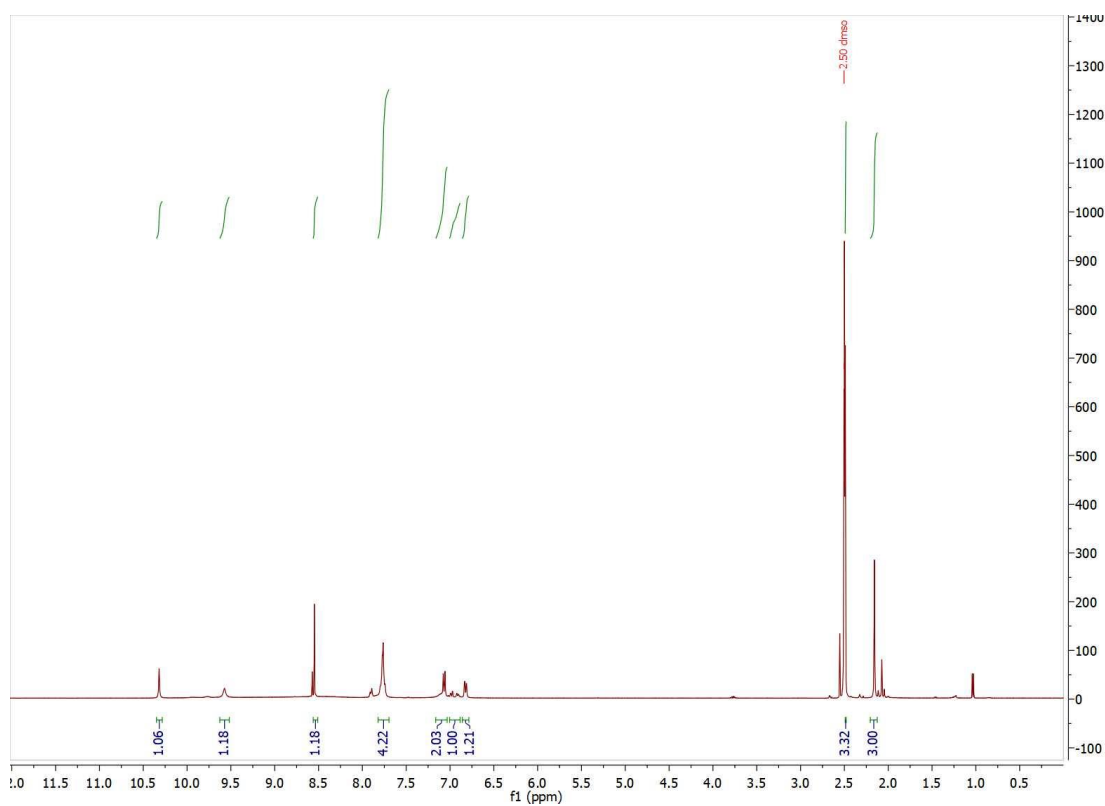
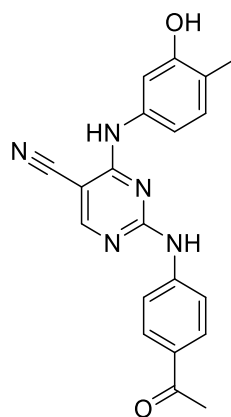
Compound 3d



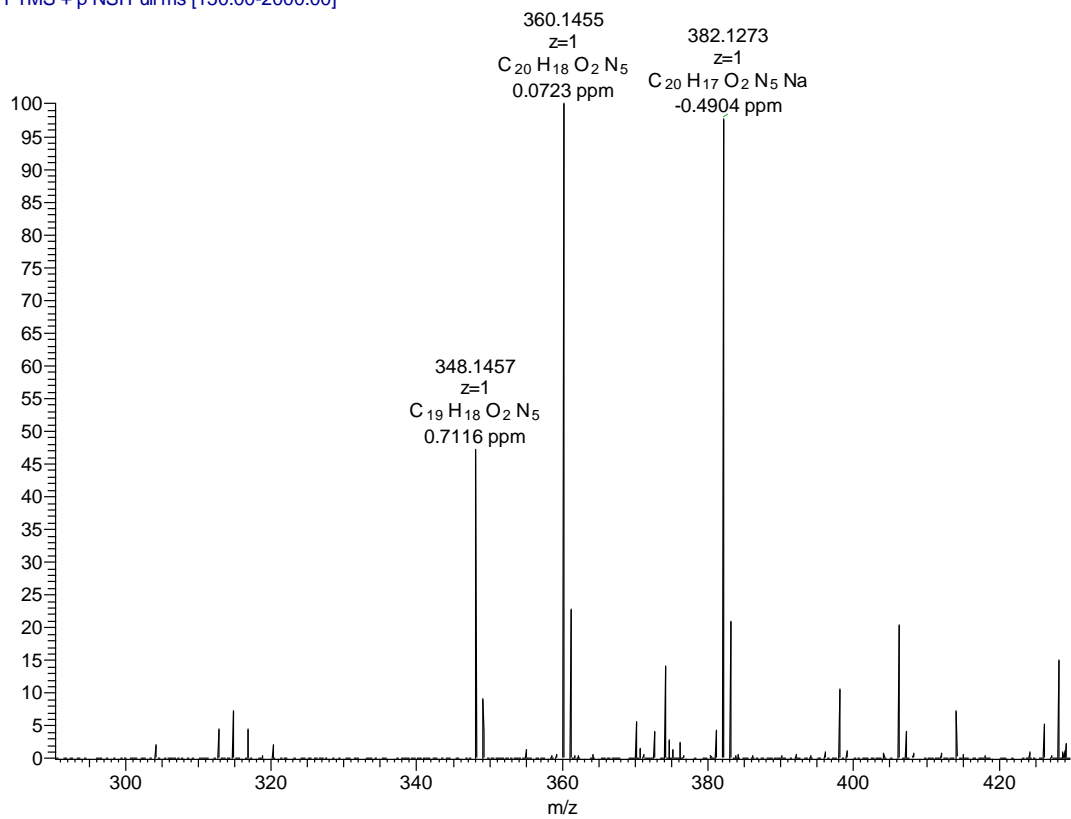
NE65 #1-13 RT: 0.02-0.46 AV: 13 NL: 1.57E6
T: FTMS + p NSI Full ms [150.00-2000.00]



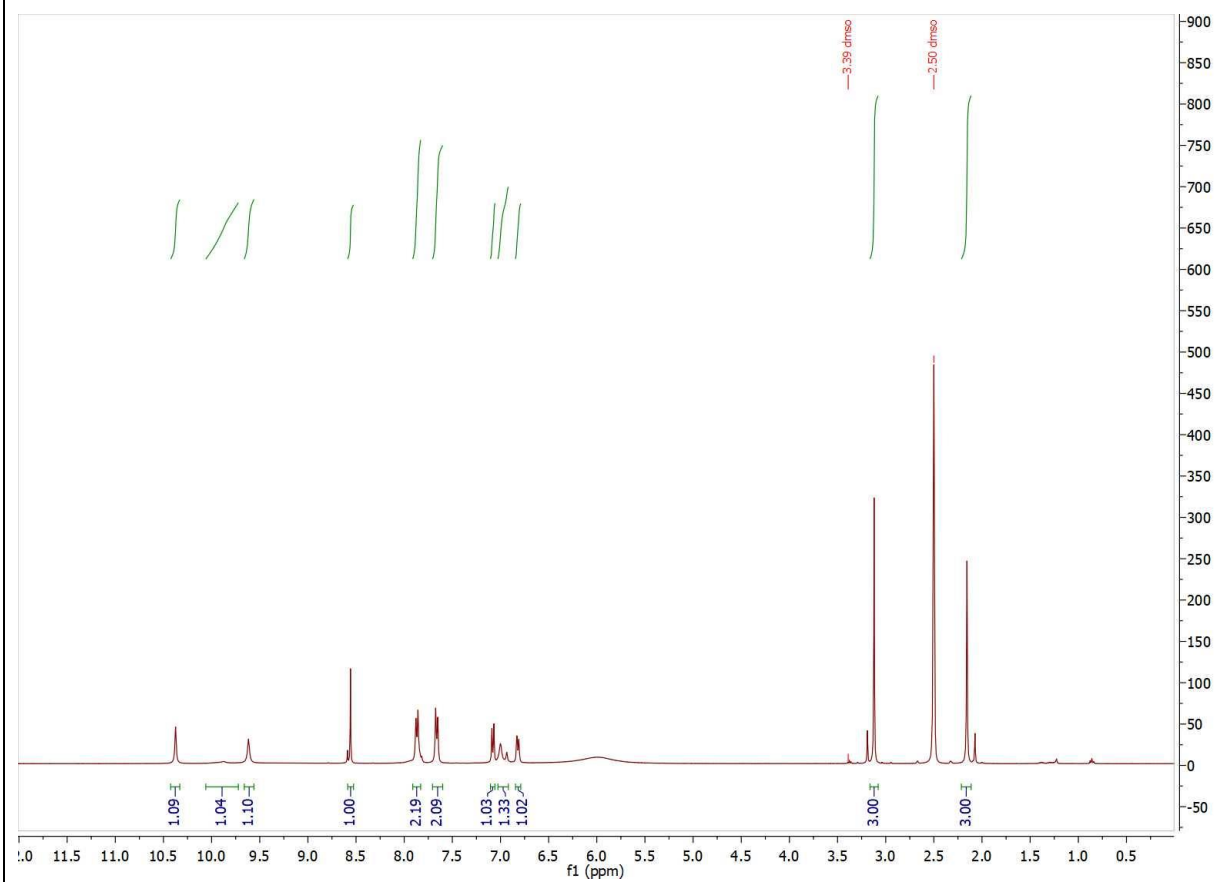
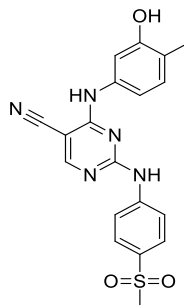
Compound 3e

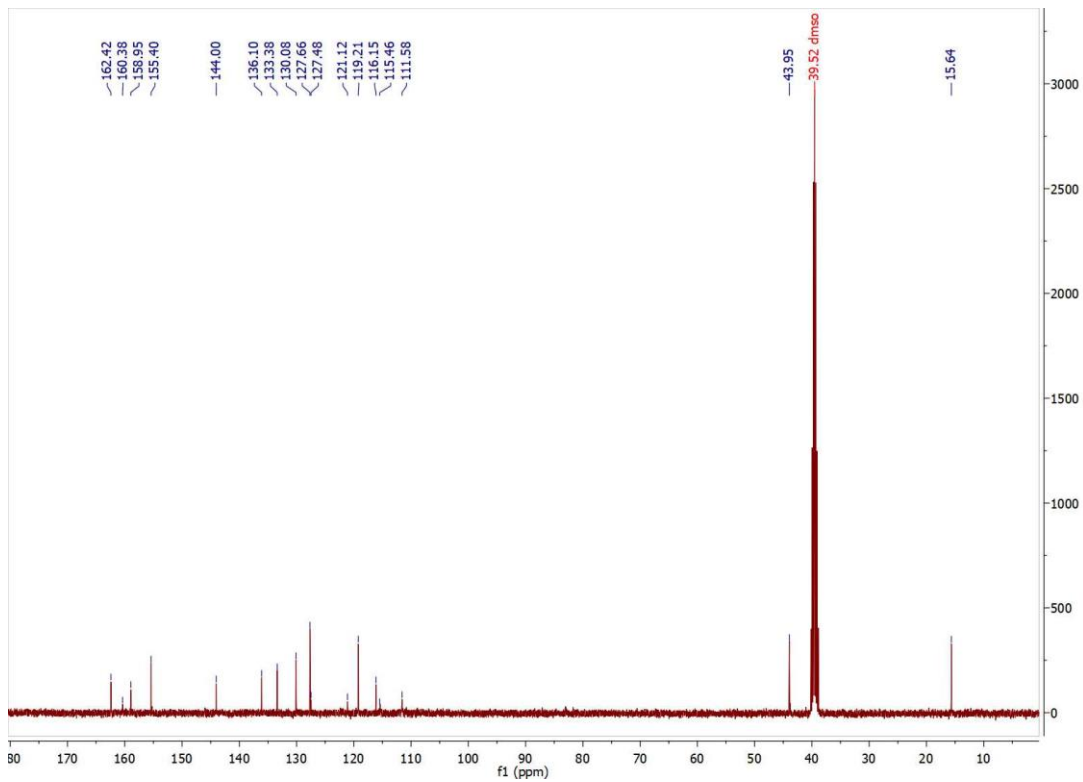


NE63 #1-13 RT: 0.02-0.46 AV: 13 NL: 1.61E5
T: FTMS + p NSI Full ms [150.00-2000.00]

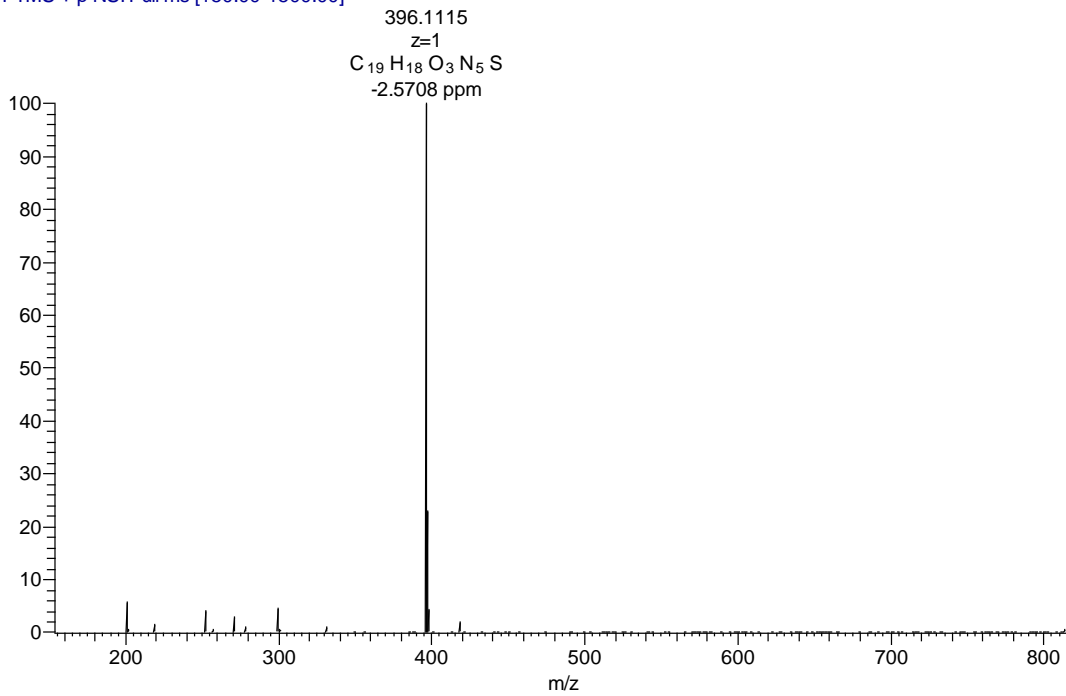


Compound 3f

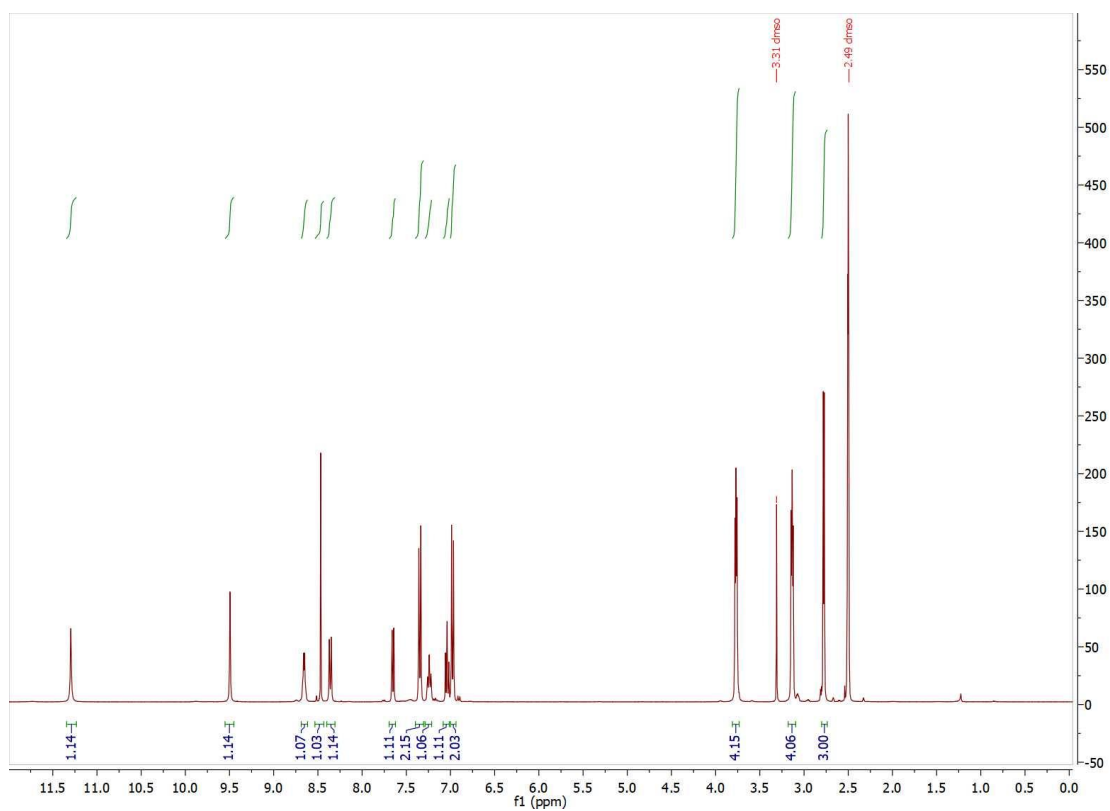
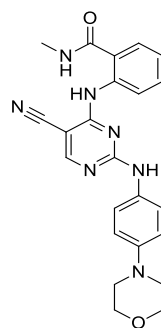


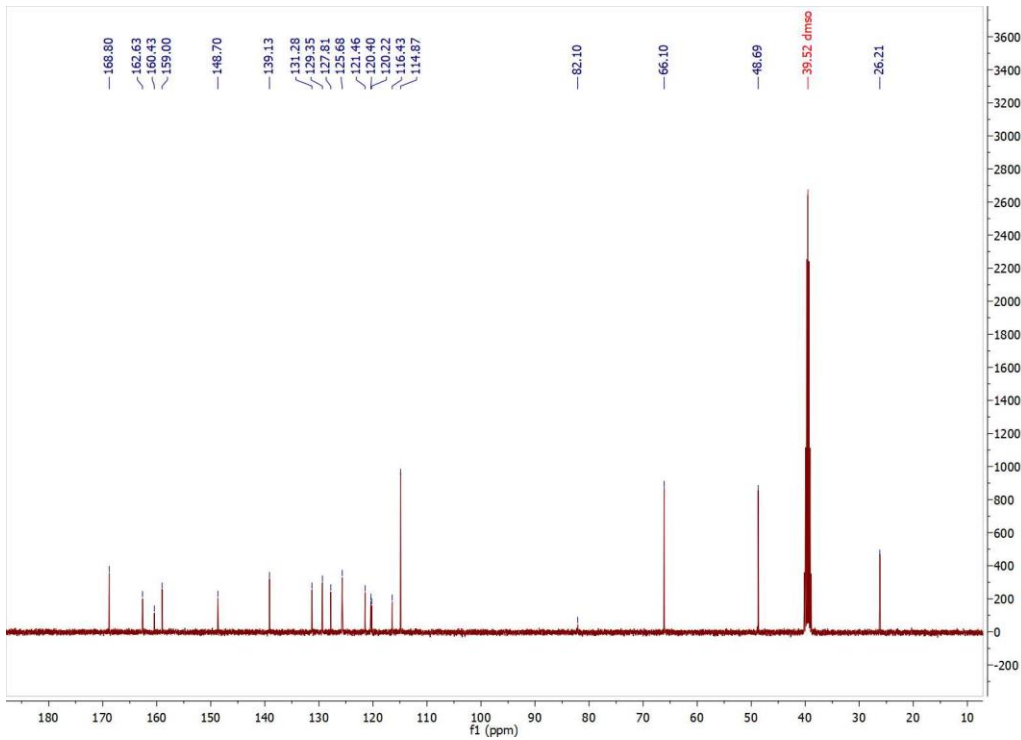


NE43pos #3-12 RT: 0.05-0.31 AV: 10 NL: 9.04E7
 T: FTMS + p NSI Full ms [150.00-1500.00]

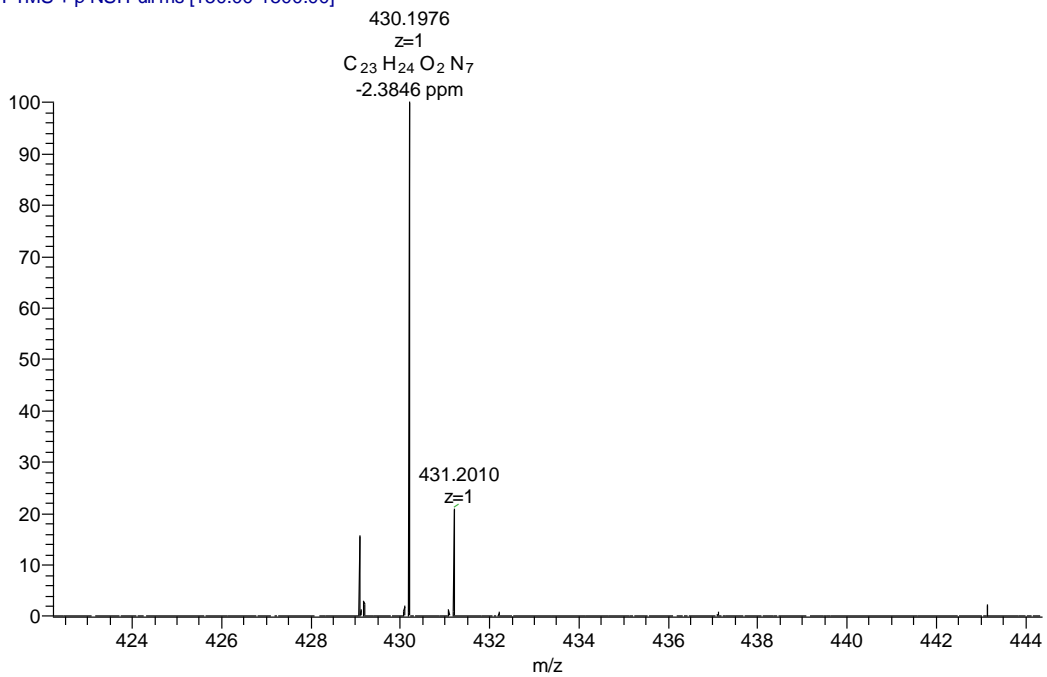


Compound 5

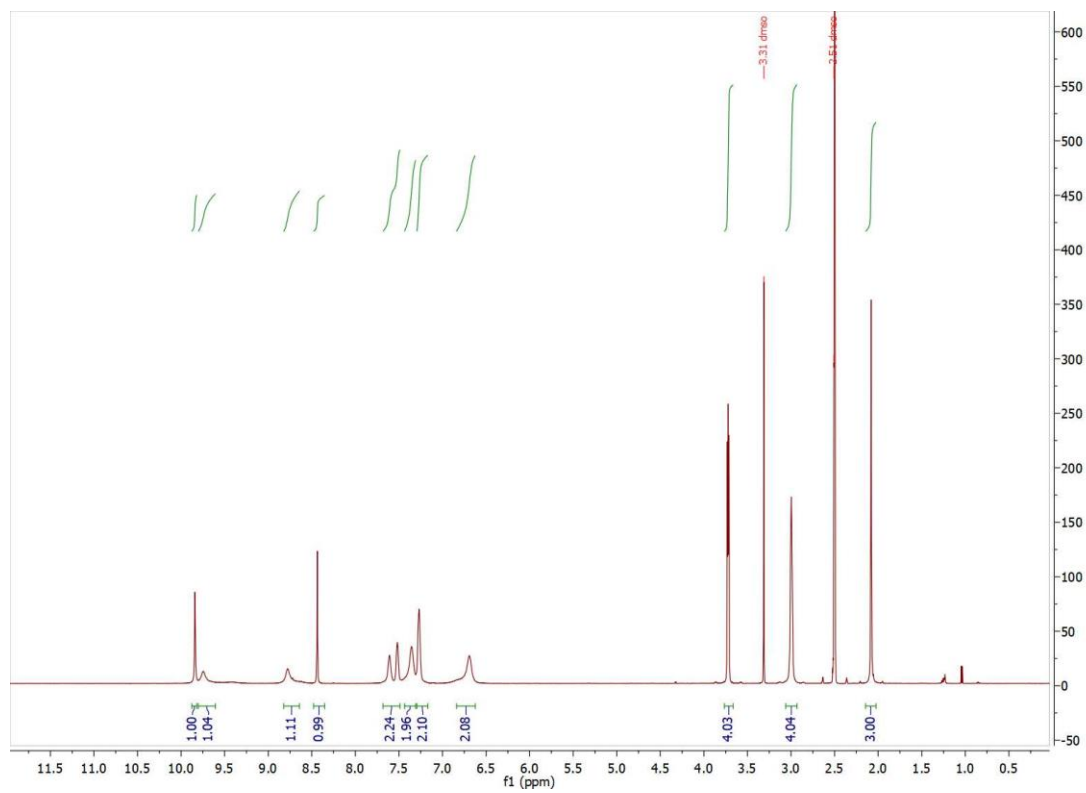
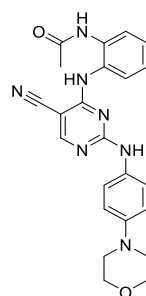


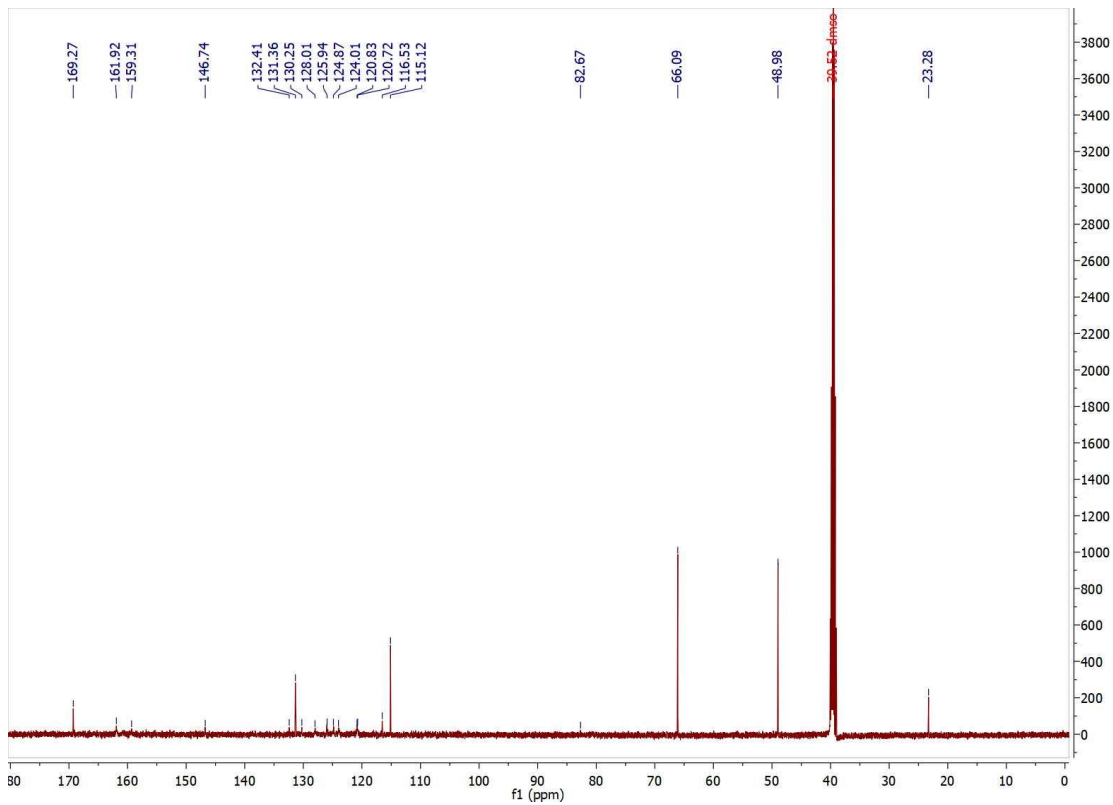


NE11pos #2-10 RT: 0.05-0.28 AV: 9 NL: 2.28E6
 T: FTMS + p NSI Full ms [150.00-1500.00]

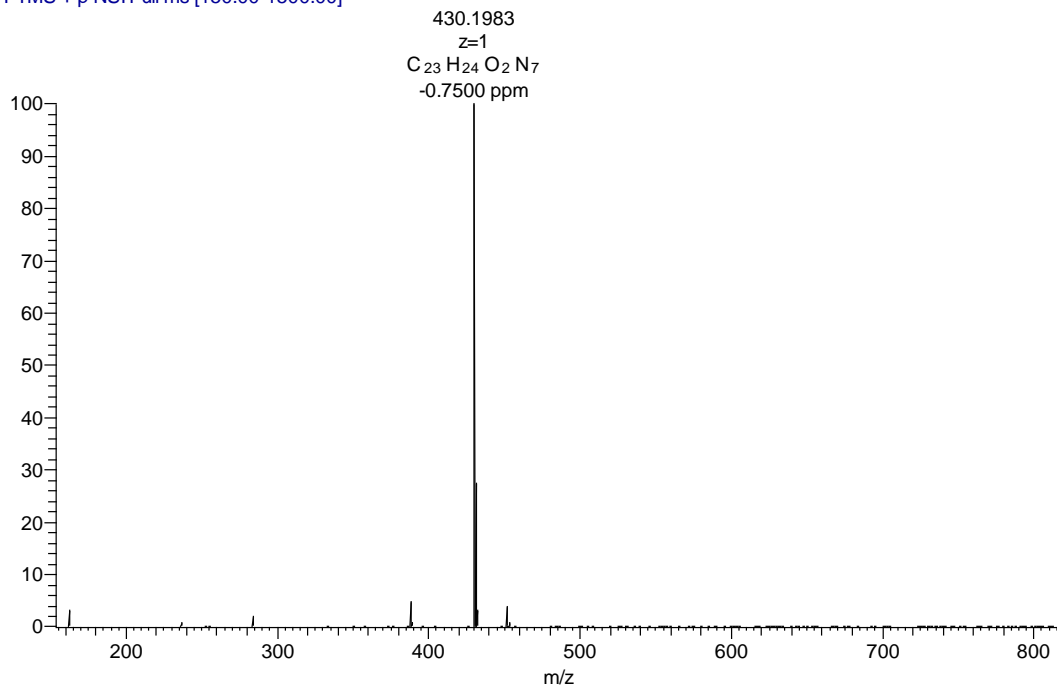


Compound 7

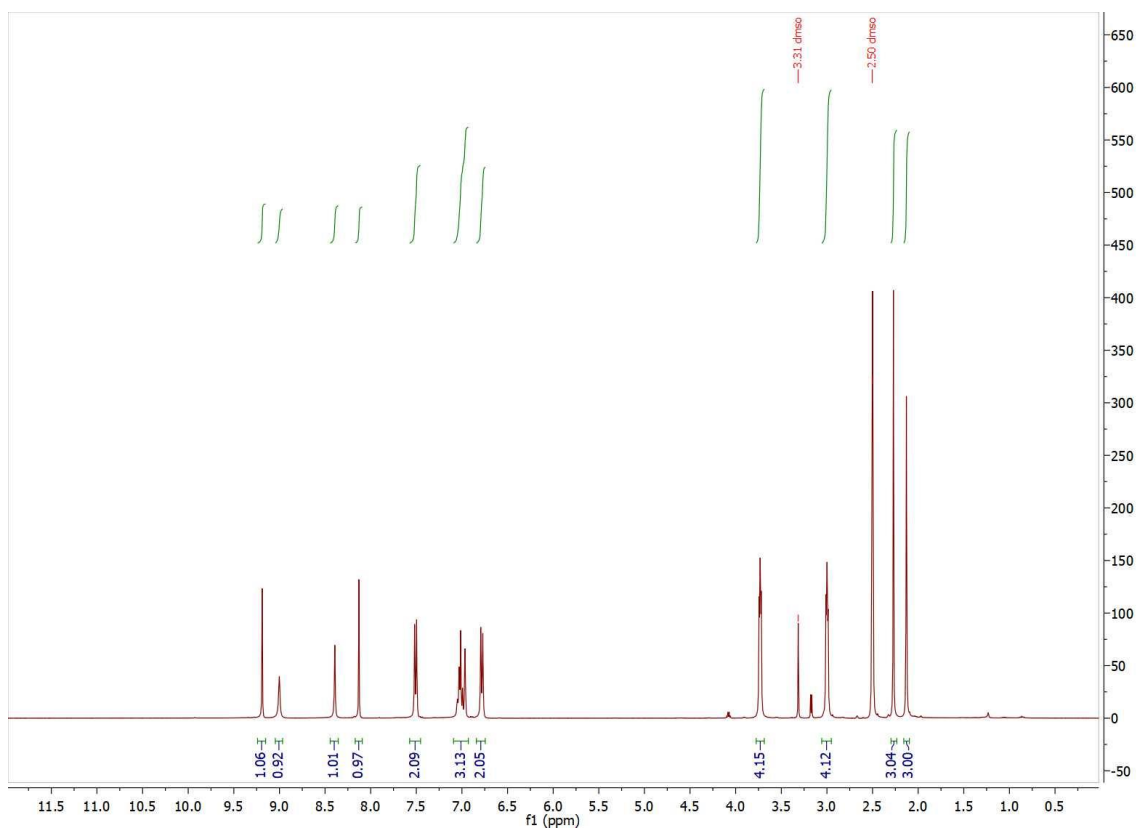
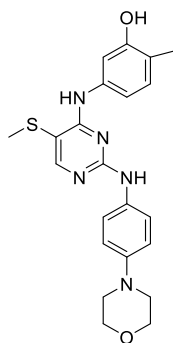


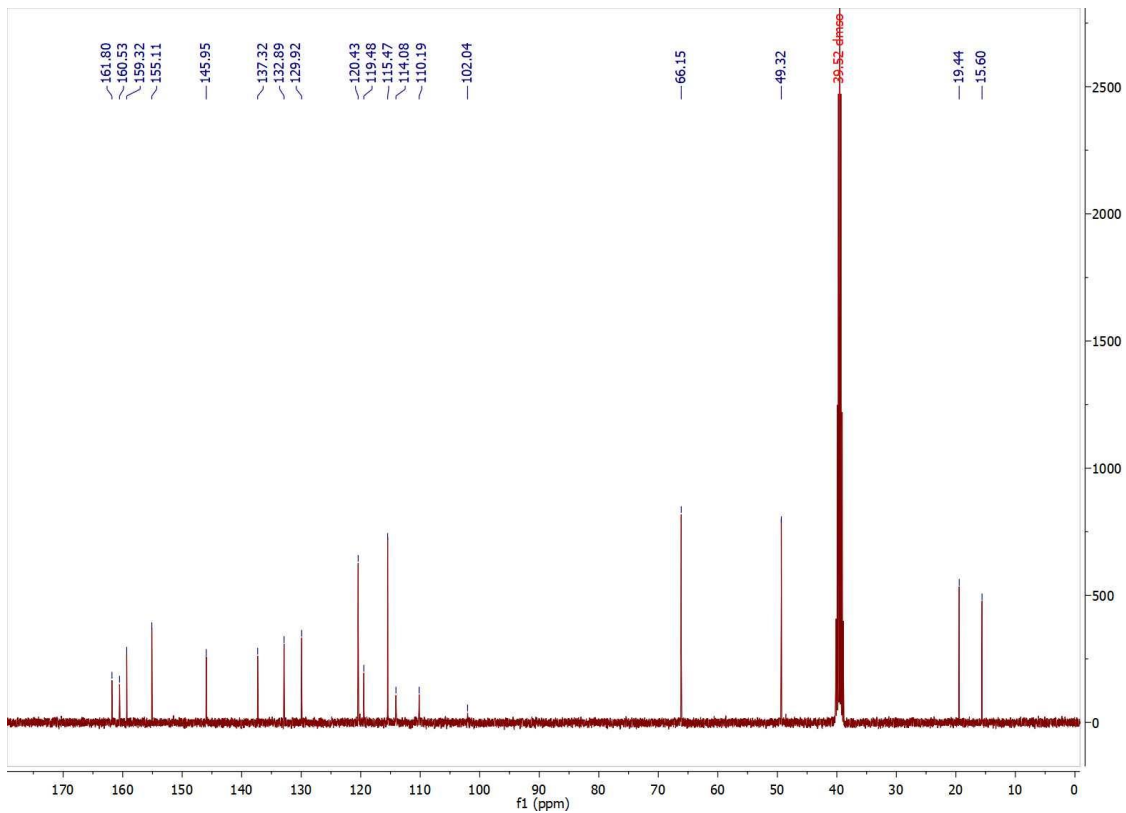


NE61pos #3-11 RT: 0.06-0.29 AV: 9 NL: 1.35E8
 T: FTMS + p NSIFull ms [150.00-1500.00]

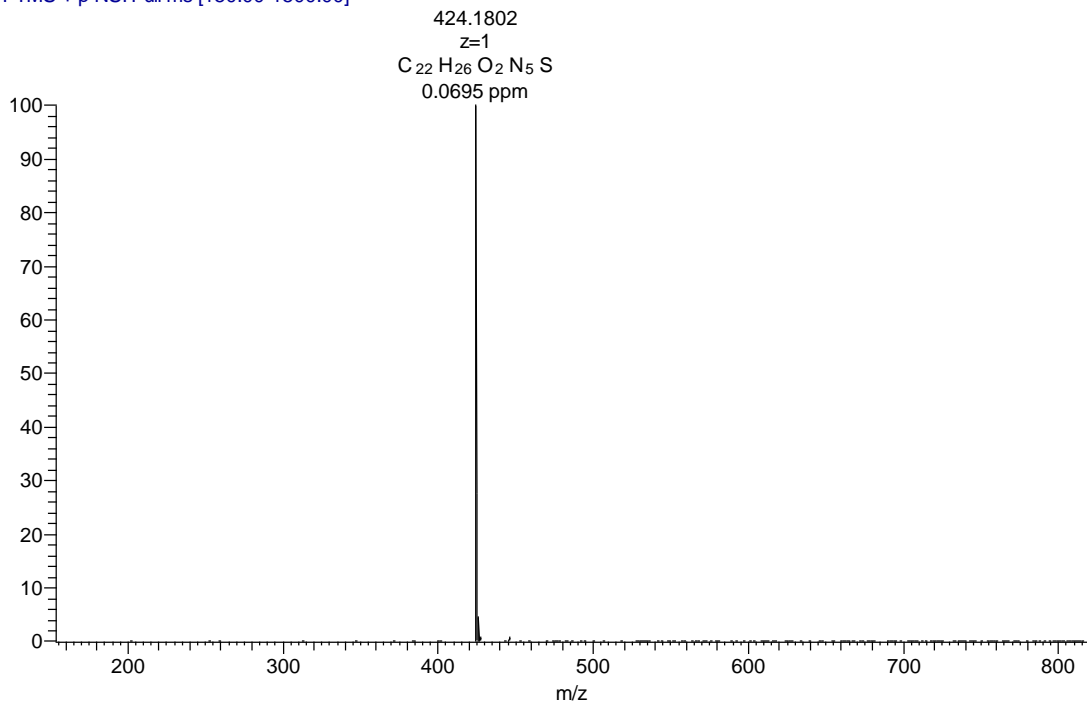


Compound 10a

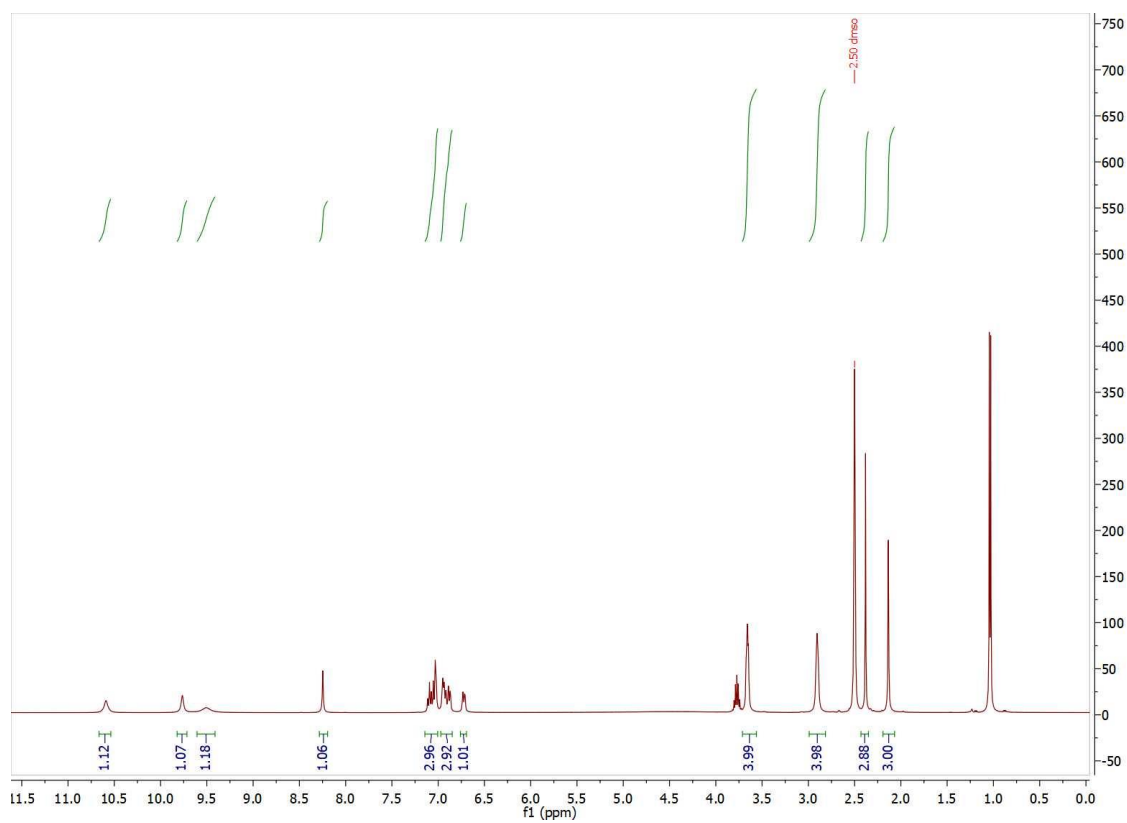
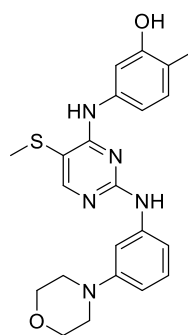


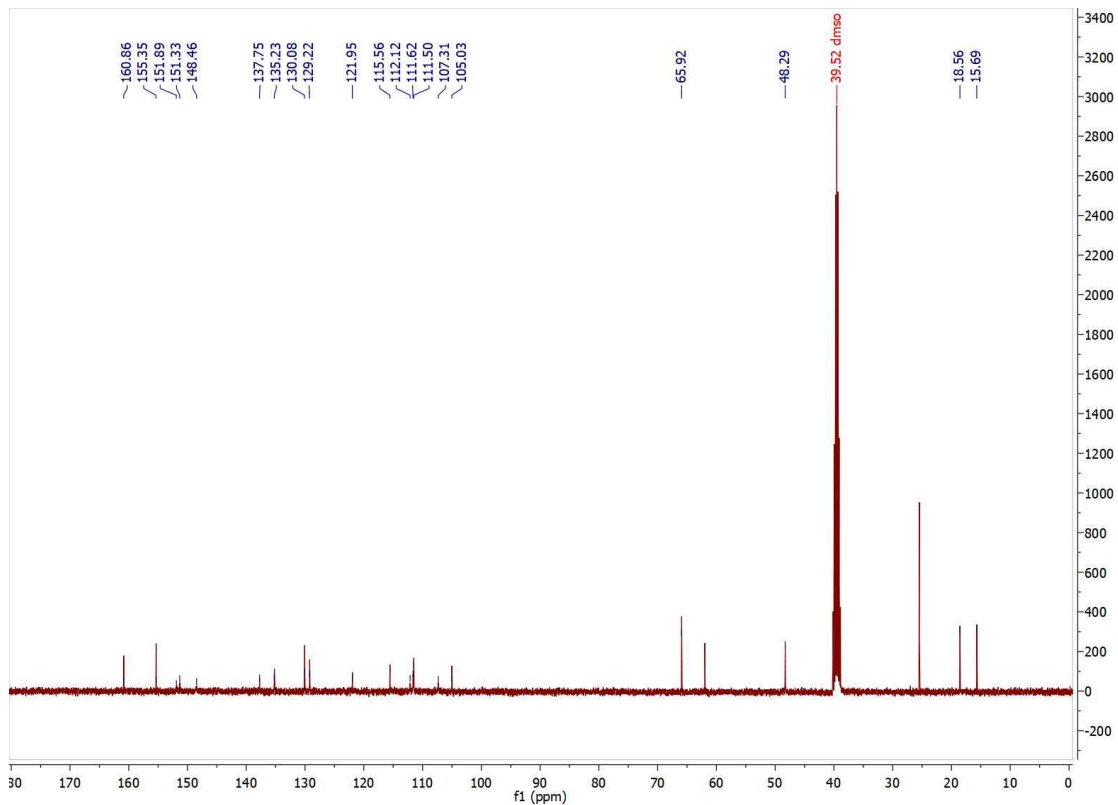


NE15pos #3-10 RT: 0.07-0.27 AV: 8 NL: 2.13E8
 T: FTMS + p NSI Full ms [150.00-1500.00]

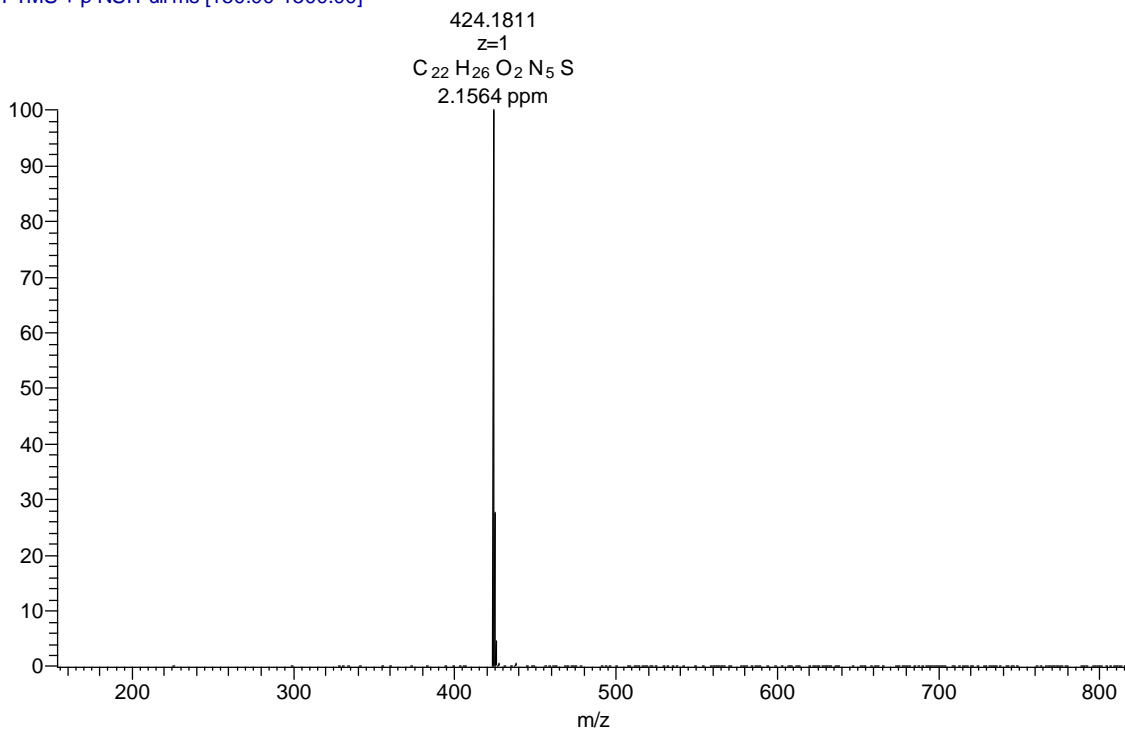


Compound 10b

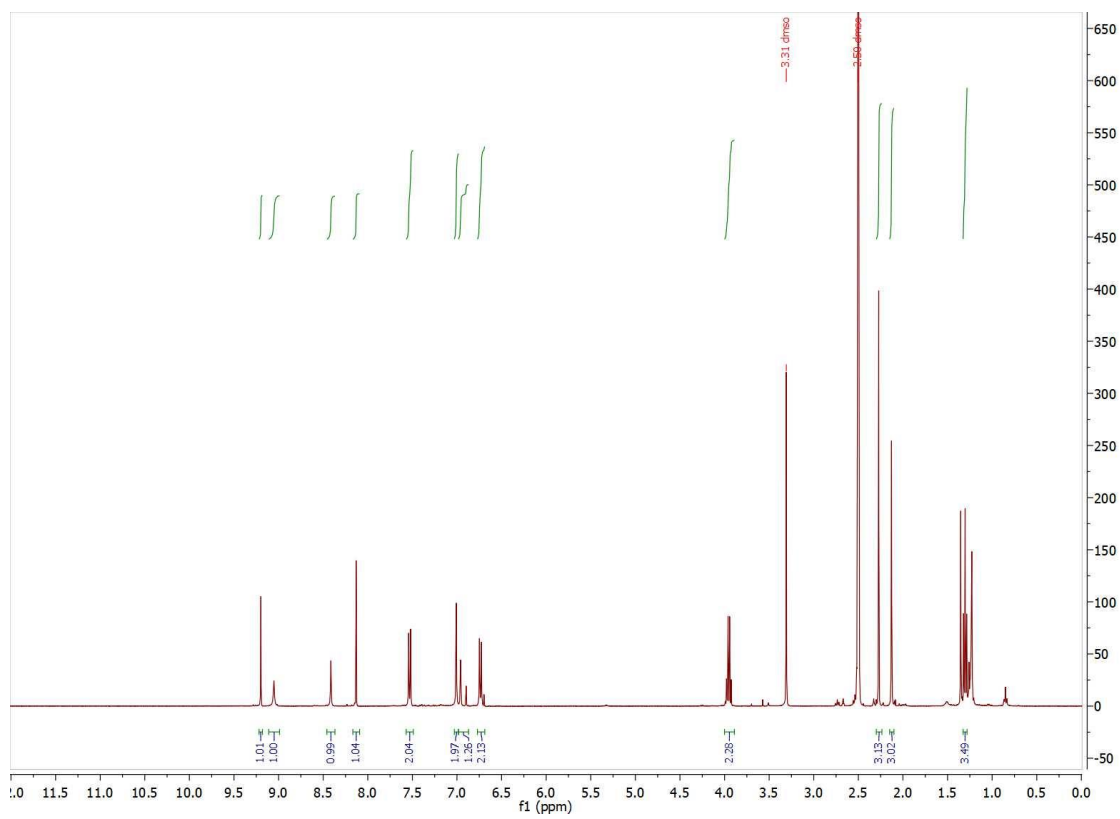
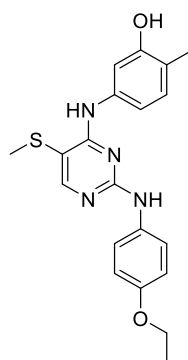




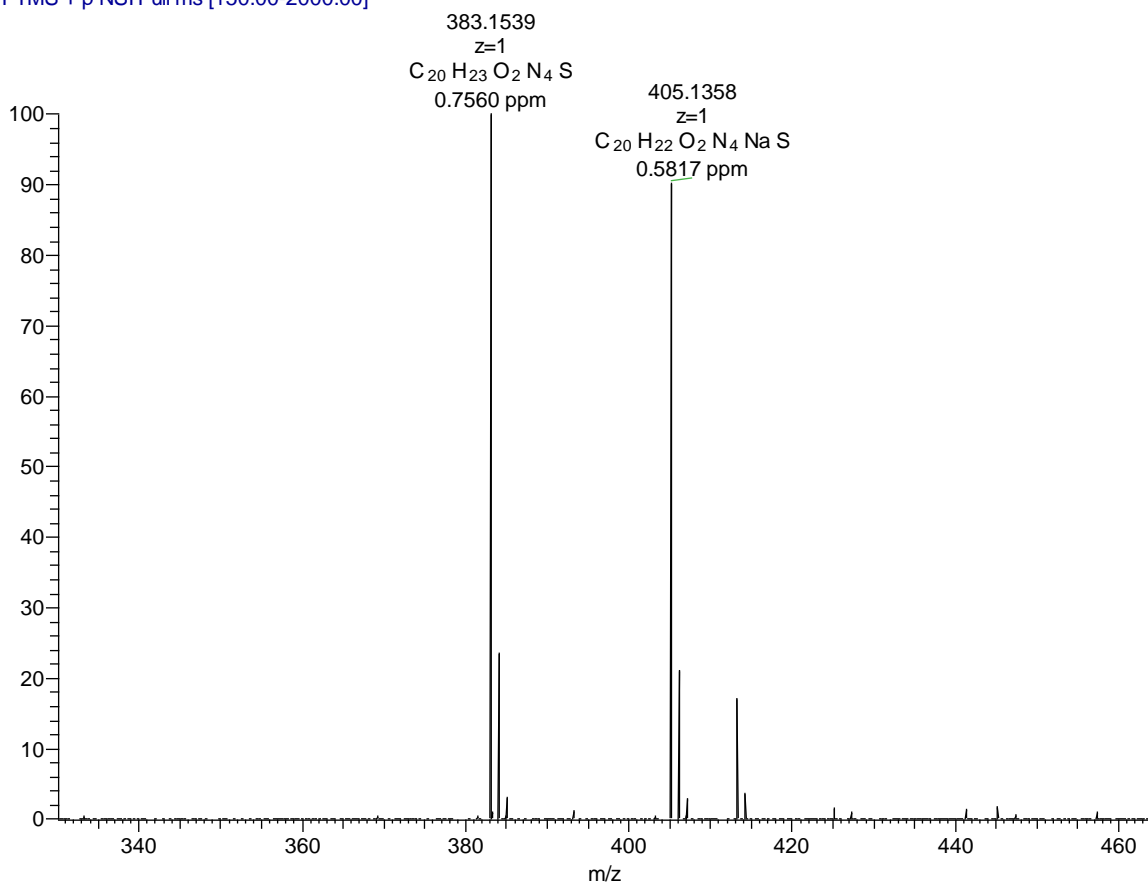
NE59pos #2-10 RT: 0.05-0.28 AV: 9 NL: 3.47E8
T: FTMS + p NSI Full ms [150.00-1500.00]



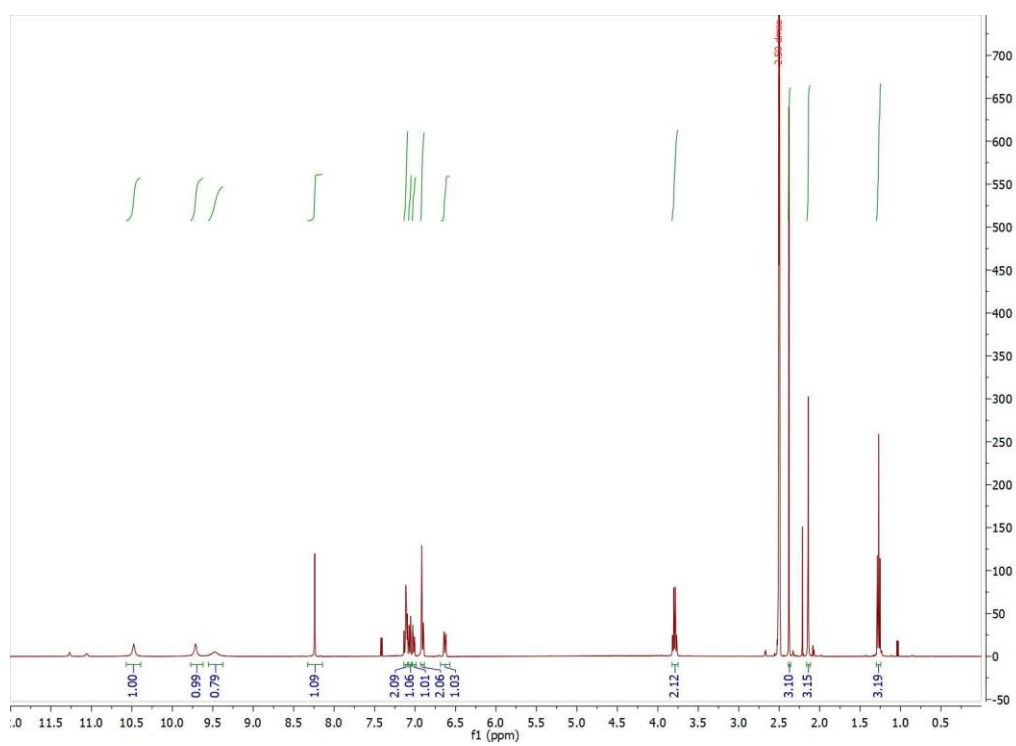
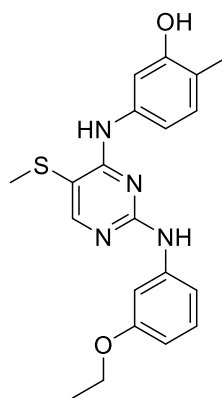
Compound 10c



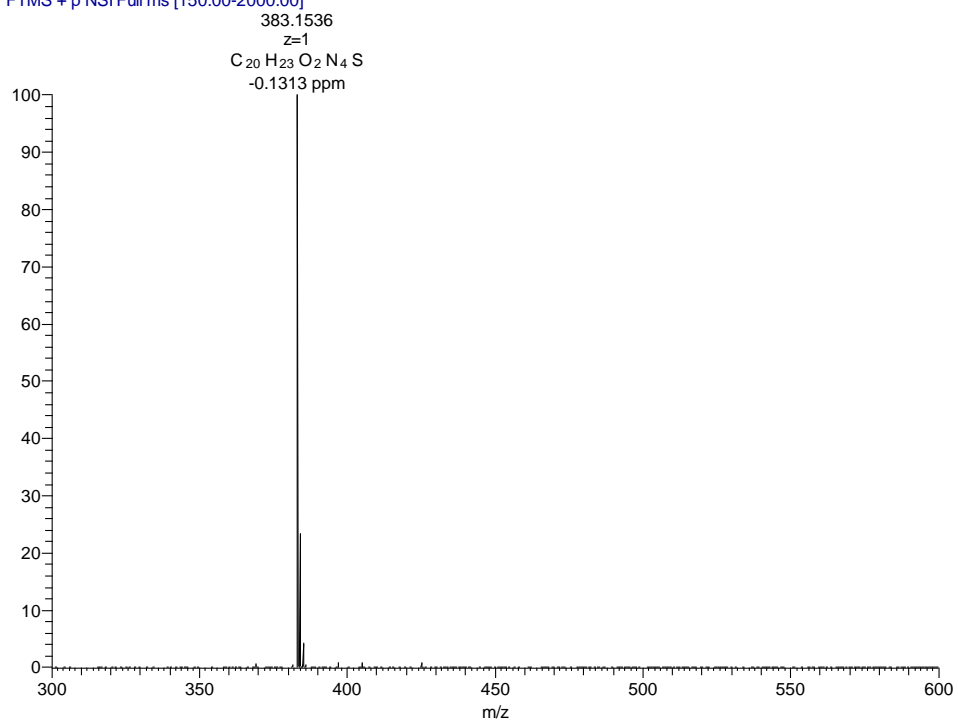
NE66 #1-13 RT: 0.01-0.45 AV: 13 NL: 3.99E5
T: FTMS + p NSI Full ms [150.00-2000.00]



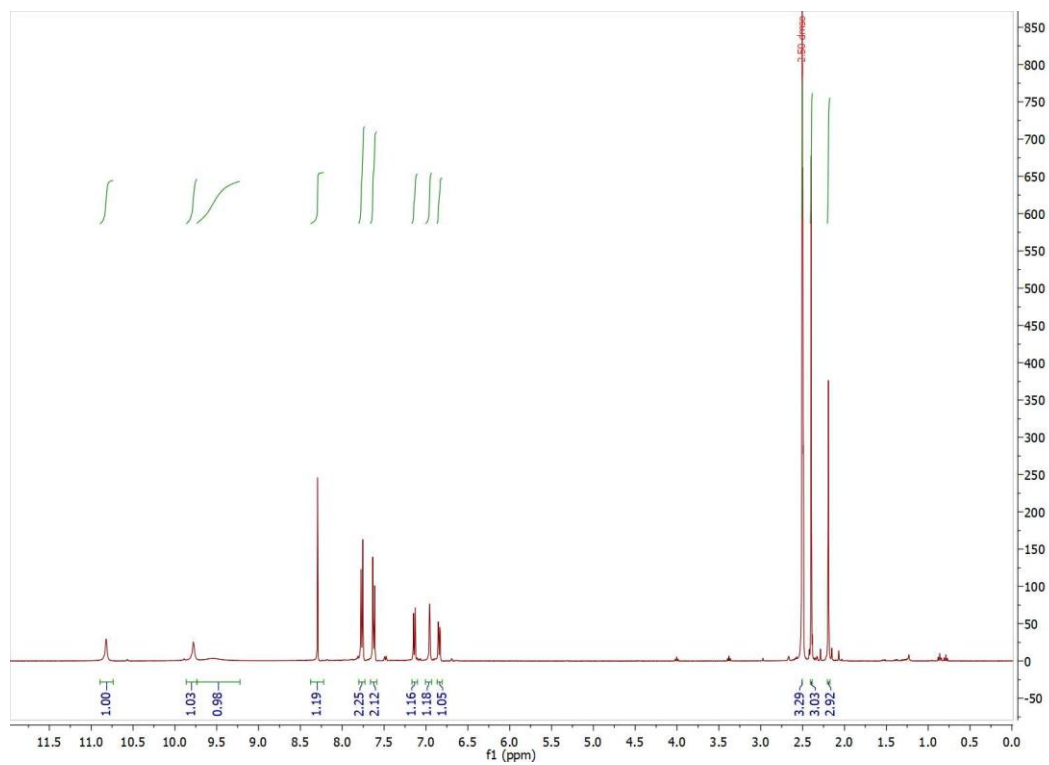
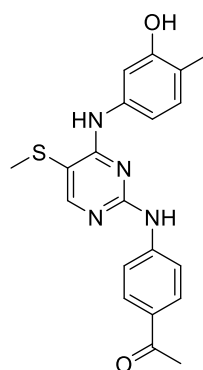
Compound 10d



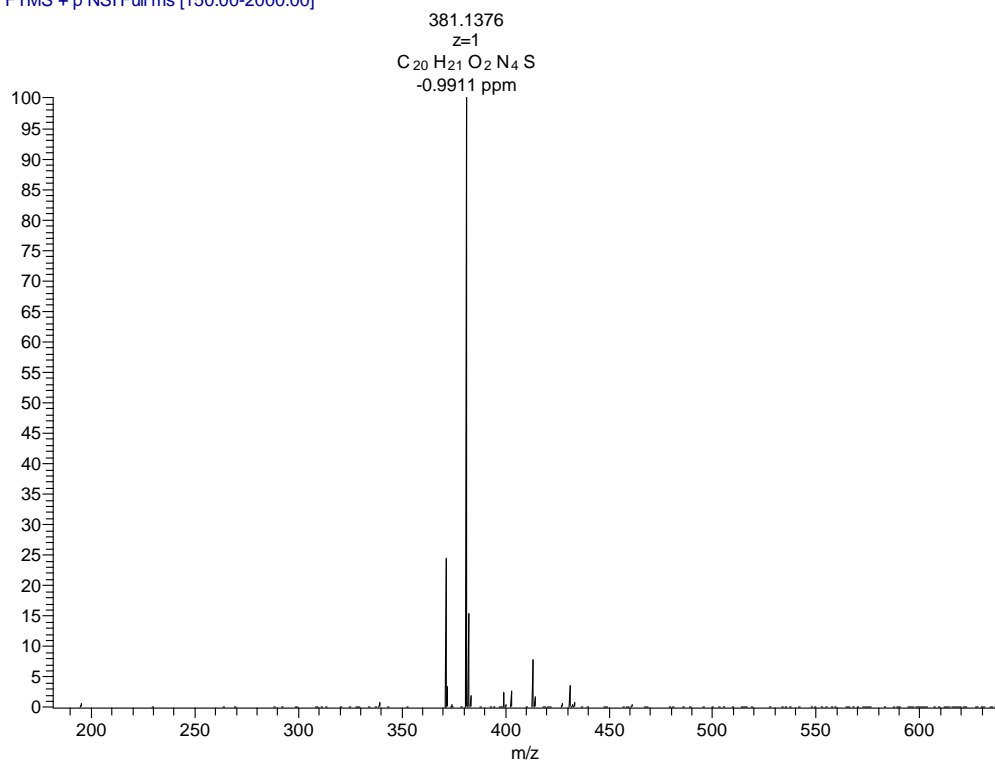
NE67 #1-12 RT: 0.02-0.42 AV: 12 NL: 1.53E6
T: FTMS + p NSI Full ms [150.00-2000.00]



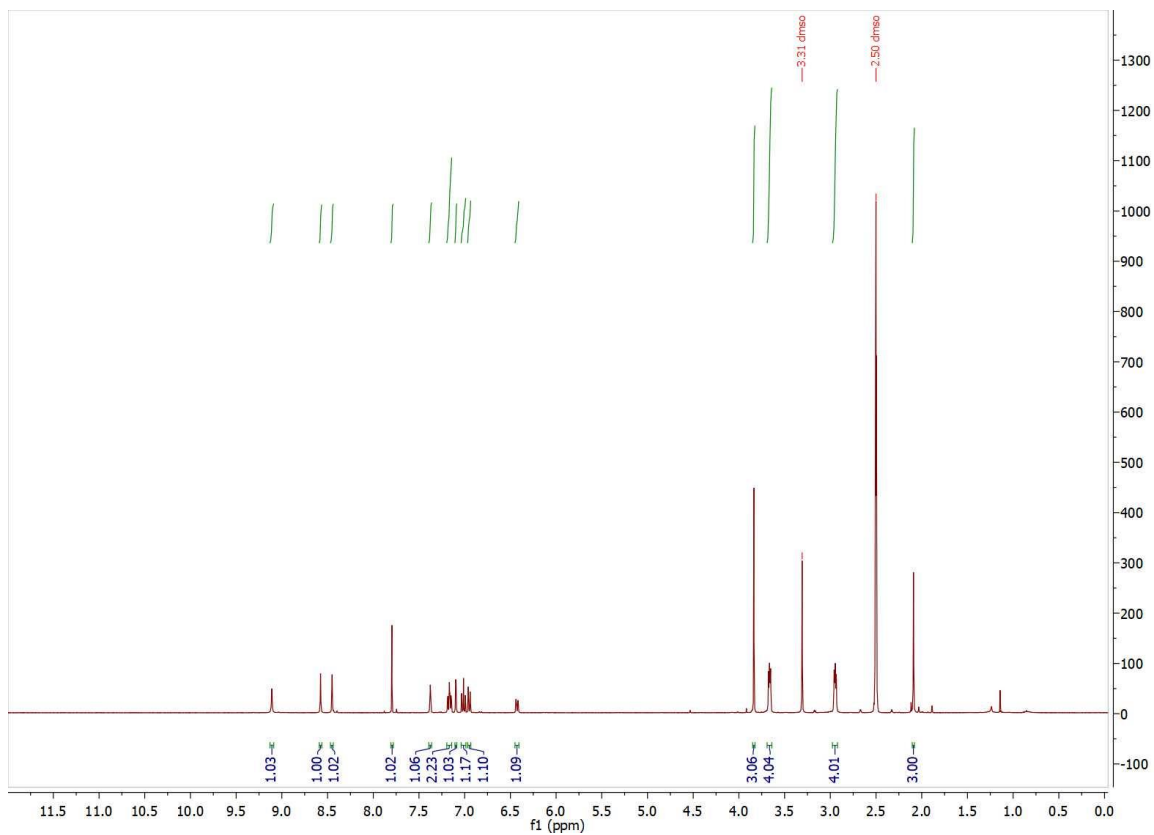
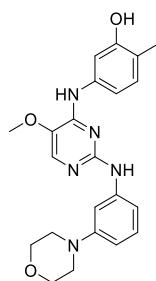
Compound 10e

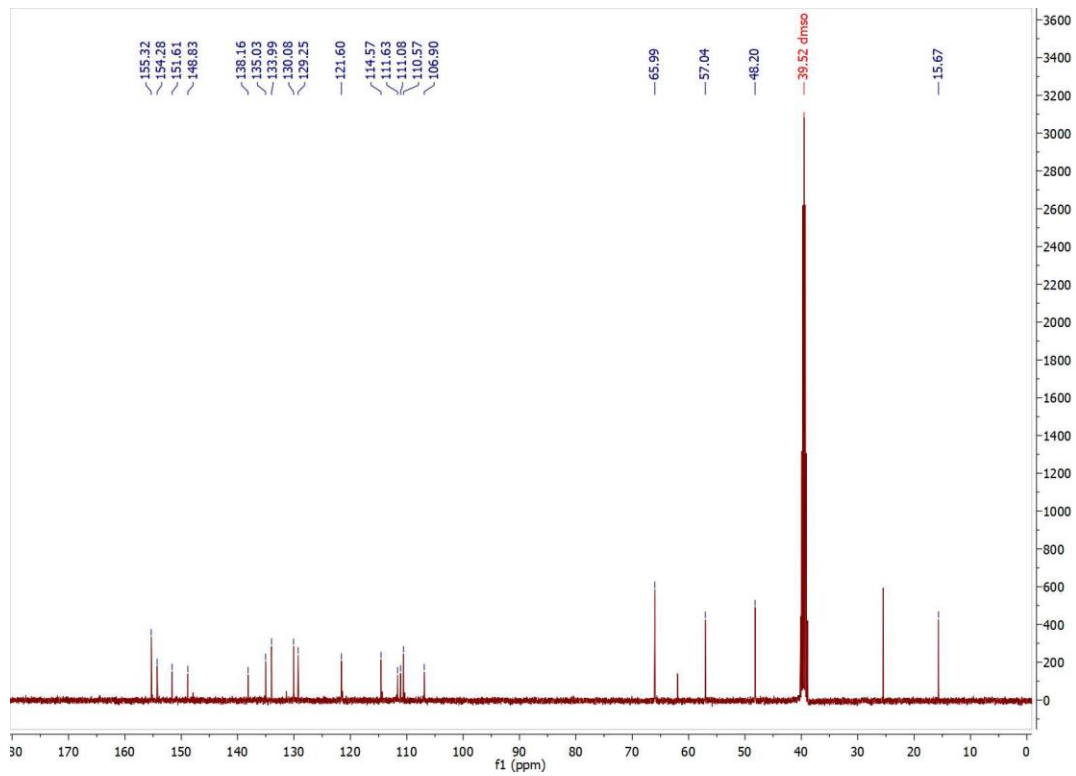


NE62 #1-14 RT: 0.01-0.49 AV: 14 NL: 3.03E4
T: FTMS + p NSI Full ms [150.00-2000.00]

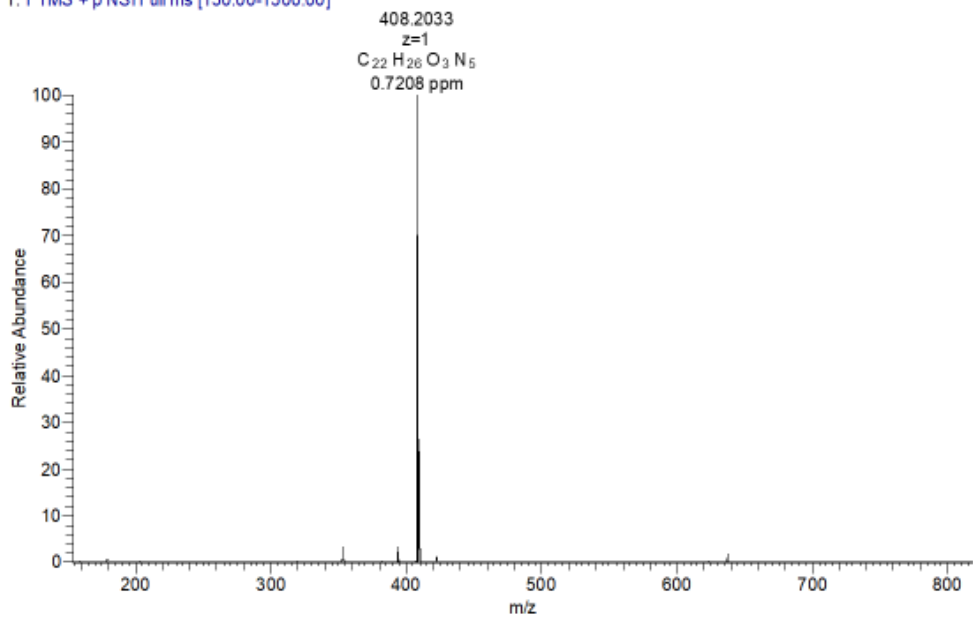


Compound 13a

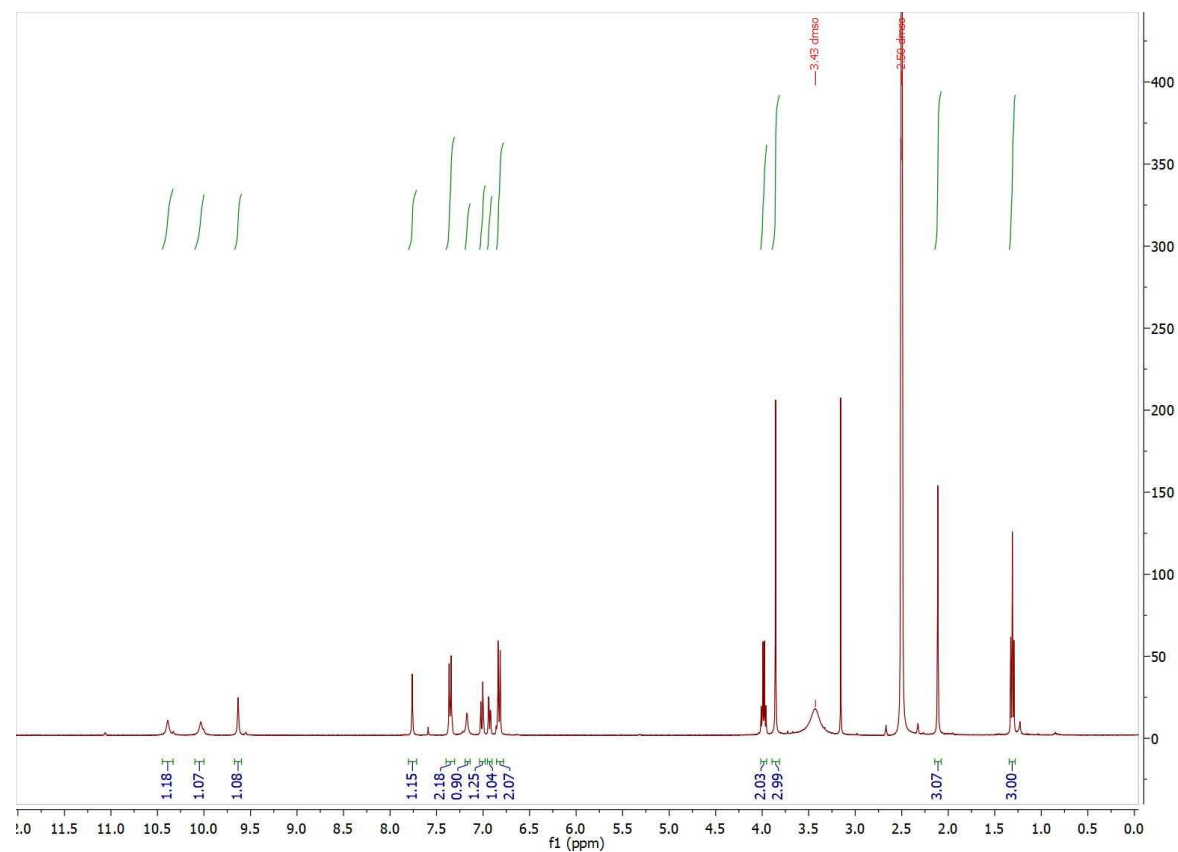
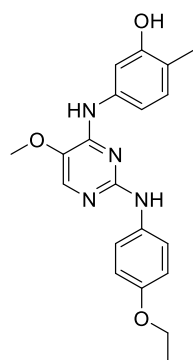


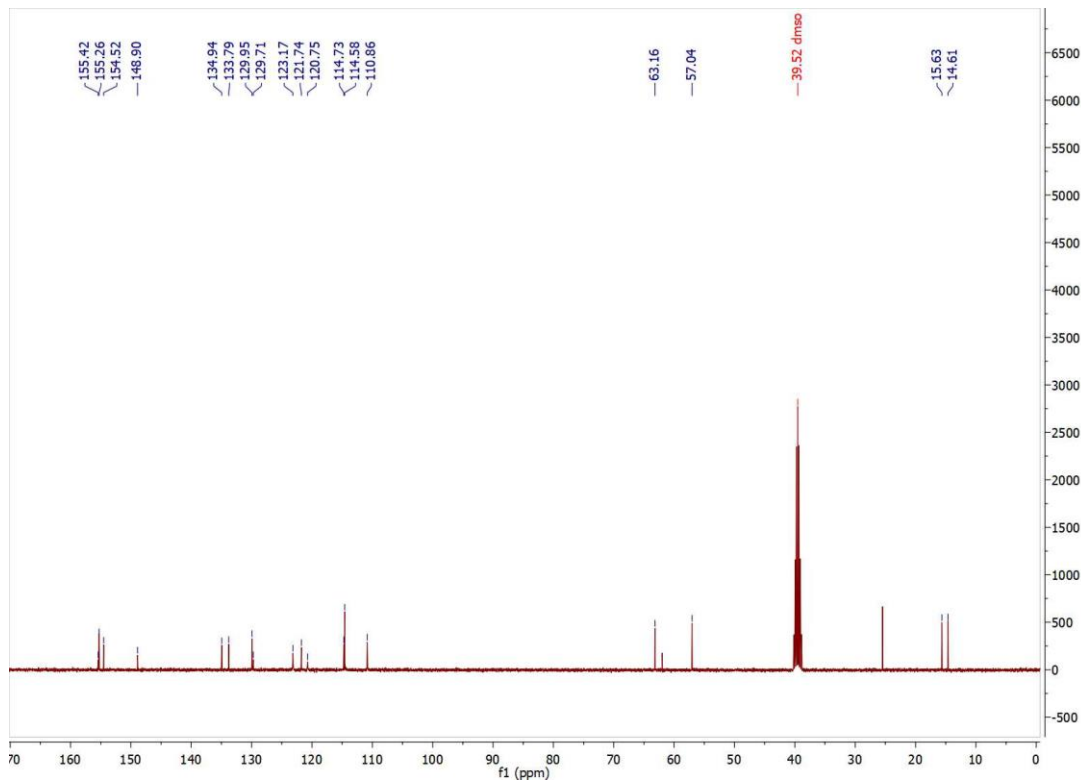


NE3pos3 #3-16 RT: 0.06-0.43 AV: 14 NL: 1.81E8
 T: FTMS + p NSI Full ms [150.00-1500.00]

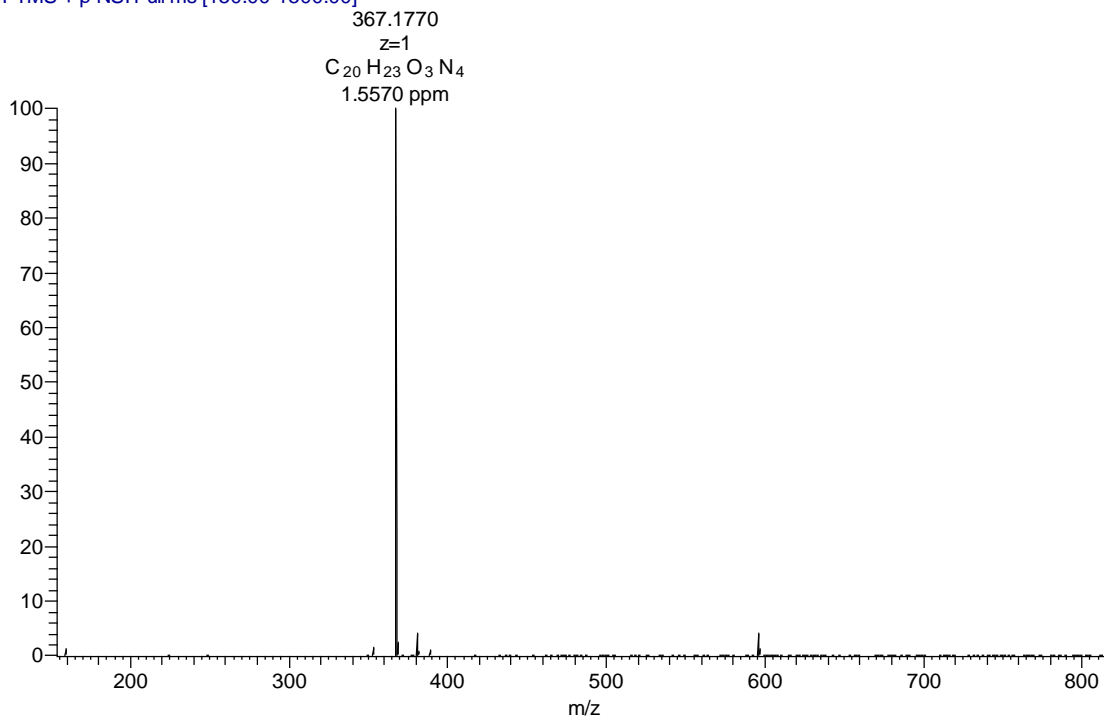


Compound 13b

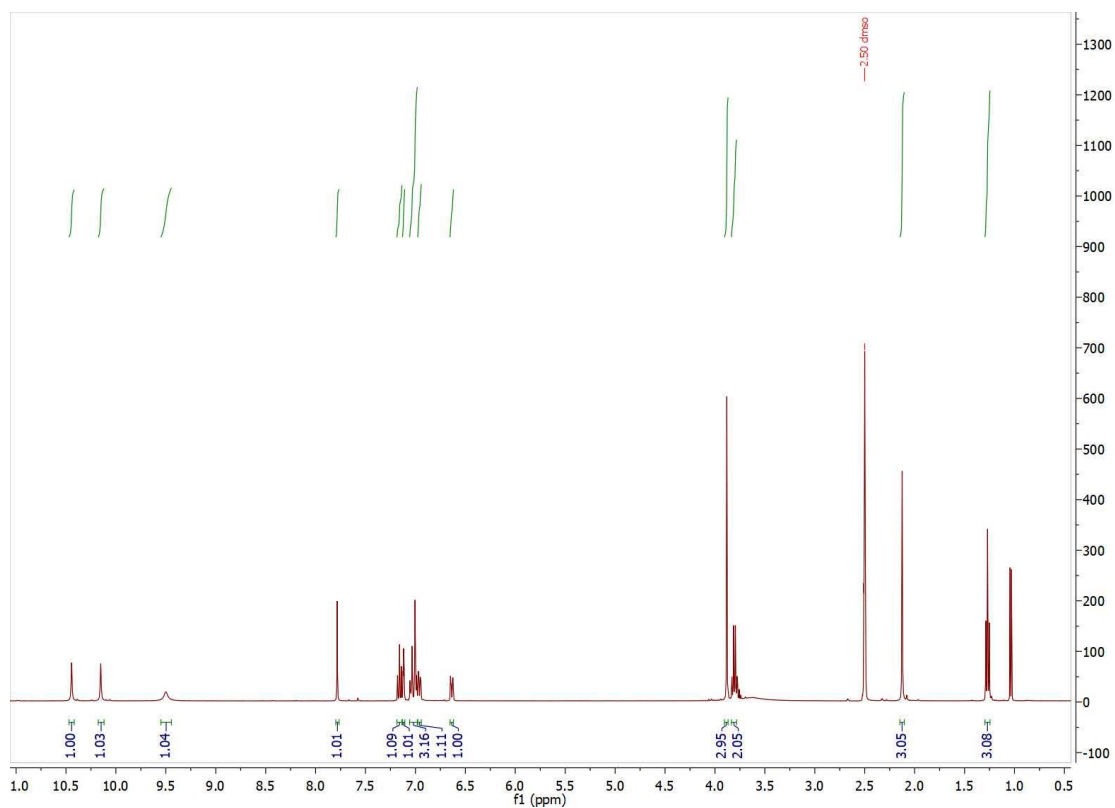
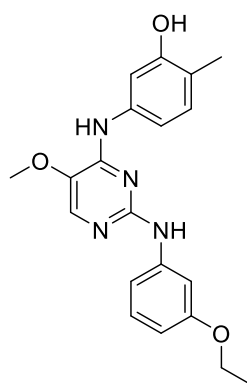


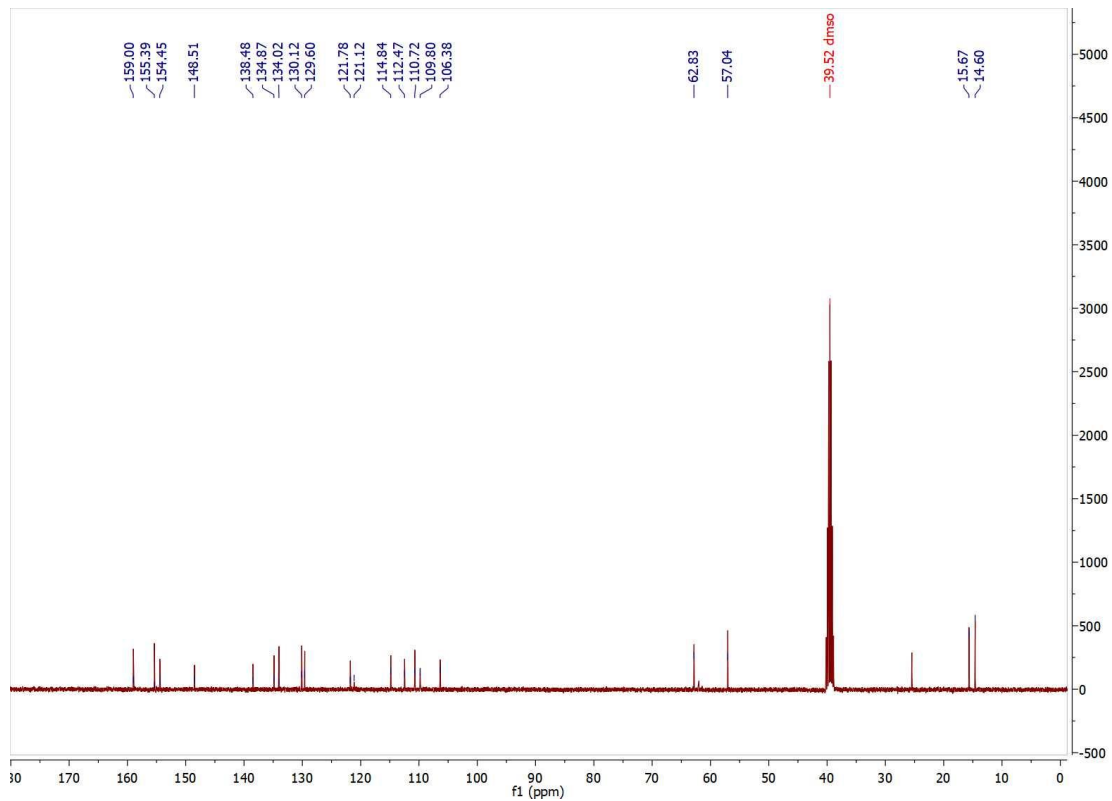


NE47pos #2-10 RT: 0.05-0.28 AV: 9 NL: 1.65E8
 T: FTMS + p NSI Full ms [150.00-1500.00]

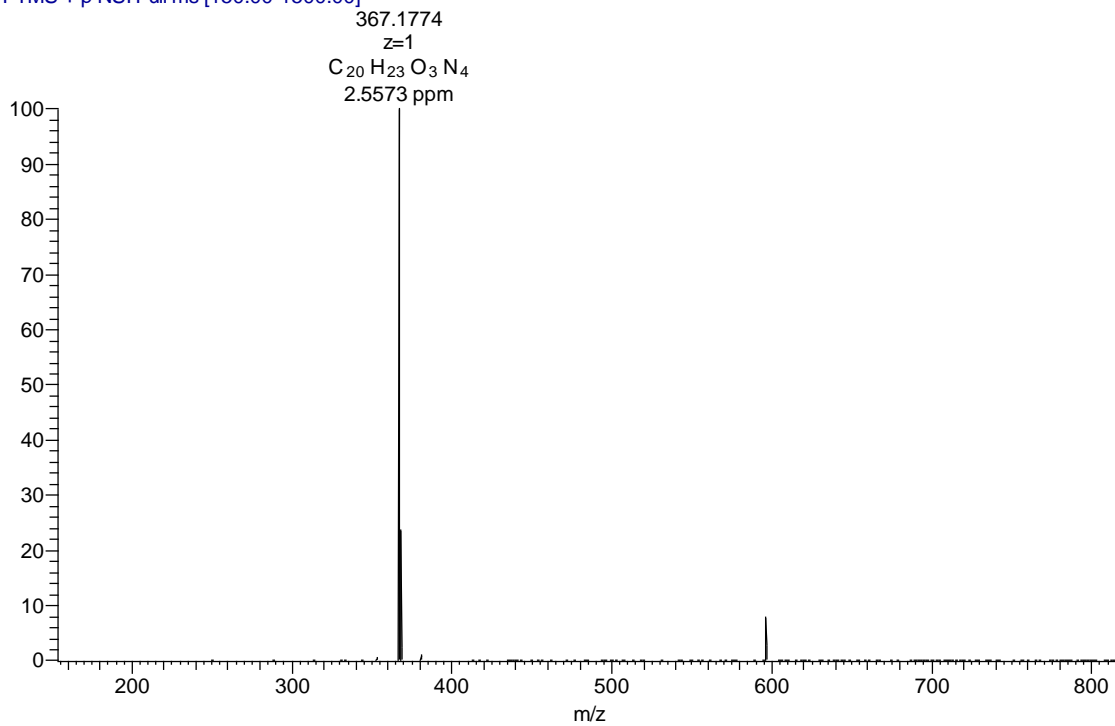


Compound
13c

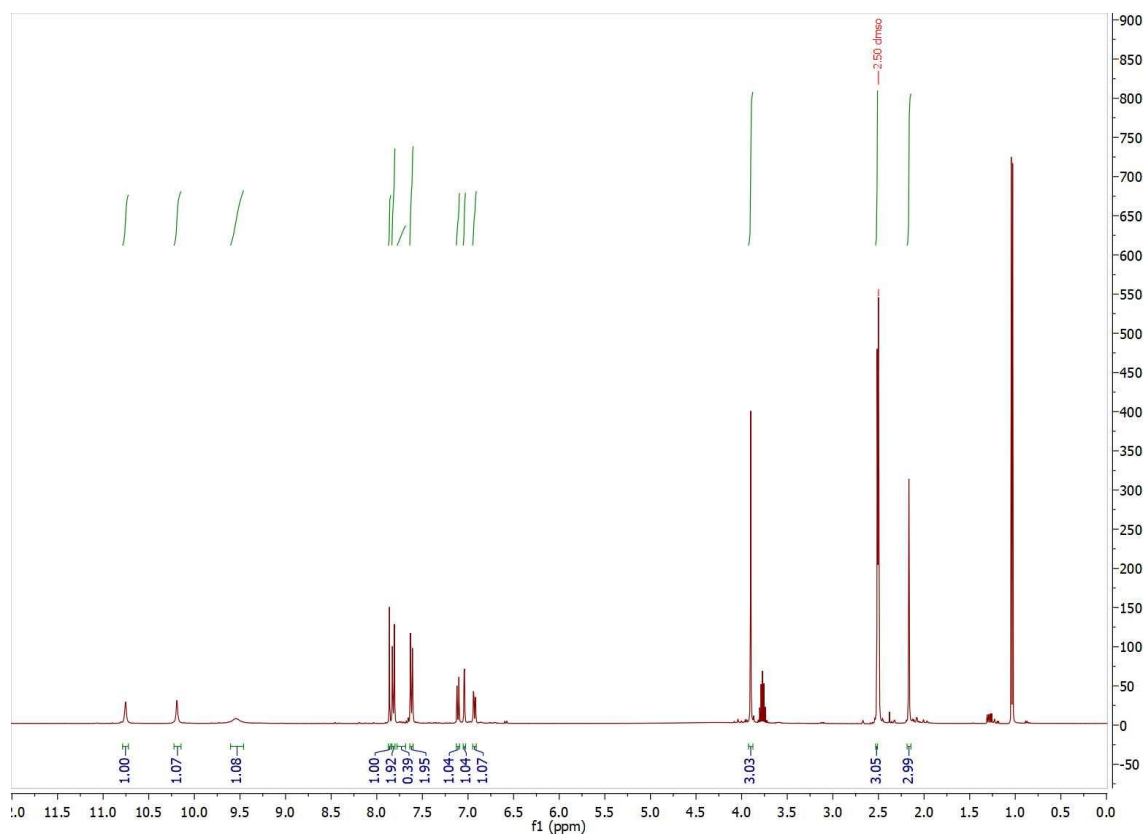
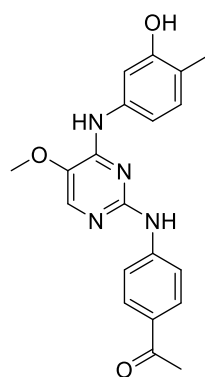


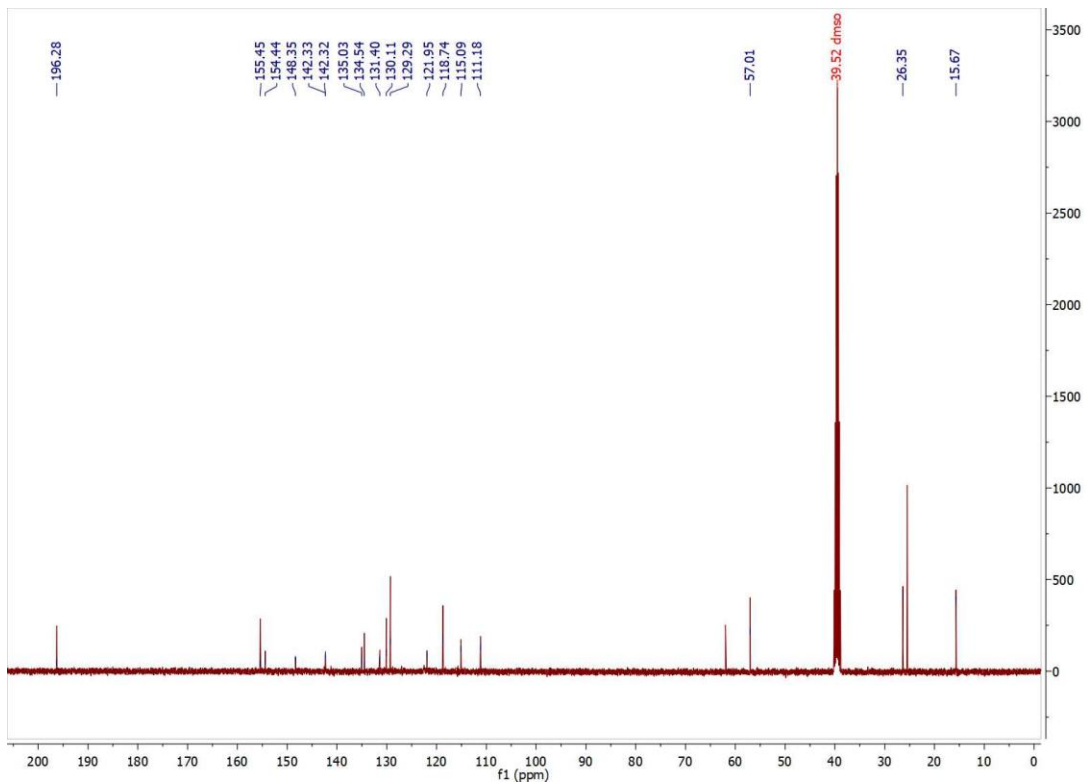


NE49pos #2-10 RT: 0.05-0.28 AV: 9 NL: 8.66E7
 T: FTMS + p NSI Full ms [150.00-1500.00]

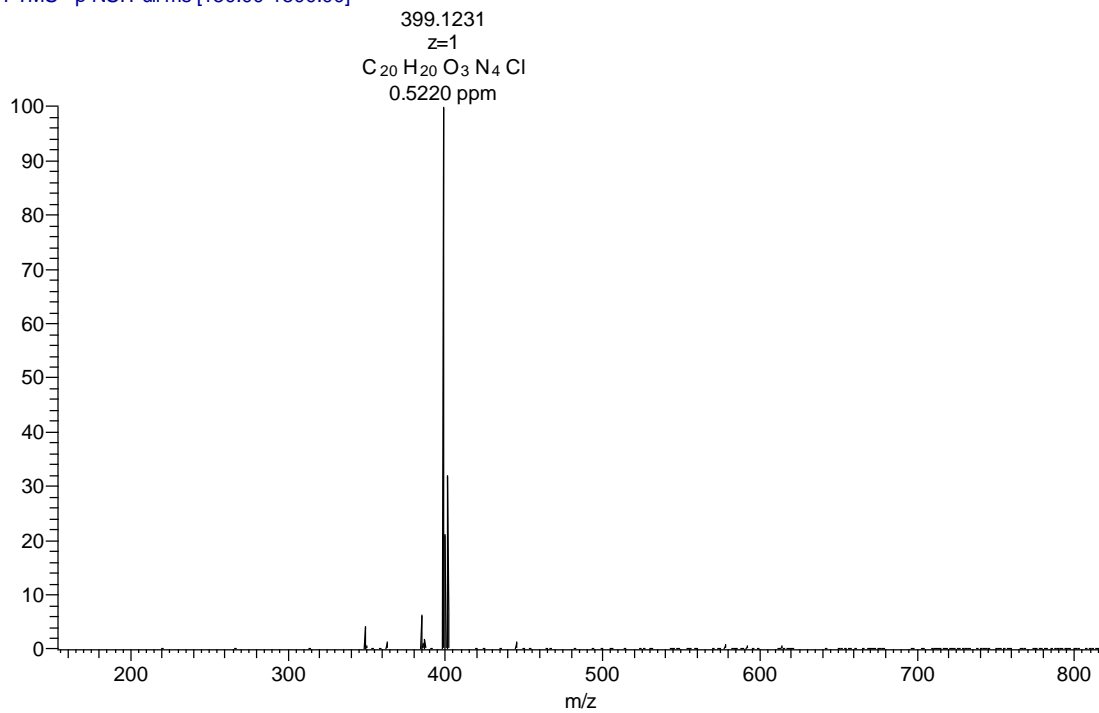


Compound 13d

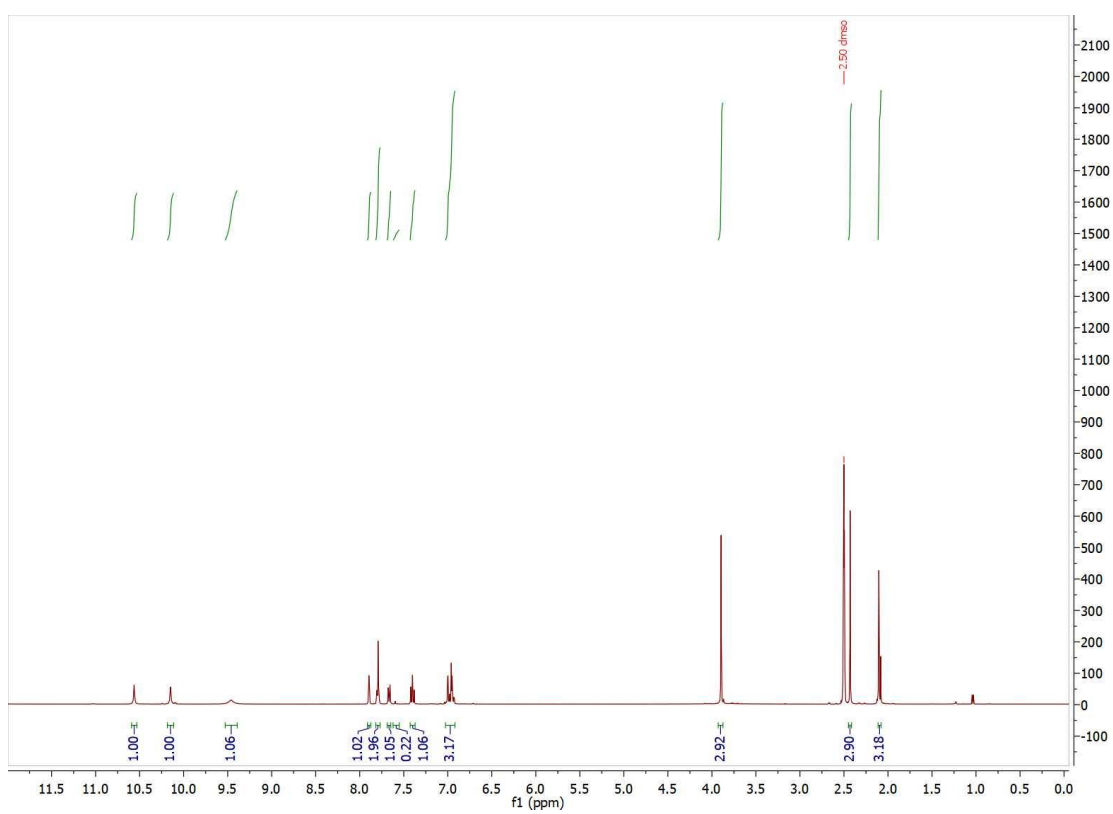
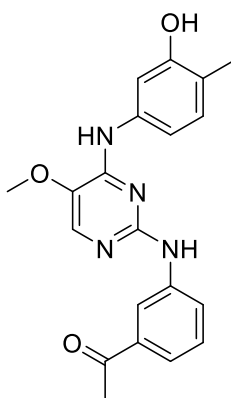


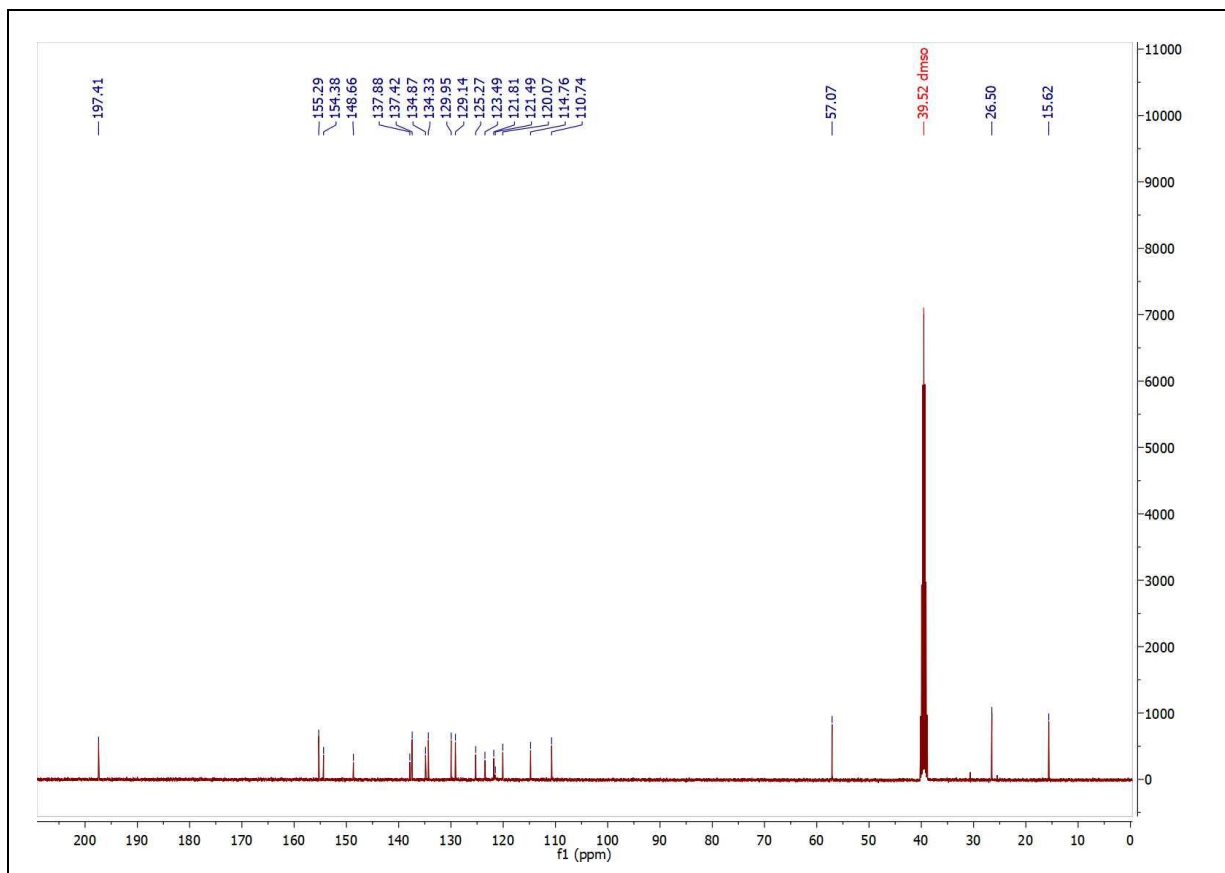


NE48neg #2-10 RT: 0.05-0.28 AV: 9 NL: 5.26E7
 T: FTMS - p NSI Full ms [150.00-1500.00]

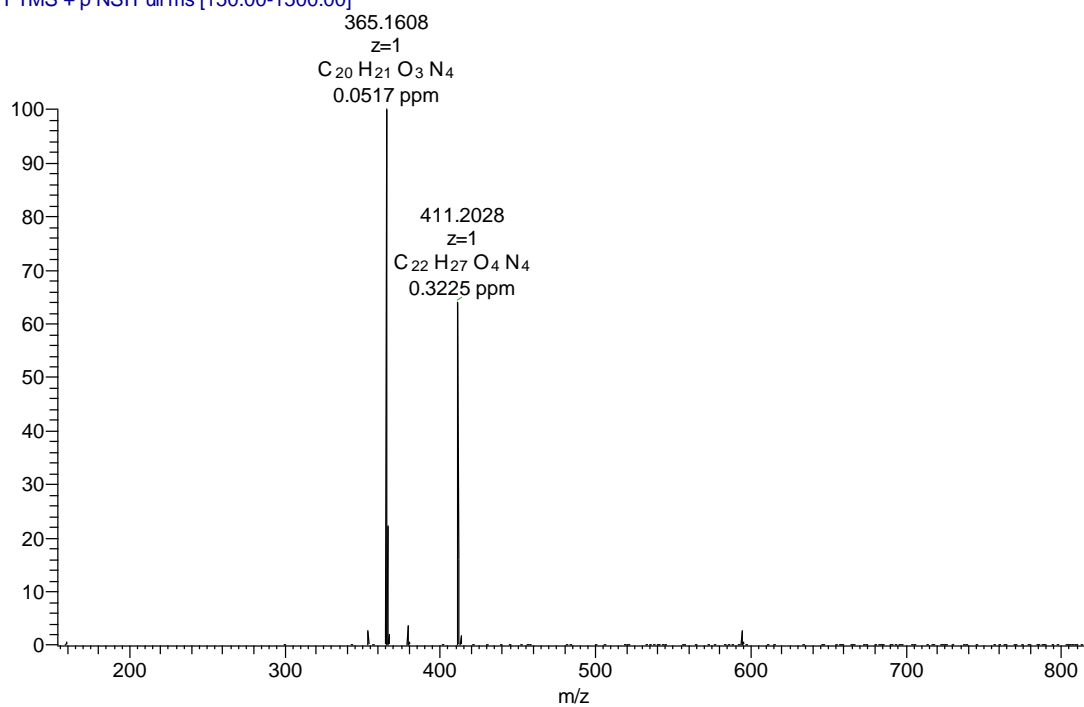


Compound 13e

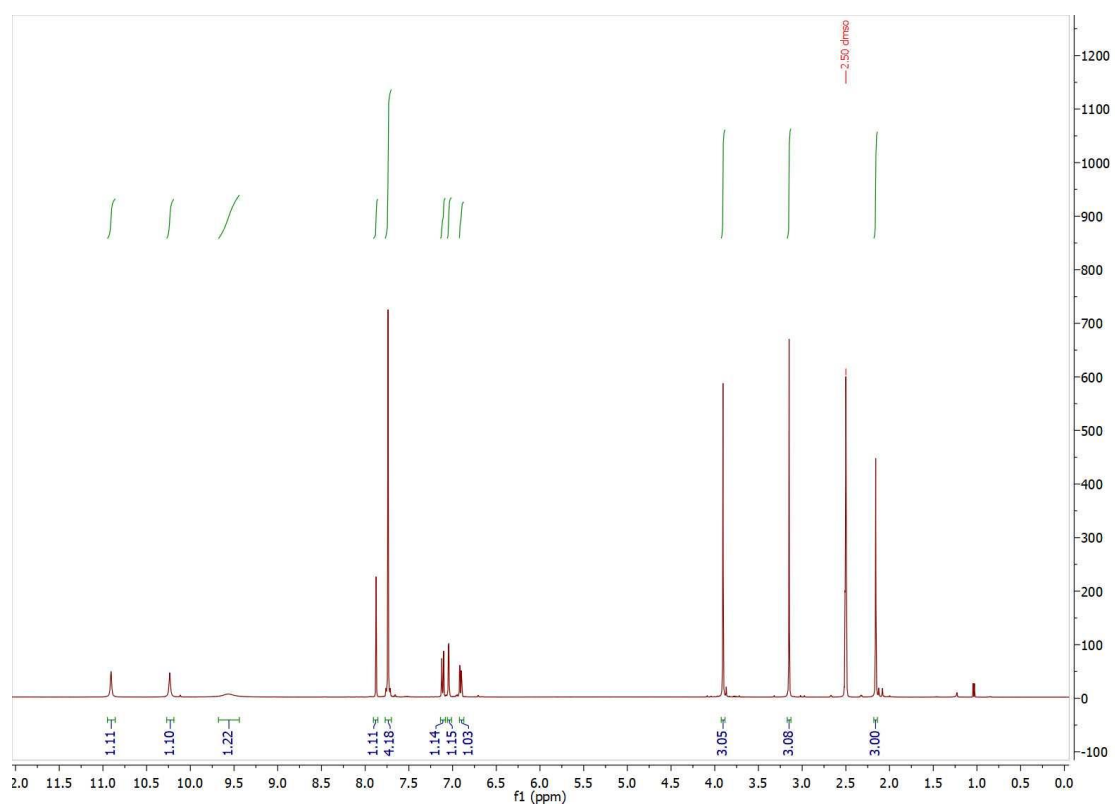
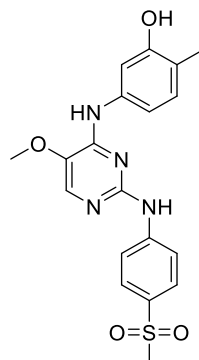




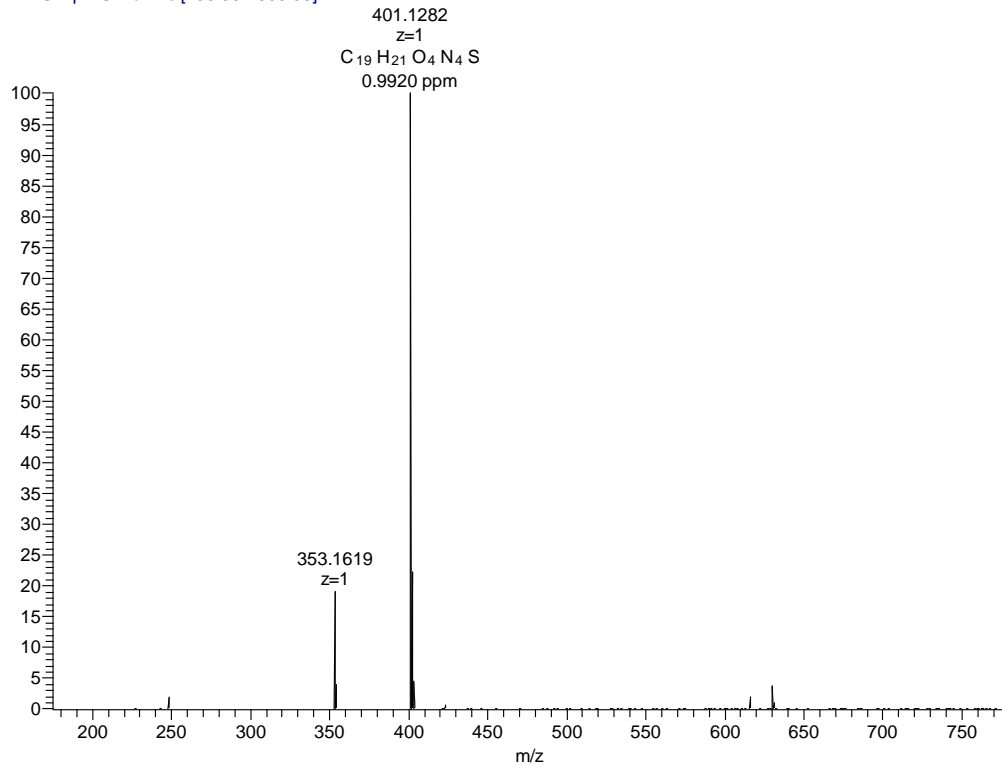
NE50pos #3-12 RT: 0.05-0.31 AV: 10 NL: 1.09E8
 T: FTMS + p NSI Full ms [150.00-1500.00]



Compounds
13f



NE38 #1-14 RT: 0.02-0.49 AV: 14 NL: 2.31E6
T: FTMS + p NSI Full ms [150.00-2000.00]



3.3. Design and synthesis of novel flexible ester-containing analogs of tamoxifen and their evaluation as anticancer agents

Nehal H. Elghazawy, Mathias Engel, Rolf W. Hartmann, Mostafa M. Hamed, Nermin S. Ahmed & Ashraf H. Abadi

Future Med. Chem. **2016**, 8, 249-56. Doi: [10.4155/fmc.15.181](https://doi.org/10.4155/fmc.15.181)

Abstract

Background: Tamoxifen (TAM) is metabolized to the more active 4-hydroxytamoxifen by CYP2D6 enzyme. Due to the genetic polymorphisms in CYP2D6, clinical outcomes of TAM treatment vary. Novel flexible TAM analogs with altered activation pathway were synthesized and were tested for their antiproliferative action on MCF-7 cell lines and their binding affinity for ER α and ER β .

Results: All compounds showed better antiproliferative activity than TAM. Compound **3** showed 80-times more ER α binding than TAM, 900-times more selectivity toward ER α . Compound **3** was tested on the entire National Cancer Institute cancerous cell lines; results indicated a broad spectrum anticancer activity.

Conclusion: The novel analogs were more potent than TAM with higher selectivity toward ER α and with potential metabolic stability toward CYP2D6.

Design and synthesis of novel flexible ester-containing analogs of tamoxifen and their evaluation as anticancer agents

Background: Tamoxifen (TAM) is metabolized to the more active 4-hydroxytamoxifen by CYP2D6 enzyme. Due to the genetic polymorphisms in CYP2D6, clinical outcomes of TAM treatment vary. Novel flexible TAM analogs with altered activation pathway were synthesized and were tested for their antiproliferative action on MCF-7 cell lines and their binding affinity for ER α and ER β . **Results:** All compounds showed better antiproliferative activity than TAM. Compound **3** showed 80-times more ER α binding than TAM, 900-times more selectivity toward ER α . Compound **3** was tested on the entire National Cancer Institute cancerous cell lines; results indicated a broad spectrum anticancer activity. **Conclusion:** The novel analogs were more potent than TAM with higher selectivity toward ER α and with potential metabolic stability toward CYP2D6.

First draft submitted: 16 September 2015; Accepted for publication: 27 November 15; Published online: 22 February 2016

Keywords: allelic variation • breast cancer • CYP2D6 • esterases • MCF7 • McMurry • metabolism • personalized medicine • SERM • tamoxifen

Breast cancer is the second most common cancer in the world and, by far, the most frequent cancer among women with an estimated 1.67 million new cancer cases diagnosed in 2012 (25% of all cancers) [1,2]. Since almost 80% of breast cancer cases are hormone-dependent, estradiol acting via the estrogen receptor (ER) plays a major role in the growth and development of (ER+) breast cancer. Endocrine therapies have played an essential role in the treatment of breast cancer and have improved the outcomes of postmenopausal women with all stages of the disease [3]. Selective estrogen receptor modulators (SERMs) are chemically diverse compounds that have been available for decades. Although they lack the steroid structure of estrogens, they possess a specific structure that allows them to bind to the ERs [4]. SERMs are known to exhibit partial agonist and antagonist properties in different tissues and organs [5,6].

TAM was the first SERM to be utilized in the treatment of metastatic breast cancer.

It is considered the most effective drug in ER-positive breast cancers. Moreover, it has shown to reduce the risk of recurrence and death when used as adjuvant therapy in early stage or in metastatic cancer [7].

TAM efficacy depends on the formation of clinically active metabolites 4-OH-TAM and endoxifen (Figure 1). These metabolites have a greater affinity to ER α and a much higher antiestrogenic potency in breast cancer cells compared with the parent drug.

The TAM metabolism is mediated via two main enzymes: CYP2D6 and CYP3A4 [8,9]. CYP2D6 is considered to have highly variable enzymatic activity; this variation has been attributed to genetic polymorphisms in the genes encoding the enzyme. Such polymorphisms can result in formation of inactive proteins that lack enzymatic activity or may lead to an enzyme with reduced activity [10–13].

This study aims to synthesize new TAM analogs having the main pharmacophoric features of TAM, yet with potential differ-

Nehal H Elghazawy^{*,1}, Mathias Engel², Rolf W Hartmann², Mostafa M Hamed², Nermin S Ahmed^{*,1} & Ashraf H Abadi¹

¹Department of Pharmaceutical Chemistry, Faculty of Pharmacy & Biotechnology, German University in Cairo, 11835 Cairo, Egypt

²Helmholtz Institute for Pharmaceutical Research Saarland (HIPS) Department Drug Development and Optimization (DDOP) Campus, C2.3Saarland University D-66123 Saarbrücken

*Author for correspondence:

Tel.: +20 227 590 715

Fax: +20 227 581 041

nermin.salah@guc.edu.eg

[†]Authors contributed equally

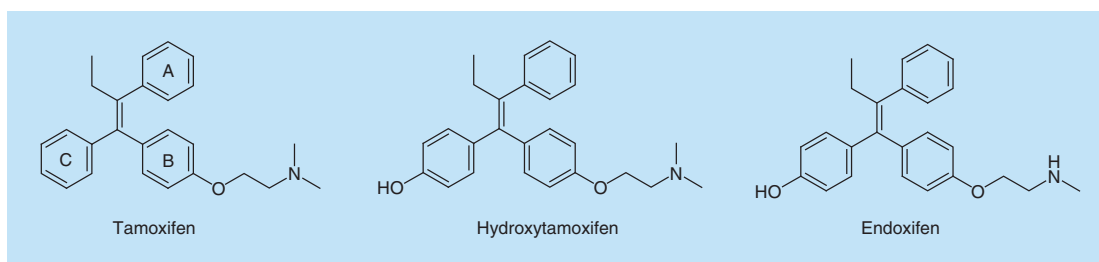


Figure 1. Chemical structures of tamoxifen, hydroxytamoxifen and endoxifen.

ent metabolic activating pathway. These novel analogs are designed to overcome the genetic polymorphism of the CYP2D6 enzyme, thus giving potential equal clinical benefits to all patients. This aim was achieved through blocking the site for metabolic *para*-hydroxylation either by hydroxy group or by ester groups, namely acetate, butanoate or decanoate. Additionally, the compounds were designed to endorse flexibility to the rigid triphenylethylene backbone through introduction of a benzylic methylene spacer between Ring A of TAM and the ethylene group, such modification is reported to increase selectivity toward ER α versus ER β , the new analogs can further reveal the nature of estrogen receptors in terms of ligand flexibility tolerance. Since the alkylaminoethoxy side chain of Ring B of TAM has been reported to be a key player for the antagonistic action of SERMs [14,15]. The novel analogs are synthesized bearing a dimethylaminoethoxy, pyrrolidinylethoxy or piperidinylethoxy side chains. The effect of cyclization, size of the cyclic structure and the effect of alteration of the basicity of nitrogen have all been extensively investigated. All novel TAM analogs were tested for their antiproliferative effect on MCF-7 cell lines as well as their binding affinity to ER α . Compounds showing highest IC₅₀ for MCF-7 cells inhibition as well as ER α binding were tested for the binding affinity to ER β and the differential selectivity between ER α and ER β was calculated (Table 1).

Results & discussion

Chemistry

Compound **1** was synthesized using standard McMurry coupling reaction of 4,4'-dihydroxybenzophenone with 1-phenyl-2-butanone using titanium tetrachloride/zinc as catalyst to give the triphenyl ethylene backbone in yield 87%. Compound **1** was confirmed from its spectral data where ¹H-NMR showed a singlet at 3.45 ppm for the benzylic CH₂, a multiplet at δ 1.94 – 1.85 and a triplet at δ 0.87 for the CH₂–CH₃. The infrared spectra of compound **1** showed a broad band at 3321.8 cm⁻¹ for the OH stretching. Moreover, the formation of the C = C has been confirmed by an absorption band at (1600–1660 cm⁻¹) [16,17].

Compound **1** was then treated with the appropriate base hydrochloride salt in the presence of potassium carbonate to form monoalkylated and dialkylated ether derivatives. Products were purified using column chromatography to provide the monoalkylated derivative **2–4** with yield 45%. The esterification of the monoalkylated compounds was then achieved via using commercially available acid chlorides in a basic medium (Figure 2). The success of esterification reaction was detected by appearing of upfield multiplets integrating for the number of alkyl protons. The infrared spectrum of all final and esterified compounds showed a peak at 1750 cm⁻¹ for (C = O) with a disappearance of characteristic OH band.

Compounds **2–13** were obtained as 1:1 mixture of *E/Z* isomers. Attempts to isolate the *E/Z* isomers using column chromatography as well as prep HPLC were not successful. The *E/Z* isomeric ratio for the products was assigned using the relative peak heights in the ¹H-NMR spectrum where all compounds displayed two signals only for the benzylic methylene protons, signals appeared as singlet δ 3.52 and 3.54.

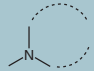
Except for the benzylic protons, all protons of both isomers appeared exactly the same chemical shift, yet integrate for double the number of protons of each pure isomer. Moreover, ¹³C-NMR confirmed the formation of isomers since most of the signals were duplicated. The duplication of signal has been previously reported by Bedford and Richardson [18].

Assessment of compounds' activity against MCF-7 cancer cell lines

For the inhibitory effect on MCF7 cell lines, all the compounds **2–13** have shown IC₅₀ values that ranged from 2.54 to <0.25 μ M that is better than IC₅₀ of TAM and 4-OH-TAM, this may be partially affiliated to the higher lipophilicity of the flexible analogs when compared with rigid TAM and 4-OH-TAM.

Compounds **5–13** bearing ester groups of different alkyl chains are hypothesized to undergo hydrolysis via esterases. MCF-7 cells have been reported to have carboxyl esterases activity, the enzyme is located entirely intracellularly and is not secreted by the MCF-7 cells [19], the novel compounds exhibit variable lipo-

Table 1. IC₅₀ of synthesized compounds on MCF-7 cells and binding to estrogen receptor.

Code		R	IC ₅₀ (μM) MCF-7 cells	IC ₅₀ (μM) ERα	IC ₅₀ (μM) ERβ	Selectivity ERα/ERβ
2	-CH ₃ , -CH ₃	----	2.12	0.00079	ND	ND
3	Pyrrolidine	----	<0.25	0.00011	>0.09	>900
4	Piperidine	----	2.51	0.00065	ND	ND
5	-CH ₃ , -CH ₃	-CH ₃	2.42	0.022	ND	ND
6	-CH ₃ , -CH ₃	-C ₃ H ₇	2.54	0.036	ND	ND
7	-CH ₃ , -CH ₃	-C ₉ H ₁₉	1.88	0.183	ND	ND
8	Pyrrolidine	-CH ₃	1.72	0.00910	0.14	15.38
9	Pyrrolidine	-C ₃ H ₇	1.60	0.036	ND	ND
10	Pyrrolidine	-C ₉ H ₁₉	1.06	0.153	ND	ND
11	Piperidine	-CH ₃	0.83	0.0225	ND	ND
12	Piperidine	-C ₃ H ₇	0.93	0.0236	ND	ND
13	Piperidine	-C ₉ H ₁₉	2.26	0.117	ND	ND
TAM			4.40	0.00808	0.18	22.2
OH-TAM			2.79	0.00058	0.1	172.4

Values are an average of at least three experiments for each concentration for MCF-7 cells and ERα and ERβ.
ND: Not determined.

philicity which in turn facilitates their uptake by the MCF-7 cells for hydrolysis. The different ester groups are expected to have different rates of hydrolysis *in vivo*.

Compound **13** with the most lipophilic decyl group did not show the highest growth inhibition effect, this may be attributed to the fact that esterases are intracellular enzymes in the MCF-7 cell lines; no experimental data are available neither to quantify the exact amount of test compounds exposed to esterase effect, nor to determine its amount that was solubilized in the aqueous media during the *in vitro* assay. Since the IC₅₀s of compounds **7**, **11–13** were lower than their hydroxyl derivatives **2** and **4**, thus the activity may be referred to the whole intact molecule rather than the hydroxyl precursor, nevertheless a mixed effect is also possible.

Regarding the nitrogenous side chain, it seems that incorporating the terminal nitrogen in a cyclized form provides higher potency, compounds **8–13** versus **5–7**, increasing the basicity of the amino group seems to enhance the growth inhibition activity.

NCI assay results for compound 3

Compound **3** (NSC 783098) showed an IC₅₀ <0.25 μM on MCF7 cell line. The compound has been further tested for its *in vitro* antitumor activity against 60 human tumor cell lines by the National Cancer Institute, three response parameters (GI₅₀, TGI and LC₅₀) were calculated for each cell line; most sensitive tumor cell lines were reported versus TAM (NSC-180973) as control (Table 2).

Compound **3** exhibited GI₅₀ = 0.02 μM on MCF-7 human breast cancer cell lines, this value is 60-times higher than TAM GI₅₀ = 1.25 μM, compound **3** was of broad spectrum activity with higher selectivity toward MCF-7. The only selectivity was for MCF-7 cells within the breast cancer cells subpanel. Compound **3** depicted antiproliferative activity on MDA-MB-231 (ER-) breast cancer cell line. The three measured parameters (GI₅₀, TGI and LC₅₀) indicated that compound **3** still exhibits an appreciable activity indicating their ability to induce ER-independent cell death. Compound **3** still exhibits an appreciable activity indicating their ability to induce ER-independent cell death in a similar fashion to TAM; previous reports stated that TAM can potentially affect cellular functions by binding to calmodulin [20] or inhibiting protein kinase C [21,22], it has been studied for its ability to inhibit cell growth and induce apoptosis independently of the presence of ER. Moreover other targets have been identified that could account for its cytotoxicity, mainly through binding to microsomal antiestrogen binding site and inhibiting cholesterol esterification, this has been linked to TAM ability to induce breast cancer cell differentiation, apoptosis and autophagy independently of the presence of ER [23–25].

Assessment of compounds' estrogen receptor binding affinity

A competitive ER binding assay was carried out for the novel compounds. Ligand-binding affinity of the

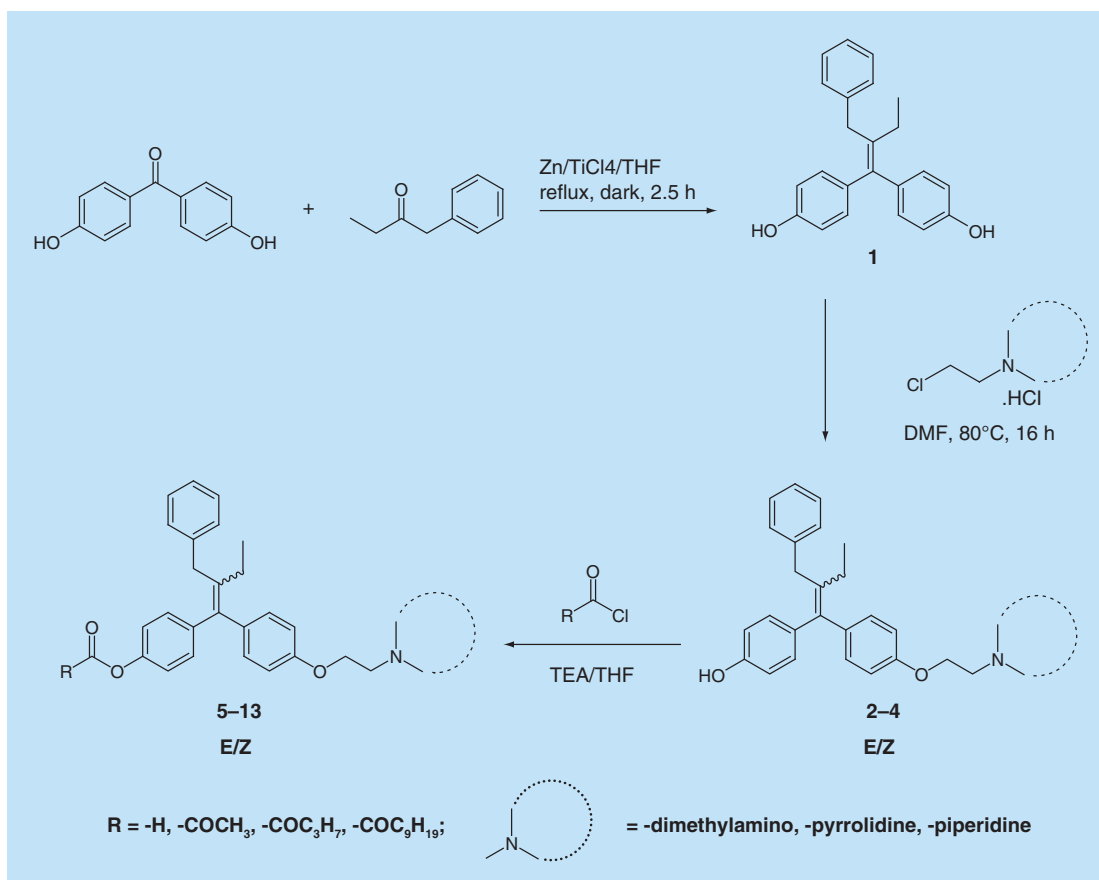


Figure 2. Synthesis of flexible tamoxifen analogs.

specified compounds for ER α is determined (Table 1). The three hydroxylated compounds 2–4 showed lower IC₅₀ values than TAM (IC₅₀ = 8 nM), and are nearly equipotent to 4-OH-TAM (IC₅₀ = 0.5 nM) except for compound 3 with (IC₅₀ = 0.1 nM), this indicates that

introducing flexibility to the triphenylethylene scaffold, together with a cyclic basic pyrrolidine substituent have contributed to better ER α binding. Comparing the three flexible analogs 2–4 reveals an essential role for the basic nitrogen, where compound 3 bearing

	Cpd	SR [†]	EKVX [‡]	HCT15 [§]	SNB-75 [¶]	LOX IMVI [#]	SK-OV3 ^{**}	A498 ^{**}	MCF7 ^{§§}	MDA-MB-231 ^{§§}	T-47D ^{§§}
GI ₅₀	3	1.35	1.44	1.50	1.30	1.60	1.70	1.20	0.02	3.90	1.20
	TAM	5.01	7.9	5.01	6.32	3.98	10	3.16	1.25	2.1	3.16
TGI	3	3.20	2.89	3.78	2.98	3.05	3.32	2.72	2.22	4.05	3.32
	TAM	79.4	19.95	10.00	12.58	7.94	15.84	6.30	6.31	12.59	10.00
LC ₅₀	3	7.54	5.78	6.26	6.79	5.76	6.34	5.85	6.13	7.79	8.80
	TAM	251	39.81	19.95	25.11	15.84	31.62	12.58	19.95	25.11	19.95

Data obtained from National Cancer Institute's *in vitro* disease-oriented human tumor cell screen (see reference [26,27] for details)

[†]Leukemia.
[‡]Non-small-cell lung cancer.
[§]Colon.
[¶]CNS.
[#]Melanoma.
^{**}Ovarian.
^{**}Renal.
^{§§}Breast cell lines.
 TAM: Tamoxifen.

the most basic nitrogen in its pyrrolidine ring has the highest binding affinity whereas compound **2** bearing the least basic dimethylamino group has the lowest affinity ($IC_{50} = 0.7$ nM), thus cyclization and a readily protonated basic nitrogen should allow better interaction with the ER, the results showed that for the hydroxylated analogs the base change does not have a dramatic effect on the binding affinity whereas it has a pronounced effect on growth inhibitory activity. Compound **3** (most active hydroxylated analog) and compound **8** (most active esterified analog) were tested for their binding affinity to ER β ; both compounds showed better binding to the ER α . Compound **3** showed 900-times more binding affinity to ER α versus ER β . All the ester containing compounds **5–13** have shown a lower binding affinity for the ER α than that of TAM and 4-OH-TAM except for compounds **8** which was equipotent to TAM ($IC_{50} = 9$ nM). The less binding affinity can be interrelated to the lack of esterases in the *in vitro* binding assays leading to lack of formation of hydroxylated analogs or endoxifen like structures. However, such lack does not affect the IC_{50} s of MCF7 cells as shown above.

In silico study

The mode of binding of the novel compounds **3** and **8** (highest ER α binding affinity) was investigated through a brief computational docking study using MOE.2009. The crystal structure used in the dock-

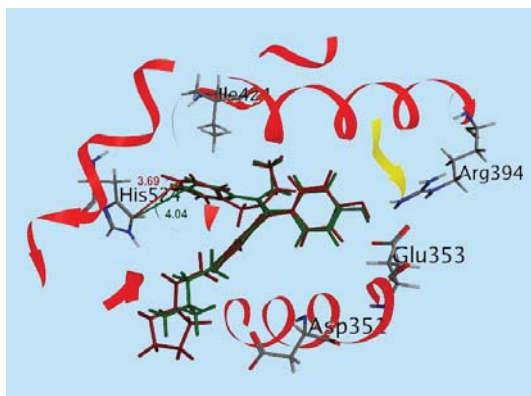


Figure 3. Overlay of compound **3 (red) on 4-OH-TAM (green).**

ing studies was obtained from the co-crystallization of ER α with 4-OH-TAM as found in the PDB database (PDB: 3ERT) [28]

The docked geometry for compound **3** showed that incorporation of the additional methylene group still allows the compounds to adopt the required arrangement for binding in an established antiestrogenic mode; this is confirmed by a nearly complete overlap of the docked geometries for **3** and 4-OH-TAM (Figure 3). The only difference is obvious in the areas of the structure where the benzylic methylene is introduced. Aiming to investigate the reason of higher affinity of flexible analog **3** compared with rigid 4-OH-TAM, the area accommodating the benzyl group was visually exam-

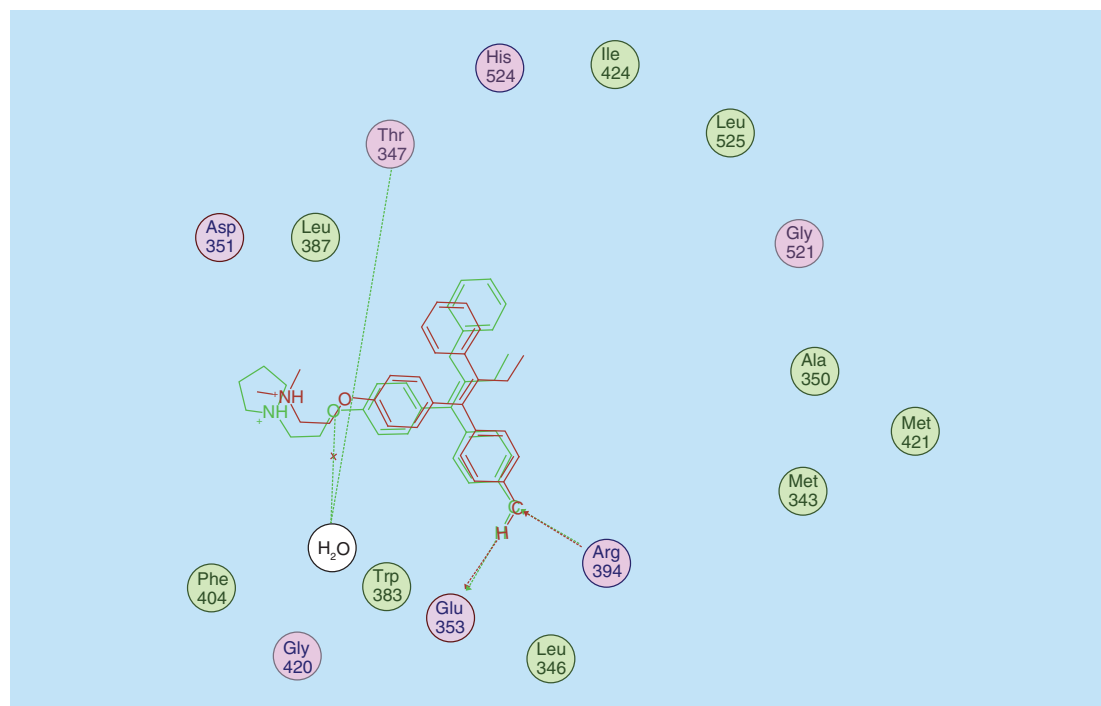


Figure 4. Interactions of 4-OH-TAM and compound **3 with ER α ligand-binding domain.**

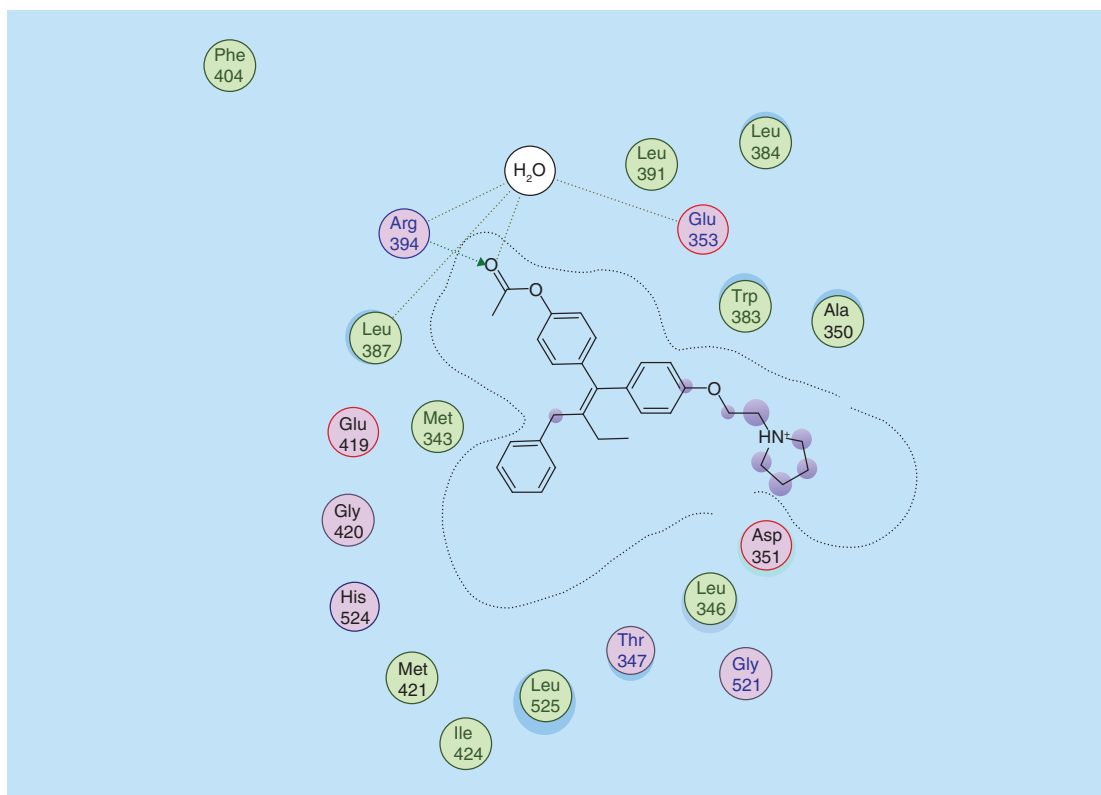


Figure 5. Interactions of compound 8 with ER α ligand-binding domain.

ined, the extra methylene carbon has pushed the phenyl ring into a small lipophilic cavity maintained by Ile424 and His524, this pocket is previously reported by Lloyd *et al* [29]. The higher affinity of compound **3** indicated that the benzylic moiety is probably held in a more favorable position by this hydrophobic cleft (Figure 3).

To quantify the relative interactions for the compounds, the 2D interactions with ligand **3**, **8** were predicted, the residues depicted are those that have been previously reported to be crucial for the binding process: Asp351, Glu353, Arg394, His524 and Ile 424 [30,31] (Figures 4 & 5).

Compound **3** interacts with ER α in a similar fashion to OH-TAM, where two H-bonds are formed between the free phenolic hydroxy group (OH) and the two amino acids residues Arg394 and Glu353 of the binding pocket as acceptor and donor, respectively. Moreover, the basic amino group of pyridine is protonated creating a cationic which augments the binding with Asp 351 (anionic carboxylate site) on the estrogen receptors. The SERM profiles have been previously ascribed to the charge neutralization between the basic amine of SERMs and the negatively charged residue Asp351 in the ligand-binding domain [32]. This has been correlated to the distances measured between O ^{δ} 351 and N^{h δ} in the crystal structures. The

distances of 3.8Å are found in 4-OHT complex in 3ERT, whereas compounds **3** and **8** showed a distance of 3.17 Å and 2.97 Å, respectively.

Compound **8** showed that the acetate group is involved in two hydrogen bonds acceptor interactions with ER α , in other words, the carbonyl group picked up similar interactions to OH-TAM but of semidifferent natures (Figure 4).

The interactions of the esterified compound **8** (IC₅₀ = 9 nM) showed that only direct H-bond was formed between the oxygen of carbonyl group and amino acid Arg394 while an indirect H-bond via water (H₂O) molecule was formed with Glu353. These findings can explain the high binding affinity of compound **8** to the ER α . This confirms that the esterification on the *para*-position did not lead to loss of any essential interactions although of partial altered nature.

Conclusion

In an attempt to synthesize compounds that have a different activation pathway than TAM to overcome the CYP2D6 enzyme genetic polymorphism, 12 novel compounds were synthesized. These compounds have showed better antiproliferative effect than TAM on MCF-7 cells. Moreover, the novel flexible analogs have shown better activity as well as higher selectivity toward

ER α receptors, providing a promising future for novel flexible TPE derivatives. Further metabolic studies are required to determine the exact rate of metabolism of the novel compounds and their potential metabolism compared with TAM. Pharmacokinetics–pharmacodynamics modeling are planned to study the effect of changes of the length of the ester alkyl groups.

Future perspective

Still today TAM and raloxifene are only two SERMs approved for reducing (ER) positive breast cancer risk in USA and still only a few women eligible for the drugs are using them. The new era of personalized medicine will attract much interest from the pharmaceutical and medical sector to our work; our research group is currently working on drug metabolism and pharmacokinetics model for those analogs to confirm their success as SERMs for individuals with CYP2D6 inactive alleles. Preliminary results indicate the possibility of preparing long acting analogs with superior pharmacokinetic properties to existing SERMs. In this study, an attempt to overcome CYP2D6 polymor-

phism through designing compounds with alternative metabolic pathway has been addressed. Success in synthesizing compounds with higher antiproliferative effect than TAM needs to be followed by metabolic studies to determine the exact rate of metabolism of the novel compound under the study conditions. Further *in vivo* testing for these compounds is planned.

Acknowledgments

The authors are deeply grateful to the authority of the National Cancer Institute, USA, for the antitumor screening.

Financial & competing interests disclosure

This project was supported financially by the Science and Technology Development Fund (STDF), Egypt, Grant No: 5386. The authors have no other relevant affiliations or financial involvement with any organization or entity with a financial interest in or financial conflict with the subject matter or materials discussed in the manuscript apart from those disclosed.

No writing assistance was utilized in the production of this manuscript.

Executive summary

- Twelve novel compounds have been synthesized in an attempt to overcome the CYP2D6 enzyme genetic polymorphism via having different metabolic pathway
- Flexibility added to the TAM backbone resulted in compounds with better antiproliferative effect than TAM on MCF-7 cell lines as well as higher selectivity toward ER α receptors.
- Further metabolic studies and pharmacokinetics–pharmacodynamics modeling are required to have full idea about the novel compounds' properties.

References

Papers of special note have been highlighted as:

• of interest; •• of considerable interest

- 1 Ferlay J, Soerjomataram I, Ervik M *et al.* GLOBOCAN 2012 v1.0. *Cancer Incidence and Mortality Worldwide: IARC CancerBase No. 11* (2012).
- 2 Ferlay J, Shin HR, Bray F, Forman D, Mathers C, Parkin DM. GLOBOCAN 2008 v1.2. *Cancer Incidence and Mortality Worldwide: IARC Cancer Base No. 10*. (2010).
- 3 Johnston SR. New strategies in estrogen receptor-positive breast cancer. *Clin. Cancer Res.* 16(7), 1979–1987 (2010).
- 4 Palacios S. The future of the new selective estrogen receptor modulators. *Menopause Int.* 13(1), 27–34 (2007).
- 5 Manni A, Verderame MF. *Selective Estrogen Receptor Modulators. Research and Clinical Applications*. Springer, NJ, USA (2002).
- 6 Ellis AJ, Hendrick VM, Williams R, Komm BS. Selective estrogen receptor modulators in clinical practice: a safety overview. *Expert Opin. Drug Saf.* 14(6), 921–934 (2015).
- 7 Fisher B, Costantino JP, Wickerham DL *et al.* Tamoxifen for the prevention of breast cancer: current status of the National Surgical Adjuvant Breast and Bowel Project P-1 study. *J. Natl Cancer Inst.* 97(22), 1652–1662 (2005).
- 8 Zanger UM, Schwab M. Cytochrome P450 enzymes in drug metabolism: regulation of gene expression, enzyme activities, and impact of genetic variation. *Pharmacol. Ther.* 138(1), 103–141 (2013).
- 9 Saladores P, Murdter T, Eccles D *et al.* Tamoxifen metabolism predicts drug concentrations and outcome in premenopausal patients with early breast cancer. *Pharmacogenomics J.* 15(1), 84–94 (2015).
- 10 Brauch H, Schwab M. Prediction of tamoxifen outcome by genetic variation of CYP2D6 in post-menopausal women with early breast cancer. *Br. J. Clin. Pharmacol.* 77(4), 695–703 (2014).
- Gives a recent update of the role of CYP2D6 in tamoxifen (TAM) metabolism and its effect on clinical outcomes.
- 11 Schmidt C. Third-generation SERMs may face uphill battle. *J. Natl Cancer Inst.* 102(22), 1690–1692 (2010).
- 12 Brauch H, Schroth W, Goetz MP *et al.* Tamoxifen use in postmenopausal breast cancer: CYP2D6 matters. *J. Clin. Oncol.* 31(2), 176–180 (2013).
- Gives a recent update of the role of CYP2D6 in TAM metabolism and its effect on clinical outcomes.
- 13 Shah IG, Breslin C, Wittayanarakul K, Mackay S. Pharmacogenetics of cytochrome P450 2D6: a translational

- medicine perspective. *Open Conf. Proc. J.* 1, 103–108 (2010).
- 14 Maximov PY, Myers CB, Curpan RF, Lewis-Wambi JS, Jordan VC. Structure-function relationships of estrogenic triphenylethylenes related to endoxifen and 4-hydroxytamoxifen. *J. Med. Chem.* 53(8), 3273–3283 (2010).
- **A review on the SAR of TPEs which give an insight on design of novel TAM analogs.**
- 15 Ohta K, Chiba Y, Kaise A, Endo Y. Structure–activity relationship study of diphenylamine-based estrogen receptor (ER) antagonists. *Bioorg. Med. Chem.* 23(4), 861–867 (2015).
- 16 Gauthier S, Mailhot J, Labrie F. New highly stereoselective synthesis of (Z)-4-hydroxytamoxifen and (Z)-4-hydroxytoremifene via McMurry reaction. *J. Org. Chem.* 61(11), 3890–3893 (1996).
- **Explains the detailed experimental work for preparation of triphenylethylene backbone via McMurry reaction.**
- 17 Lv W, Liu J, Lu D, Flockhart DA, Cushman M. Synthesis of mixed (E,Z)-, (E)-, and (Z)-norendoxifen with dual aromatase inhibitory and estrogen receptor modulatory activities. *J. Med. Chem.* 56(11), 4611–4618 (2013).
- **Explains the detailed experimental work for preparation of TAM analogs with 4,4' substituents.**
- 18 Bedford G, Richardson D. Preparation and Identification of *cis* and *trans* isomers of a substituted triarylethylene. *Nature* 212, 733–734 (1966).
- **Explains the detailed experimental work for preparation of geometric isomers of TAM analogs and their separation and identification.**
- 19 Katz J, Levitz M, Kadner SS, Finlay TH. Estradiol esters can replace 17 beta-estradiol in the stimulation of DNA and esterase synthesis by MCF-7 cells: a possible role for the estrogen-sensitive MCF-7 cell esterase. *J. Steroid Biochem. Mol. Biol.* 38(1), 17–26 (1991).
- **Highlights possible availability of esterases in MCF7 cell lines.**
- 20 Lam HY. Tamoxifen is a calmodulin antagonist in the activation of cAMP phosphodiesterase. *Biochem. Biophys. Res. Commun.* 118(1), 27–32 (1984).
- 21 O'brian CA, Ward NE, Anderson BW. Role of specific interactions between protein kinase C and triphenylethylenes in inhibition of the enzyme. *J. Natl Cancer Inst.* 80(20), 1628–1633 (1988).
- 22 Horgan K, Cooke E, Hallett MB, Mansel RE. Inhibition of protein kinase C mediated signal transduction by tamoxifen. Importance for antitumour activity. *Biochem. Pharmacol.* 35(24), 4463–4465 (1986).
- 23 De Medina P, Paillasse MR, Segala G *et al.* Importance of cholesterol and oxysterols metabolism in the pharmacology of tamoxifen and other AEBs ligands. *Chem. Phys. Lipids* 164(6), 432–437 (2011).
- **Reference highlights other mechanisms involved in TAM pharmacology with an insight on the involvement of cholesterol and its metabolites.**
- 24 Silvente-Poirot S, Poirot M. Cancer. Cholesterol and cancer, in the balance. *Science* 343(6178), 1445–1446 (2014).
- 25 Poirot M, Silvente-Poirot S, Weichselbaum RR. Cholesterol metabolism and resistance to tamoxifen. *Curr. Opin. Pharmacol.* 12(6), 683–689 (2012).
- 26 Grever MR, Schepartz SA, Chabner BA. The National Cancer Institute: cancer drug discovery and development program. *Semin. Oncol.* 19(6), 622–638 (1992).
- 27 Monks A, Scudiero D, Skehan P *et al.* Feasibility of a high-flux anticancer drug screen using a diverse panel of cultured human tumor cell lines. *J. Natl Cancer Inst.* 83(11), 757–766 (1991).
- 28 Shiau AK, Barstad D, Loria PM *et al.* The structural basis of estrogen receptor/coactivator recognition and the antagonism of this interaction by tamoxifen. *Cell* 95(7), 927–937 (1998).
- 29 Lloyd DG, Smith HM, O'sullivan T, Knox AS, Zisterer DM, Meegan MJ. Antiestrogenically active 2-benzyl-1,1-diarylbut-2-enes: synthesis, structure–activity relationships and molecular modeling study for flexible estrogen receptor antagonists. *Med. Chem.* 2(2), 147–168 (2006).
- 30 Grese TA, Cho S, Finley DR *et al.* Structure–activity relationships of selective estrogen receptor modulators: modifications to the 2-arylbenzothiophene core of raloxifene. *J. Med. Chem.* 40(2), 146–167 (1997).
- 31 Li W, Li X, Sun S, Liang J, Wang R., Wang S. Agonist and antagonist recognition studies for oestrogen receptor by molecular dynamics simulation. *Mol. Simulat.* 39(3), 228–233 (2013).
- 32 Liu H, Park WC, Bentrem DJ *et al.* Structure-function relationships of the raloxifene-estrogen receptor-alpha complex for regulating transforming growth factor-alpha expression in breast cancer cells. *J. Biol. Chem.* 277(11), 9189–9198 (2002).

3.4. Design and synthesis of novel tamoxifen analogues that avoid CYP2D6 metabolism

Nermin S. Ahmed, Nehal H. Elghazawy , Ahmed K. ElHady , Matthias Engel, Rolf W. Hartmann , Ashraf H. Abadi

Eur. J. Med. Chem. **2016**, *112*, 171-179. Doi: [10.1016/j.ejmech.2016.02.026](https://doi.org/10.1016/j.ejmech.2016.02.026)

Abstract

Tamoxifen (TAM) is a widely used drug in the prophylaxis and treatment of breast cancer. TAM is metabolized to the more active 4-hydroxytamoxifen (4-OH-TAM) and endoxifen by cytochrome P450 (CYP) mainly CYP2D6 and CYP3A4 enzymes. Due to the genetic polymorphisms in CYP2D6 genes, high variation in the clinical outcomes of TAM treatment is observed among women of different populations. To address this issue, novel TAM analogues with possible altered activation pathways were synthesized. These analogues were tested for their antiproliferative action on MCF-7 breast cancer cell lines as well as their binding affinity for estrogen receptor (ER) ER-a and ER-b receptors. These entire novel compounds showed better antiproliferative activity than did TAM on the MCF-7 cells. Moreover, compound 10 exhibited a half maximal growth inhibition (GI_{50}) that was 1000 times more potent than that of TAM ($GI_{50} < 0.005$ mM vs 1.58 mM, respectively). Along with a broad spectrum activity on various cancer cell lines, all the TAM analogues showed considerable activity on the ER-negative breast cancer cell line. For further study, compound 10 was incubated in human liver microsomes (HLM), human hepatocytes (hHEP) and CYP2D6 supersomes. The active hydroxyl metabolite was detected after incubation in HLM and hHEP, implicating the involvement of other enzymes in its metabolism. These results prove that this novel series of TAM analogues might provide improved clinical outcomes for poor 2D6 metabolizers.



Contents lists available at ScienceDirect

European Journal of Medicinal Chemistry

journal homepage: <http://www.elsevier.com/locate/ejmech>

Short communication

Design and synthesis of novel tamoxifen analogues that avoid CYP2D6 metabolism

Nermin S. Ahmed^a, Nehal H. Elghazawy^a, Ahmed K. ElHady^a, Matthias Engel^b, Rolf W. Hartmann^b, Ashraf H. Abadi^{a,*}^a Department of Pharmaceutical Chemistry, Faculty of Pharmacy and Biotechnology, German University in Cairo, 11835 Cairo, Egypt^b Helmholtz Institute for Pharmaceutical Research Saarland and Pharmaceutical and Medicinal Chemistry, Saarland University, Campus C2.3, 66123 Saarbrücken, Germany

ARTICLE INFO

Article history:

Received 3 December 2015
 Received in revised form
 7 February 2016
 Accepted 8 February 2016
 Available online 9 February 2016

Keywords:

CYP2D6
 Estrogen receptors
 MCF-7
 Personalized medicine
 SERM
 Tamoxifen

ABSTRACT

Tamoxifen (TAM) is a widely used drug in the prophylaxis and treatment of breast cancer. TAM is metabolized to the more active 4-hydroxytamoxifen (4-OH-TAM) and endoxifen by cytochrome P450 (CYP) mainly CYP2D6 and CYP3A4 enzymes. Due to the genetic polymorphisms in CYP2D6 genes, high variation in the clinical outcomes of TAM treatment is observed among women of different populations. To address this issue, novel TAM analogues with possible altered activation pathways were synthesized. These analogues were tested for their antiproliferative action on MCF-7 breast cancer cell lines as well as their binding affinity for estrogen receptor (ER) ER- α and ER- β receptors. These entire novel compounds showed better antiproliferative activity than did TAM on the MCF-7 cells. Moreover, compound **10** exhibited a half maximal growth inhibition (GI_{50}) that was 1000 times more potent than that of TAM ($GI_{50} < 0.005 \mu\text{M}$ vs $1.58 \mu\text{M}$, respectively). Along with a broad spectrum activity on various cancer cell lines, all the TAM analogues showed considerable activity on the ER-negative breast cancer cell line. For further study, compound **10** was incubated in human liver microsomes (HLM), human hepatocytes (hHEP) and CYP2D6 supersomes. The active hydroxyl metabolite was detected after incubation in HLM and hHEP, implicating the involvement of other enzymes in its metabolism. These results prove that this novel series of TAM analogues might provide improved clinical outcomes for poor 2D6 metabolizers.

© 2016 Elsevier Masson SAS. All rights reserved.

1. Introduction

Breast cancer is considered to be the most common cancer among women worldwide, with 1.7 million women diagnosed with the disease in 2012 [1]. The majority of breast cancer cases (almost 80%) are classified as hormone-dependent cancer, since estrogen, acting via estrogen receptor alpha (ER- α) or estrogen receptor beta (ER- β), is the major inducer of the development and growth of the tumor. These are also called ER-positive breast cancers. The

remaining cases are not induced by estrogen and are classified as hormone-independent, or ER-negative, cancers. Since the growth of hormone-dependent cancer cells can be down-regulated by the oppositely active hormones, several endocrine therapies that limit the actions of estrogen have been developed over the past years. These endocrine therapies have played an important part in treating and improving the outcomes of postmenopausal women with all stages of the disease [2]. Selective estrogen receptor modulators (SERMs) have also been studied for their anti-cancer activity. These are chemically diverse compounds that lack the steroidal structure of estrogens yet can bind to ERs [3]. In addition, SERMs exhibit partial agonist and antagonist properties in different tissues and organs [4,5].

Tamoxifen (TAM) was the first SERM to be utilized in the treatment of metastatic breast cancer and is considered to be among the most effective drug in treating ER-positive breast cancers, either alone or better in combination with aromatase inhibitors. Moreover, the drug reduces the risk of recurrence and

Abbreviations: TAM, Tamoxifen; 4-OH-TAM, 4-hydroxytamoxifen; CYP, Cytochrome P450; ER, Estrogen receptor; GI_{50} , Half Maximal growth inhibition; HLM, Human microsomal enzymes; hHEP, Human hepatocytes; SERM, Selective estrogen receptor modulator; TPE, Triphenyl ethylenes; IC_{50} , Half maximal inhibitory concentration; TGI, Total growth inhibition; LC_{50} , half maximal lethal concentration; PDB, Protein data bank; UGT, Uridine 5'-diphospho-glucuronosyltransferase; SULF, Sulfotransferase.

* Corresponding author.

E-mail address: ashraf.abadi@guc.edu.eg (A.H. Abadi).<http://dx.doi.org/10.1016/j.ejmech.2016.02.026>

0223-5234/© 2016 Elsevier Masson SAS. All rights reserved.

death when used as adjuvant therapy in early stage or in metastatic cancer [6]. The efficacy of TAM is derived from its two clinically active metabolites, 4-hydroxytamoxifen (4-OH-TAM) and endoxifen, both of which have a greater affinity towards ER- α and a much higher antiestrogenic potency in breast cancer cells than does the parent drug (Fig. 1).

TAM metabolism and activation to the more active endoxifen is mediated mainly *via* cytochrome P450 (CYP) enzymes, specifically the CYP2D6 and CYP3A4 isoforms. Other non CYP as UGT and SULT genes are contributing to the clearance of TAM. All these enzymes are polymorphic with many well-characterized variants [7]. CYP2D6 is known to have highly variable enzymatic activity as a result of polymorphisms in the genes that encode the enzyme. Such genetic polymorphisms can lead to the formation of proteins that lack enzymatic activity or to enzymes with reduced activity [5,8].

The aim of this study was to synthesize new TAM analogues that maintain the main pharmacophoric features of TAM yet are metabolized *via* a metabolic pathway that does not involve the CYP2D6 enzyme, thus avoiding the genetic polymorphisms of this enzyme and giving more equal clinical benefits to patients. During the course of this work, several structural modifications to TAM were investigated, including substitution of a methyl in place of an ethyl group on the triphenylethylene (TPE) backbone. The effects of such a change on binding affinity to ER- α receptors, growth inhibition of MCF-7 cancerous cell line and selectivity were investigated. In addition, the effect of blocking the metabolic *para*-hydroxylation on ring C was studied by placing a hydroxyl group or an ester group, namely acetate, butanoate or decanoate. Furthermore, the dimethylaminoethoxy side chain at ring B of TAM that plays a crucial role in TAM antagonistic action [9] was modified to a pyrrolidinylethoxy or a piperidinylethoxy group. The effect of cyclization, size of the cyclic structure and alteration of the basicity of nitrogen were all extensively investigated (Fig. 2). The novel TAM analogues were prepared as depicted in (Scheme 1).

Compounds **1** was synthesized using standard McMurry coupling reaction of 4,4'- dihydroxybenzophenone with acetophenone using titanium tetrachloride/zinc as catalyst to give the triphenyl ethylene backbone in yield 87% [10,11].

Compound **1** was then treated with the appropriate base hydrochloride salt in the presence of potassium carbonate to form monoalkylated and dialkylated ether derivatives. Products were purified using column chromatography to provide the monoalkylated derivative **2–4** with yield 45%. The esterification of the monoalkylated compounds was then achieved *via* using commercially available acid chlorides in a basic medium. Compounds **2–13** were obtained as 1:1 mixture of *E/Z* isomers. Attempts to isolate the *E/Z* isomers using column chromatography as well as preparative HPLC were not successful.

¹³C NMR confirmed the formation of isomers since most of the signals were duplicated. Such duplication of signal has been previously reported by Bedford and Richardson [12].

2. Results and discussion

All novel TAM analogues were tested for their antiproliferative effect on MCF-7 cell lines and for their binding affinity to ER- α . Compound **8**, the esterified analogue with the highest ER- α binding affinity (half maximal inhibitor concentration [IC₅₀] = 0.0077 μ M), and compound **3**, its hydroxyl congener (IC₅₀ = 0.0008 μ M), were additionally tested for their binding affinity to ER- β . The differential selectivities between ER- α and ER- β were calculated for these two compounds (Table 1).

All of the novel TAM analogues, including the hydroxyl-containing molecules (compounds **2–4**) and ester-containing molecules (compounds **5–13**), showed IC₅₀ values in the range of (<1–3.17 μ M) on MCF-7 cell lines, which is lower than the IC₅₀ of TAM (4.40 μ M). These results confirmed that placing a hydroxyl or an ester group at position 4 of TAM enhances activity of the compounds. Compound **2** (IC₅₀ = 1.48 μ M) achieved twice the activity of 4-OH-TAM with only one structural difference: a methyl rather than an ethyl group on the TPE backbone. This modification did not have a consistent effect on all analogues, indicating that TPE can tolerate a range of alkyl spacers. A more pronounced effect was observed when a basic nitrogen was incorporated into the molecule in a cyclic pyrrolidine ring, as seen in compound **3** (IC₅₀ < 1 μ M).

Introduction of an ester group at position 4 of ring C increased the growth inhibition potency of almost all compounds. Analogues bearing a decanoate ester (compounds **7**, **10** and **13**) were the most active of the ester-bearing compounds, indicating a correlation between lipophilicity and growth inhibition that may be attributed to an improved cellular uptake. Carboxyl esterases are located entirely intracellular in MCF-7 cells, and, therefore, the conversion of the lipophilic esterified analogues to the more potent hydroxyl analogues may be facilitated by a successful uptake of the compounds [13]. We cannot, however, exclude the possibility that the improved activity is a combined effect coming from both the ester analogues and their hydroxyl metabolites.

In addition, incorporation of a cyclic nitrogen moiety on ring B provides a better inhibitory profile than acyclic nitrogen. Compounds **5**, **8** and **11** all contain an acetate at ring B, but the addition of a pyrrolidine or piperidine in compounds **8** and **11**, respectively, resulted in lower IC₅₀ values against MCF-7 (2.60 and 2.46 μ M for compounds **8** and **11**, respectively, vs. 2.74 μ M for compound **5**). A similar pattern is seen for the butanoate -bearing analogues when compounds **9** and **12**, which contain a pyrrolidine or a piperidine, respectively, are compared to compound **6** (1.20 and 2.42 μ M vs. 3.17 μ M, respectively).

Compounds **3** and **10** (NSC-783093, NSC-783094) were selected by the National Cancer Institute (NCI) for further testing for *in vitro* antitumor activity against 60 human tumor cell lines. The (GI₅₀), total growth inhibition (TGI) and half maximal lethal concentration (LC₅₀) were measured for each cell line (see Supplemental Information). The GI₅₀ values of these two compounds on the

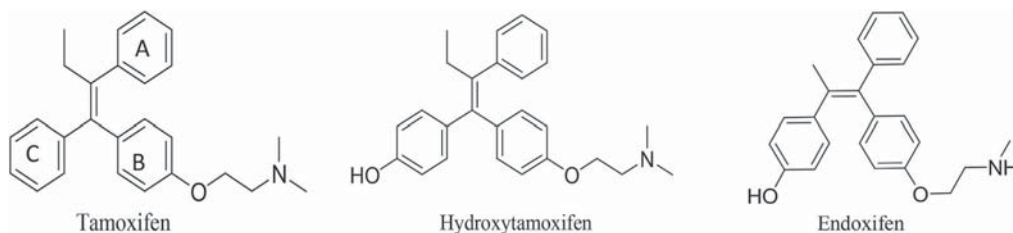


Fig. 1. Chemical structures of tamoxifen, hydroxytamoxifen and endoxifen.

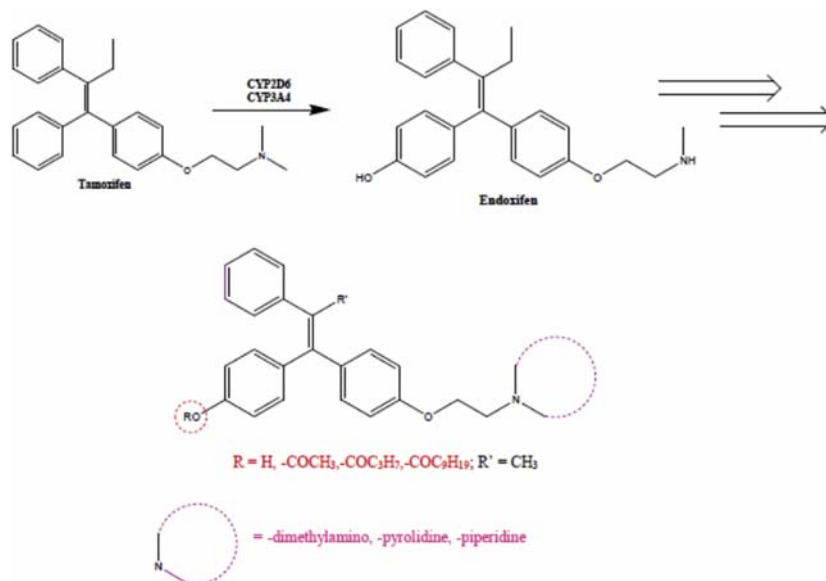
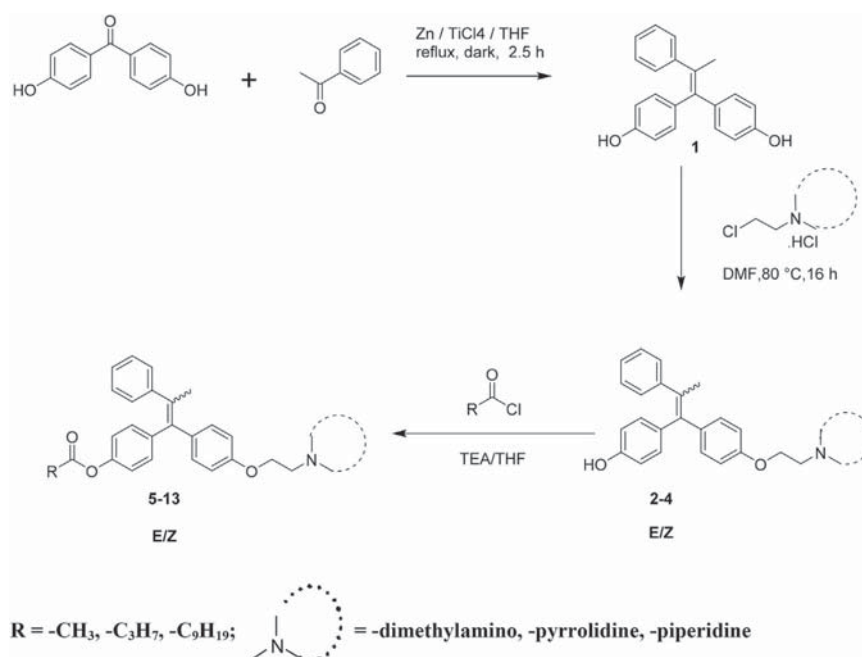


Fig. 2. Structural modifications of novel tamoxifen analogues.



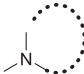
Scheme 1. Synthesis of the tamoxifen analogues (compounds 1–13).

most sensitive tumor cell lines are shown in comparison with TAM (NSC-180973) as the control in Table 2. For the MCF-7 human breast cancer cell line, compounds **3** and **10** had GI_{50} values of less than $0.01 \mu\text{M}$ and less than $0.005 \mu\text{M}$, respectively. These values represent an activity between 100 and 1000 times higher than that for TAM ($\text{GI}_{50} = 1.58 \mu\text{M}$), indicating that compounds **3** and **10** exhibit a high selectivity for MCF-7 cells and that they act mainly via an ER antagonistic mechanism. Interestingly, compound **3** showed to be more active than TAM on most cell lines tested.

The appreciable activity displayed by compounds **3** and **10** on the ER-negative breast cancer cell line MDA-MB-468 indicates that

these compounds have the ability to induce ER-independent cell death in a fashion similar to TAM. Previous reports stated that TAM potentially affects cellular functions by binding to calmodulin [14] or by inhibiting protein kinase C [15,16], and for this reason TAM has been studied for inhibition of cell growth and induction of apoptosis independently of ER. Other targets that could account for the cytotoxicity of TAM have been identified. TAM can bind to microsomal antiestrogen binding sites (AEBS), thus inhibiting cholesterol esterification. This mechanism has been linked to TAM's ability to induce breast cancer cell differentiation, apoptosis and autophagy independently of ER [17–19].

Table 1
Antiproliferative effect of TAM analogues in MCF-7 cells and binding affinities to ER- α and ER- β

Cpd		R ^b	R'	IC ₅₀ (μ M) ^a			ER- α /ER- β selectivity ratio
				MCF-7	ER- α	ER- β	
2	–(CH ₃) ₂	–H	–CH ₃	1.48	0.0013	ND	ND
3	pyrrolidine	–H	–CH ₃	<1	0.0008	0.04	44.9:1
4	piperidine	–H	–CH ₃	1.24	0.0004	ND	ND
5	–(CH ₃) ₂	–COCH ₃	–CH ₃	2.74	0.0220	ND	ND
6	–(CH ₃) ₂	–COC ₃ H ₇	–CH ₃	3.17	0.0345	ND	ND
7	–(CH ₃) ₂	–COC ₉ H ₁₉	–CH ₃	1.12	0.0319	ND	ND
8	pyrrolidine	–COCH ₃	–CH ₃	2.60	0.0077	0.26	37.14:1
9	pyrrolidine	–COC ₃ H ₇	–CH ₃	1.20	0.0271	ND	ND
10	pyrrolidine	–COC ₉ H ₁₉	–CH ₃	<1	0.0484	ND	ND
11	piperidine	–COCH ₃	–CH ₃	2.46	0.0124	ND	ND
12	piperidine	–COC ₃ H ₇	–CH ₃	2.42	0.0333	ND	ND
13	piperidine	–COC ₉ H ₁₉	–CH ₃	1.52	0.0810	ND	ND
TAM	–(CH ₃) ₂	–	–C ₂ H ₅	4.40	0.0080	0.18	22.2:1
4-OH-TAM	–(CH ₃) ₂	–OH	–C ₂ H ₅	2.79	0.0005	0.10	172.4:1

^a Values are an average of at least three experiments for each concentration for MCF-7 cells, ER- α and ER- β .

^b The R and R' sites are located as shown in Fig. 2. 4-OH-TAM, 4-hydroxytamoxifen; ER, estrogen receptor; MCF-7, estrogen receptor alpha positive breast cancer cell line; ND, not determined; TAM, tamoxifen.

Table 2
GI₅₀ of TAM, compound **3** and compound **10** over a panel of human tumor cell lines.

Cell lines	GI ₅₀ (μ M)		
	Compound 3	Compound 10	TAM
MOLT-4	2.94	8.61	2.5
EKVX	2.46	6.92	6.3
HCT15	1.81	6.69	3.16
SNB-75	3.07	6.55	5.01
MDA-MB-435	1.88	7.47	3.16
SK-OV3	3.25	7.36	10
UO-31	1.87	6.72	6.3
MCF-7	<0.01	<0.005	1.58
MDA-MB-468	1.84	7.26	1.99
T-47D	0.71	ND	2.50

Data obtained from NCI's *in vitro* disease-oriented human tumor cell screen (see Refs. [25] and [26] for details). EKVX, non-small lung cancer cell line; GI₅₀ = half maximal growth inhibition; HCT15, colon cancer cell line; MCF-7, estrogen receptor alpha positive breast cancer cell line; MDA-MB-435, melanoma cell line; MDA-MB-468, estrogen receptor negative breast cancer cell line; MOLT-4, leukemia cell line; SNB-75, central nervous system cancer cell line; SK-OV3, ovarian cancer cell line; TAM, tamoxifen; T-47D, estrogen receptor alpha positive breast cancer cell line; UO-31, renal cancer cell line.

Additionally, compound **10** was evaluated for *in-vitro* metabolite identification by incubation in CYP2D6 supersomes with and without the presence of NADPH, HLM or hHEP. A hydroxylated metabolite (M1) was observed in all incubation conditions, and a

Table 3
Relative abundances of compound **10**, its hydroxyl metabolite (M1) and glucuronide metabolite (M2) under incubation conditions.

		Peak area	Relative abundance (%)				
			Cpd 10				
			Cpd 10	M1	M2		
HLM	0 h –NADPH	5.9 × 10 ⁷	1.3 × 10 ⁷	ND	82	18	ND
	3 h –NADPH	3.4 × 10 ⁷	4.1 × 10 ⁷	ND	54	46	ND
	3 h + NADPH	2.5 × 10 ⁷	4.3 × 10 ⁷	ND	63	37	ND
2D6	0 h –NADPH	4.5 × 10 ⁶	6.2 × 10 ⁷	ND	93	7	ND
	3 h –NADPH	2.0 × 10 ⁷	5.6 × 10 ⁷	ND	74	26	ND
	3 h + NADPH	7.4 × 10 ⁷	6.5 × 10 ⁷	ND	90	10	ND
hHEP	0 h –	8.1 × 10 ⁶	2.0 × 10 ⁷	1.1 × 10 ⁵	29	71	<1%
	3 h –	7.0 × 10 ⁶	3.3 × 10 ⁶	9.2 × 10 ⁶	36	17	47

CYP2D6, cytochrome P450 2D6; hHEP, human hepatocytes; HLM, human liver microsomes, ND, not detected.

glucuronidated metabolite (M2) was seen after 3 h incubation in hHEP (Table 3).

A competitive ER binding assay was carried out for all the novel compounds, and the IC₅₀ values are listed in Table 1. A comparison of the ER binding affinities of the three hydroxylated analogues (compounds **2–4**) reveals the influence of the basic nitrogen; compounds **3** and **4** contain a highly basic nitrogen in the pyrrolidine and piperidine rings, respectively, and are nearly 10-fold more active than compound **2** and TAM (IC₅₀ = 0.0008 and 0.0004 vs 0.0013 and 0.008 μ M, respectively). Compound **2** contains the least basic nitrogen (the dimethylamine moiety) among this group of compounds and also has the lowest affinity. Cyclization and efficient protonation of the basic nitrogen probably allow for better positioning and, hence, a better antiestrogenic mode of interaction with ER.

Compounds **3** and **4** are equipotent to 4-OH-TAM (IC₅₀ = 0.0005 μ M), whereas compound **2** showed a 10-fold decrease in binding affinity compared to 4-OH-TAM. This difference in potency can be attributed to the presence of an ethyl group in 4-OH-TAM as opposed to a methyl group on the TPE backbone of compound **2**. Further investigations are needed to understand the effect of an alkyl spacer on binding affinity in these compounds.

The esterified molecule, compound **8** (ER- α IC₅₀ = 0.0077 μ M), and its hydroxylated derivative, compound **3** (ER- α IC₅₀ = 0.0008 μ M), we retested for binding affinity to ER- β . Both compounds exhibited a higher selectivity to ER- α than to ER- β . Except for compound **8**, which was more potent than TAM (IC₅₀ = 0.008 μ M), the ester containing compounds **5–13** exhibited a lower binding affinity to ER- α than did TAM and 4-OH-TAM. The decreased binding affinity might be due to a lack of esterases in the *in vitro* binding assays, leading to minimal formation of active hydroxylated analogues and resulting in a lack of essential interactions between phenolic OH and Arg394 and Glu353 residues.

Compound **10** (GI₅₀ < 0.005 μ M) was incubated in CYP2D6 supersomes in the presence of NADPH, HLM or hHep, and the resultant metabolites were characterized using LC-UV/MS. A hydrolyzed product was observed at t = 0 under all incubation conditions. To investigate the nature of this degradation product, the compound was subjected to a preparative HPLC run. Two peaks were integrated and were determined to represent the E and Z isomers of each compound (see Supplemental Information). The pure compound was incubated again and the degradation product still appeared at t = 0, indicating that hydrolysis was probably due

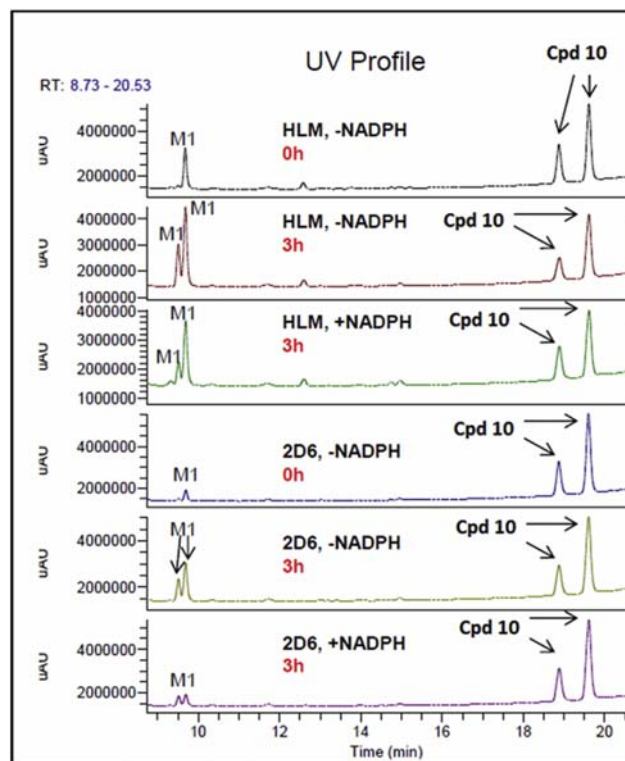


Fig. 3. Extracted ion chromatogram of compound **10** after incubation in HLM or CYP2D6 supersomes, both with and without NADPH. The analysis was conducted using liquid chromatography coupled to ultraviolet and mass spectrometry.

to the experimental conditions.

After incubation of compound **10** for 3 h in either CYP2D6 supersomes in the absence of NADPH or HLM, an increase in the concentration of the hydroxyl metabolite (M1) was observed, implicating the involvement of non-CYP enzymes in the formation of the active hydroxyl metabolite (Table 3, Fig. 3). After 3 h

incubation of compound **10** in hHEP, a decrease in the relative peak area of M1 was observed, accompanied by the formation of the glucuronide (M2), a common phase II metabolite (Table 3, Fig. 4). These results indicate the successful design and synthesis of TAM analogues that undergo significant non-CYP mediated hydrolysis. The molecular ion peak of compound **10** was recognized at 554.36; the hydroxyl metabolite at 400.022 and the glucouronide metabolite at 576.26 (supporting information).

To develop a deeper insight into the mode of binding of these novel compounds, a brief computational docking study using MOE.2009 was undertaken for compounds **3**, **4** and **8**, the most potent of the hydroxylated and esterified analogues. The crystal structure used in the docking studies was obtained from the co-crystallization of ER- α with 4-OH-TAM as found in the protein data bank (PDB: 3ERT) [20].

The docked geometries of compounds **3** and **4** were compared to the experimental binding mode for 4-OH-TAM, showing that the presence of a methyl group (instead of an ethyl group) on the TPE backbone still allows the compounds to adopt the required arrangement for binding in an established antiestrogenic mode. This is confirmed by a nearly complete overlap of the docked geometries for both **3** and **4** when overlaid over that of 4-OH-TAM (Fig. 5a).

Examination of the 2D interactions of compounds **3**, **4** and **8** with ER- α clearly shows that the incorporated residues are consistent with those that were previously reported to be crucial for binding, namely Asp351, Glu 353, Arg 394, His 524 and Ile 424 [21–23]. Compounds **3** and **4** interact with ER- α in a similar fashion as does 4-OH-TAM; two hydrogen-bonds form between the free phenolic hydroxyl moiety of the compounds and the two amino acids residues, Arg394 and Glu353, of the binding pocket (Figs. 6 and 7).

SERM profiles have been previously ascribed to charge neutralization between the basic amine of a SERM and the negatively charged residue Asp351 (an anionic carboxylate site) in the ligand binding domain (LBD) of the ER [24]. Since the basic amino group on the pyrrolidine and piperidine on compounds **3** and **4**, respectively, is protonated, a cation is created that strengthens the binding between these compounds and Asp 351. Moreover, the extent of charge neutralization can be correlated to the distance measured between O δ 351 of Asp 351 and N^{lig} of the compound in

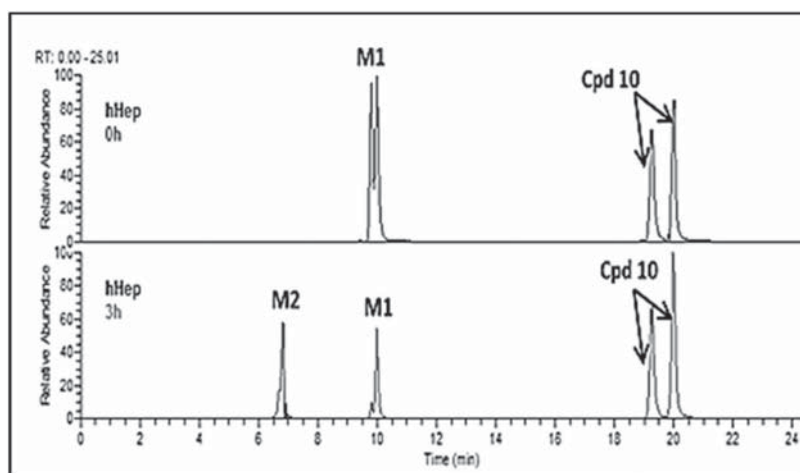


Fig. 4. Extracted ion chromatogram of compound **10** after incubation in hHEP. The analysis was conducted using liquid chromatography coupled to ultraviolet and mass spectrometry.

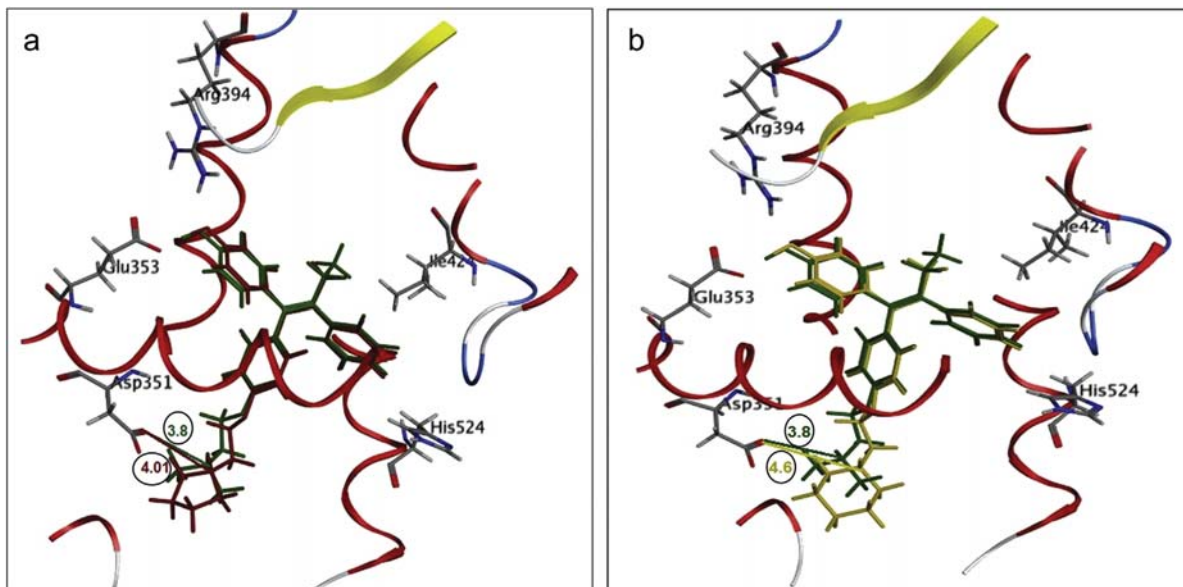


Fig. 5. a) The docking geometry of compound 3 (red) overlaid with that of 4-OH-TAM (green) in the estrogen receptor- α ligand binding domain. b) The docking geometry of compound 4 (yellow) overlaid with that of 4-OH-TAM (green) in the estrogen receptor- α ligand binding domain. (For interpretation of the references to colour in this figure legend, the reader is referred to the web version of this article.)

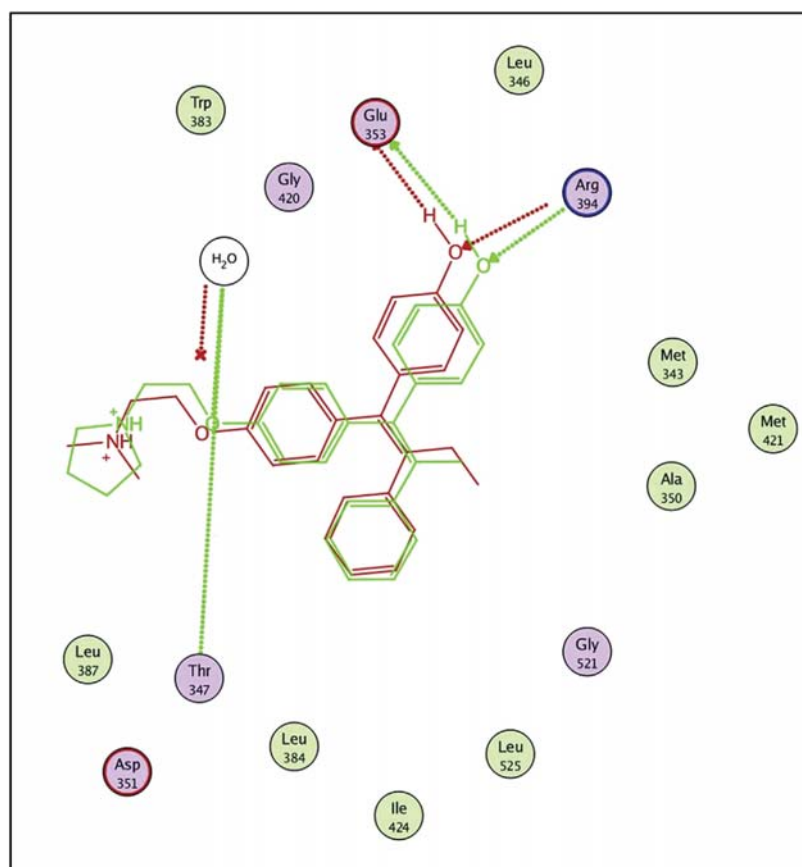


Fig. 6. 2D interactions of 4-hydroxytamoxifen (red) and compound 3 (green) in the estrogen receptor- α ligand binding domain. (For interpretation of the references to colour in this figure legend, the reader is referred to the web version of this article.)

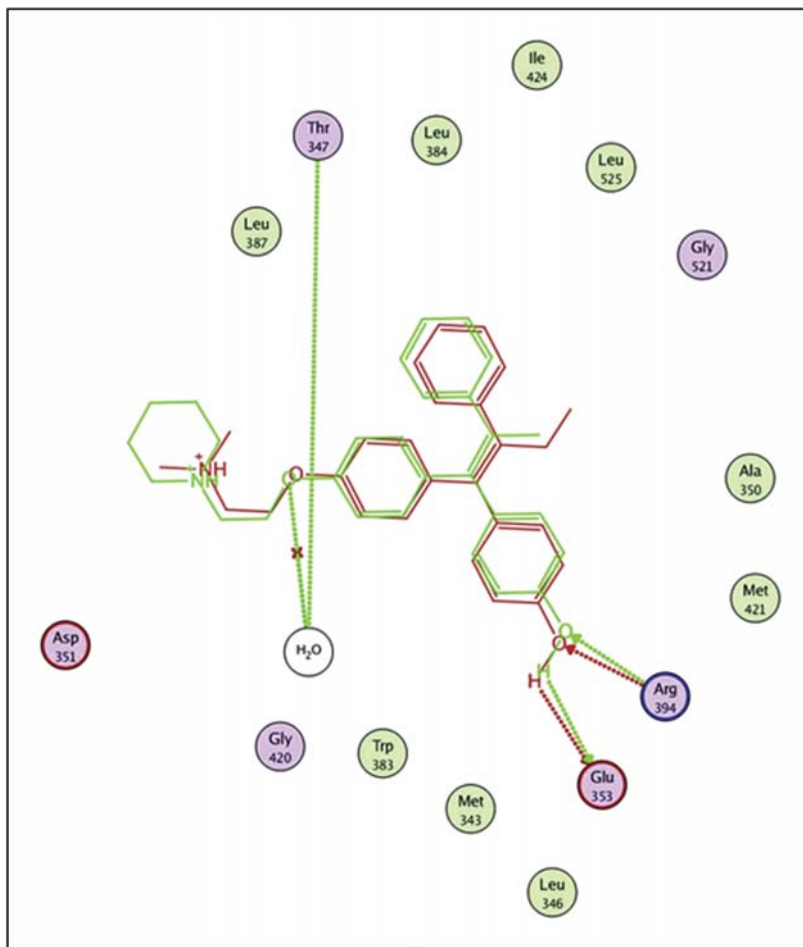


Fig. 7. 2D interactions of 4-hydroxytamoxifen (red) and compound 4 (green) in the estrogen receptor- α ligand binding domain. (For interpretation of the references to colour in this figure legend, the reader is referred to the web version of this article.)

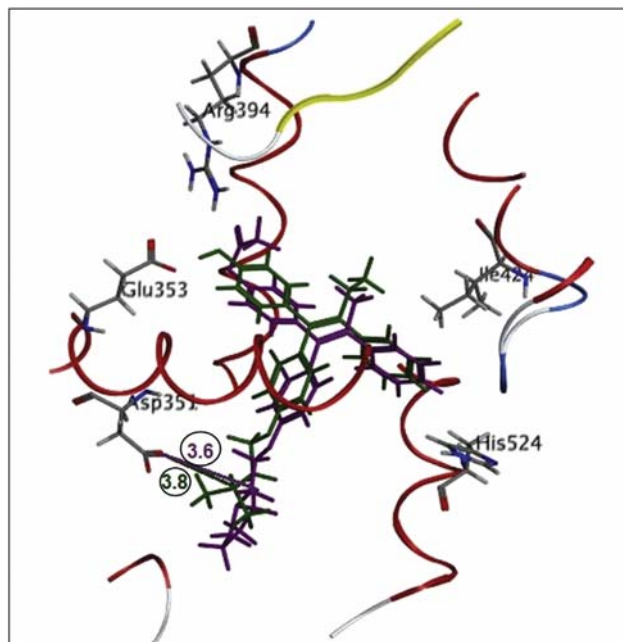


Fig. 8. Compound 8 overlaid with 4-hydroxytamoxifen in the estrogen receptor- α ligand binding domain.

the crystal structures. A distance of 3.8 Å was measured for the 4-OH-TAM complex in 3ERT, whereas compounds 3 and 4 showed distances of 4.01 Å and 4.60 Å, respectively. The small difference between the distances measured for compounds 3 and 4 and the distance for 4-OH-TAM indicates that the TAM analogues can possibly attain an antiestrogenic activity comparable to that of 4-OH-TAM.

The interactions of the esterified compound 8 ($IC_{50} = 0.0077 \mu M$) showed a single direct hydrogen-bond between the oxygen of the carbonyl group and amino acid Arg394. An indirect hydrogen-bond via a water molecule was also formed with Glu353. Compound 8, which contains an acetate ester group at position 4 and a pyrrolidine ring at position 4', exhibited interactions with ER- α similar to those of 4-OH-TAM. The high binding affinity of compound 8 to ER- α can be attributed to these interactions. These results confirm that neither the replacement of the ethyl moiety with a methyl group nor the esterification on the *para* position leads to loss of any essential interactions.

The phenyl group of compound 8 was accommodated in the small lipophilic cavity maintained by His524 and Ile424, indicating an improved fit in the receptor (Figs. 8 and 9). Additionally, the distance between $O^{\delta 351}$ of Asp351 and N^{lig} of compound 8 is 3.62 Å, which is a smaller distance than that seen with 4-OH-TAM. These observations indicate that the introduced acetate group pushed the ligand closer to Asp351, possibly leading to a better antiestrogenic effect.

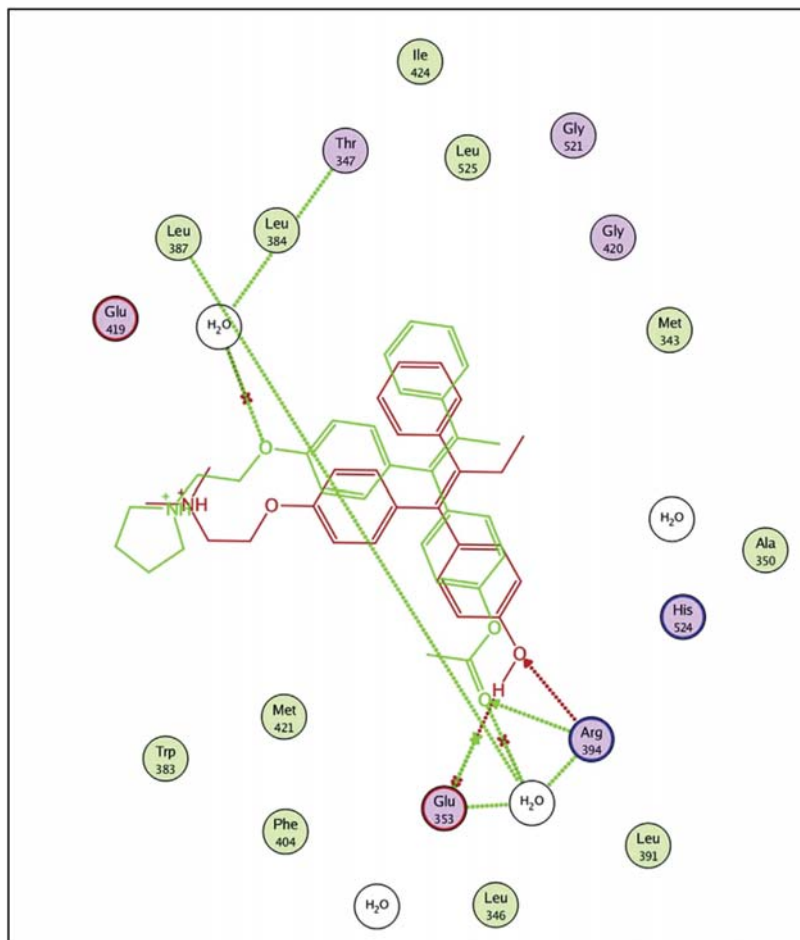


Fig. 9. 2D interactions of 4-hydroxytamoxifen (red) and compound **8** (green) in the estrogen receptor- α ligand binding domain. (For interpretation of the references to colour in this figure legend, the reader is referred to the web version of this article.)

3. Conclusion

We designed and synthesized a series of TAM analogues that are metabolized *via* activation pathways that do not involve the CYP2D6 enzyme, thus avoiding the variability in response caused by genetic polymorphism of this enzyme. All these novel compounds have a better antiproliferative effect on MCF-7 cells than does TAM. Moreover, these novel, rigid analogues show improved activity and high selectivity towards ER- α receptors compared to TAM. It is worth to mention that for compounds **3**, **8** and TAM, the ratio of binding to ER α /ER β is proportional to their IC₅₀ on MCF-7 cell lines, this is in agreement with studies suggesting that ER- β may oppose the actions of estrogen receptor alpha (ER- α) in cancer cells [27]. A simple metabolite identification experiment proved that these novel esterified analogues can act as stable, long-acting, non-CYP2D6 mediated SERMs.

Acknowledgements

The authors are deeply grateful to the authority of the National Cancer Institute, USA, for the antitumor screening. This project was supported financially by the Science and Technology Development Fund (STDF), Egypt, Grant No: 5386.

The authors are deeply grateful to Dr. Bianca Liederer, Dr. Peter Fan and Ms. Teresa Mulder, Drug Metabolism & Pharmacokinetics,

Genentech, South San Francisco, CA for their support in the metabolite ID study.

Appendix A. Supplementary data

Supplementary data related to this article can be found at <http://dx.doi.org/10.1016/j.ejmech.2016.02.026>.

References

- [1] J. Ferlay, I. Soerjomataram, M. Ervik, R. Dikshit, S. Eser, C. Mathers, M. Rebelo, D.M. Parkin, D. Forman, F. Bray, *GLOBOCAN 1* (2012).
- [2] S.R. Johnston, *Clin. Cancer Res.* 16 (2010) 1979–1987.
- [3] S. Palacios, *Menopause Int.* 13 (2007) 27–34.
- [4] A. Manni, M.F. Verderame, *Selective Estrogen Receptor Modulators, Research and Clinical Applications*, 2002.
- [5] A.J. Ellis, V.M. Hendrick, R. Williams, B.S. Komm, *Expert Opin. Drug Saf.* 14 (2015) 921–934.
- [6] B. Fisher, J.P. Costantino, D.L. Wickerham, R.S. Cecchini, W.M. Cronin, A. Robidoux, T.B. Bevers, M.T. Kavanah, J.N. Atkins, R.G. Margolese, C.D. Runowicz, J.M. James, L.G. Ford, N. Wolmark, *J. Natl. Cancer Inst.* 97 (2005) 1652–1662.
- [7] Z. Desta, B.A. Ward, N.V. Soukhova, D.A. Flockhart, *J. Pharmacol. Exp. Ther.* 310 (2004) 1062–1075.
- [8] I.G. Shah, C. Breslin, K. Wittayanarakul, S. Mackay, *Open Conf. Proc. J.* 1 (2010) 103–108.
- [9] P.Y. Maximov, C.B. Myers, R.F. Curpan, J.S. Lewis-Wambi, V.C. Jordan, *J. Med. Chem.* 53 (2010) 3273–3283.
- [10] S. Gauthier, J. Mailhot, F. Labrie, *J. Org. Chem.* 61 (1996) 3890–3893.

- [11] W. Lv, J. Liu, D. Lu, D.A. Flockhart, M. Cushman, *J. Med. Chem.* 56 (2013) 4611–4618.
- [12] G. Bedford, D. Richardson, *Nature* 733 (1966) 734.
- [13] J. Katz, M. Levitz, S.S. Kadner, T.H.J. Steroid, *Biochem. Mol. Biol.* 38 (1991) 17–26.
- [14] H.Y. Lam, *Biochem. Biophys. Res. Commun.* 118 (1984) 27–32.
- [15] C.A. O'Brian, N.E. Ward, B.W. Anderson, *J. Natl. Cancer Inst.* 80 (1988) 1628–1633.
- [16] K. Horgan, E. Cooke, M.B. Hallett, R.E. Mansel, *Biochem. Pharmacol.* 35 (1986) 4463–4465.
- [17] P. de Medina, M.R. Paillasse, G. Segala, F. Khallouki, S. Brillouet, F. Dalenc, F. Courbon, M. Record, M. Poirot, S. Silvente-Poirot, *Chem. Phys. Lipids* 164 (2011) 432–437.
- [18] S. Silvente-Poirot, M. Poirot, *Cancer. Sci.* 343 (2014) 1445–1446.
- [19] M. Poirot, S. Silvente-Poirot, R.R. Weichselbaum, *Curr. Opin. Pharmacol.* 12 (2012) 683–689.
- [20] A.K. Shiau, D. Barstad, P.M. Loria, L. Cheng, P.J. Kushner, D.A. Agard, G.L. Greene, *Cell* 95 (1998) 927–937.
- [21] T.A. Grese, S. Cho, D.R. Finley, A.G. Godfrey, C.D. Jones, C.W. Lugar 3rd, M.J. Martin, K. Matsumoto, L.D. Pennington, M.A. Winter, M.D. Adrian, H.W. Cole, D.E. Magee, D.L. Phillips, E.R. Rowley, L.L. Short, A.L. Glasebrook, H.U. Bryant, *J. Med. Chem.* 40 (1997) 146–167.
- [22] J. MacGregor Schafer, H. Liu, D.J. Bentrem, J.W. Zapf, V.C. Jordan, *Cancer Res.* 60 (2000) 5097–5105.
- [23] W. Li, X. Li, S. Sun, J. Liang, R. Wang, S. Wang, *Mol. Simul.* (2013) 228–233.
- [24] H. Liu, W.C. Park, D.J. Bentrem, K.P. McKian, L. Reyes Ade, J.A. Loweth, J.M. Schafer, J.W. Zapf, V.C. Jordan, *J. Biol. Chem.* 277 (2002) 9189–9198.
- [25] M.R. Grever, S.A. Schepartz, B.A. Chabner, *Semin. Oncol.* 19 (1992) 622–638.
- [26] A. Monks, D. Scudiero, P. Skehan, R. Shoemaker, K. Paull, D. Vistica, C. Hose, J. Langley, P. Cronise, A. Vaigro-Wolff, et al., *J. Natl. Cancer Inst.* 83 (1991) 757–766.
- [27] M. Madeira, A. Mattar, A.F. Logullo, F.A. Soares, L.H. Gebrim, *BMC Cancer* 13 (2013) 425–436.

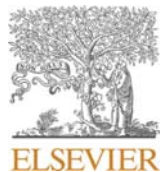
3.5. Control of ER-positive breast cancer by ER α expression inhibition, apoptosis induction, cell cycle arrest using semi-synthetic isoeugenol derivatives.

Mohamed S. Nafie*, **Nehal H. Elghazawy***, Salma M. Owf , Kholoud Arafa , Mohamed A. Abdel-Rahman , Reem K. Arafa

Chem. Biol. Interact. **2021**, 351, 109753. Doi:[10.1016/j.cbi.2021.109753](https://doi.org/10.1016/j.cbi.2021.109753)

Abstract

New semi-synthetic effective and safe anticancer agents isoeugenol derivatives were synthesized, characterized, and screened for their cytotoxic activity against MCF-7. Moreover, their selective cytotoxicity was assessed against MCF-10A. Three derivatives, 2, 8 and 10 were significantly more active than the reference drug 5-FU with IC₅₀ values of 6.59, 8.07 and 9.63 and 30.93 μ M, respectively. Also interestingly, these derivatives demonstrated some degree of selectivity to cancer cells over normal cells. Furthermore, derivative 2 was subjected to other in vitro experiments against MCF-7 where it inhibited colony formation by 87.5% and lowered ER α concentration to 395.7 pg/mL compared to 1129 pg/mL in untreated control cells. In continuation of the investigation, the apoptotic activity of compound 2, was assessed where it significantly enhanced total apoptotic cell death by 9.16-fold (18.70% compared to 1.64% for the untreated MCF-7 control cells) and arrested the cell cycle at the G₂/M phase. Furthermore, the molecular mechanism of apoptotic activity was investigated at both the gene (RT-PCR) and protein (western plotting) levels where upregulation of pro-apoptotic and down regulation of anti-apoptotic genes was detected. Additionally, compound 2 treatment enhanced the antioxidant (GSH, CAT, SOD) activities. Finally, in vivo experiments verified the effective anticancer activity of compound 2 through inhibition of tumor proliferation by 47.6% compared to 22.9% for 5-FU and amelioration of the hematological, biochemical, and histopathological examinations near normal. In effect, compound 2 can be viewed as a promising semi-synthetic derivative of isoeugenol with some degree of selectivity for management of breast cancer through apoptotic induction and ER α downregulation.



Control of ER-positive breast cancer by ER α expression inhibition, apoptosis induction, cell cycle arrest using semisynthetic isoeugenol derivatives

Mohamed S. Nafie^{a,1}, Nehal H. Elghazawy^{b,1}, Salma M. Owf^c, Kholoud Arafa^d,
Mohamed A. Abdel-Rahman^c, Reem K. Arafa^{b,e,*}

^a Chemistry Department, Faculty of Science, Suez Canal University, Ismailia, 41522, Egypt

^b Drug Design and Discovery Lab, Zewail City of Science and Technology, Giza, 12578, Egypt

^c Zoology Department, Faculty of Science, Suez Canal University, Ismailia, 41522, Egypt

^d Center for Material Sciences-NanoSciences, Zewail City of Science and Technology, Giza, 12578, Egypt

^e Biomedical Sciences Program, University of Science and Technology, Zewail City of Science and Technology, Giza, 12578, Egypt

ARTICLE INFO

Keywords:

Isoeugenol derivatives
Antiestrogenic effect
Antitumor activity
Apoptotic cell death

ABSTRACT

New semi-synthetic effective and safe anticancer agents isoeugenol derivatives were synthesized, characterized, and screened for their cytotoxic activity against MCF-7. Moreover, their selective cytotoxicity was assessed against MCF-10A. Three derivatives, **2**, **8** and **10** were significantly more active than the reference drug 5-FU with IC₅₀ values of 6.59, 8.07 and 9.63 and 30.93 μ M, respectively. Also interestingly, these derivatives demonstrated some degree of selectivity to cancer cells over normal cells. Furthermore, derivative **2** was subjected to other *in vitro* experiments against MCF-7 where it inhibited colony formation by 87.5% and lowered ER α concentration to 395.7 pg/mL compared to 1129 pg/mL in untreated control cells. In continuation of the investigation, the apoptotic activity of compound **2**, was assessed where it significantly enhanced total apoptotic cell death by 9.16-fold (18.70% compared to 1.64% for the untreated MCF-7 control cells) and arrested the cell cycle at the G2/M phase. Furthermore, the molecular mechanism of apoptotic activity was investigated at both the gene (RT-PCR) and protein (western plotting) levels where upregulation of pro-apoptotic and down regulation of anti-apoptotic genes was detected. Additionally, compound **2** treatment enhanced the antioxidant (GSH, CAT, SOD) activities. Finally, *in vivo* experiments verified the effective anticancer activity of compound **2** through inhibition of tumor proliferation by 47.6% compared to 22.9% for 5-FU and amelioration of the hematological, biochemical, and histopathological examinations near normal. In effect, compound **2** can be viewed as a promising semi-synthetic derivative of isoeugenol with some degree of selectivity for management of breast cancer through apoptotic induction and ER α downregulation.

1. Introduction

Breast cancer remains a worldwide public health concern and a major cause of morbidity and mortality among females [1]. Treatment of breast cancer is mainly multimodal in nature comprising tumor resection, hormonal replacement therapy, ionizing radiation, systemic chemotherapy and immuno-therapy [2]. Despite advancements achieved so far, yet resistance to conventional forms of therapies and tumor recurrence are very frequent. Additionally, the complexity of this disease emanates from its heterogeneity where breast cancer is namely

classified based on the type of overexpressed receptors including human epidermal growth factor receptor-2 (HER-2), estrogen receptors (ERs), and progesterone receptors (PRs). The diversity of genotypic aberrations underlying the different types of breast cancer makes it a necessity to search for new agents capable of selectivity targeting the underlying molecular mechanism of pathogenesis. Traditional medicine deploying bioactive agents derived from plant species constitutes 74% of the drug panel used as anticancer agents [3,4]. Hence, the ubiquitously abundant phytochemicals including alkaloids, terpenoids, quinonoids, flavonoids and related polyphenols, served and still offer a wide myriad of compounds with potential cytostatic or cytotoxic agents. Natural products

* Corresponding author. Zewail City of Science and Technology, Ahmed Zewail Road, October Gardens, Giza, 12578, Egypt.

E-mail addresses: Mohamed.nafie@science.suez.edu.eg (M.S. Nafie), nelghazawy@zewailcity.edu.eg (N.H. Elghazawy), scisalma2018@gmail.com (S.M. Owf), karafa@zewailcity.edu.eg (K. Arafa), mohamed.hassanain@science.suez.edu.eg (M.A. Abdel-Rahman), rkhidr@zewailcity.edu.eg (R.K. Arafa).

¹ Authors with equal contribution.

List of abbreviations

ALT	alanine transaminase
AST	aspartate transaminase
BAX	Bcl-2 Associated X
Bcl-2	B-cell lymphoma 2
CAT	catalase
ER α	Estrogen Receptor alpha
GSH	Glutathione
IHC	Immunohistochemistry
p53	tumor protein p53
PI	propidium iodide;
PUMA	p53 upregulated modulator of apoptosis
ROS	reactive oxygen species
RT-PCR	Real Time polymerase chain reaction
SEC	Solid Ehrlich Ascites
SOD	Super oxide dismutase
TDP-2	Tyrosyl-DNA phosphodiesterase-2

were found to corroborate anti-tumor activity *via* promoting apoptosis. Several of these products such as curcumin, genistein, quercetin, and procyanidins are currently in clinical trials for the treatment of various forms of cancer [5].

Amongst the most studied phytochemicals for its anticancer effect is eugenol, an allyl benzene derivative found in essential oils from clove, nutmeg and cinnamon. Piling evidence proved that eugenol causes a dose-dependent cell death of estrogen positive MCF-7 cells, and to a lesser extent estrogen negative MDA-MB-231 cells [6,7]. In MCF-7 cell-line, eugenol cytotoxic effect has been mediated through an estrogen receptor- α (ER α)-dependent mechanism culminating into apoptosis induction. Additionally, a study demonstrated that eugenol promotes ROS propagation resulting in mitochondrial failure concomitantly with down-regulation of proliferating cell nuclear antigen (PCNA) leading to G2/M cell cycle arrest and DNA damage [8]. Taken together, eugenol can negatively impact the survival of different breast cancer types by regulating a myriad of complex interconnected pathways as proven by the different studies.

Isoeugenol is a phenylpropanoid produced by plants which is an isomer of eugenol with known potent antiproliferative activity. The structural similarity of isoeugenol with eugenol stimulates advances in pharmacological studies to explore their therapeutic potential in cancer treatment [9]. Both eugenol and isoeugenol were reported to induce apoptotic cell death in cancer cells, and their synthetic analogues demonstrated and enhanced anticancer activity. This sheds light on the potential of isoeugenol to be used as a lead compound for further optimization to promote its antitumor activity [10]. The work done by Chalcogen et al. further stipulates the effective cytotoxic effect of isoeugenol against several cancer cell-lines *via* inhibiting potent COX-2 and 5-LOX inflammatory proteins which are critical components to cancer development and progression [11]. Also, docking experiments demonstrated the ability of isoeugenol to reside into the active site of COX-2 protein with similar orientation with indomethacin. Likewise, derivatives of isoeugenol namely methyl isoeugenol which occurs as a natural constituent found in lemongrass was found to possess chemical carcinogens detoxification capacity *via* induction of glutathione S-transferase enzyme [12]. Additionally, isoeugenol was found to effectively bind into the 5-LOX cavity of the active site near arachidonic acid moiety [13,14]. Atsumi et al. synthesized dimer compounds from eugenol or isoeugenol and reported their potential antitumor activity through the inhibition of DNA synthesis. In this study, isoeugenol derivatives were proven to be superior to their eugenol counterparts due to their better interaction with cell membranes *via* the lipophilic radical [15]. Furthermore, isoeugenol was recently reported to synergistically

enhance the antitumor effect of camptothecin on MCF-7 cells [16]. Mechanistically, isoeugenol was found to hinder TDP-2 mediated DNA repair mechanisms thus sensitizing cancer cells to cytotoxic chemotherapeutic agents.

Motivated by all the above-mentioned evidences, the current study intends to fill a knowledge gap by investigating the therapeutic potential of isoeugenol in breast cancer treatment. The study rationale is based on the structural similarity of isoeugenol to eugenol being its positional isomer. To this effect, new isoeugenol derivatives were chemically synthesized and structurally validated. Anticancer activity of the new compounds was tested *in-vitro* on the ER+ breast carcinoma cell-line MCF-7. Mechanistically, the apoptosis induction as well as cell-cycle abrogation capability of the most active compound was evaluated. The effect of the most potent compound as antioxidant was also investigated. Finally, *in vivo* studies were implemented using the most promising compound on SEC-bearing mice to validate its pharmacological efficacy at the preclinical level.

2. Material and methods

2.1. Chemistry

2.1.1. General method for preparation of benzyloxypropenylbenzene derivatives 2–11

A solution of isoeugenol (0.5 g, 3 mmol) in absolute ethanol (20 mL) was treated with the appropriate benzyl chloride (4.5 mmol) in the presence of sodium ethoxide (7 mmol) where the mixture was allowed to reflux overnight. After completion of the reaction, the reaction mixture was poured onto ice/water and extracted using ethyl acetate to afford the corresponding benzyloxypropenylbenzene derivative. The product was then purified by column chromatography using silica gel 60–120 mesh as the stationary phase and ethyl acetate:hexane (gradient form 0.5% till 7%) as the mobile phase. All compounds were either oils or low melting solids at ambient temperature. All structures of the compounds were confirmed by spectral and elemental analyses (data not shown).

2.2. Cytotoxic activity

Cytotoxic activity of all synthesized compounds against MCF-7 (ER α -dependent) breast cancer cell line; and the MCF-10A as the normal breast cell line were determined by the MTT assay. Cells were acquired from ATCC and cultured according to standard protocols [17]. Serial concentrations of (100, 25, 6.25, 1.56, 0.39 μ M) of tested compounds were prepared for treatment the cultured cells for 48 h of incubation. After treatment, percentages of cell survival were determined by measuring the optical absorbance λ 570 nm according to the following equation: % of cell viability = $\frac{A_{sample}}{A_{control}} \times 100$, then IC₅₀ calculation was calculated using the EXCEL software.

2.3. Colony forming assay

MCF-7 cells were seeded at 200 cells/well, then incubated for 24 h, and the cells were then allowed to attach to form a complete monolayer of cells. Five concentrations (0.01, 0.1, 1, 10, 100 μ M) of the compound 2 were added to the cell culture, following which the cells were incubated for 72 h, then washed with PBS and the colonies thus formed were fixed using methanol. The cells were stained with crystal violet for 20 min and then counted using a light microscope [18].

2.4. ER α level detection

The compound with the lowest IC₅₀ against the MCF-7 cells was tested for its effect on the quantitative expression of ER α upon treatment therewith using the Human ER Alpha/Estrogen Receptor ELISA Kit (Catalog No. LS-F23792) [19].

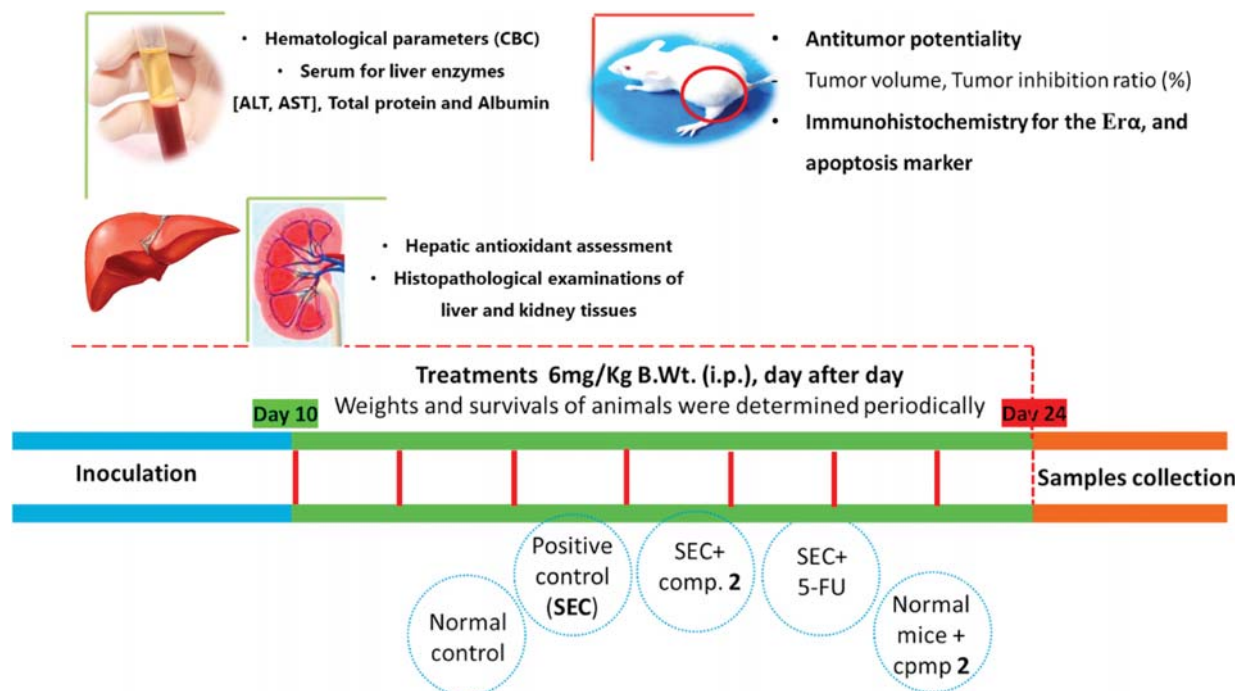


Fig. 1. *In vivo* experiment's workflow.

2.5. Apoptotic investigation

The apoptotic impact of MCF-7 treatment with **2** was investigated through the flow cytometric analyses of Annexin V/PI staining and cell cycle analysis and follow up the expression of the apoptosis-related genes in both gene and protein expression levels using the RT-PCR and western blotting assays.

2.6. Annexin V/PI staining and cell cycle analysis

Apoptotic cell death in MCF-7 cells was quantified using annexin V-FITC (BD Pharmingen, USA). Cells were seeded into 6-well culture plates ($3-5 \times 10^5$ cells/well) and incubated for an overnight. Cells were then treated with compound **2** for 48 h. Next, media supernatants and cells were collected and rinsed with ice-cold PBS. The next step was suspending the cells in 100 μ L of annexin binding buffer solution "25 mM CaCl₂, 1.4 M NaCl, and 0.1 M HEPES/NaOH, pH 7.4" and incubation with annexin V-FITC solution (1:100) and propidium iodide (PI) at a concentration equals 10 μ g/mL" in the dark for 30 min. Stained cells were then acquired by CytExpert FACS machine. Data was analyzed using cytExpert software [20].

2.7. RT-PCR analysis

MCF-7 cancer cells were treated with compound **2** ($IC_{50} = 6.59 \mu$ M, 48 h), then total RNA was extracted from cells using Qiagen's RNA

extraction in both treated and untreated. The synthesis of cDNA was then performed, followed by the qPCR test in one tube. The perfect primer pairs (Supplementary, Table 1) were selected for the tested genes (p53, PUMA, BAX, CASP-3 & -9, Bcl-2, ER α) and β -actin as a house-keeping gene. The results were given in cycle thresholds (Ct), and $\Delta\Delta$ Ct for calculation of the relative quantities of each gene tested as previously described [21].

2.8. Western blotting

Furthermore, for validation of the apoptotic pathway at the protein expression level, we used the immunoblotting (Western blot) for ER α and some apoptosis proteins. Untreated and treated MCF-7 cancer cells were treated with compound **2** ($IC_{50} = 6.59 \mu$ M, 48 h) were washed in PBS and lysed in boiling sample buffer for sodium dodecyl sulfate polyacrylamide gel electrophoresis (SDS-PAGE). The lysates were boiled for 5 min with lamellae buffer, and the proteins were separated by SDS-PAGE and transferred to an Immobilon membrane (Millipore). The membranes were blocked in 5% non-fat milk for 1 h and probed with P53, Bax, Bcl2, ER α , caspase 3 and caspase 9 primary antibodies overnight at 4 °C. Appropriate secondary antibodies were conjugated, then densitometric analysis of the immunoblots was performed to quantify the amounts of P53, Bax, Bcl2, ER α , caspase-3 and caspase-9 in both untreated and treated cells by total protein normalization to β -actin. Image analysis was done using the software on the ChemiDoc MP imaging system (version 3) produced by Bio-Rad (Hercules, CA).

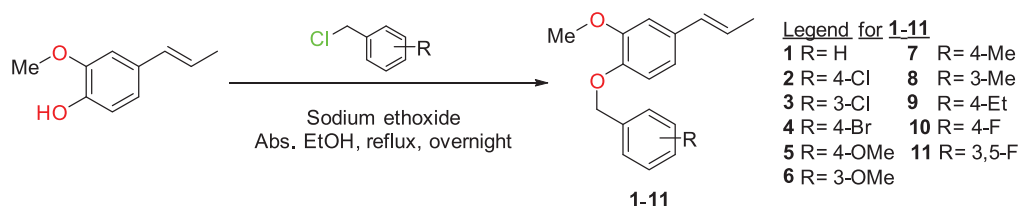


Fig. 2. Synthesis of the target isoeugenol derivatives 1–11.

Table 1

IC₅₀ values of the tested compounds against the MCF-7 breast cancer cell line and MCF-10A normal breast cells using the MTT assay.

Compounds	IC ₅₀ (μM) ^a	
	MCF-7 (ERα-dependent)	MCF-10A
Isoeugenol	11.14 ± 0.6	NT ^b
1	32.92 ± 1.9	NT
2	6.59 ± 0.4	28.0 ± 0.7
3	90.66 ± 5.2	NT
4	13.28 ± 0.8	NT
5	43.61 ± 2.5	NT
6	11.24 ± 0.6	NT
7	27.99 ± 1.6	NT
8	8.07 ± 0.5	18.1 ± 0.5
9	14.55 ± 0.8	NT
10	9.63 ± 0.6	17.3 ± 0.5
11	82.50 ± 4.7	NT
5-FU	30.93 ± 1.8	20.4 ± 0.5

^a Values are expressed as Mean ± SD of 3 independent experiments and are calculated through non-linear regression curve fit of EXCEL software.

^b NT = not tested.

2.9. In vivo work

Experiment design is summarized in Fig. 1, including antitumor potentiality, hematological, biochemical and histopathological examinations as previously described [21,22]. Detailed experimental procedures are presented in the supplementary materials.

3. Results and discussion

3.1. Chemistry

The target isoeugenol derivatives 1–11 were synthesized as depicted in Fig. 2. A solution of isoeugenol in absolute ethanol was refluxed with the appropriate benzyl chloride derivative in the presence of sodium ethoxide as a base catalyst. Derivatives obtained were structurally confirmed by spectral and elemental analyses. All pertaining synthesis and spectral analysis details are presented in the supplementary

material.

3.2. Cytotoxicity against breast cancer cell lines

The synthesized derivatives were screened for their cytotoxic activity against the ERα+ breast cancer cell line (MCF-7) and normal breast cell line (MCF-10A). As seen in Table 1, compounds 2, 8, and 10 exhibited significant cytotoxic activities against MCF-7 cells with IC₅₀ values range 6.59–9.63 μM being almost 3–5 folds more active than the reference cytotoxic drug 5-FU possessing IC₅₀ value of 30.93 μM. Additionally, the three most promising compounds 2, 8 and 10 were tested against the MCF-10A normal breast cells and were found to be selectively toxic exhibiting relatively large IC₅₀ values ranging from 17.3 to 28 μM. These results agreed with previous studies that investigated several eugenol derivatives with good IC₅₀ values against the MCF-7 breast cancer cell line [2,23]. Hence, the effective and selective activity of 2, 8 and 10 was strongly highlighted, that is why the most active compound in this study, derivative 2, was further inspected as a representative of this series for its effect on ERα expression, cell cycle progression and apoptotic cell death.

3.3. Colony forming assay

Colony forming assay measures the ability of tumor cells to grow and form colonies in a way that was not restricted by growth contact inhibition, which is characteristic in normal untransformed cells, and therefore clonogenicity was commonly employed as an indirect evaluation of tumor cells undergoing neoplastic transformation. Isoeugenol derivative 2 (IC₅₀ = 6.59 μM, 48 h) was assessed for its ability to inhibit colony formation in MCF-7 cells. As shown in Fig. 3, fewer and smaller colonies cells were observed after treatment of MCF-7 cells with the compound 2 in a concentration dependent manner. At the maximum tested dose of 100 μM, the number of counted colonies was 125 compared to 464 colonies of the untreated control with colony formation inhibition rate reaching around 87.5%. Our results are in line with the study by Barbosa et al. [3], which investigated the colony formation activity of some phenylpropanoid-based derivatives in estrogen positive MCF-7 cells.

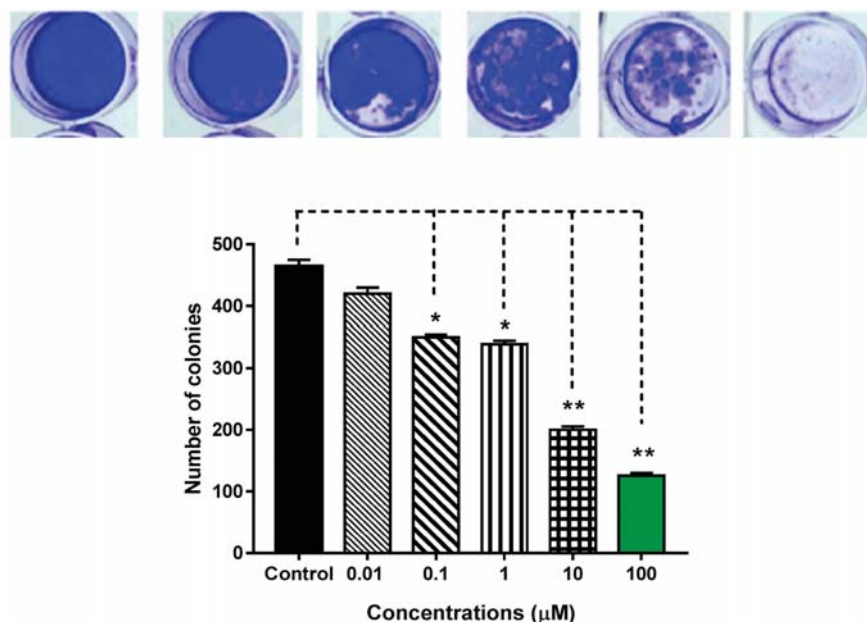


Fig. 3. Effect of treatment of MCF-7 cells with derivative 2 in serial concentrations from 0.01 to 100 μM on the number of colonies. * Significant difference between control and treated group ($p < 0.05$, unpaired t -test), ** highly significant difference between control and treated group ($p < 0.01$, unpaired t -test).

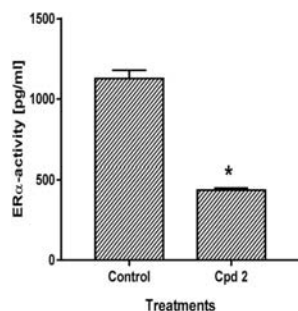


Fig. 4. ER α concentration in isoeugenol derivative 2-treated MCF-7 cells. * Significant difference between control and treated group ($p < 0.05$, unpaired t -test).

3.4. Estrogen-receptor (ER α) level alteration upon treatment

MCF-7 cells treated with isoeugenol derivative 2 were examined for their ER α concentration. As seen in Fig. 4, treatment of MCF-7 cells by 2 lowered ER α concentration to 395.7 pg/mL compared to 1129 pg/mL in untreated control cells. Hence, this infers that the observed cytotoxic activity of this isoeugenol derivative can be partly correlated with the inhibition of ER α expression in treated MCF-7 cells.

3.5. Apoptotic investigation

- Annexin V/PI staining with cell cycle analysis

Following the cytotoxic results of the tested derivatives against breast cancer MCF-7 cells, compound 2 was further tested employing flow cytometric analysis using the Annexin V/PI staining for detecting its apoptotic and necrotic effect and assessing the alteration in cell cycle progression. Therefore, MCF-7 cells were treated with compound 2 at the IC₅₀ concentration of 6.59 μ M for 48 h. As seen in Fig. (5), compound 2 significantly enhanced MCF-7 apoptotic cell death by 9.16-fold (18.70% compared to 1.64% for the untreated MCF-7 control cells). It raised the population of cells in early apoptosis to 4.54% and in late apoptosis to 14.16%, compared to 0.51% and 0.26%, respectively in the untreated control cells. Moreover, this isoeugenol derivative stimulated cell death via necrosis through inducing a 6.54-fold increase in necrotic cells population (8.31% compared 1.27% for the negative control cells). Thus, it can be inferred that compound 2 induced prominent apoptosis and necrosis in MCF-7 cells.

Our results of apoptosis-induction activity of the tested isoeugenol derivatives in the MCF-7 cells agree with Vidhya et al. [4] who investigated the inhibition of MCF-7 cell growth both in dose and time dependent manner. Additionally, our results agree with Jaganathan et al. [14], who highlighted the antiproliferative activity and molecular mechanism as apoptosis-induction of the eugenol against the cancer cells and animal models.

Additionally, cell cycle analysis was assessed to investigate the percentage of cells accumulation in each phase during cell growth after treatment with compound 2. As seen in Fig. (6), compound 2 induced arrest of the cell cycle phases G2/M and Pre-G1 and blocked progression of the MCF-7 cells. The compound significantly increased cell population at G2/M phase (23.43% compared to 8.62% for control untreated cells) and the Pre-G1 phase (27.01% compared to 2.04% for the negative

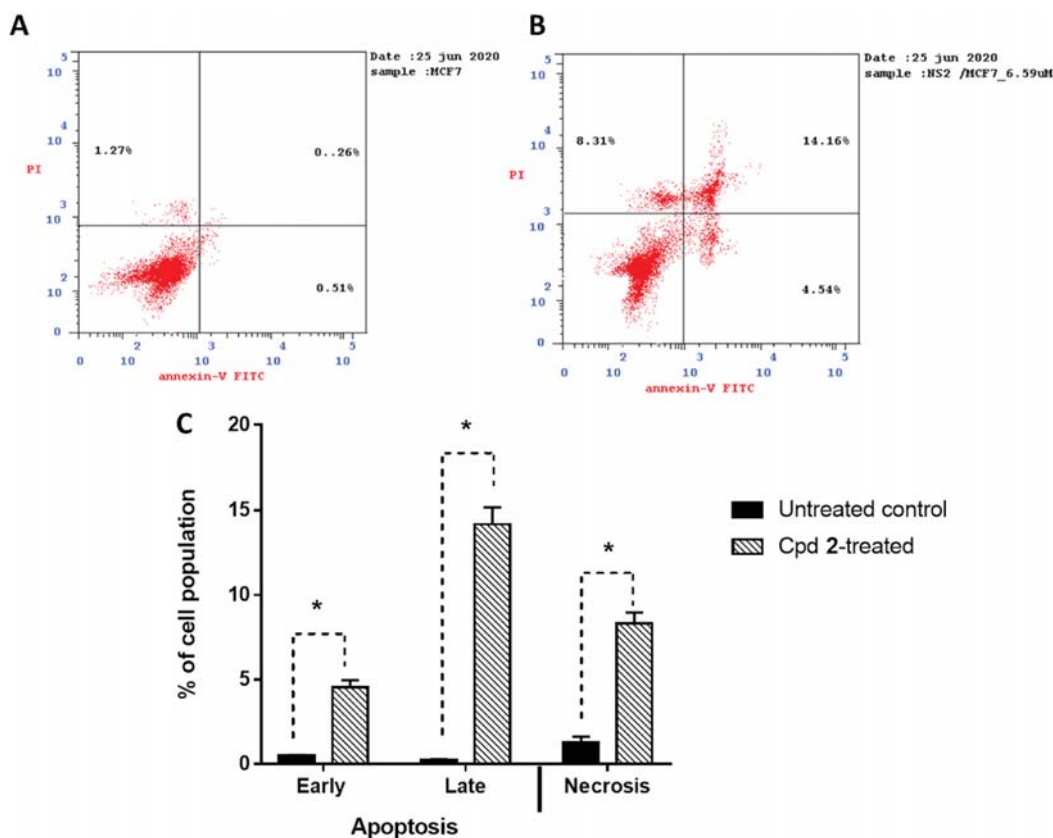


Fig. 5. Cryptographs of annexin-V/Propidium Iodide staining of A: Untreated and B: Treated MCF-7 cells with compound 2 (IC₅₀ = 6.59 μ M, 48 h), "Q2-1 (intermediate apoptosis, AV-/PI+), Q2-2 (late apoptotic cells, AV+/PI+), Q2-3 (normal cells, AV-/PI-), Q2-4 (early apoptotic cells, AV+/PI-), and C: Bar-representation of the percentage of cell population in early, late apoptotic and necrotic cell. * Significant difference between control and treated group ($p < 0.05$, unpaired t -test).

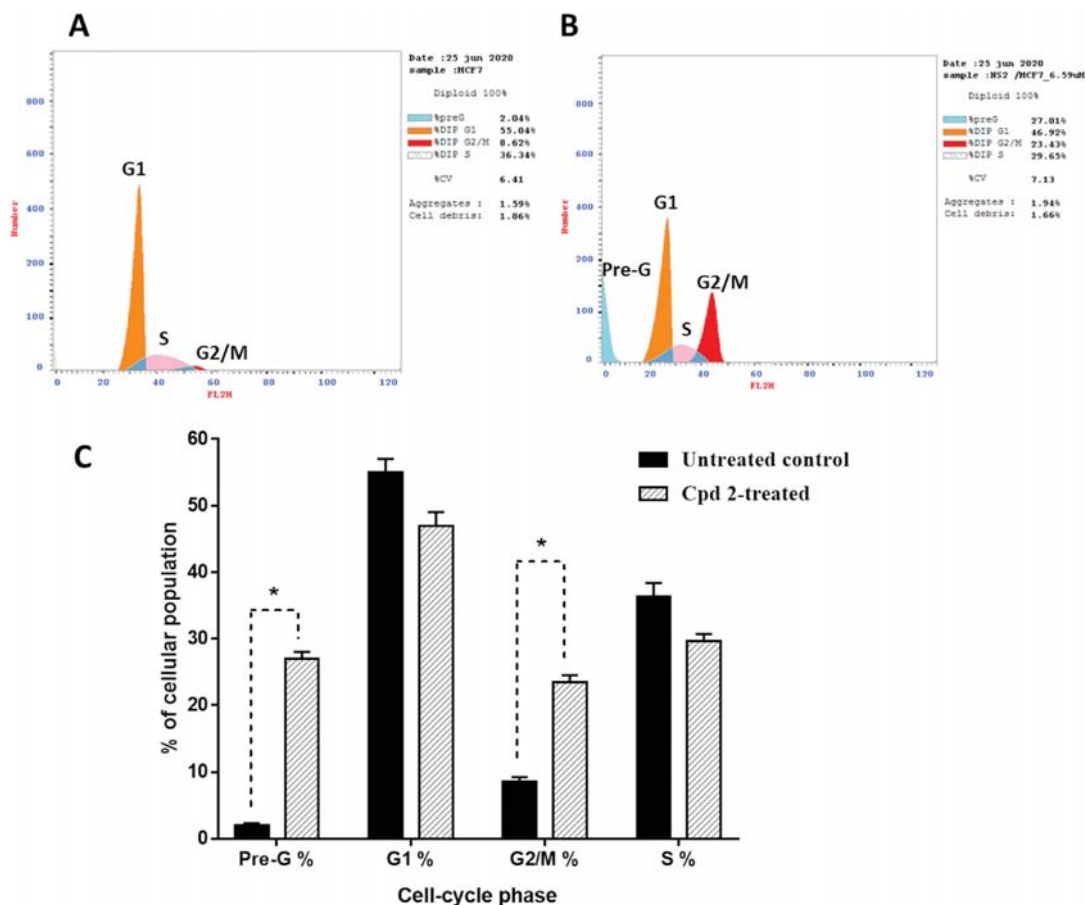


Fig. 6. Histograms DNA content-flow cytometry aided cell cycle analysis of A: Untreated and B: Treated MCF-7 cells with **2** ($IC_{50} = 6.59 \mu M$, 48 h), and C: Bar-representation of the percentage of cell population at each cell cycle. * Significant difference between control and treated group ($p < 0.05$, unpaired *t*-test).

control cells), while treatment decreased cellular populations at both G1 and S phases.

This is in agreement with Junior et al. [8], who investigated the apoptotic effect of eugenol in MCF-7 by arresting the cell cycle at G2/M phase abrogation associated with intense ROS production and mitochondrial toxicity triggering apoptosis in cancer cells. Additionally, our results are compliant with Pathak et al. [5], who investigated a novel eugenol-based derivative as the most active molecule, which inhibited proliferation of cancer cells by inducing apoptosis and causing a cell cycle accumulation at the G2/M phase.

3.6. RT-PCR analysis of pro-apoptotic and anti-apoptotic genes

Based on the significant cytotoxic activity of compound **2**, and its apoptosis inducing activity in the MCF-7 cells, and for elucidation the ER α -signalling-dependent apoptosis, herein the RT-PCR analysis of pro-apoptotic and anti-apoptotic genes were further investigated. Relative gene expression of p53, PUMA, caspases-3, -8 & -9, and Bcl-2, was assessed by RT-PCR (Fig. 7). Additionally, the ER α gene expression level was also evaluated in treated and untreated MCF-7 cells. As shown in Fig. 7, compound **2** significantly increased the gene expression level of p53 gene (≈ 7.54 -fold) with concomitant activation of Bax and PUMA levels by 5.43 and 4.34-fold, respectively. Also, the compound significantly increased the mRNA levels of caspases-3, -8, -9 genes with ≈ 8.75 -fold, 3.23-fold and 6.34-fold, respectively, while it significantly down-regulated the anti-apoptotic Bcl-2 gene (decrease of ≈ 0.35 -fold). Additionally, it inhibited the expression levels ER α with ≈ 0.34 -fold. Thus, these results propose induction of intrinsic and extrinsic apoptosis

pathway in treated MCF-7 breast cancer cells. These obtained results are in line with the flow cytometric data of apoptosis-induction, and ER α -dependency in the MCF-7 cells. Additionally, they agree with other previous studies, in which the eugenol-related apoptosis through up-regulation of proapoptotic genes and down-regulation of anti-apoptotic genes was investigated [24] and through the mitochondrial pathway via Bax, p53 increase [6], Bcl-2 decrease [25], and casapase-3 and 9 elevation in breast cancer cell lines [7,11].

3.7. Western blotting

Employing western blotting technique, we measured the expression levels of p53, Bax, caspase-3, & -9, Bcl-2, and ER α proteins to confirm the mechanism of apoptosis induction caused by compound **2** in MCF-7 cells. Results implied that p53, Bax, caspases-3 & -9 proteins were upregulated. In contrast, the Bcl-2, and ER α proteins were down-regulated in compound **2** treated cells, and this is indicated by visualizing both thick and thin bands and in their relative quantification data shown in Fig. 7. These results are consistent with the upregulation of pro-apoptotic and downregulation of anti-apoptotic genes witnessed in the RT-PCR results.

3.8. In vivo results

A preliminary experiment was first conducted to test the lethal dose of **2**. The performed experiment demonstrated the LD₅₀ of derivative **2** to be 6 mg/kg BW. The anti-breast cancer activity of compound **2**, was evaluated in SEC-bearing mice and was compared to both 5-FU treated

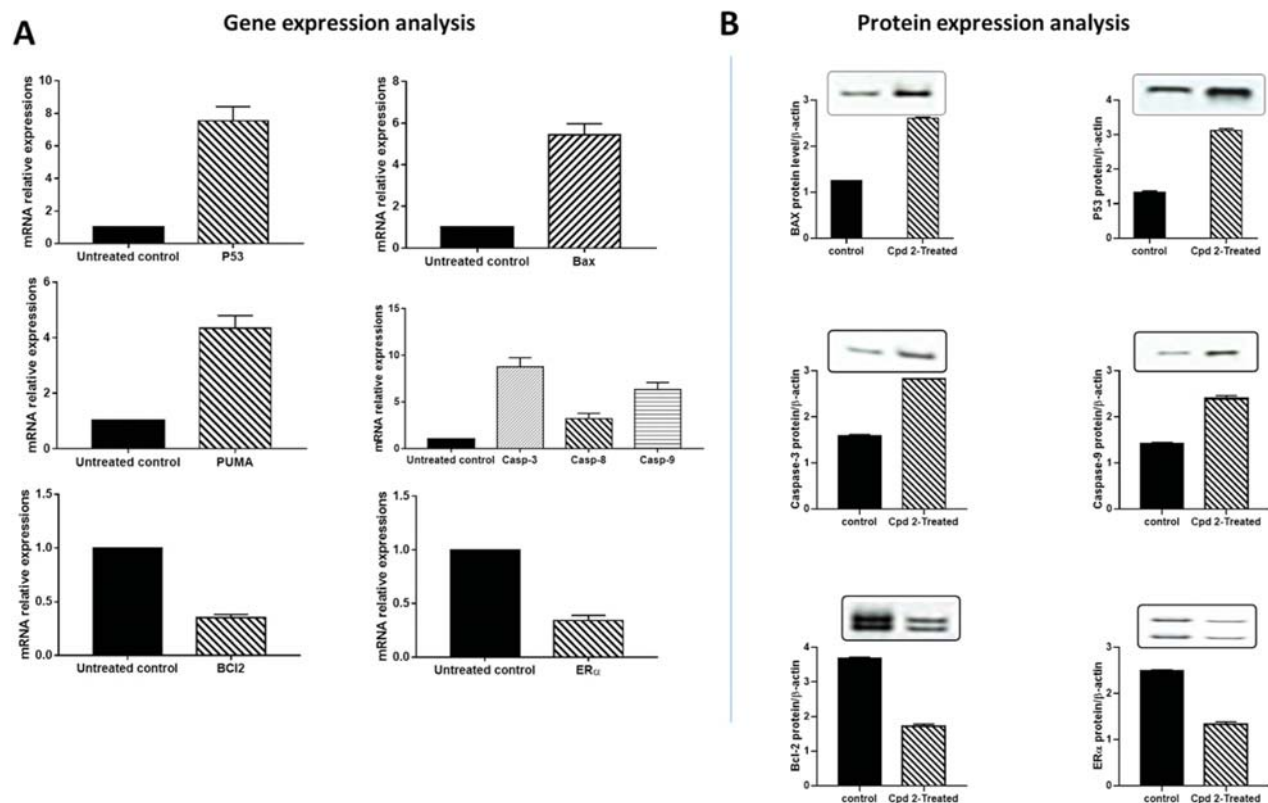


Fig. 7. A; Gene expression level, B; Protein expression level of genes in both untreated and treated MCF-7 with 2 ($IC_{50} = 6.59 \mu M$, 48 h).

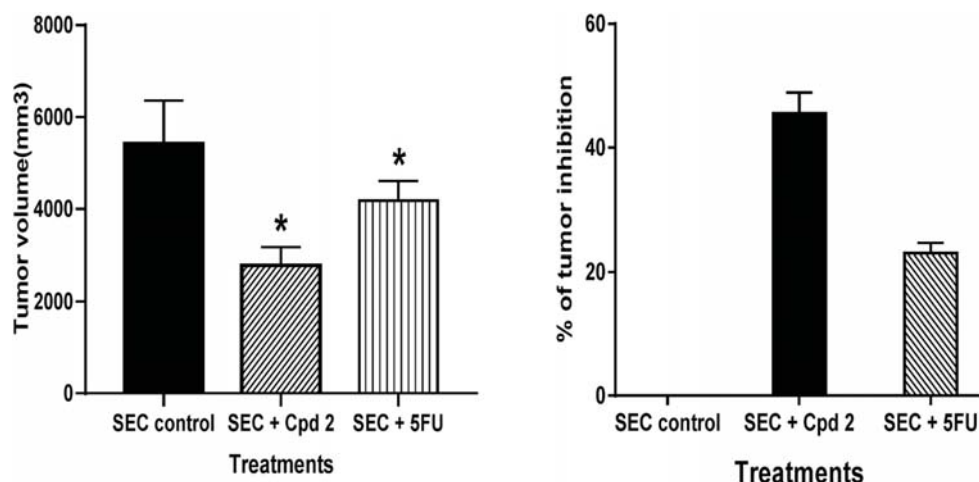


Fig. 8. Tumor volume and TIR% in SEC-bearing mice with treatment of compound 2 and 5-FU ($TIR\% = \frac{C-T}{C} \times 100$). * Significant difference between control and treated group ($p < 0.05$, unpaired *t*-test).

mice as a standard drug and SEC-bearing untreated mice as positive control.

3.8.1. Antitumor potentiality

Propagation of SEC cells into mice increased the tumor volume in the SEC-control mice, while treatment with compound 2 significantly reduced the tumor volume (2790 mm^3) as compared with SEC group (5423 mm^3) and 5-FU group (4177 mm^3). In addition, compound 2 caused a commitment decrease in the tumor inhibition ratio percentage (TIR%) by 47.6%, being more effective than 5-FU (22.9%) (Fig. 8). The

obtained *in vivo* results support the encouraging *in vitro* therapeutic potential that compound 2 has as an antitumor agent.

3.8.2. Hematological parameters

As seen in Table 2, normal mice treatment by 2 did not confer any significant change in CBC parameters compared to normal control, thus proving safety of the tested compound. Comparing SEC groups, all CBC parameters changes were compared to normal control due to the effect of solid tumor propagation during the experiment on the CBC parameters. Both Hemoglobin level and RBC's count were decreased to 9.8 g/

Table 2

Hematological, liver and kidney parameters in different tested groups of SEC-bearing and normal mice.

Parameter Treatments	Hematological parameters			Liver parameters				Kidney parameters	
	Hb (g/ dL)	RBC's (× 10 ⁶ /μL)	WBC's (× 10 ³ /μL)	ALT (U/ L)	AST (U/ L)	Total protein (mg/dL)	Albumin (mg/ dL)	Urea (mg/ dL)	Creatinine (mg/ dL)
Normal control	13.3 ± 0.6	8.9 ± 0.3	9.4 ± 1.2	38.7 ± 4.7	38.7 ± 2.9	6.7 ± 0.4	4.2 ± 0.4	27.3 ± 2.5	1.5 ± 0.2
Normal mice + Cpd 2 (6 mg/kg BW)	13.7 ± 0.1	9.6 ± 0.1	6 ± 0.6	30 ± 5.2	35.8 ± 5	7.4 ± 0.4	3.9 ± 0.1	24.5 ± 4.3	1.8 ± 0.2
SEC control	9.8* ± 0.7	7.9 ± 0.5	16.8* ± 3.4	64.6* ± 6.5	62.4* ± 6.1	4.9* ± 0.4	2.3* ± 0.5	46.8* ± 3	1.9 ± 0.1
SEC + Cpd 2 (6 mg/kg BW)	12.5 [#] ± 0.1	8.6 ± 0.3	10.4 [#] ± 1.7	39 [#] ± 7.4	38.7 [#] ± 9.4	6.9 [#] ± 0.4	3.3 [#] ± 0.06	24.4 [#] ± 2.3	0.7 [#] ± 0.02
SEC + 5-FU (6 mg/kg BW)	10.5 ± 1.1	7.5 ± 0.7	13 ± 4.1	39.1 ± 3.6	38 ± 4.6	7.2 ± 0.4	4.1 ± 0.3	26 ± 2.6	0.8 ± 0.1

- Results are expressed as Mean ± SE (n = 9).

- * Significant difference between SEC control and normal control using unpaired *t*-test ($P \leq 0.05$) using the GraphPad prism7.- [#] Significant difference between SEC control and compound 2 SEC-treated groups using unpaired *t*-test ($P \leq 0.05$) using the GraphPad prism7.**Table 3**

Assessment of hepatic antioxidant activities in the studied groups.

Treatments	Parameter		
	GSH (mg/g. tissue)	CAT (U/g. tissue)	SOD (U/g. tissue)
Normal control	51.78 ± 1.08	50.87 ± 1.06	48.76 ± 1.08
SEC control	21.67* ± 0.08	17.86* ± 0.07	19.54* ± 0.19
SEC + Cpd 2 (6 mg/kg BW)	42.45 [#] ± 1.03	21.65 ± 0.98	38.76 [#] ± 0.90

- Results are expressed as Mean ± SE (n = 9).

- * Significant difference between SEC control and normal control using unpaired *t*-test ($P \leq 0.05$) using the GraphPad prism7.- [#] Significant difference between SEC control and compound 2 SEC-treated groups using unpaired *t*-test ($P \leq 0.05$) using the GraphPad prism7.

dL, and $7.9 \times 10^6/\mu\text{L}$, while the WBC's count was increased to $16.4 \times 10^3/\mu\text{L}$. Compared to SEC-bearing mice, treatment with compound 2 significantly increased hemoglobin content from 9.8 (g/dL) to 12.5 (g/dL), while RBC's count was non-significantly increased to $8.6 \times 10^6/\mu\text{L}$. On the other hand, 2 significantly decreased the WBC's count in the SEC-bearing mice from $16.810^3/\mu\text{L}$ to $10.4 \times 10^3/\mu\text{L}$.

3.8.3. Biochemical parameters

Other biochemical parameters like AST, ALT, total protein, albumin, urea and creatinine blood levels were also examined to determine alterations in biochemical profile upon treatment with 2 in SEC-bearing mice in comparison with normal mice, 5-FU treated SEC-bearing mice and untreated SEC-bearing mice as demonstrated in Table 2. Like with the hematological profile, 2 did not induce any significant change in liver and kidney parameters on normal treated mice demonstrating its safety profile. Comparing the SEC groups, liver enzymes ALT and AST were elevated to 64.6 U/L and 62.4 U/L, respectively compared to normal mice as a consequence of cancer propagation, but treatment by 2 decreased the elevated ALT, AST values to 39 U/L and 38.7 U/L, respectively, like 5-FU treatment. In addition, treatment by 2 maintained both total protein and albumin, urea, and creatinine levels near normal.

3.8.4. Antioxidant activity

Antioxidant levels of GSH, CAT and SOD in both untreated and 2-treated mice compared to normal mice group are presented and summarized in Table 3. Results demonstrate that the three tested antioxidants were significantly decreased in the SEC-bearing mice compared to normal mice as cancer poses an oxidative stress. On the other hand, comparing the 3 antioxidants levels in SEC control and compound 2 SEC treated mice, it was observed that GSH increased to 42.45 mg/g.tissue compared to 21.67 mg/g.tissue, and SOD increased to 38.76 U/g.tissue

compared to 19.54 U/g.tissue. However, CAT levels was not significantly different in treated and untreated SEC mice. These results agree with antioxidant activation of isoeugenol and its derivatives [26,27].

3.8.5. Histopathology assay

3.8.5.1. Liver tissues. Livers of normal mice, isoeugenol derivative 2 treated normal mice, untreated SEC-bearing mice, 5-FU, and 2 treated SEC-bearing mice were subjected to histopathological examination. Fig. 9 displays the findings where normal control group showed normal structure of central vein surrounded with hepatocytes while normal treated control group injected with 2 showed near normal hepatocytes with a little hydropic degeneration (panels A and B, respectively). With regards to SEC-bearing mice, SEC control group showed hydropic degeneration of hepatocytes, loss of cell boundaries, pyknosis (arrows) & karyolysis (arrowhead) and ballooning degeneration (panel C). On the other hand, SEC group treated with 5-FU showed some tissue enhancement, yet some hepatocytes still showed hydropic degeneration, pyknosis (arrows) & karyolysis (arrowhead) (panel D). Finally, SEC group treated with 2 (panel E) demonstrated near normal hepatic cells with better tissue enhancement as compared to (C) and (D) groups.

3.8.5.2. Kidney tissues. Additionally, animal test groups were also examined for their kidney tissues hisopathology as shown in Fig. 9. Normal control group showed normal structure of renal corpuscles and renal tubules, proximal convoluted tubules and distal convoluted tubules, glomerulus (Bowman's capsule) and urinary spaces, with a similar behavior by 2-treated normal control group (panels A and B, respectively). SEC control group showed inflammatory infiltration in the interstitial spaces (arrows), renal corpuscles showed congestion and hypercellularity and hyperemia (arrow heads) (panel C). SEC group treated with 5-FU displayed some tissue enhancement like normal group but still had inflammatory infiltration in the interstitial spaces (arrow) and hyperemia (arrow heads) (panel D). Finally, SEC group treated with 2 showed more near normal texture almost close to that of the normal group.

3.8.6. Immunohistochemistry assay

Solid tumor sections from untreated and 2-treated SEC-bearing mice were subjected to immunohistochemistry staining to determine their ER α expression levels. Tumor mice were treated with derivative 2 day after day for 20 days then sacrificed and solid tumor was eradicated to resort to IHC examinations. Untreated SEC group displayed positive expression of ER α indicating an active progression of tumor (Fig. 10, A). Mice with solid tumor treated with 2 displayed enhanced immunohistochemical staining of reduced intensity of the staining of ER α indicating a positive response to treatment and a behavior supportive of tumor

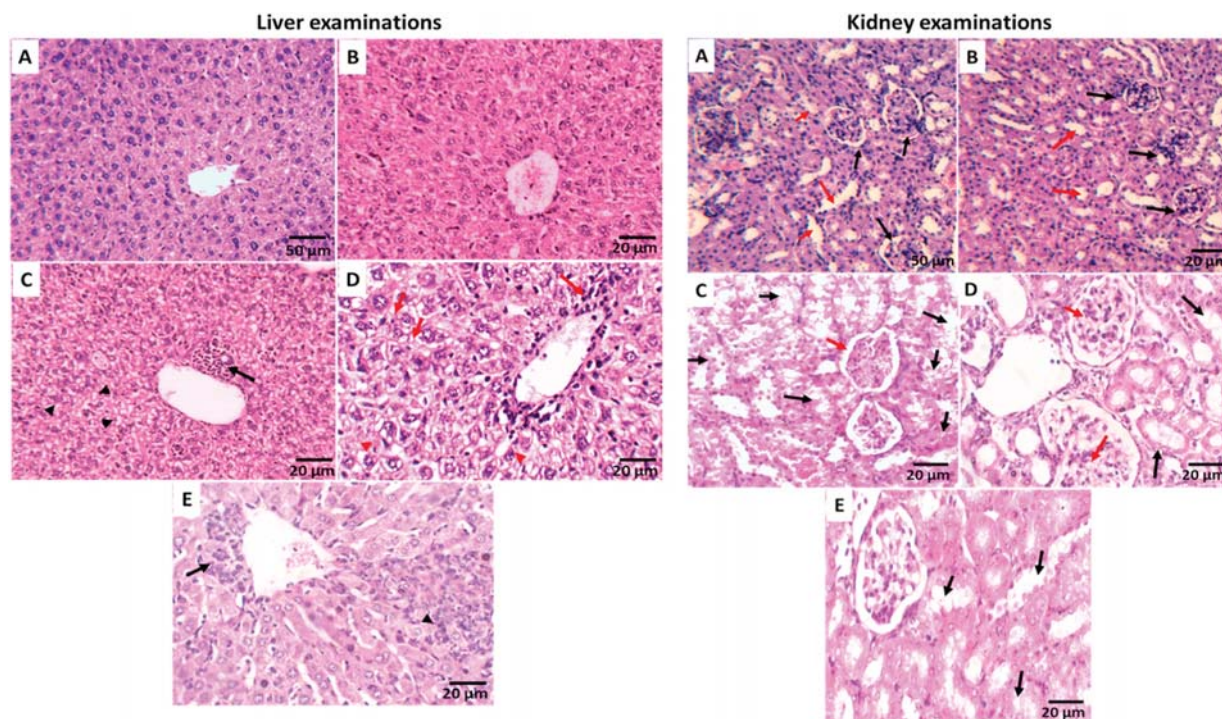


Fig. 9. Liver examinations: T.S in liver displays the effect of 2 on SEC bearing mice (A) Normal control group that shows normal structure of central vein surrounded with Hepatocytes. (B) Normal treated control group that injected with a dose of 2, uniform liver architecture, with no detected pathological changes. (C): SEC control group shows mild expansion of a portal tract with chronic inflammation (Black arrow). Hepatocytes showing hydropic degeneration (Arrow heads). (D) SEC group treated with compound 2 (6 mg/kg BW) that shows of chronic inflammatory cell infiltrate replacing hepatocytes (Black arrow), around central vein. Hepatocytes show hydropic degeneration (Arrow heads). (E) SEC group treated with 5-FU that shows expansion of portal tract with chronic inflammation (Black arrow) and area of confluent necrosis with chronic inflammatory cell infiltrate replacing hepatocytes (Arrowhead). Hepatocytes show no hydropic degeneration. (H&E, A, magnification of 10 \times , while others are of magnification 40 \times for better details).

Kidney examinations: L.S. in kidney displays the effect of 2 on SEC bearing mice. (A) Normal control group that shows uniform renal tissue, showing normal glomeruli (Black arrows), urinary spaces and tubules (Red arrows); proximal convoluted tubules and distal convoluted tubules (B) Normal treated control group that injected with a dose of 2, show normal structure as uniform renal tissue, showing normal glomeruli (Black arrows) and tubules (Red arrows). (C) SEC control group, many tubules show evidence of acute tubular injury, flattening of tubular epithelial cells, necrosis of cells, loss of brush border and apical vacuolization (Black arrows). Some glomeruli show mild mesangial expansion (Red arrow). (D) SEC group treated with (6 mg/kg BW) that shows few tubules with manifestations of mild tubular injury (Black arrows). Glomerular show mild mesangial expansion. (E) SEC group treated with 5-FU that shows Few tubules show manifestations of mild tubular injury (Black arrows). No detected glomerular injury was seen. (H&E, A, magnification of 10 \times , while others are of magnification 40 \times for better details. (For interpretation of the references to colour in this figure legend, the reader is referred to the Web version of this article.)

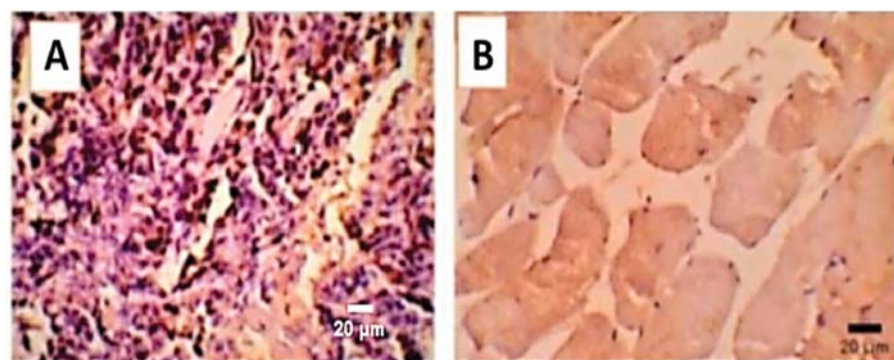


Fig. 10. Immunohistochemistry of solid tumor sections for ER- α . Tumor mice were treated with 2 day after day for 20 day then sacrificed and solid tumor eradicated to resort to IHC examinations. (A) SEC Group display positive expression as an indicator of tumor cells. (B) Mice with solid tumor treated with 2, display immunohistochemical staining of ER α (Anti-apoptotic factor) as an indicator for tumor reduction (magnification \times 400).

reduction (Fig. 10, B).

3.8.7. Statistical analysis

Data were statistically analyzed using GraphPad prism 7 and

expressed as mean \pm standard error. Unpaired *t*-test was used to find out if there is a significant difference between every two groups (control and treated). * Significant different ($p < 0.05$), while ** highly significant difference ($p < 0.01$).

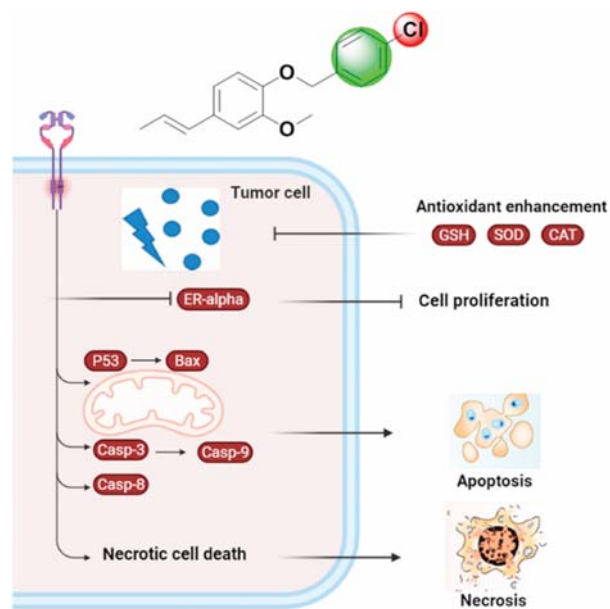


Fig. 11. Collective mechanism of action of the isoeugenol derivative 2.

4. Conclusion

Taken together, ER α plays an essential role in MCF-7, and its inhibition represents a practical approach for breast cancer treatment. This work sheds light on the chemotherapeutic activity of some isoeugenol derivatives (compound 2 being the most active and a representative of the class) as promising apoptotic anti-breast cancer agents through apoptosis induction and ER α reduced level expression. Compound 2 exhibited effective and selective cytotoxicity against MCF-7 with apoptosis induction arresting cell cycle at G2/M phase. Apoptosis-induction along with ER α inhibition pathway was validated as the effective molecular target for the tested compound through both gene and protein expression levels of pro- and anti-apoptotic markers. Restoration of the levels of endogenous antioxidants in SCE mice near to normal upon treatment by 2 also reflect its effectiveness in reducing the oxidative stress imposed by tumor growth. Finally, *in vivo* studies validated the anticancer activity and safety of treatment through amelioration of hematological, biochemical parameters and histopathological examinations. Thus, in conclusion, compound 2 can be viewed as a promising derivative from isoeugenol with good cytotoxic and apoptotic inducing activity against breast cancer due to its combined effect on ER + breast cancer cells as antioxidant, antiproliferative and pro-apoptotic (Fig. 11).

Novelty and impact

New semisynthetic isoeugenol derivatives were found to be cytotoxic on MCF-7 breast cancer cell lines and affect apoptosis on these ER + breast cancer cells being with low toxicity on normal breast cells. A representative promising derivative also induced antioxidant pathway activation and reduced ER α expression levels in treated cells. Additionally, *in vivo* testing of a representative on SEC mouse model demonstrated a very good cytotoxicity and safety profile compared to 5-FU drug standard.

Authors contributions

K.A., M.S.N. M.A.A. & R.K.A. design of the biology part; M.S.N. conducting *in vivo* experiments; M.S.N. and S.M.O. conducting *in vitro*

experiments; R.K.A. design of the chemical synthesis schemes; N.H.E. conducting chemical synthesis; all authors, writing, results interpretation, data analysis and revision of the manuscript at relevant sections.

Ethics statement

Suez Canal University Research Ethical Committee (Approval number REC-07-2020; Date August 2020).

Data availability statement

The data that support the findings of this study are available from the corresponding author upon reasonable request.

Declaration of competing interest

The authors declare that they have no known competing financial interests or personal relationships that could have appeared to influence the work reported in this paper.

Appendix A. Supplementary data

Supplementary data to this article can be found online at <https://doi.org/10.1016/j.cbi.2021.109753>.

References

- 1] M. Ma, Y. Ma, G.-J. Zhang, R. Liao, X.-F. Jiang, X.-X. Yan, F.-J. Bie, X.-B. Li, Y.-H. Lv, Eugenol alleviated breast precancerous lesions through HER2/PI3K-AKT pathway-induced cell apoptosis and S-phase arrest, *Oncotarget* 8 (2017) 56296–56310.
- 2] F.M. Abdel Bar, M.A. Khanfar, A.Y. Elnagar, F.A. Badria, A.M. Zaghoul, K. F. Ahmad, P.W. Sylvester, K.A. El Sayed, Design and pharmacophore modeling of biaryl methyl eugenol analogs as breast cancer invasion inhibitors, *Bioorg. Med. Chem.* 18 (2010) 496–507.
- 3] H. Azevedo-Barbosa, G.Á. Ferreira-Silva, C.F. Silva, T.B. de Souza, D.F. Dias, A.C. C. de Paula, M. Ionta, D.T. Carvalho, Phenylpropanoid-based sulfonamide promotes cyclin D1 and cyclin E down-regulation and induces cell cycle arrest at G1/S transition in estrogen positive MCF-7 cell line, *Toxicol. Vitro* 59 (2019) 150–160.
- 4] N. Vidhya, S.N. Devaraj, Induction of apoptosis by eugenol in human breast cancer cells, *Indian J. Exp. Biol.* 49 (2011) 871–878.
- 5] V. Pathak, I. Ahmad, A.K. Kahlon, M. Hasanain, S. Sharma, K.K. Srivastava, J. Sarkar, K. Shankar, A. Sharma, A. Gupta, Syntheses of 2-methoxyestradiol and eugenol template based diarylpropenes as non-steroidal anticancer agents, *RSC Adv.* 4 (2014) 35171.
- 6] I. Al-Sharif, A. Rammal, A. Aboussekhra, Eugenol triggers apoptosis in breast cancer cells through E2F1/survivin down-regulation, *BMC Cancer* 13 (2013) 600.
- 7] R. Al Wafai, W. El-Rabih, M. Katerji, R. Safi, M. El Sabban, O. El-Rifai, J. Usta, Chemosensitivity of MCF-7 cells to eugenol: release of cytochrome-c and lactate dehydrogenase, *Sci. Rep.* 7 (2017) 43730.
- 8] P.L.D.S. Júnior, D.A.D. Câmara, A.S. Costa, J.L.M. Ruiz, D. Levy, R.A. Azevedo, K.F. M. Pasqualoto, C.F. De Oliveira, T.C. De Melo, N.D.S. Pessoa, P.M.M. Fonseca, A. Pereira, et al., Apoptotic effect of eugenol involves G2/M phase abrogation accompanied by mitochondrial damage and clastogenic effect on cancer cell in vitro, *Phytomedicine* 23 (2016) 725–735.
- 9] A.A. Carvalho, L.N. Andrade, E.B.V. De Sousa, D.P. De Sousa, Antitumor phenylpropanoids found in essential oils, *BioMed Res. Int.* 2015 (2015) 1–21.
- 10] A.H. Carrasco, C.L. Espinoza, V. Cardile, C. Gallardo, W. Cardona, L. Lombardo, M. K. Catalán, F.M. Cuellar, A. Russo, Eugenol and its synthetic analogues inhibit cell growth of human cancer cells (Part I), *J. Braz. Chem. Soc.* 19 (2008) 543–548.
- 11] M.L. Abdullah, M.M. Hafez, A. Al-Hoshani, O. Al-Shabanah, Anti-metastatic and anti-proliferative activity of eugenol negative and HER2 positive breast cancer cells, *BMC Compl. Alternative Med.* 18 (2018) 321.
- 12] G.Q. Zheng, P.M. Kenney, L.K.T. Lam, Potential anticarcinogenic natural products isolated from lemongrass oil and galanga root oil, *J. Agric. Food Chem.* 41 (1993) 153–156.
- 13] A. Zarlaha, N. Kourkoumelis, T. Stanojkovic, D. Kovala-Demertzi, Cytotoxic activity of essential oil and extracts of *Ocimum Basilicum* against human carcinoma cells. Molecular docking study of isoeugenol as a potent cox and lox inhibitor, *Digest J. Nanomater. Biostruct.* 9 (2014) 907–917.
- 14] S.K. Jaganathan, E. Supriyanto, Antiproliferative and molecular mechanism of eugenol-induced apoptosis in cancer cells, *Molecules* 17 (2012) 6290–6304.
- 15] T. Atsumi, S. Fujisawa, K. Satoh, H. Sakagami, I. Iwakura, T. Ueha, Y. Sugita, I. Yokoe, Cytotoxicity and radical intensity of eugenol, isoeugenol or related dimers, *Anticancer Res.* 20 (2000) 2519–2524.

- [16] W. Elsayed, L. El-Shafie, M.K. Hassan, M.A. Farag, S.F. El-Khamisy, Isoeugenol is a selective potentiator of camptothecin cytotoxicity in vertebrate cells lacking TDP1, *Sci. Rep.* 6 (2016) 26626.
- [17] T. Jokela, M. Labarge, *Culture of Animal Cells: A Manual of Basic Technique and Specialized Applications*, seventh ed., Culture of Cancer stem cells ed., 2015, pp. 583–587.
- [18] D. Katz, E. Ito, K.S. Lau, J.D. Mocanu, C. Bastianutto, A.D. Schimmer, F.-F. Liu, Increased efficiency for performing colony formation assays in 96-well plates: novel applications to combination therapies and high-throughput screening, *Biotechniques* 44 (2008) ix–xiv.
- [19] M. He, W. Ning, Z. Hu, J. Huang, C. Dong, H.B. Zhou, Design, synthesis and biological evaluation of novel dual-acting modulators targeting both estrogen receptor α (ER α) and lysine-specific demethylase 1 (LSD1) for treatment of breast cancer, *Eur. J. Med. Chem.* 195 (2020) 112281.
- [20] S.W. Kattan, M.S. Nafie, G.A. Elmgeed, W. Alelwani, M. Badar, M.A. Tantawy, Molecular docking, anti-proliferative activity and induction of apoptosis in human liver cancer cells treated with androstane derivatives: implication of PI3K/AKT/mTOR pathway, *J. Steroid Biochem. Mol. Biol.* 198 (2020) 105604.
- [21] A.A.M. Sarhan, A.T.A. Boraie, A. Barakat, M.S. Nafie, Discovery of hydrazide-based pyridazino[4,5-b]indole scaffold as a new phosphoinositide 3-kinase (PI3K) inhibitor for breast cancer therapy, *RSC Adv.* 10 (2020) 19534–19541.
- [22] E.M. Gad, M.S. Nafie, E.H. Eltamany, M.S.A.G. Hammad, A. Barakat, A.T.A. Boraie, Discovery of new apoptosis-inducing agents for breast cancer based on ethyl 2-amino-4,5,6,7-tetra hydrobenzo[b]Thiophene-3-carboxylate: synthesis, in vitro, and in vivo activity evaluation, *Molecules* 25 (2020) 2523.
- [23] E. Dervis, A. Yurt Kilcar, E.I. Medine, V. Tekin, B. Cetkin, E. Uygur, F.Z.B. Muftuler, In vitro incorporation of radioiodinated eugenol on adenocarcinoma cell lines (Caco2, MCF7, and PC3), *Cancer Biother. Rad.* 32 (2017) 75–81.
- [24] X. Sun, V.P. Veeraraghavan, K.M. Surapaneni, S. Hussain, M. Mathanmohun, S. A. Alharbi, A.A.M. Aladresi, A. Chinnathambi, Eugenol–piperine loaded polyhydroxy butyrate/polyethylene glycol nanocomposite-induced apoptosis and cell death in nasopharyngeal cancer (C666-1) cells through the inhibition of the PI3K/AKT/mTOR signaling pathway, *J. Biochem. Mol. Toxicol.* 35 (2021) 22700.
- [25] M.A. Fouad, M.M. Sayed-Ahmed, E.A. Huwait, H.F. Hafez, A.-M.M. Osman, Epigenetic immunomodulatory effect of eugenol and astaxanthin on doxorubicin cytotoxicity in hormonal positive breast Cancer cells, *BMC Pharmacol. Toxicol.* 22 (2021) 8.
- [26] E. Findik, M. Ceylan, M. Elmastaş, Isoeugenol-based novel potent antioxidants: synthesis and reactivity, *Eur. J. Med. Chem.* 46 (2011) 4618–4624.
- [27] H. Vijay Kumar, N. Naik, Synthesis and antioxidant properties of some novel 5H-dibenz[b,f]azepine derivatives in different in vitro model systems, *Eur. J. Med. Chem.* 45 (2010) 2–10.

3.6. Preparation and nanoformulation of new quinolone scaffold-based anticancer agents: Enhancing solubility for better cellular delivery.

Nehal H. Elghazawy, Amr Hefnawy, Nada K. Sedky, Ibrahim M. El-Sherbiny, Reem K. Arafa

Eur. J. Pharm. Sci. **2017**, *105*, 203-211. Doi: [10.1016/j.ejps.2017.05.036](https://doi.org/10.1016/j.ejps.2017.05.036)

Abstract

A new series of 5,7-dibromoquinoline scaffold-based derivatives with varied flexibility substituents at position 8 of the ring system has been synthesized as potential anticancer agents. The new compounds were evaluated for their in vitro antiproliferative activity versus the human breast cancer cell lines MCF-7 and MDA-MB231. Generally, both cell lines were responsive to the cytotoxic effect of the synthesized analogues. Compounds 4a, 5c and 7b were chosen for nanoformulation studies to assess the effect of enhancing their solubility profile on their cytotoxic ability. Indeed, the pluronic nanomicelles of the three formulated derivatives showed an observable significant increase in their cytotoxic efficacy demonstrating a positive impact of the used nanoformulations on the delivery of the active compounds to their cellular biological targets.



Contents lists available at ScienceDirect

European Journal of Pharmaceutical Sciences

journal homepage: www.elsevier.com/locate/ejps

Preparation and nanoformulation of new quinolone scaffold-based anticancer agents: Enhancing solubility for better cellular delivery

Nehal H. Elghazawy^a, Amr Hefnawy^b, Nada K. Sedky^a, Ibrahim M. El-Sherbiny^{b,1}, Reem K. Arafa^{a,*,1}^a University of Science and Technology, Zewail City of Science and Technology, 12588 Giza, Egypt^b Center for Materials Science, Zewail City of Science and Technology, 6th October City, 12588, Giza, Egypt

ARTICLE INFO

Keywords:

Quinolines
Antiproliferative agents
Cytotoxicity
MCF-7
MDA-MB231
Poloxamers

ABSTRACT

A new series of 5,7-dibromoquinoline scaffold-based derivatives with varied flexibility substituents at position 8 of the ring system has been synthesized as potential anticancer agents. The new compounds were evaluated for their in vitro antiproliferative activity versus the human breast cancer cell lines MCF-7 and MDA-MB231. Generally, both cell lines were responsive to the cytotoxic effect of the synthesized analogues. Compounds **4a**, **5c** and **7b** were chosen for nanoformulation studies to assess the effect of enhancing their solubility profile on their cytotoxic ability. Indeed, the pluronic nanomicelles of the three formulated derivatives showed an observable significant increase in their cytotoxic efficacy demonstrating a positive impact of the used nanoformulations on the delivery of the active compounds to their cellular biological targets.

1. Introduction

Cancer is identified by the American cancer society as a group of diseases characterized by the uncontrolled growth and spread of abnormal cells (Society, 2016). The ability of these abnormal cells to outgrow their normal boundaries leads to cancer invasiveness and metastasis (Anand et al., 2008; Moscow and Cowan, 2007; Thun, 2007). Statistics showed an estimate of 14.1 million cancer cases and 8.2 cancer deaths worldwide in 2012. These numbers are expected to reach about 21.7 million new cancer cases and 13.0 million cancer deaths by year 2030 (Society, 2016). That terrifying rapid increase in cancer incidence and mortality rates has put researchers in a constant advent to develop new chemical moieties to work as anticancer agents. On the other hand, rapid emergence of the resistance to currently clinically used chemotherapeutic anticancer agents calls for exploration of new chemotypes.

Among the promising widely investigated chemical classes stands the quinolone-based nucleus (Solomon and Lee, 2011) that is found in many biologically active natural as well as synthetic molecules (Yan et al., 2013). Interestingly, the quinoline ring system is also known to be one of the most prominent scaffolds in the field of designing novel active anticancer agents where decorations on various positions around the quinoline ring would pave a way to modify the pharmacokinetic as well as the pharmacodynamic properties of the designed derivatives

(Jasinski et al., 2008; Jasinski et al., 2011; Wang et al., 2011). This new dimension of quinoline development in anticancer drug development was added by the advent of Camptothecin in 1966 (Wall et al., 1966) and its synthetic analogs like Topotecan, Irinotecan and Exatecan (Fig. 1). The anticancer potential of several of these derivatives has been proven on various cancer cell lines (Bawa et al., 2010). Currently reported are many quinolone-based anticancer agents possessing diverse mechanisms of action like topoisomerase inhibition, telomerase inhibition, Hsp90 inhibition (Afzal et al., 2015), tubulin inhibition (Alqasoumi et al., 2009), free radical regulation and increasing the activity of superoxide dismutase (Rashad et al., 2010). Also, explored was the ability of quinoline derivatives to induce cytotoxicity through carbonic anhydrase inhibition (Ghorab et al., 2010), cMet kinase inhibition (Wang et al., 2011), VEGFR inhibition (Ghorab et al., 2011), increase in the protein expression of Bad, Bax and decrease in Bcl-2, and PARP with consequent cell death (Tseng et al., 2011), and down regulation or alteration of gap junction intercellular communication activities (Heiniger et al., 2010).

In line with our previous attempts to explore new quinoline derivatives (Arafa et al., 2013), we herein report a series of novel compounds based on the 5,7-dibromoquinoline scaffold backbone.

The design strategy adopted for the new series was to introduce various groups at position 8 of the quinoline nucleus. Those groups were varied with respect to their conformational/physicochemical

* Corresponding author.

E-mail address: rkhidr@zewailcity.edu.eg (R.K. Arafa).¹ Both authors share seniority in authorship.

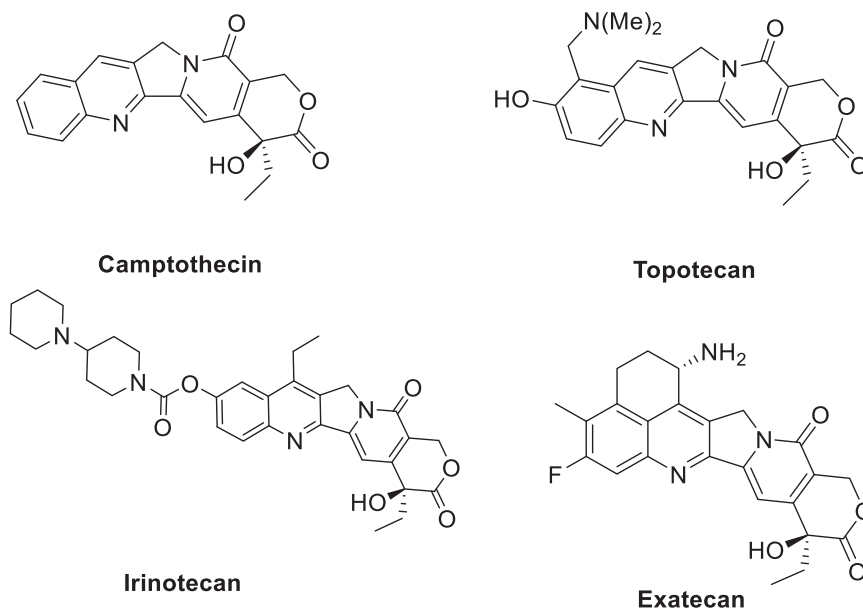


Fig. 1. Structures of some quinoline-based anticancer compounds.

parameters being altered between flexible and rigid, hydrophilic and hydrophobic as well as hydrogen bond donating and/or accepting characters. The antiproliferative biological effect of all the synthesized compounds were assessed against MDA-MB231 and MCF-7 human breast cancer cell lines.

As is the case with drug development, the use of compounds with promising bioactivity may be hindered by other factors rather than the activity itself. This may include pharmacokinetic factors as poor solubility, limited bioavailability and lack of stability or difficulties in formulating the bioactive compound into a suitable dosage form for delivery. Overcoming these obstacles via further structural modifications is not a preferred approach as it may affect the desired activity or selectivity of the compound. A more simple way is to incorporate the compound into a suitable carrier system that maintains the desired bioactivity of the compound and at the same time evades the aforementioned drawbacks. In this study, three of the synthesized compounds among those showing the most promising anticancer activity were incorporated into pluronic nanomicelles to enhance their aqueous solubility, and consequently their cancer cell penetrability as well as allowing their sustained release.

Pluronic polymers or poloxamers are a class of non-ionic block copolymers that consist of a central hydrophobic poly(propylene glycol) block conjugated from both sides with hydrophilic poly(ethylene glycol) blocks (Israelachvili, 1997). Pluronic are present in the molecular state at concentrations and temperatures below their critical micelle concentration and temperature, respectively. At higher concentrations or temperatures, pluronic chains aggregate forming micelles that are arranged to minimize the interactions between the aqueous environment and the hydrophobic poly(propylene glycol) portion of the copolymer. The use of pluronic nanomicelles for loading of hydrophobic drugs has been reported in several studies. These drugs include, for instance, naproxen (Yardimci et al., 2005), indomethacin (Sharma and Bhatia, 2004), ibuprofen (Foster et al., 2009), aspirin (Basak and Bandyopadhyay, 2013), and silymarin (El-Far et al., 2016).

2. Experimental

2.1. Chemistry

Melting points were measured employing in an open capillary

method with a DMP100 melting point device and are uncorrected. IR spectra were recorded on Thermo Scientific™ Nicolet™ iS™10 FT-IR spectrometer. ^1H NMR and ^{13}C NMR spectra were obtained using Bruker high performance digital FT-NMR Spectrometer Avance III 400 MHz using TMS as an internal standard. Elemental analyses and Mass spectra were carried out at the Microanalytical center, Faculty of Pharmacy, Al-Azhar University, Egypt and are within ± 0.4 of the calculated values. All chemical and solvents were purchased from Sigma Aldrich and used as provided. Compounds **2** and **3** were prepared according to the reported methods (Mosmann, 1983; Scudiero et al., 1988).

2.1.1. General Method for Preparation of *N'*-(substituted)benzylidene-2-(5,7-dibromoquinolin-8-yloxy)acetohydrazides (**4a,b**)

A suspension of the hydrazide **3** (0.5 g, 1.33 mmol) in absolute ethanol (20 mL) was treated with the appropriate aromatic aldehyde (1.59 mmol) in the presence of a catalytic amount of glacial acetic acid (1 mL) and the reaction mixture was refluxed for 5 h. After half an hour of reflux, **3** dissolved completely and within 1 h a new precipitate of the Schiff's base started forming. After completion of reflux, the reaction mixture was poured onto ice/water and the formed precipitate was collected by filtration, washed, dried and recrystallized from DMF/H₂O.

2.1.1.1. 2-((5,7-Dibromoquinolin-8-yl)oxy)-*N'*-(4-Hydroxybenzylidene)Acetohydrazide (**4a**). Yield: 81%; m.p. 245–248 °C. IR (cm^{-1}): 3304 (OH), 3200 (NH), 3060 (CH aromatic), 1666 (C = O). ^1H NMR (300 MHz, DMSO-*d*₆): δ 12.09 (s, 1H), 9.93 (s, 1H), 9.13 (dd, J = 8.6, 1.2 Hz, 1H), 8.56 (dd, J = 8.6, 1.2 Hz, 1H), 8.27 (s, 1H), 7.86 (s, 1H), 7.84–7.79 (m, 1H), 7.62 (d, J = 8.5 Hz, 2H), 6.86 (d, J = 8.5 Hz, 2H), 4.97 (s, 2H). ^{13}C NMR (75 MHz, DMSO-*d*₆): δ 168.5, 163.8, 159.4, 151.2, 148.1, 143.8, 136.0, 133.2, 128.9, 127.3, 125.0, 123.2, 116.2, 115.6, 108.8, 72.7. MS *m/z*: 476.87 (M^+). Anal. Calcd. for C₁₈H₁₃Br₂O₃ (476.93): C, 45.12; H, 2.73; N, 8.77. Found: 45.43; H, 2.45; N, 8.57.

2.1.1.2. 2-((5,7-Dibromoquinolin-8-yl)oxy)-*N'*-(4-nitrobenzylidene)acetohydrazide (**4b**). Yield: 93%; m.p. 258–260 °C. IR (cm^{-1}): 3171 (NH), 3060 (CH aromatic), 2973 (CH aliphatic), 1689 (C = O). ^1H NMR (300 MHz, DMSO-*d*₆): δ 12.57 (s, 1H), 9.16 (s, 1H), 8.60 (s, 1H), 8.55 (dd, J = 8.5, 3.9 Hz, 1H), 8.32 (s, 1H), 8.19 (d, J = 6.2 Hz, 2H), 7.85

(dd, $J = 8.5, 3.9$ Hz, 1H), 7.80 (d, $J = 8.6$ Hz, 2H), 5.05 (s, 2H). MS m/z : 508.40 (M^+). Anal. Calcd. for $C_{18}H_{12}Br_2N_4O_4$ (508.13): C, 42.55; H, 2.38; N, 11.03. Found: C, 42.94; H, 2.19; N, 10.67.

2.1.2. General Method for Preparation of 2-(5,7-dibromoquinolin-8-yloxy)-*N'*-(1-(Substituted)phenylethylidene)acetohydrazides (**5a,b**)

The same method employed for synthesis of derivatives **4a,b** was adopted for preparation of the quinolines **5a,b** but replacing aromatic aldehydes with the appropriate substituted aromatic acetophenone.

2.1.2.1. 2-((5,7-Dibromoquinolin-8-yl)oxy)-*N'*-(1-(4-nitrophenyl)ethylidene) acetohydrazide (5a**)**. Yield, 40%; m.p. 259–261 °C. IR (cm^{-1}): 33,087 (OH), 3226 (NH), 3036 (CH aromatic), 2924 (CH aliphatic), 1678 (C = O). 1H NMR (400 MHz, DMSO- d_6): δ 11.19 (s, 1H), 9.74 (s, 1H), 8.99 (dd, $J = 4.3, 1.5$ Hz, 1H), 8.53–8.47 (m, 1H), 8.19 (s, 1H), 7.74 (dd, $J = 8.6, 4.3$ Hz, 1H), 7.40 (d, $J = 8.4$ Hz, 2H), 6.75 (d, $J = 8.4$ Hz, 2H), 4.93 (s, 2H), 2.34 (s, 3H). ^{13}C NMR (100 MHz, DMSO- d_6) δ 169.92, 164.47, 159.36, 152.30, 152.00, 148.80, 142.86, 136.58, 133.70, 128.50, 127.94, 124.28, 116.85, 115.56, 115.49, 73.47, 14.18. MS m/z : 492.94 (M^+). Anal. Calcd. for $C_{19}H_{15}Br_2N_3O_3$ (493.15): C, 46.27; H, 3.07; N, 8.52. Found: C, 46.18; H, 2.88; N 8.48.

2.1.2.2. 2-((5,7-Dibromoquinolin-8-yl)oxy)-*N'*-(1-(4-nitrophenyl)ethylidene) acetohydrazide (5b**)**. Yield: 92%; m.p. 238–240 °C. IR (cm^{-1}): 3184 (NH), 3079 (CH aromatic), 2929 (CH aliphatic), 1702 (C = O). 1H NMR (400 MHz, DMSO- d_6): δ 11.04 (s, 1H), 9.00 (s, 1H), 8.62 (d, $J = 7.8$ Hz, 1H), 8.53 (d, $J = 7.8$ Hz, 1H), 8.18 (d, $J = 9.4$ Hz, 2H), 7.89 (d, $J = 9.1$ Hz, 2H), 7.80 (m, 1H), 5.70 (s, 2H), 2.33 (s, 3H). MS m/z : 522.46 (M^+). Anal. Calcd. for $C_{19}H_{14}Br_2N_4O_4$ (522.15): C, 43.71; H, 2.70; N, 10.73. Found: C, 44.03; H, 2.67; N, 11.06.

2.1.3. General Method for Preparation of the Amino Arylidene Derivatives (**4c** and **5c**)

To a suspension of the nitro compounds **4b** or **5b** (0.01 mol) in EtOH (10 mL), Fe powder (0.03 mol) and $CaCl_2$ (0.01 mol) were added. The resulting suspension was allowed to reflux for 3 h. Progress of the reaction was monitored by TLC. After completion of the reaction it was filtered and the filtrate was washed with ethyl acetate (3 \times 20 mL). The organic extract was washed with H_2O (3 \times 10 mL) and dried over anhydrous Na_2SO_4 . The organic phase was then evaporated to dryness under vacuum to obtain products **4c** and **5c**.

2.1.3.1. *N'*-(4-Aminobenzylidene)-2-((5,7-dibromoquinolin-8-yl)oxy)acetohydrazide (4c**)**. Yield, 66%; m.p. 223–225 °C. IR (cm^{-1}): 3380 (NH), 3190 (NH), 2999 (CH aliphatic), 1684 (C=O). 1H NMR (300 MHz, DMSO- d_6): δ 12.56 (s, 1H), 11.78 (s, 1H), 9.14 (m, 1H), 8.96 (s, 1H), 8.56 (d, $J = 9.4$ Hz, 2H), 8.25 (d, $J = 10.0$ Hz, 2H), 7.43 (d, $J = 8.2$ Hz, 1H), 6.60 (d, $J = 8.1$ Hz, 1H), 5.63 (s, 2H), 5.03 (s, 2H). MS m/z : 478.84 (M^+). Anal. Calcd. for $C_{18}H_{14}Br_2N_4O_2$ (478.14): C, 45.22; H, 2.95; N, 11.72. Found: C, 45.47; H, 2.98; N, 11.97.

2.1.3.2. *N'*-(1-(4-Aminophenyl)ethylidene)-2-((5,7-dibromoquinolin-8-yl)oxy)acetohydrazide (5c**)**. Yield, 89%; m.p. 215–217 °C. IR (cm^{-1}): 3412 (NH), 3327 (NH), 3181 (CH aromatic), 1705 (C=O). 1H NMR (400 MHz, DMSO- d_6): δ 11.16 (s, 1H), 10.44 (s, 2H), 9.00 (d, $J = 9.4$ Hz, 1H), 8.51 (d, $J = 9.4$ Hz, 1H), 8.4–8.1 (m, 1H), 7.65 (d, $J = 7.8$ Hz, 2H), 7.35 (s, 1H), 6.54 (d, $J = 7.8$ Hz, 2H), 4.98 (s, 2H), 2.36 (s, 3H). ^{13}C NMR (100 MHz, DMSO- d_6): δ 170.6, 164.1, 154.5, 152.0, 151.0, 142.8, 136.1, 133.7, 128.1, 127.6, 125.3, 124.3, 123.8, 116.8, 113.6, 73.5, 13.9. MS m/z : 492.18 (M^+). Anal. Calcd. for $C_{19}H_{16}Br_2N_4O_2$ (492.16): C, 46.37; H, 3.28; N, 11.38. Found: C, 46.48; H, 3.31; N, 11.62.

2.1.4. General Method for Preparation of 2-(2-(5,7-dibromoquinolin-8-yloxy)acetyl)-*N*-phenylhydrazinecarboxamides **6a,b**

A suspension of the key intermediate hydrazide **3** (0.37 g, 1 mmol)

in dioxane (20 mL) was treated with the appropriate phenylisocyanate (1.5 mmol) and heated under reflux. After 1 h of reflux the hydrazide dissolved and a new precipitate started forming. Reflux was maintained for 8 h after which the reaction mixture was filtered while hot, the residue was washed with hot ethanol (70%, 3 \times 5 mL) and dried to afford the target compounds **6a** or **6b**.

2.1.4.1. *N*-(4-Chlorophenyl)-2-(2-((5,7-dibromoquinolin-8-yl)oxy)acetyl)hydrazine-carboxamide (6a**)**. Yield: 94%; m.p. 248–250 °C. IR (cm^{-1}): 3325 (NH), 3306 (NH), 3204 (NH), 3010 (CH aromatic), 1723 (C = O), 1697 (C = O). 1H NMR (300 MHz, DMSO- d_6): δ 10.64 (s, 1H), 9.04 (d, $J = 8.5, 1H$), 8.89 (s, 1H), 8.54 (d, $J = 8.5, 1H$), 8.33 (s, 1H), 8.25 (s, 1H), 7.80 (m, 1H), 7.49–7.42 (d, $J = 9.01$ Hz, 2H), 7.34–7.25 (d, $J = 5.96$ Hz, 2H), 5.0 (s, 2H). MS m/z : 528.8 (M^+). Anal. Calcd. for $C_{18}H_{13}Br_2ClN_4O_3$ (528.89): C, 40.90; H, 2.48; N, 10.60. Found: C, 41.24; H, 2.54; N, 10.79.

2.1.4.2. 2-(2-((5,7-Dibromoquinolin-8-yl)oxy)acetyl)-*N*-(4-(trifluoromethyl)phenyl)hydrazinecarboxamide (6b**)**. Yield, 45%; m.p. 235–237 °C. IR (cm^{-1}): 3305 (NH), 3280 (NH), 3040 (CH aromatic), 2910 (CH aliphatic), 1712 (C = O). 1H NMR (400 MHz, DMSO- d_6): δ 10.62 (s, 1H), 9.13 (s, 1H), 8.98 (dd, $J = 4.2, 1.5$ Hz, 1H), 8.48 (dd, $J = 8.6, 1.6$ Hz, 1H), 8.40 (s, 1H), 8.20 (s, 1H), 7.75 (dd, $J = 8.6, 4.2$ Hz, 1H), 7.60 (d, $J = 8.7$ Hz, 2H), 7.55 (d, $J = 8.7$ Hz, 2H), 4.92 (s, 2H). ^{13}C NMR (100 MHz, DMSO- d_6): δ 167.11, 153.86, 152.12, 151.85, 143.40, 142.90, 136.40, 133.67, 127.88, 126.54, 124.19, 118.30, 116.66, 116.10, 72.95, 61.02, 14.87. MS m/z : 562.50 (M^+). Anal. Calcd. for $C_{19}H_{13}Br_2F_3N_4O_3$ (562.13): C, 40.60; H, 2.33; N, 9.97. Found: C, 40.57; H, 2.19; N, 9.72.

2.1.5. General method for preparation of 5-((5,7-dibromoquinolin-8-yloxy)methyl)-4-phenyl-4H-1,2,4-triazol-3-(thio)ol **7a,b**

The hydrazinecarboxamides were refluxed in ethanol (15 mL) in the presence of sodium ethoxide (1.5 mmol) for 5 h. The reaction mixture was then cooled and extracted using ethyl acetate (20 mL \times 3). The combined organic phase extract was washed with water (20 mL \times 3) and dried over anhydrous Na_2SO_4 . Evaporating the organic solvent under vacuum afforded the corresponding quinolinyltriazole derivative **7a** or **7b**.

2.1.5.1. 4-(4-Chlorophenyl)-5-(((5,7-dibromoquinolin-8-yl)oxy)methyl)-4H-1,2,4-triazol-3-ol (7a**)**. Yield: 70%; m.p. 208–210 °C. IR (cm^{-1}): 3350 (OH), 3081 (CH aromatic). 1H NMR (400 MHz, DMSO- d_6): δ 9.19 (s, 1H), 8.63 (d, $J = 8.5$ Hz, 1H), 8.53 (s, 1H), 8.46 (d, $J = 8.6$ Hz, 1H), 7.88 (dd, $J = 8.6, 4.3$ Hz, 1H), 7.45 (d, $J = 9.2$ Hz, 2H), 7.31 (d, $J = 8.9$ Hz, 2H), 4.58 (s, 2H). MS m/z : 510.98 (M^+). Anal. Calcd. for $C_{18}H_{11}Br_2ClN_4O_2$ (510.57): C, 42.34; H, 2.17; N, 10.97. Found: C, 42.59; H, 2.12; N, 11.34.

2.1.5.2. 5-(((5,7-Dibromoquinolin-8-yl)oxy)methyl)-4-(4-(trifluoromethyl)phenyl)-4H-1,2,4-triazol-3-ol (7b**)**. Yield, 20%; m.p. 99–101 °C. IR (cm^{-1}): 3305 (OH), 3040 (CH aromatic), 2929 (CH aliphatic). 1H NMR (400 MHz, DMSO- d_6): δ 10.54 (s, 1H), 8.36 (s, 1H), 8.21–8.14 (m, 1H), 7.77 (d, $J = 8.1$ Hz, 2H), 7.71–7.66 (m, 1H), 7.55 (d, $J = 8.1$ Hz, 2H), 7.50–7.43 (m, 1H), 4.14 (s, 2H). MS m/z : 544.14 (M^+). Anal. Calcd. for $C_{19}H_{11}Br_2F_3N_4O_2$ (544.12): C, 41.94; H, 2.04; N, 10.30. Found: C, 42.19; H, 2.03; N, 10.56.

2.2. Nanoformulations

2.2.1. Materials

Poly(ethylene glycol)-block-poly(propylene glycol)-block-poly(ethylene glycol) (Pluronic F108) was purchased from Aldrich (Germany). Acetone and all other solvents were of analytical grade and used as received. Water used was ultrapure (Type 1 water) obtained using Direct-Q® UV.

2.2.2. Experimental

2.2.2.1. Assessment of Solubility for Selected Compounds. The selected compounds were practically assessed for their solubility in aqueous environment. 10 mg of each compound were dispersed in 1 mL of double distilled H₂O and incubated overnight on the orbital shaker at ambient temperature. Undissolved particles were then separated by centrifuge for 30 min at 10,000 rpm. The supernatant was analyzed using UV–Vis spectrometer to determine the concentration of dissolved substance. Samples were prepared as triplicates and the values were taken as average of three measurements.

The partition coefficients (Log P) of the compounds were also evaluated experimentally by partitioning of 5 mg of each compound between 25 mL of octanol and equal volume of aqueous medium. The organic layer was then separated in a separating funnel dried and dissolved in excess known volume of DMSO to measure the concentration using UV–Vis spectrophotometric analysis.

2.2.2.2. Preparation of Bioactive Compounds-Loaded Pluronic Nanomicelles. The nanomicelles were prepared using nanoprecipitation method. Briefly, 100 mg of pluronic F108 was dissolved in mixture of 4.75 mL acetone and 0.25 mL distilled water. Afterwards, the bioactive compound (**4a**, **5c** or **7b**) was dissolved or dispersed in pluronic solution via probe sonication at 40 KW for 5 min. The resulting solution or suspension was then added dropwise to 12 mL of distilled water, and the solvent was evaporated to obtain dry bioactive compounds-loaded nanomicelles.

2.2.2.3. Determination of the Particle Size and Charge of the Formed Nanomicelles. Size and charge of the developed plain and loaded nanomicelles were measured using dynamic light scattering zeta sizer (DLS, Malvern Instruments Ltd., UK). Measurements were done by dispersion of 100 μ L of the formed nanomicelles suspensions in 10 mL of deionized water at $\lambda = 480$ nm and a refractive index of 1.363. The samples were measured in triplicates using automatic mode to determine the proper number of runs of each sample. Transmission electron microscope (TEM, JEOL, JEM-1230, Tokyo, Japan) was also used to confirm the size of the particles and to determine their shape, and the measurements were performed at an accelerating voltage of 200 kV.

2.2.2.4. In-Vitro Enzymatic Degradation Study. In-vitro enzymatic degradation study of the prepared nanomicelles was carried out in presence of lysozyme in phosphate buffer saline (PBS) (1.5 mg/mL PBS at pH 7.4). An initial weight (W_0) of the nanomicelles (10–15 mg) was transferred to a microcentrifuge tube, and incubated with 1 mL of lysozyme solution at 37 °C in a shaking incubator at 130 rpm (VWR® incubating orbital shaker, VWR International, Brisbane, CA, USA) for 60 min. Afterwards, samples were centrifuged for 3 min at 14000 rpm. Then, the final weight of the particles (W_t) was determined after discarding the supernatant. A fresh lysozyme solution (1 mL) was added to the pluronic nanomicelles. At certain time intervals, the steps of centrifugation and weighing were repeated, and the final weight (W_t) of the particles at these intervals was determined. The percent weight remaining (W_r %) of the particles due to degradation was calculated according to the following equation:

$$W_r (\%) = 100 - \left(\frac{W_0 - W_t}{W_0} \times 100 \right)$$

where W_0 and W_t are the initial weight of particles, and after incubation with lysozyme for a certain time, t , respectively.

2.2.2.5. Determination of Loading Efficiency and Release Profiles of the Bioactive Compounds. The loading efficiency and release profiles of the selected three bioactive compounds were determined spectrophotometrically (UV–Vis Spectrophotometer, Evolution 600-

ThermoScientific, USA). UV–Vis spectra of the compounds were first obtained to determine their maximum absorption wavelengths to be used further for getting their calibration curves and release profiles. The release profiles were obtained via monitoring the diffusion of the free bioactive compounds rather than the carrier nanomicelles through a semipermeable membrane. A two compartment system separated by a semipermeable dialysis membrane of a cutoff 12,000 MW was used. The inner compartment contained the bioactive compound-loaded nanomicelles dispersed in 0.5 mL of DMSO while the outer receiving compartment contained 10 mL of phosphate buffer (pH 7.4). At predetermined time intervals, 1 mL of the external medium was withdrawn for spectrophotometric analysis, and replaced with buffer to maintain constant volume. The concentration of the bioactive compounds released at different time intervals were assessed by UV–Vis analysis.

2.3. Antiproliferative Screening

2.3.1. Effect on Cancer Cell Lines

2.3.1.1. Cell Culture. Human breast adenocarcinoma cell lines (MDA-MB-231 and MCF-7) were originally purchased from American type culture collection (ATCC, Wesel, Germany) and grown in the tissue culture lab of the Egyptian company for production of vaccines, sera and drugs (Vacsera, Giza, Egypt). The cells were transferred to our laboratory and MDA-MB-231 were maintained in Dulbecco Modified Eagle's medium (DMEM) while MCF-7 were maintained in Roswell Park Memorial Institute medium (RPMI1640) both are supplemented with 100 mg/mL of streptomycin, 100 units/mL of penicillin and 10% of heat-inactivated fetal bovine serum (Invitrogen, Carlsbad, CA) in a humidified, 5% (v/v) CO₂ atmosphere at 37 °C.

2.3.1.2. Cytotoxicity Assay by 3-[4,5-dimethylthiazole-2-yl]-2,5-diphenyltetrazolium bromide (MTT). Exponentially growing cells were trypsinized, counted and seeded at the appropriate densities (5000 cells/0.33 cm² well) into 96-well microtiter plates. Cells were incubated in a humidified atmosphere at 37 °C for 24 h. Then, cells were exposed to different compounds at the desired concentrations, (0.1, 1, 10, 100 & 1000 μ M) for 72 h. At the end of the treatment period, media were removed; cells were incubated with 200 μ L of 5% MTT solution/well (Sigma Aldrich, MO) and allowed to metabolize the dye into a colored-insoluble formazan complex for 2 h. Medium was discarded from the wells and the formazan crystals were dissolved in 200 μ L/well acidified isopropanol for 30 min, covered with aluminum foil and with continuous shaking using a MaxQ 2000 plate shaker (ThermoFisher Scientific Inc., MI) at room temperature. Absorbance was measured at 570 nm using a SpectraMax plus Microplate Reader (Molecular Devices, CA). The cell viability was expressed relative to the untreated control cells (Mosmann, 1983; Scudiero et al., 1988).

2.3.2. Effect on Normal Cells

2.3.2.1. Cell Culture. Proliferating fibroblast cells obtained from the skin of a healthy rat were cultured as a monolayer in a humidified atmosphere at 37 °C under 5% CO₂ environment in Dulbecco's modified Eagle's medium DMEM media (Lonza, Switzerland; 12-707F) supplemented with 10% fetal bovine serum (Analysis, 10270106), 1% antibiotic–antimycotic (Lonza, Switzerland; 17-745E), and L-glutamine (Lonza, Switzerland; 17-605E) under standard culture conditions (Doyle and Griffiths, 1998). Media was changed every 2 days. Cells were trypsinized upon reaching 70–75% confluency using Trypsin-EDTA (Life technologies; 25200-056).

2.3.2.2. Cell Viability Assay. Cell viability was determined using a modified MTT assay. The tested compounds were each dissolved in Dimethyl Sulfoxide to form a stock of 2 mM concentration. 30,000 cells were plated in 24-well plate with 497.5 μ L medium per well. After 24 h, 2.5 μ L of the investigated drug was added to each of the three wells

containing cells to form a final volume of 500 μL with a final test agent concentration of 10 μM per well. While, three other wells containing the same amount of cells were left untreated with the addition of only equivalent amount (2.5 μL) of Dimethyl Sulfoxide and these cells were considered the control group. Furthermore, to avoid any misinterpretation with the colorimetric MTT assay, the tested agents were added to three wells containing medium alone as a blank. On the next day, 80 μL of 5 mg/mL MTT was added to each well, and plates were incubated for 3 h. Finally, the growth medium was removed carefully and 600 μL of solubilizing solution (Dimethyl Sulfoxide) was added followed by 15 min shaking using the orbital shaker. Absorption readings were performed at 500 nm using Floustar BMG Lab Tech. The equation used in calculating the percentage viability was as follows;

$$\frac{\text{Avg. Abs. of drug treated cells} - \text{Avg. Abs. of blank}}{\text{Avg. Abs. of non-treated cells} - \text{Avg. Abs. of blank}} \times 100$$

3. Results and Discussion

3.1. Chemistry

The synthesis pathway that has been used for preparing the target compounds is shown in [Scheme 1](#). The key synthetic intermediate in this work, 2-(5,7-dibromo quinolin-8-yloxy)acetohydrazide **3**, was prepared from the starting material 5,7-dibromo-8-hydroxyquinoline **1** in two steps. Starting material **1** was allowed to react with ethyl chloroacetate in absolute ethanol in the presence of anhydrous K_2CO_3 giving ethyl 2-(5,7-dibromoquinolin-8-yloxy)acetate **2**. Afterwards, a solution of **2** in absolute ethanol was treated with hydrazine hydrate in the presence of glacial acetic acid as a catalyst giving hydrazide **3** that is considered the key intermediate for the synthesis of the target quinolines. ([Scheme 1](#)). Preparation of *N'*-(substituted) benzylidene-2-(5,7-dibromoquinolin-8-yloxy)acetohydrazide Schiff's bases **4a**, **4b** started with treating a solution of **3** in ethanol with the appropriate aromatic aldehyde and allowing them to reflux for 5 h. Afterwards, compound **4c** has been obtained through the reduction of Fe/CaCl_2 catalyzed of the nitro group of **4b**. Similarly, 2-(5,7-dibromoquinolin-8-yloxy)-*N'*-(1-phenylethylidene) acetohydrazides **5a–c** have been prepared using same conditions to prepare analogues **4** but using the appropriate acetophenones instead of the aldehydes. Finally compounds **6a,b** were synthesized from reaction of intermediate **3** with substituted phenylisocyanates and refluxing for 8 h. Finally, reflux of the hyrazinocarboxamides **6a** & **6b** in sodium ethoxide yielded the corresponding quinolinyltriazole derivatives **7a** & **7b** through affecting the side chain cyclization.

3.1.1. Physicochemical Properties Exploration

The synthesized compounds' partition coefficients (Log *P*) and their water solubility (Log *S*) have been calculated using Molinspiration property engine and ChemDraw Pro 14.0, respectively ([Table 1](#)). By comparing the benzylidenes (**4a–c**) to their corresponding phenylethylidene bioisosteres (**5a–c**), the solubility of the latter derivatives demonstrated a reduction in their water solubility influenced by the presence of the extra methyl group, however, no significant change has been noticed in their Log *P* values. On the other hand, reduction of the nitro group in compounds **4b** (log *P* = 4.79, log *S* = –6.63) and **5b** (log *P* = 4.70, log *S* = –6.79) to furnish their amino counterparts **4c** (log *P* = 3.90, log *S* = –6.11) and **5c** (log *P* = 3.82, log *S* = –6.26) respectively, lead to an increases in the solubility of the resulting compounds. This effect can be explained in terms of the higher potential of the amino group containing derivatives to make H-bonds with the surrounding water molecules thus enhancing their solubility.

To discover the role of the cyclization step on the compounds' lipophilicity and solubility; compounds **6a** (log *P* = 4.64, log *S* = –6.67) and **7a** (log *P* = 5.03, log *S* = –7.98) were compared to their respective cyclized analogues **6b** (log *P* = 4.86, log

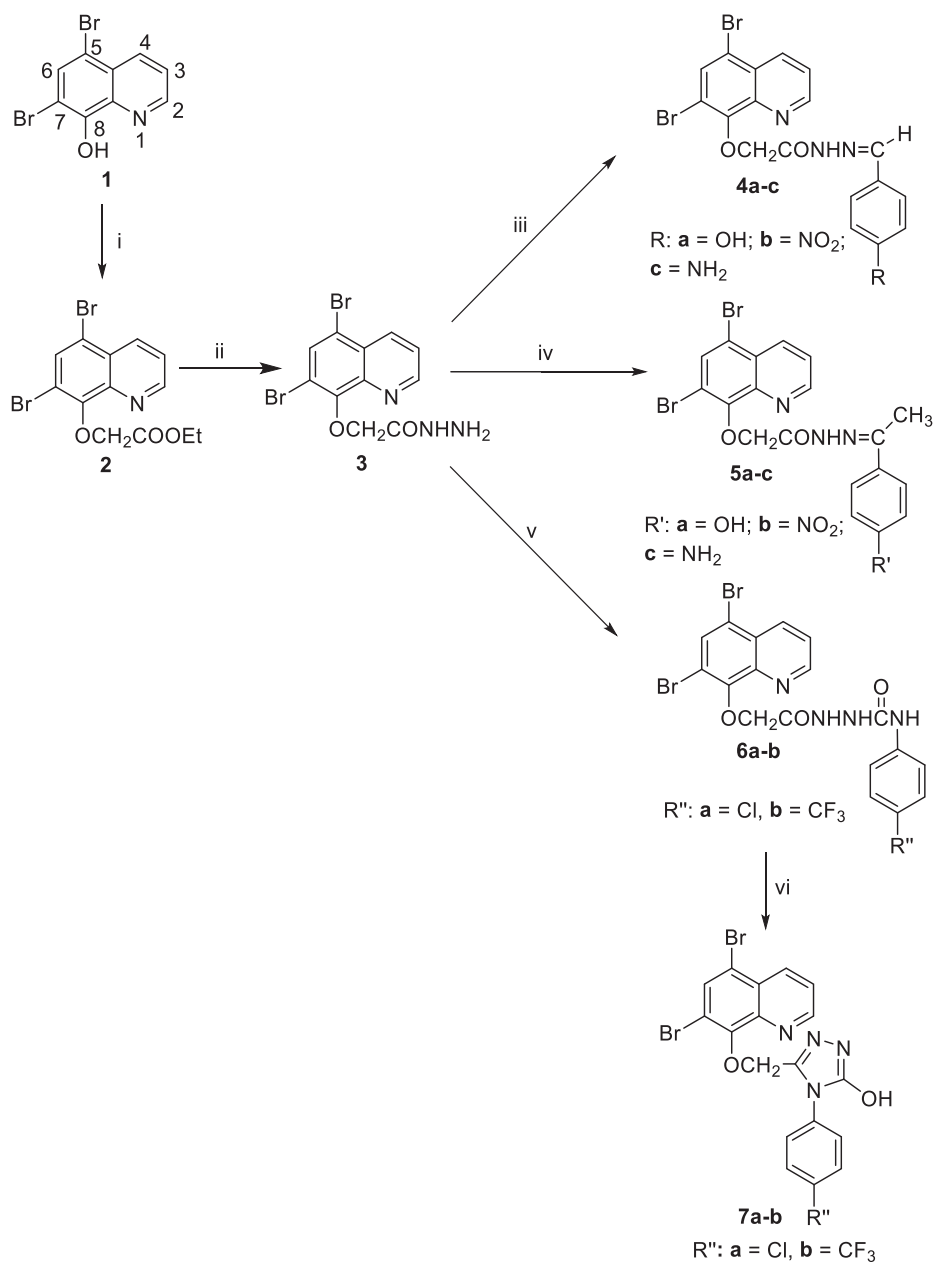
S = –7.00) and **7b** (log *P* = 5.25, log *S* = –8.29). Apparently, cyclization causes an observable increase in lipophilicity and decrease in solubility. Also, compounds bearing a CF_3 substituted phenyl represented by **7a,b** showed higher lipophilicity than those having a Cl group in the same position as exemplified by **6a,b**. Finally, it seems that introduction of a strong electron withdrawing group as CF_3 at the para position of the phenyl ring side chain of **7b** (log *S* = –8.29) decreases the solubility compared to substitution with a weaker electron withdrawing group as Cl in **7a** (log *S* = –7.98). Such an observation may be attributed to the electronic effect of the electron withdrawing groups on the OH group of the triazole ring reducing its ability to be involved in H-bonds with surrounding water molecules thus decreasing the compound's water solubility.

3.2. Nanoformulation

Three of the synthesized compounds with the most promising anticancer activity were evaluated for possible methods to enhance their physicochemical properties. Practical assessment of the solubility showed that the selected compounds were practically insoluble (< 0.1 mg/1 mL, full data not shown) which conforms to the calculated log *S* values for the compounds. This demonstrated the need to enhance this poor solubility of the compounds which was performed through incorporation into an appropriate nanocarrier system. Pluronic nanomicelles were developed to encapsulate the selected compounds eliciting the most promising anticancer activity from the synthesized series of compounds. Compounds-loaded nanomicelles were prepared using the nanoprecipitation technique through a modified procedure as illustrated in [Scheme 2](#). This preparation technique is ultimate for entrapment of hydrophobic moieties such as bioactive compounds under investigation. Besides, the entrapment of these water-insoluble compounds into nano-sized polymeric particles would improve their dissolution, and consequently their bioavailability. This role played by nanoformulation is apparent from [Fig. 2](#) which shows the aqueous suspension of the compounds ([Fig. 2a](#)) as compared to that of their corresponding nano-formulated forms ([Fig. 2b](#)). As apparent from the figure, the very limited solubility of the synthesized compounds in water has been improved significantly upon nanoformulation. Besides, the nanoencapsulation of the compounds led to a stable colloidal dispersion with strong color, indicating their homogenous distribution in aqueous medium at a significantly higher concentration. This in consequence will improve the extent of their in vivo bioavailability and absorption.

3.2.1. Particle Size and Zeta Potential

The size of the formed compounds-loaded nanomicelles was found to be in the range from 416.1 ± 4.2 nm to 818.2 ± 117 nm as compared to 161 ± 31 nm for the plain nanomicelles ([Table 1](#)). As apparent also from the Table, the loaded particles showed a wide range of zeta potential ranging from -12.3 ± 0.75 to 2.1 ± 0.25 mV while the compounds-free pluronic nanomicelles demonstrated a zeta potential of -15.7 ± 1 mV. It can be noted that the compound **5c** with an aromatic amino groups yielded neutral nanomicelles or nanomicelles of weakly positive charge. Transmission electron microscopy (TEM) was also used to confirm the successful formation of pluronic nanomicelles ([Fig. 3](#)), and the TEM micrographs also revealed an agreement in particle size with that measured by DLS. Although the size of the particles is relatively larger than the conventional definition of nano-systems (< 100 nm), the particles have demonstrated good efficiency in improving the physicochemical properties of the loaded bioactive compounds including the ability to form stable homogenous solutions that are more suitable for delivery as well as sustained release of the drugs for > 3 days. It is worth mentioning that the developed nanocarriers still fit into the size range reported by many previous studies indicating that for polymeric nanoparticles, the systems can maintain their nano characteristics and desired properties for sizes up to



Reagents and conditions: i) ClCH₂CO₂Et, K₂CO₃ (anhyd.), DMF, 6h, reflux, yield: 84 %; ii) NH₂NH₂-H₂O, gl. HOAc, Abs. EtOH, 3h, r.t., yield: 89 %; iii) RCHO, gl. HOAc, abs. EtOH, 5h, reflux, yield: 81-93 %; iv) Subs. PhC(O)CH₃, gl. HOAc, abs. EtOH, 5h, reflux, yield: 87-92 %; v) PhNCX, abs. EtOH, 8h, reflux, yield: 63-84 %; vi) 2N NaOH, 5h, reflux, yield: 68-79 %

Scheme 1. Synthesis of the quinolone scaffold-based derivatives 4–7.

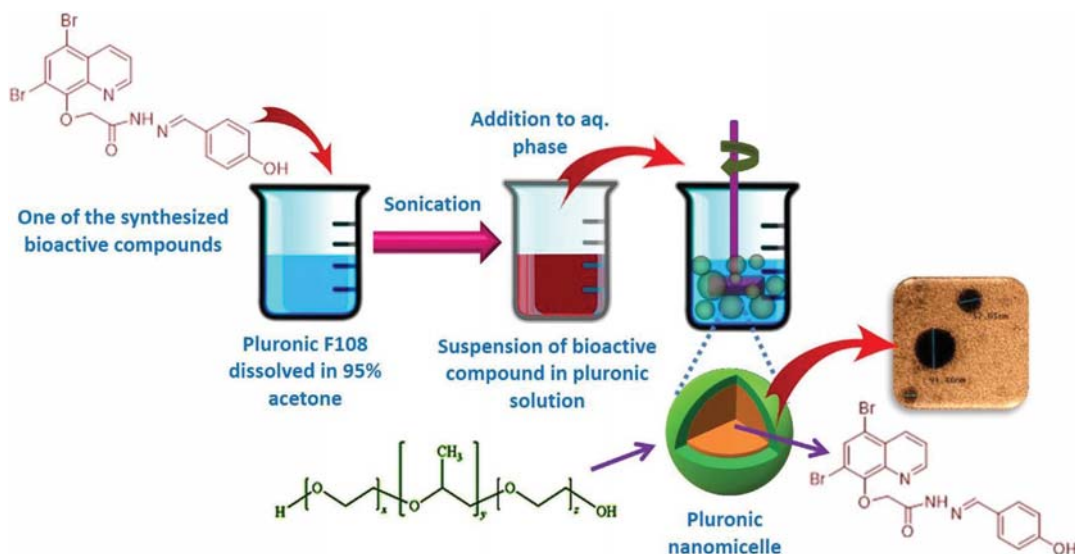
Table 1
Size and charge of the prepared formulations as measured using DLS.

Formula	Loaded compound	Size (nm)	Charge (mV)	EE%
F0	None (Plain)	161 ± 31	- 15.7 ± 1	-
F1	4a	818.2 ± 117	- 8.28 ± 0.18	82.4%
F2	5c	461.3 ± 95.6	2.1 ± 0.25	86.1%
F3	7b	416.1 ± 4.2	- 12.3 ± 0.75	78.6%

1000 nm including enhancement of solubility, stability, dispersion and ability to control the delivery of active agents. (Bhatia, 2016; Nahar et al., 2006). However, it should be mentioned here that such large size nanoparticles will not provide the potential to the encapsulated active substances to be passively targeted to cancerous tissues, via the EPR effect.

3.2.2. In-Vitro Biodegradation Study

An in-vitro enzymatic biodegradation study of the developed pluronic nanomicelles was performed in PBS (pH 7.4) in presence of lysozyme as shown in Fig. 4. The weight loss (%) of the nanomicelles as



Scheme 2. A schematic illustration of the preparation of pluronic nanomicelles loaded with the selected bioactive compounds.

a function of time was determined and taken as a measure of the biodegradation. As apparent from the figure, the polymeric micelles attained a higher degradation rates in presence of lysozyme. For example, the percentage of remaining weights of the nanomicelles was only 18.4% after 2 days.

3.2.3. Entrapment Efficiency and In-Vitro Cumulative Release Studies

The entrapment efficiency and the release profiles of the loaded bioactive compounds from the developed nanomicelles were studied using UV-Vis spectrophotometry (Table 1). The first step was to determine the wavelength of maximum absorption specific for each of the three investigated compounds. It was found that all of the three synthesized compounds had a maximum absorption in the UV range between 258 and 320 nm. This can be explained by the fact that all of the three synthesized compounds have high degree of conjugation having at least three aromatic rings with double bonds in between. As can be noted from Table 1, the entrapment efficiency (*EE%*) of the bioactive compounds was found to be in the range from 78.6 to 86.1%.

Formulations that allow sustained release of bioactive compounds are considered more advantageous compared to the instant release ones with regards to improving patient compliance and maintaining more uniform blood drug concentration avoiding fluctuations that may cause reduced therapeutic efficiency or undesired toxic effects.

The cumulative release profiles of the loaded bioactive compounds from the carrier nanomicelles at 37 °C in PBS of pH 7.4 are shown in Fig. 4. As can be noted from the figure, the compounds 5c and 7b (F2

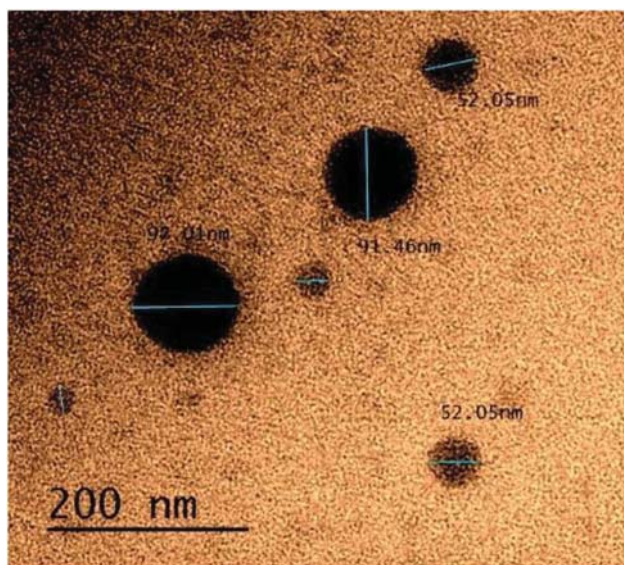


Fig. 3. Transmission electron micrograph of the developed plain pluronic nanomicelles.

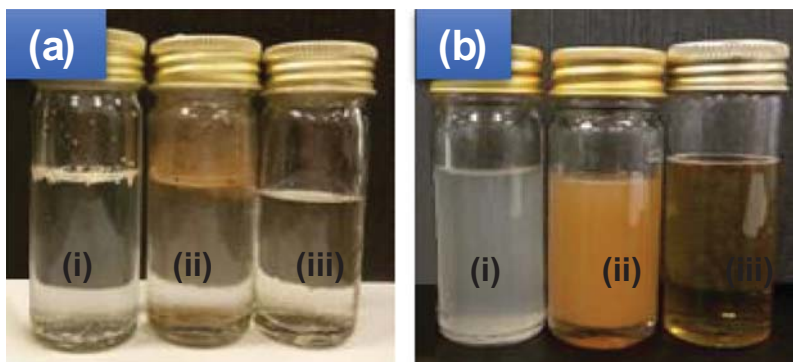


Fig. 2. (a) Lack of homogeneity, insolubility and instability of the aqueous suspensions of the free bioactive compounds [4a (i), 5c (ii) and 7b (iii)] as compared to (b) their corresponding nanomicelles formulations.

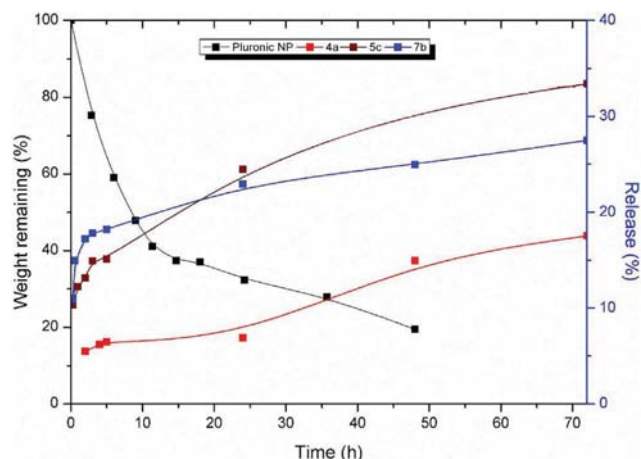


Fig. 4. Degradation pattern of the pluronic nanomicelles, and the release profiles of the synthesized bioactive compounds from the nanomicelles.

and F3, respectively) showed an initial burst release of about 30% in the first hour as compared to **4a** (F1) which attained an initial release of about 16%. Afterwards, the percent of the bioactive compounds released increased gradually with time to show sustained release profiles.

3.3. Antiproliferative Screening

3.3.1. Free Compounds

The antiproliferative activity of all the synthesized final 5,7-dibromo-8-substituted quinolines was evaluated in vitro against two human breast cancer cell lines MCF-7 and MDA-MB231. Compounds were evaluated in triplicates for their percent proliferation inhibition, followed by determination of their IC_{50} values (Table 2). Cytotoxicity data demonstrated that the tested compounds have been active on both cell lines except for compound **5c** that was inactive on MDA-MB231 yet showing good activity on MCF-7 with IC_{50} 12.9 μ M. Moreover, with the exception of **4a**, all compounds showed better activity towards MCF-7 breast cancer cell lines rather than MDA-MB231 proposing the possible selectivity of these novel analogues towards the MCF-7 cells. This observation is currently under investigation in an attempt to uncover the underlying molecular basis of biological action of these chemotypes.

SAR exploration showed that generally the *N'*-benzylideneacetohydrazide derivatives (**4a–c**) seem to have higher activity when compared

to their *N'*-phenylethylidene acetohydrazides bioisosteric counterparts (**5a–c**) on both MCF-7 and MDA-MB231 cell lines.

Moreover, the *N*-phenylhydrazine(thio)carboxamides **6a,b** and their rigid cyclic 4-phenyl-4H-1,2,4-triazol-3-(thiol)ol analogues **7a,b** have shown activity towards both MCF-7 and MDA-MB231 cell lines with significant higher activity of the cyclic analogues. This can be explained by the higher lipophilicity introduced through cyclization that may contribute to the cell membrane penetration and/or better conformational orientation for biotarget binding. Consequently, it came to expectations that among the four compounds **6a,b** and **7a,b**, derivative **7b** (4-(trifluoromethyl)phenyl)-4H-1,2,4-triazol-3-ol) exhibited the best activity towards both MCF-7 and MDA-MB231 cell lines with IC_{50} of 6.2 μ M and 13.5 μ M, respectively.

Regarding the antiproliferative efficacy against MCF-7 cell lines, 5 out of 10 compounds (**4a**, **4c**, **5a**, **5c**, **7a** and **7b**) have shown IC_{50} values < 20 μ M. These compounds bear either an OH or NH_2 group in their side chains indicating the significance of these groups as being hydrophilic, hydrogen bond donating/accepting and electron donating behaviors on their pharmacokinetic/pharmacodynamics behavior.

Finally, with respect to the antiproliferative efficacy against the tested breast cancer cell line MDA-MB231, compounds **4a**, **5a**, **7a** and **7b** have shown IC_{50} values 5.95 μ M, 34.7 μ M, 26.9 μ M and 13.5 μ M, respectively. Interestingly, all these derivatives possess an OH group on their cyclic side chain (phenyl in **4a** and **5a** or triazole in **7a** and **7b**). This observation indicates a potentially important role of the OH group for cytotoxicity towards the MDA-MB231 cell lines.

3.3.2. Loaded Pluronic Nanomicelles

The bioactive compounds-loaded nanomicelles showed a higher activity for compounds **4a**, **7b** against both tested cell lines and an enhanced activity of **5c** against MDA-MB231 cells as compared to the cytotoxicity of the corresponding free compounds (Table 2). While cytotoxicity of the tested compounds showed a 1.27 to 2.48 fold increase in MCF-7 cell lines, a 1.4 to > 5.4 fold enhancement of cytotoxicity was observed against MDA-MB231. This can be attributed to the improved dispersion of the nano form of these compounds in aqueous medium as compared to the poor water solubility of the corresponding free unloaded forms. However, more studies need to be performed to understand the lack of effectiveness of nanomicelles of compound **5c** against MCF-7 cells.

3.3.3. Cytotoxicity Assay

All the synthesized compounds were tested for their cytotoxic effect against normal rat skin fibroblast. The cells have shown high viability percentage (86.8–122.2% viability, Table 2) for all compounds at a

Table 2

LogP values, LogS and antiproliferative effect against MCF-7 and MDA-MB231 breast cancer cell lines and cytotoxic effect against rat skin fibroblast cells of the synthesized quinoline derivatives and their loaded nanoparticles.

Compound code	Calc. LogP	Exp. Log P	LogS	Rat skin fibroblasts % viability	MCF-7* (IC_{50} , μ M)		MDA-MB231* (IC_{50} , μ M)	
					Free compound	Loaded nanoparticles	Free compound	Loaded nanoparticles
4a	4.36	4.54	−6.11	86.8	11	8.6	5.95	4
4b	4.79	NT**	−6.63	122.2	45.7	NT	436.5	NT
4c	3.90	NT	−6.11	94.5	9	NT	60.3	NT
5a	4.26	NT	−6.25	91.3	19.5	NT	34.7	NT
5b	4.70	NT	−6.79	107.4	195	NT	490	NT
5c	3.82	3.61	−6.26	115.8	12.9	143	> 1000	184
6a	4.64	NT	−6.67	102.1	57.5	NT	95.5	NT
6b	4.86	NT	−7.00	97.0	45.7	NT	426.6	NT
7a	5.03	NT	−7.98	93.4	17.4	NT	26.9	NT
7b	5.25	4.82	−8.29	92.6	6.2	2.5	13.5	2.5
DOX	−1.34	NT	−3.15	NT	1.2	NT	0.4	NT

* IC_{50} values are the average of 3 independent runs.

**NT = not tested.

single dose (10 μM) exposure to the test agents. Obtained results indicate that these chemotypes are not toxic eliciting a good safety profile for normal cells under the adopted experimental conditions.

4. Conclusion

This study presents the synthesis of 10 new quinoline derivatives. These compounds were tested against 2 breast cancer cell lines MCF-7 and MDA-MB231. Results have shown that compounds bearing a hydroxyl-containing side chains or cyclic side chain have the best activity for both cell lines. Consequently, compound **7b** demonstrated the best cytotoxicity towards MCF-7 cell line with IC_{50} of 6.2 μM . Safety profile of the compounds was assessed through evaluating their toxicity against rat skin fibroblasts where they demonstrated good safety profile under the adopted experimental conditions.

The study involves also the incorporation of three of the synthesized compounds among those showing the most promising anticancer activity into pluronic nanomicelles to enhance their aqueous solubility, and consequently their cancer cell penetrability as well as allowing their sustained release. Indeed and as expected, there was an observable significant increase in the cytotoxicity of the nanoformulated compounds. Interestingly, compound **7b** also showed the best activity upon its loading in the nanomicelles introducing it as a promising compound in terms of bioactivity as well as delivery. The choice of the pluronic polymer was made based on a tendency to keep the formulation process as simple as possible in addition to the well-established safety profile of the polymer as an FDA approved ingredient. Additionally, pluronic was shown to overcome some drug resistance mechanism by inhibition of efflux transporters. (Diniz et al., 2015; Geller, 2012; Liu et al., 2012).

To conclude, the results obtained through this research activity demonstrate that the cytotoxicity of quinolone scaffold-based small molecules can be modulated by structural manipulation of the physicochemical properties of the functional groups decorating the quinolone nucleus. On the other hand, fine-tuning of activity can be achieved by enhancing the solubility profile of the designed compounds to augment their delivery to their cellular biological targets through adopting nanoformulation strategies.

Acknowledgement

The authors are thankful to Professor Sameh Ali (CAAD, Zewail City) for providing the rat skin fibroblasts.

References

Afzal, O., Kumar, S., Haider, M.R., Ali, M.R., Kumar, R., Jaggi, M., Bawa, S., 2015. A review on anticancer potential of bioactive heterocycle quinoline. *Eur. J. Med. Chem.* 97, 871–910.

Alqasoumi, S.I., Al-Taweel, A.M., Alafeefy, A.M., Hamed, M.M., Noaman, E., Ghorab, M.M., 2009. Synthesis and biological evaluation of 2-amino-7,7-dimethyl 4-substituted-5-oxo-1-(3,4,5-trimethoxy)-1,4,5,6,7,8-hexahydro-quinoline-3-carbonitrile derivatives as potential cytotoxic agents. *Bioorg. Med. Chem. Lett.* 19, 6939–6942.

Anand, P., Kunnumakkara, A.B., Sundaram, C., Harikumar, K.B., Tharakan, S.T., Lai, O.S., Sung, B., Aggarwal, B.B., 2008. Cancer is a preventable disease that requires major lifestyle changes. *Pharm. Res.* 25, 2097–2116.

Arafa, R.K., Hegazy, G.H., Piazza, G.A., Abadi, A.H., 2013. Synthesis and in vitro antiproliferative effect of novel quinoline-based potential anticancer agents. *Eur. J. Med. Chem.* 63, 826–832.

Basak, R., Bandyopadhyay, R., 2013. Encapsulation of hydrophobic drugs in Pluronic F127 micelles: effects of drug hydrophobicity, solution temperature, and pH. *Langmuir* 29, 4350–4356.

Bawa, S., Kumar, S., Drabu, S., Kumar, R., 2010. Structural modifications of quinoline-

based antimalarial agents: recent developments. *J. Pharm. Bioallied Sci.* 2, 64–71.

Bhatia, S., 2016. Nanoparticles Types, Classification, Characterization, Fabrication Methods and Drug Delivery Applications, Natural Polymer Drug Delivery Systems. Springerpp. 33–93.

Diniz, I.M., Chen, C., Xu, X., Ansari, S., Zadeh, H.H., Marques, M.M., Shi, S., Moshaverinia, A., 2015. Pluronic F-127 hydrogel as a promising scaffold for encapsulation of dental-derived mesenchymal stem cells. *J. Mater. Sci. Mater. Med.* 26, 1–10.

El-Far, Y.M., Zakaria, M.M., Gabr, M.M., El Gayar, A.M., El-Sherbiny, I.M., Eissa, L.A., 2016. A newly developed silymarin nanoformulation as a potential antidiabetic agent in experimental diabetes. *Nanomedicine* 11, 2581–2602.

Foster, B., Cosgrove, T., Espidel, Y., 2009. PFGSE-NMR study of pH-triggered behavior in pluronic-ibuprofen solutions. *Langmuir* 25, 6767–6771.

Geller, J., 2012. Food and drug administration approves devices through premarket approval application process. *J. Clin. Eng.* 37, 4–6.

Ghorab, M.M., Ragab, F.A., Heiba, H.I., Arafa, R.K., El-Hossary, E.M., 2010. In vitro anticancer screening and radiosensitizing evaluation of some new quinolines and pyrimido[4,5-b]quinolines bearing a sulfonamide moiety. *Eur. J. Med. Chem.* 45, 3677–3684.

Ghorab, M.M., Ragab, F.A., Heiba, H.I., Ghorab, W.M., 2011. Design and synthesis of some novel quinoline derivatives as anticancer and radiosensitizing agents targeting VEGFR tyrosine kinase. *Heterocycl. Chem.* 48, 1269–1279.

Heiniger, B., Gakhar, G., Prasain, K., Hua, D.H., Nguyen, T.A., 2010. Second-generation substituted quinolines as anticancer drugs for breast cancer. *Anticancer Res.* 30, 3927–3932.

Israelachvili, J., 1997. The different faces of poly(ethylene glycol). *Proc. Natl. Acad. Sci. U. S. A.* 94, 8378–8379.

Jasinski, P., Welch, B., Galvez, J., Land, D., Zwolak, P., Ghandi, L., Terai, K., Dudek, A.Z., 2008. A novel quinoline, MT477: suppresses cell signaling through Ras molecular pathway, inhibits PKC activity, and demonstrates in vivo anti-tumor activity against human carcinoma cell lines. *Investig. New Drugs* 26, 223–232.

Jasinski, P., Zwolak, P., Terai, K., Vogel, R.I., Borja-Cacho, D., Dudek, A.Z., 2011. MT477 acts in tumor cells as an AURKA inhibitor and strongly induces NRF-2 signaling. *Anticancer Res.* 31, 1181–1187.

Liu, L., Yong, K.-T., Roy, I., Law, W.-C., Ye, L., Liu, J., Liu, J., Kumar, R., Zhang, X., Prasad, P.N., 2012. Bioconjugated Pluronic Triblock-Copolymer Micelle-Encapsulated Quantum Dots for Targeted Imaging of Cancer: In Vitro and In Vivo Studies.

Moscow, J., Cowan, K., 2007. Biology of cancer. In: Goldman, L., Ausiello, D. (Eds.), *Cecil Medicine*, 23rd ed. Saunders Elsevier, Philadelphia, PA.

Mosmann, T., 1983. Rapid colorimetric assay for cellular growth and survival: application to proliferation and cytotoxicity assays. *J. Immunol. Methods* 65, 55–63.

Nahar, M., Dutta, T., Murugesan, S., Asthana, A., Mishra, D., Rajkumar, V., Tare, M., Saraf, S., Jain, N.K., 2006. Functional Polymeric Nanoparticles: An Efficient and Promising Tool for Active Delivery of Bioactives. *Critical Reviews™ in Therapeutic Drug Carrier Systems.* 23.

Rashad, A.E., El-Sayed, W.A., Mohamed, A.M., Ali, M.M., 2010. Synthesis of new quinoline derivatives as inhibitors of human tumor cells growth. *Arch. Pharm.* 343, 440–448.

Scudiero, D.A., Shoemaker, R.H., Paull, K.D., Monks, A., Tierney, S., Nofziger, T.H., Currens, M.J., Seniff, D., Boyd, M.R., 1988. Evaluation of a soluble tetrazolium/formazan assay for cell growth and drug sensitivity in culture using human and other tumor cell lines. *Cancer Res.* 48, 4827–4833.

Sharma, P.K., Bhatia, S.R., 2004. Effect of anti-inflammatories on Pluronic F127: micellar assembly, gelation and partitioning. *Int. J. Pharm.* 278, 361–377.

Society, A.C., 2016. *Cancer Facts & Figures 2016*. American Cancer Society, Atlanta.

Solomon, V.R., Lee, H., 2011. Quinoline as a privileged scaffold in cancer drug discovery. *Curr. Med. Chem.* 18, 1488–1508.

Thun, M., 2007. Epidemiology of cancer. In: Goldman, L., Ausiello, D. (Eds.), *Cecil Medicine*, 23rd ed. Saunders Elsevier, Philadelphia.

Tseng, C.H., Chen, Y.L., Chung, K.Y., Wang, C.H., Peng, S.I., Cheng, C.M., Tzeng, C.C., 2011. Synthesis and antiproliferative evaluation of 2,3-diarylquinoline derivatives. *Org. Biomol. Chem.* 9, 3205–3216.

Wall, M.E., Wani, M.C., Cook, C.E., Palmer, K.H., McPhail, A.I., Sim, G.A., 1966. Plant antitumor agents. I. The isolation and structure of camptothecin, a novel alkaloidal leukemia and tumor inhibitor from *Camptotheca acuminata*. *J. Am. Chem. Soc.* 88, 3888–3890.

Wang, Y., Ai, J., Wang, Y., Chen, Y., Wang, L., Liu, G., Geng, M., Zhang, A., 2011. Synthesis and c-Met kinase inhibition of 3,5-disubstituted and 3,5,7-trisubstituted quinolines: identification of 3-(4-acetyl piperazin-1-yl)-5-(3-nitrobenzylamino)-7-(trifluoromethyl)quinoline as a novel anticancer agent. *J. Med. Chem.* 54, 2127–2142.

Yan, R., Liu, X., Pan, C., Zhou, X., Li, X., Kang, X., Huang, G., 2013. Aerobic synthesis of substituted quinoline from aldehyde and aniline: copper-catalyzed intermolecular C-H active and C-C formative cyclization. *Org. Lett.* 15, 4876–4879.

Yardimci, H., Chung, B., Harden, J.L., Leheny, R.L., 2005. Phase behavior and local dynamics of concentrated triblock copolymer micelles. *J. Chem. Phys.* 123, 244908.

4. Summary of the results

4.1. Identification of novel inhibitors for PKMYT-1

This part will briefly discuss the results obtained in studies **3.1** and **3.2**. These studies focused on studying the ATP pocket of PKMYT-1 and its inhibitors' binding interactions. Using computational, synthetic, and biological evaluations, we managed to introduce novel potent PKMYT-1 inhibitors.

Our previous published work on PKMYT-1 inhibitors was the first reported attempt to screen a chemical compound dataset against the PKMYT-1. Upon screening 800 known kinase inhibitors from the kinase inhibitor data sets I and II from GSK against PKMYT-1, several hits were identified as nanomolar inhibitors. Out of the ten compounds showing promising PKMYT-1 inhibition, three novel scaffolds emerged: azastilbenes, 4-aminoquinolines, and aminopyrimidines, thus providing new scaffolds used to develop novel selective PKMYT-1 inhibitors [85, 92].

For identifying new PKMYT-1 inhibitors, we first elucidated the proposed binding mechanism via exploration of the PKMYT-1 ATP binding pocket and molecular docking of all identified PKMYT-1 inhibitors against PKMYT-1 crystal structure (*PDB ID: 5VCW*) (**Figure 20**). Despite their chemical diversity, all the inhibitors formed a hydrogen bond with the backbone of conserved hinge region residue Cys190, akin to ATP. Furthermore, substituted phenyl or small chemical groups introduced π - π aromatic interactions with the side chain of Phe240, targeting the hydrophobic back-pocket. In addition, more interactions were observed with the front-pocket residues such as Leu116, Pro191, and Gln196. Finally, polar interactions with Asp251 and Tyr121 were commonly observed in most PKMYT-1 inhibitors.

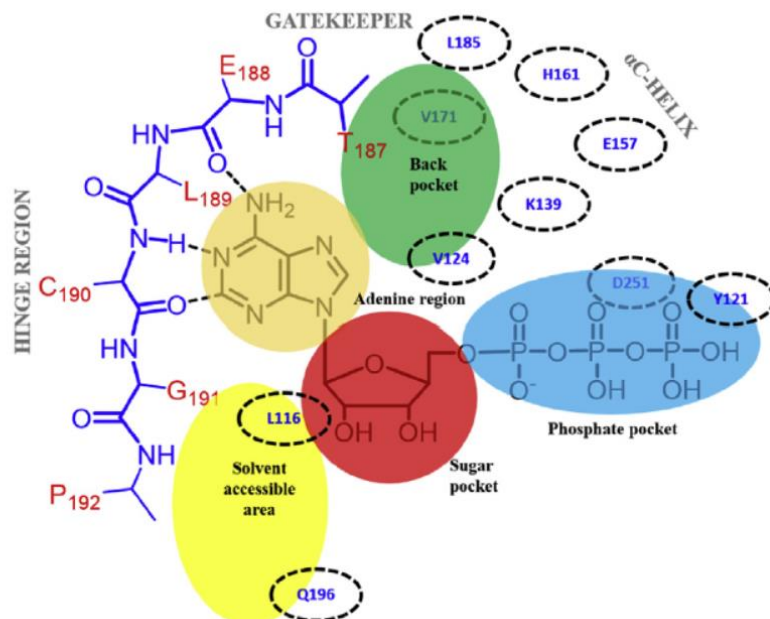


Figure 20: Scheme of the ATP-binding pocket of PKMYT-1. The backbone of the PKMYT-1 key residues is colored blue. Solvent-accessible area: (yellow sphere), ribose-binding pocket (red sphere), phosphate region (blue sphere), adenine region (beige sphere), back pocket (green sphere).

After determining the anticipated interactions in designing new PKMYT-1 kinases, we focused on introducing diaminopyrimidine derivatives since azastilbenes and aminoquinolines have limited structural synthetic variabilities. Starting with the diaminopyrimidine scaffold, we implemented fragment growing methodology since the Fragment-based drug design (FBDD) technique is known for its efficacy in exploring diverse chemical spaces compared to other methods [176]. Keeping the default interactions of PKMYT-1 inhibitors in mind, the fragment-growing approach can guarantee the presence of those interactions with nearby pockets in hits and lead optimization [177, 178]. As for the diaminopyrimidine scaffold, extensions were selected to interact with the front-pocket, hydrophobic back-pocket, and ribose and phosphatase pockets of the kinase (**Figure 21**). All proposed structures have to be evaluated using previously derived computational calculations models, including binding free energy, QSAR models, Ligand efficiency (LE) and ligand lipophilicity efficiency (LLE) all of which serve as metrics for fragment hit selection and optimization. The output candidates from those tests were then selected for synthesis and biologically evaluated against PKMYT-1.

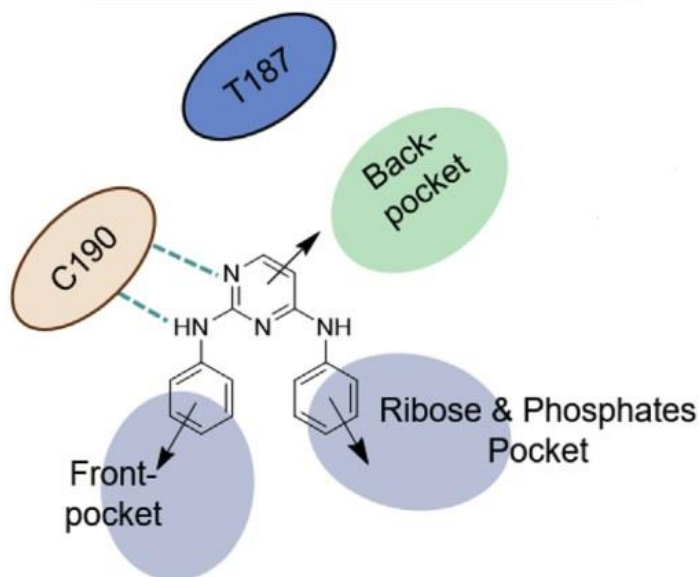


Figure 21: Diphenyldiaminopyrimidine scaffold and three possible vectors to start a fragment growing process

Synthesis of the diaminopyrimidine derivatives was realized in a two-step scheme where it started with the reaction of the respective 5-substituted-2,4-dichloropyrimidine derivatives with the selected aniline derivatives followed by the reaction of the intermediate with morpholinoaniline which has been proposed as the best moiety to address the front pocket. Among all the synthesized compounds, **5d** and **5k** showed 75% displacement at 20 μM while **5l** and **5n** have shown 100% displacement. The IC_{50} values of the compounds were in the low-micromolar and sub-micromolar when measured using fluorescence polarization immunoblot activity assay activity (FPIA) and fluorescence polarization binding (FPBA) assays (**Figure 22**). While docking and scoring methods had limitations in predicting the activity of new PKMYT-1 inhibitors, binding free energy calculations showed better predictive capabilities. In a nutshell, fragment growing led to the generation of multiple active diaminopyrimidine-derived PKMYT-1 inhibitors and allowed the assessment of initial structure-activity relationships for them. The obtained results serve as a foundation for future chemical modifications aimed at designing more potent PKMYT-1 inhibitors.

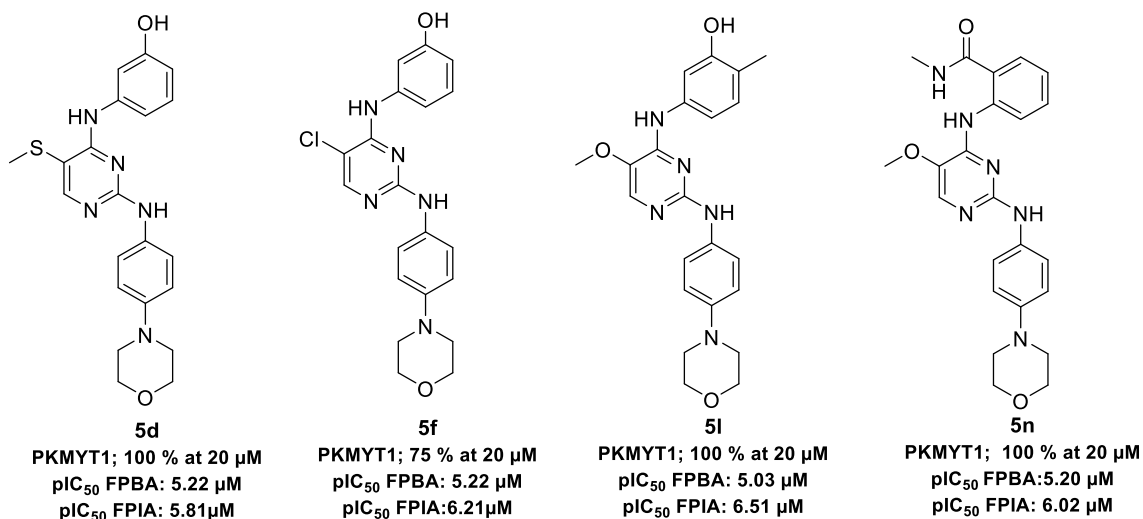


Figure 22: The most promising synthesized PKMYT-1 inhibitors

Considering all the results in study **3.1**, a new series of diaminopyrimidines were designed and synthesized in study **3.2**. All the new compounds have been tested for their potential PKMYT-1 inhibition as well as their anticancer activities. These compounds have been divided into 3 main groups based on the substituent at position 5, which varies between CN in compounds **3a-f**, **5** and **7**, S-CH₃ in compounds **10a-e** and OCH₃ in compounds **13a-e**. The rest of the structural variation of the compounds were in positions of 2 and 5 of the diaminopyrimidine ring. Similarly to compounds reported in section **3.1**, the new compounds were synthesized through a two-step reaction where the respective 5-substituted-2,4-dichloropyrimidine derivatives were allowed to react with corresponding aniline derivatives in each step. Due to variations in the introduced anilines, the reaction conditions have varied in terms of time, temperature, and catalysts used.

Following the synthesis of the compounds, all the compounds have been tested for their antiproliferative activity against three cancer cell lines, namely hepatoma cancer cells (Huh7), as well as neuroblastoma cell lines (BE(2)-C and NBL-S). Some synthesized compounds exhibited promising anticancer effects. Among these, compounds **3a** and **3f** from the series **3a-3f** demonstrated high inhibitory activity. Compound **3a** exhibited potent inhibition against the cell lines Huh7, BE(2)-C, and NBL-S, with EC₅₀ values in the submicromolar range of 0.428

μM , 0.227 μM , and 0.296 μM , respectively. Conversely, compound **3f** displayed slightly lower activity against these cell lines with EC_{50} values of 1.185 μM , 0.433 μM , and 0.323 μM against Huh7, BE(2)-C, and NBL-S, respectively. Unfortunately, the other synthesized compound series, **10a-e** and **13a-13f**, did not demonstrate significant activity against Huh7 cell lines. Compound **5** showed promising activity, ranking as the second most potent compound against neuroblastoma cell lines BE(2)-C and NBL-S with EC_{50} values of 0.129 μM and 0.156 μM , respectively. However, compound **7** emerged as the most compelling of the synthesized compounds. It demonstrated remarkable potency against both Huh7 and neuroblastoma cells, with particularly striking activity against the neuroblastoma cell lines falling within the nanomolar range with EC_{50} values of 0.722 μM against Huh7 and 16.5 nM and 17.9 nM against BE(2)-C and NBL-S, respectively.

Subsequently, all the compounds were tested for their binding and activity towards PKMYT-1 to discover if their anticancer activity is accredited to PKMYT-1 inhibition. Binding assays have shown that only **13a**, **13b**, **13f**, **10b**, **13c**, **10a**, **13d**, **7**, and **3b** were able to show more than 40% binding displacement at 20 μM . Retesting those compounds at 5 μM have shown that only **13a**, **13b**, **13c**, **13d**, **10b**, and **3b** show more than 25% displacement percentages. Following the PKMYT-1 activity assays, no direct correlation was found between the binding and activity assay results. For instance, while compounds **3b**, **7**, **10a**, and **10b** have the highest percentage inhibition for PKMYT-1, their binding displacement didn't exceed 72 % at 20 μM .

Finally, a docking study was performed in order to understand the key interactions between the most active compounds and PKMYT-1. The general binding mode to PKMYT-1 involves two essential hydrogen bonds between the aminopyrimidine fragment and the hinge region of the kinase (hydrogen bond to the NH backbone group of Cys190 and CO backbone group of Gly189). Still, the most active compounds in cancer cell lines **3a**, **5**, **7** have shown less favorable docking scores. This could be explained by the weak interaction between the cyano group at position 5 of the diaminopyridine ring and the gatekeeper residue Thr189. In contrast, less active methoxy derivatives **13a**, **13b**, and **13f** manage to

form van-der-Waals interactions with the gatekeeper residue Thr189 along with a hydrogen-bond to Lys139 and the conserved water molecule in PKMYT-1. Also, **13a** shows another hydrogen bond between the morpholine oxygen and Lys125 (**Figure 17**). With the observed disagreement between cellular assay and docking study, the most active compounds were docked against WEE1 kinase and Aurora A kinase.

For the WEE1 docking results, the most active compounds show more favorable binding forming classical hydrogen bond to the hinge region (NH backbone Cys379 and CO backbone Asn380). Additionally, the cyano groups **3a**, **5**, and **7** show hydrogen bond interaction with the gatekeeper residue Asn376 and the conserved water molecule, which was not possible with PKMYT-1. While all the active compounds form van-der-Waals interactions with the Lys328 side chain, compounds **3a** and **7** make a further hydrogen bond to Lys328 with their polar substituents of the terminal phenyl ring (**Figure 18**). Similarly, docking results for Aurora A Kinase revealed more favorable docking scores than for PKMYT-1. Compounds **3a**, **5**, and **7** were involved in two hydrogen bonds with the hinge backbone (CO Pro214, NH Ala213) via their aminopyrimidine ring and a hydrogen bond to Lys162 with their cyano group (**Figure 19**). Also, polar substituents on the terminal phenyl ring allowed for more H-bonds like that between the phenol group of **3a** and the backbone CO of Glu260 and between the carbonyl groups of **5** and **7** and Lys162 and Lys141. Notably, all three most active compounds from the cancer cell testing possess a morpholine ring in para position of the aniline ring that can make hydrogen bonds to Arg220 (or alternatively to Arg137)

4.2. Identification of novel tamoxifen analogs

This part will briefly discuss the results obtained in studies **3.3** and **3.4**. These studies focused on designing novel tamoxifen derivatives intended to have an alternative metabolic pathway independent of the CYP2D6 enzyme.

Considering the effect of CYP2D polymorphism in the manifestation of the effect of tamoxifen in breast cancer patients, our objective was to design compounds that bear the main pharmacophoric features of tamoxifen while adopting an alternative metabolic pathway, thus giving potential equal clinical benefits to all patients. To this end, all synthesized tamoxifen analogues were decorated with an ester group at the para position of Ring C in order to block the metabolic site of CYP2D6 enzyme. While CYP2D6 typically hydroxylate this position in TAM metabolites, our derivatives were strategically designed to be metabolically activated through esterase enzymes, which exhibit a consistent enzymatic behavior across populations. As the alkylaminoethoxy side chain of Ring B of TAM has been established as a key determinant for the antagonistic properties of SERMs, our novel analogues were thoughtfully crafted to feature dimethylaminoethoxy, pyrrolidinylethoxy, or piperidinylethoxy side chains. This investigation explored the effects of cyclization, the size of the cyclic structure, and the influence of modifying the basicity of nitrogen of the side chain on compounds' activities (**Figure 23**). In study **3.3**, all analogues were designed to endorse flexibility to the rigid triphenylethylene backbone by introducing a benzylic methylene spacer between Ring A of TAM. This flexibility is reported to increase selectivity toward ER α versus ER β . On the contrary, in compounds in study **3.4** a substitution of the ethyl group on the triphenylethylene backbone by a methyl group was attempted. After testing the antiproliferative effect of the synthesized compounds on MCF-7 cell line as well as their binding affinity to ER α , compounds showing the highest IC₅₀ were tested for the binding affinity to ER β *and* their differential selectivity between ER α and ER β was calculated.

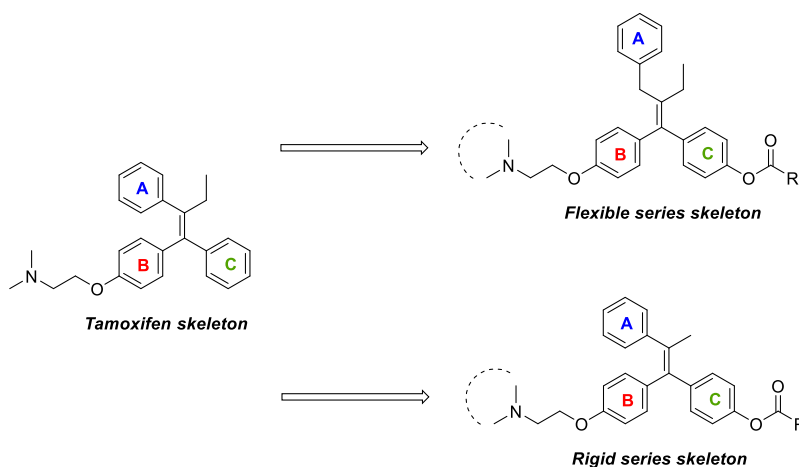
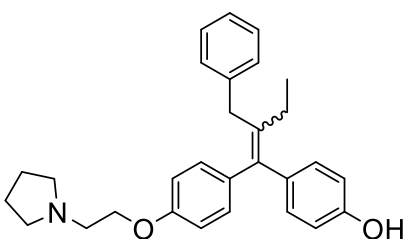


Figure 23: Design strategy of TAM derivatives

In study **3.3**, the synthesized flexible TAM analogues were tested against MCF-7 cell line, where they managed to have a remarkable antiproliferative effect even better than that of TAM and 4-OHTAM. Compound **3** specifically has managed to have $IC_{50} < 0.25\mu M$ which is more potent than both TAM and 4-OHTAM, which exhibited IC_{50} of 4.4 and 2.79, respectively. Further investigations regarding the binding of compound **3** to the $ER\alpha$ have shown IC_{50} 0.1 nM, which is more potent than 4OHTAM (showed IC_{50} 0.5 nM) (**Figure 24**). These results indicated that introducing flexibility to the triphenylethylene scaffold, together with a cyclic basic pyrrolidine substituent have contributed to better $ER\alpha$ binding. Additionally, compound **3** has shown 900 times selectivity towards $ER\alpha$ vs. $Er\beta$.



3

MCF-7, $IC_{50} < 0.25 \mu M$

$ER\alpha$; IC_{50} 0.1 nM

$ER\beta$; $IC_{50} > 90$ nM

Figure 24: Most active compound in flexible TAM analogues (Compound **3**)

In silico analysis of the binding mode of compound **3** in the binding pocket of $ER\alpha$ has been studied and compared to that of 4-OHTAM. The docked geometry

for compound **3** showed that incorporation of the additional methylene group still allows the compounds to adopt the required arrangement for binding in an established antiestrogenic mode; this is confirmed by a nearly complete overlap of the docked geometries for compound **3** and 4-OHTAM (**Figure 25A**). This overlay has permitted interactions with the essential aminoacids such as Glu353 and Arg394 (**Figure 25B**).

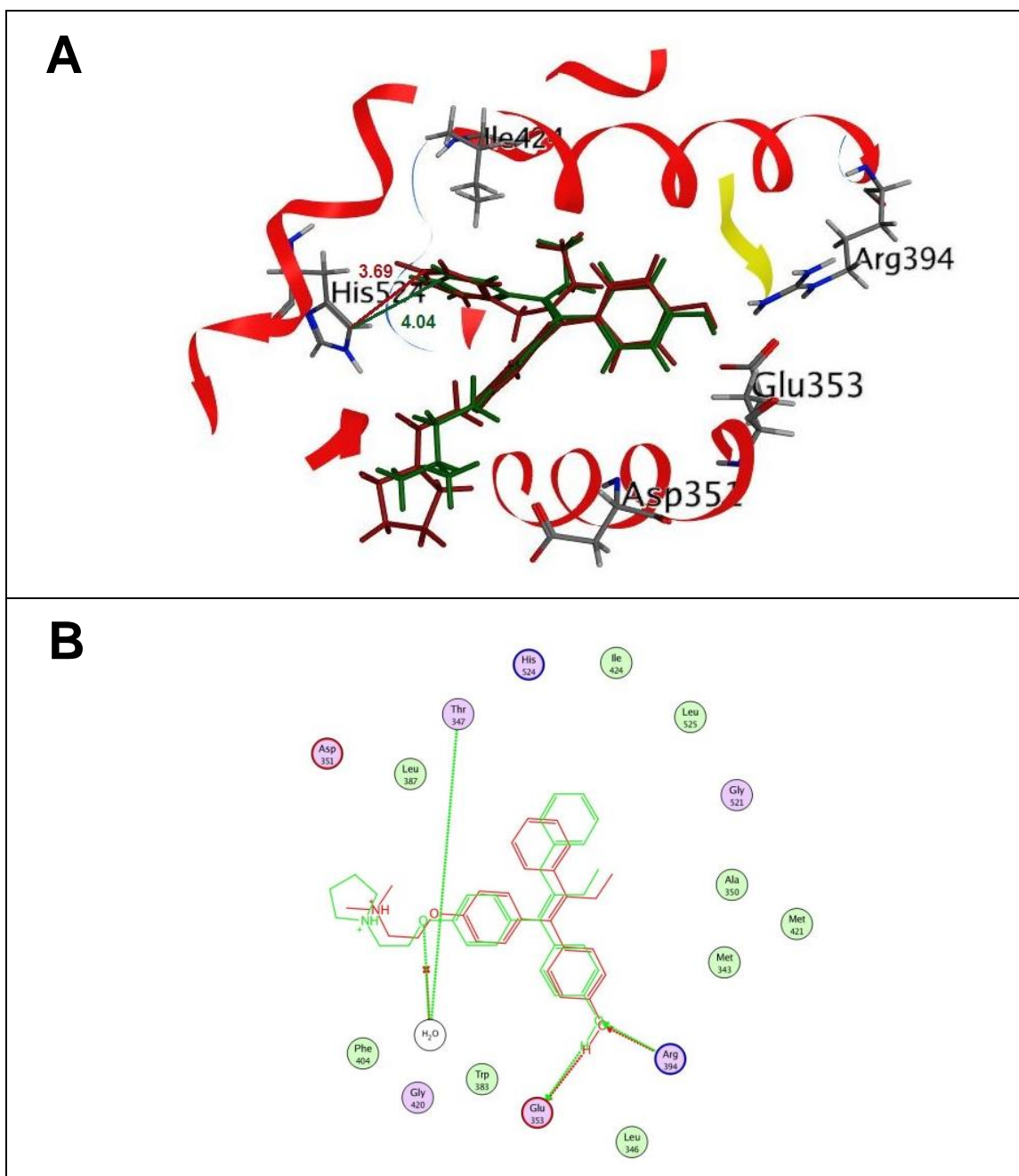


Figure 25: Overlay of compound **3** (Red) on 4-OHTAM (Green)

and the two amino acids residues, Arg394 and Glu353, of the binding pocket (Figure 27).

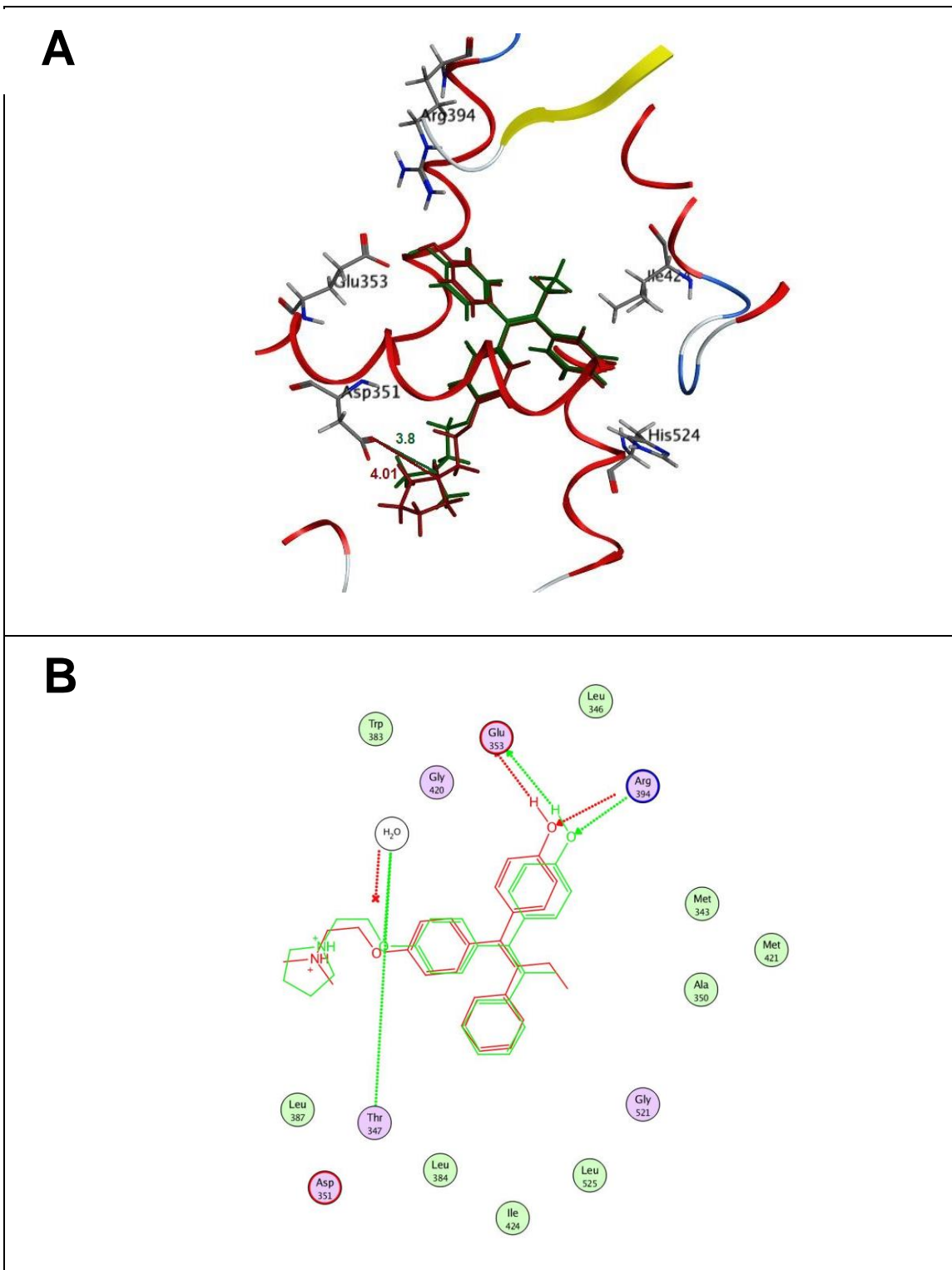


Figure 27: Overlay of compound 3 (Red) on 4-OHTAM (Green)

Finally, an in-depth metabolic investigation was conducted on compound **10** to elucidate the influence of CYP2D6 on its metabolic pathways where it was incubated in CYP2D6 supersomes in the presence of NADPH, HLM or hHep, and the resultant metabolites were characterized using LC-UV/MS. Remarkably, the identified metabolites were observed to be independent of CYP2D enzyme activity, suggesting the contribution of non-CYP enzymes in the formation of the active hydroxyl metabolite of compound **10**. These findings highlight our endeavor's success in designing and synthesizing TAM analogues that undergo significant non-CYP mediated hydrolysis (**Figure 28**).

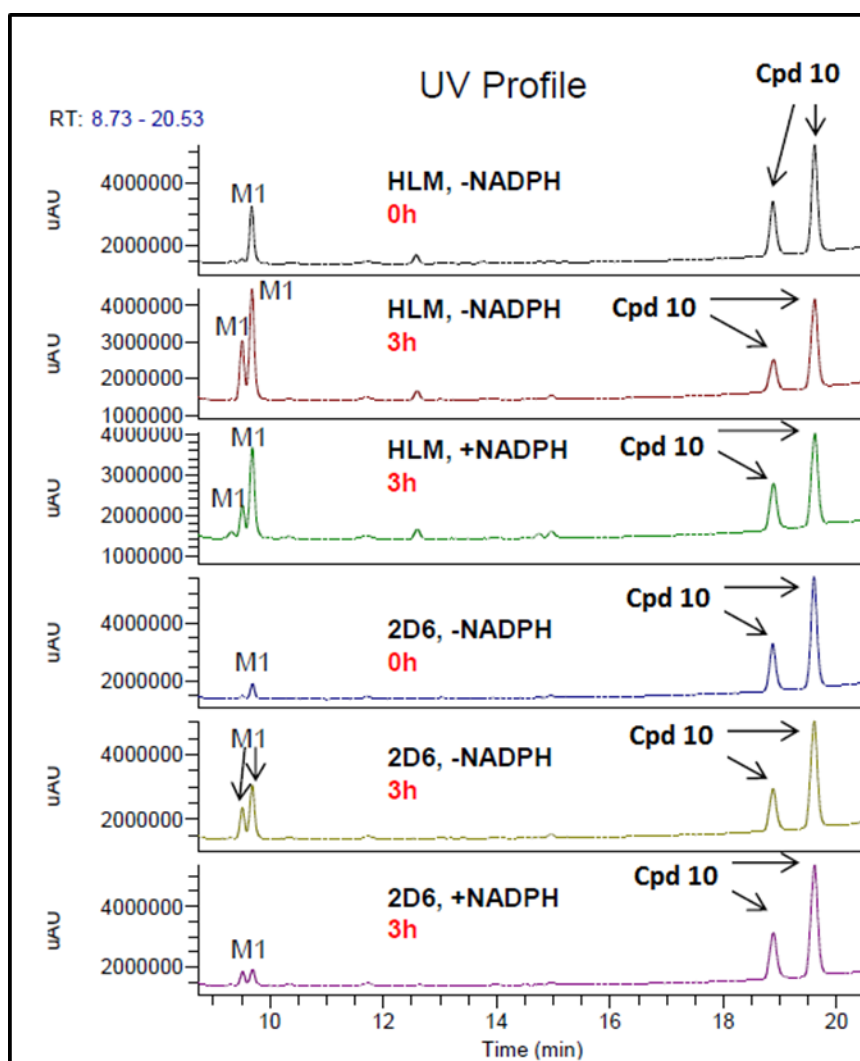


Figure 28: Extracted ion chromatogram of compound 10 after incubation in HL or CYP2D6 supersomes, both with and without NADPH. The analysis was conducted using liquid chromatography coupled to ultraviolet and mass spectrometry.

4.3. Identification of semi-synthetic isoeugenol derivatives

This part will briefly discuss the results obtained in study 3.5. In this study, we focused on synthesizing novel isoeugenol analogues, which were tested against ER+ breast cancer cells. Additional mechanistic, antioxidant, and in vivo studies were conducted to provide more evidence for the observed pharmacological efficacy.

Recently, the spotlight has turned toward natural-derived compounds for their potential role in breast cancer therapy, offering a safe and effective alternative to existing treatments and/or providing potential synergism [179]. Among the studied phytochemicals, eugenol and isoeugenol have demonstrated enhanced anticancer activity [180-183], encouraging us to utilize isoeugenol as a lead compound for further optimization to promote its antitumor activity.

Following the synthesis of diverse isoeugenol derivatives, those compounds were screened against both ER+ breast cancer cell line (MCF-7) and normal breast cell line (MCF-10A). Compounds **2**, **8**, and **10** have managed to exert higher potency when compared to the isoeugenol as well as the reference compound 5-Fluorouracil (5-FU), a chemotherapeutic agent in the treatment regimen for breast cancer [184, 185] (**Figure 29**).

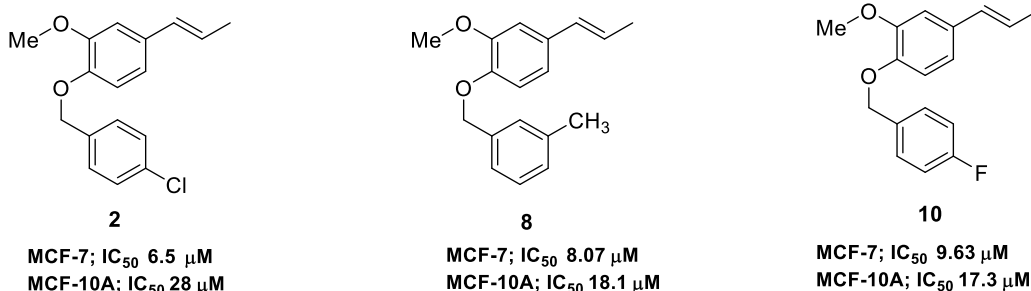


Figure 29: Most active compounds 2,8,10 and their IC₅₀s against MCF-7 and MCF-10A cells

Additionally, MCF-7 cells treated with compound **2**, the most active compound, have grown fewer and smaller colonies in a concentration-dependent manner. Cell cycle analysis showed that compound **2** induced the arrest of the cell cycle phases G₂/M and Pre-G₁ and blocked the progression of the MCF-7 cells.

By focusing on the effect of compound **2** treatment on ERα, it turned out that treated MCF-7 cells have lower expression levels of ERα as well as

downregulation of ER α proteins when compared to untreated control cells, indicating the interference of isoeugenol derivatives with ER α expression, which may account for the observed cytotoxic activity of compound **2** (**Figure 30**).

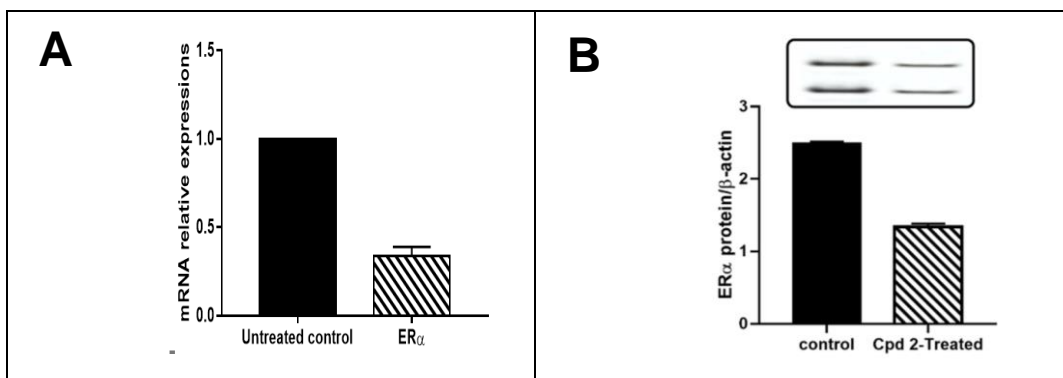


Figure 30: Downregulation of ER genes (A) and proteins(B) in case of Compound **2** treated cells vs control

Further investigations into compound **2**'s cytotoxic and apoptotic inducing activity against ER+ breast cancer have identified possible combined antioxidant, antiproliferative, and pro-apoptotic effects, as summarized in (**Figure 31**). Finally, *in vivo* results in SEC-bearing mice supported the encouraging *in vitro* therapeutic potential that compound **2** has as an antitumor agent.

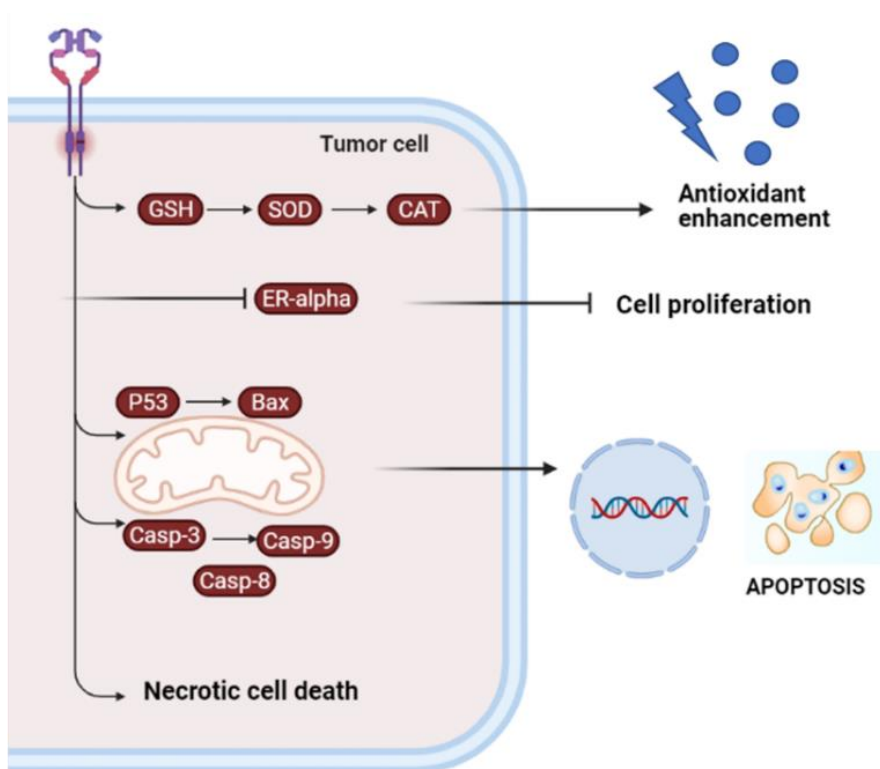


Figure 31: Summary of mixed mechanisms of action of Compound **2**

4.4. Identification of novel quinoline derivatives and their nanoformulations

This part will briefly discuss the results obtained in study 3.6. In this study, we focused on synthesizing several quinoline derivatives, testing them as anti-breast cancer agents and improving their solubility via nanoformulations.

Given that quinoline-based compounds have demonstrated remarkable potential in the field of anticancer research [186, 187], we herein adopted the development of new derivatives with potential anti-breast cancer activity. First, we set a design strategy that aimed at using the quinoline core as the main nucleus; then, we started to introduce different groups at position 8 of the nucleus (**Figure 32**). The introduced substituents have been explicitly chosen to vary in their conformational/physicochemical parameters. Their alterations spanned between flexible and rigid, hydrophilic and hydrophobic, as well as hydrogen bond donating and/or accepting characters.

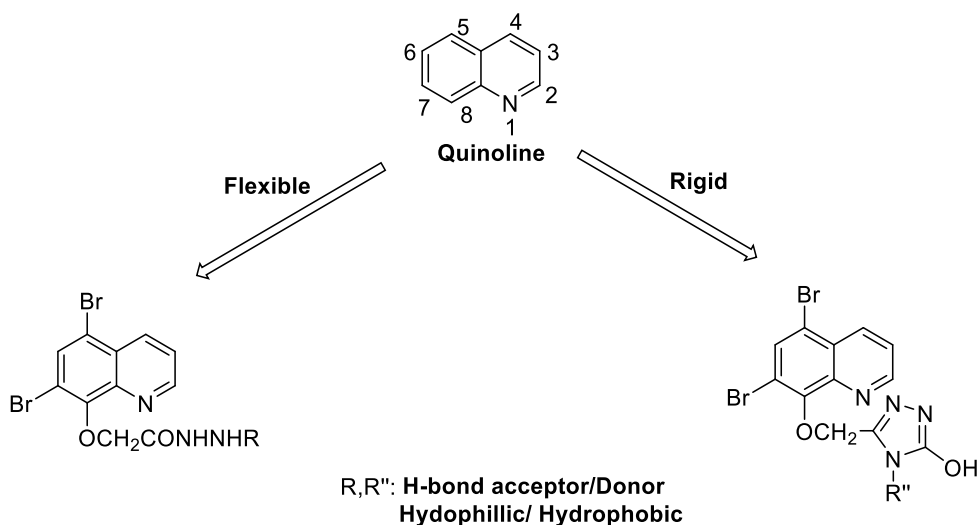
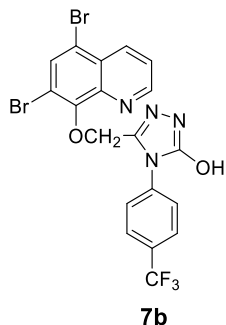


Figure 32: Design strategy for quinoline-based derivatives

Afterward, all the synthesized final 5,7-dibromo-8-substituted quinolines were evaluated for their antiproliferative activity towards two human breast cancer cell lines MCF-7 and MDA-MB231. Most of the synthesized compounds have shown better activity on MCF-7 (Luminal A subtype) rather than MDA-MB231 (TNBC subtype), proposing a possible role of hormone receptors such as ER and PR in the witnessed activity (**Figure 33**).



MCF-7; IC₅₀: 6.2 μM
MDA-MB231; IC₅₀:13.5 μM

Figure 33: Most active compound of the 5,7-dibromquinoline derivatives.

After the success of obtaining some scaffolds with observed anti-breast cancer activity, improving their solubility for better drug delivery was another objective to be addressed. It is well-known that some pharmacokinetic factors can hinder the drug development process, namely poor solubility, limited bioavailability, and difficulties in dosage form formulation. In our study, we tested the effect of incorporating synthesized compounds in pluronic nanomicelles. Assessment of the solubility of the selected compounds showed that they were practically insoluble (< 0.1 mg/1 mL); accordingly, preparation of compounds loaded nanoparticles (NP) act to enhance this poor solubility of the compounds, as seen in **Figure 34**.

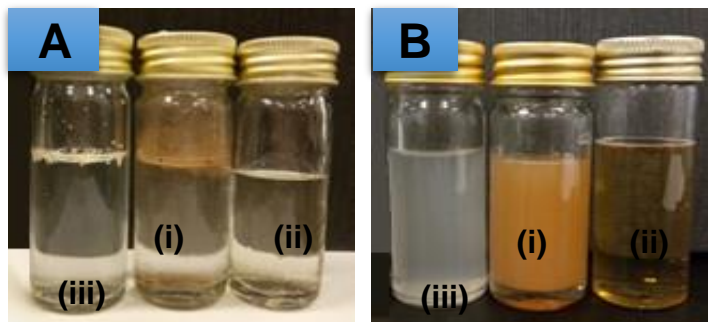


Figure 34: Free compounds vs their corresponding nanomicells formation (a) Lack of homogeneity, insolubility and instability of the aqueous suspensions of the free bioactive compounds [**4a** (i), **5c** (ii) and **7b** (iii)] as compared to (b) their corresponding nanomicelles formulations.

Finally, the compounds-loaded nanomicelles for **4a**, **5c** and **7b** showed higher activity against MCF-7 and MDA-MB231, an observation that can be attributed to the improved dispersion of the nano form of these compounds in an aqueous medium as compared to the poor water solubility of the corresponding free unloaded forms (**Figure 35**). It is worth mentioning that those formulations

have provided a sustained release of the bioactive compounds from the nanomicelles as seen in **Figure 36**.

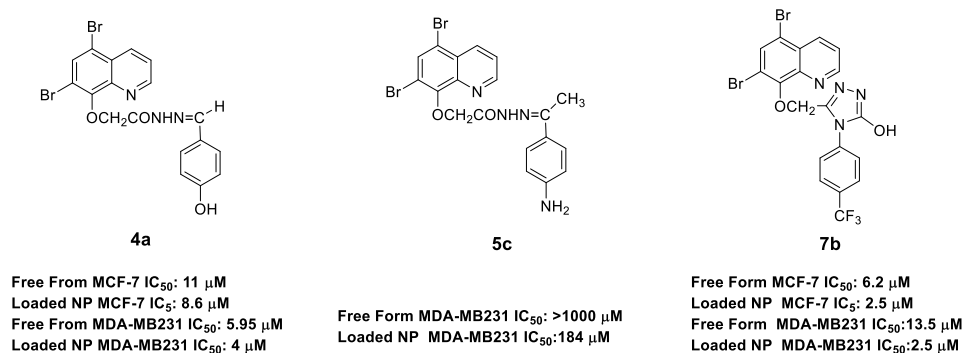


Figure 35: Free Form vs Loaded NP IC₅₀s against MCF-7 and MDA-MB231 cells

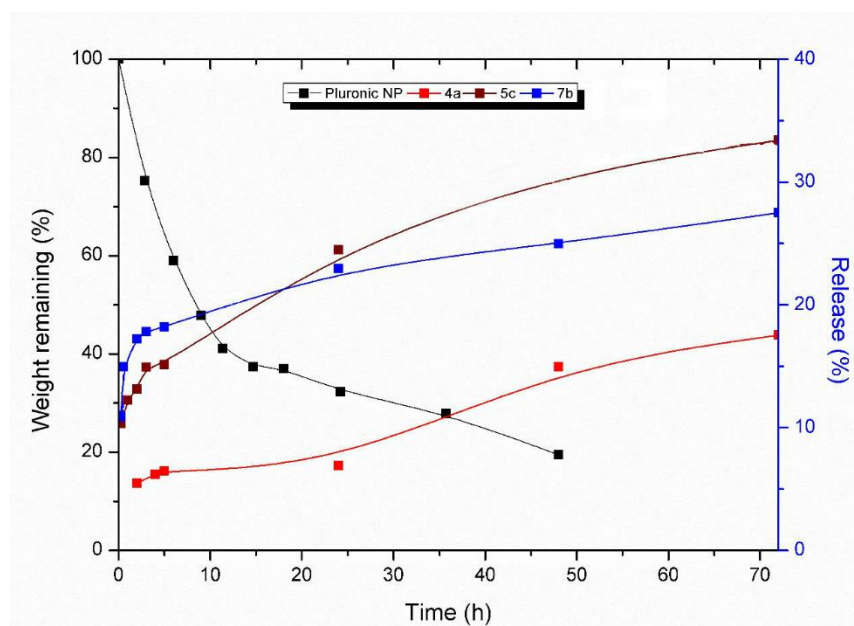


Figure 36: Degradation pattern of the pluronic nanomicelles, and the release profiles of the synthesized bioactive compounds from the nanomicelles.

5. General Conclusions

As the incidence of cancer has been increasing dramatically throughout the years, identifying new treatment options has always been one of the top research interests in different scientific fields. From a medicinal chemistry perspective, searching for active molecules that can target cancer cells is the main goal of research. Although many forms of cancer are known for their devastating prognosis, we herein have chosen to target two of the most prevailing types of cancer: neuroblastoma and breast cancer. We have adopted different methods, such as computational studies, chemical synthesis, biochemical assays, and cellular testing, to introduce new chemical compounds targeting these specific cancer types.

The first part of the work has delved into investigating PKMYT-1's ATP pocket and its inhibitors' binding interactions. Previous screening of 800 known kinase inhibitors against PKMYT-1 has identified several chemically classified inhibitors into azastilbenes, 4-aminoquinolines, and aminopyrimidines. Based on the obtained results, compounds bearing the diaminopyrimidine scaffold were designed as potential PKMYT-1 inhibitors. Consequently, the promising candidates were synthesized, structurally optimized, and tested for their PKMYT-1 inhibition and anticancer activity. The synthesized compounds have shown varying inhibition levels against different cancer cell lines; however, no direct correlation was found between PKMYT-1 binding and activity against cancer cells for most compounds. Further analysis through docking studies revealed insights into compound interactions with PKMYT-1, WEE1 kinase, and Aurora A kinase. The most active compounds displayed unique interactions with these kinases, indicating potential alternative pathways for their activity. Overall, this part has proposed some potential PKMYT-1 inhibitors and shed light on the complex interactions between these compounds and various kinases, providing valuable insights for the future development of targeted cancer therapies.

The second part of the work dealt with breast cancer, which is known to be the most common cancer type among females worldwide. Given that about 80% of breast cancers manifest Estrogen receptors, developing ER antagonists to induce estrogen deprivation stands as a logical treatment strategy. Our approach

to targeting ER was structured around three distinct concepts, each introducing novel chemical compositions. These compounds were tailored to affect MCF-7 cells, a significant model of ER+ breast cancer (Luminal A subtype), or to directly target the ER itself. Throughout our design process, we aimed to bypass the significant limitations observed in similar or approved inhibitors.

The first approach focused on creating new TAM derivatives that aim to bypass the metabolic pathway reliant on the CYP2D6 enzyme. Therefore, our work has included designing compounds maintaining TAM's main features while utilizing an alternative metabolic route. We modified tamoxifen analogues with structural variabilities that would promote alternative metabolic pathways while keeping the main pharmacophoric features of TAM. Some of the synthesized compounds have demonstrated significant antiproliferative effects on MCF-7 cells with noticeable activity and binding affinity to ER α . Additionally, the in silico analysis indicated the ability of those analogues to maintain the necessary binding arrangement for an antiestrogenic effect similar to 4-OHTAM. Finally, investigating the metabolic pathway of a representative compound showed an independent pathway of CYP2D6, indicating the involvement of non-CYP enzymes in its active hydroxyl metabolite formation. These findings highlighted the success in designing TAM analogues undergoing significant non-CYP mediated hydrolysis.

With the increasing interest in natural compounds for breast cancer treatment, our secondary focus involved seeking potentially effective semi-synthetic compounds against ER+ breast cancer cells. We investigated new derivatives of isoeugenol, evaluating their efficacy in combating these cancer cells. Some of these newly synthesized compounds demonstrated higher potency than both isoeugenol and 5-Fluorouracil, a common chemotherapy drug used in breast cancer treatment. Upon closer examination of the most active compound, it showed an ability to halt cell progression by inducing cell cycle arrest in G2/M and Pre-G1 phases. Further investigations revealed that these compounds might trigger cytotoxicity and apoptosis in ER+ breast cancer cells by combining antioxidant, antiproliferative, and pro-apoptotic effects. This data was reinforced

by observations of reduced ER α protein levels in treated MCF-7 cells and positive outcomes from in vivo experiments conducted on mice with SEC tumors.

Our final approach aimed to develop quinoline derivatives as potential anti-breast cancer agents and improve their solubility using nanoformulations. Leveraging the promising characteristics of quinoline-based compounds in cancer research, we created various derivatives by modifying the substituents of the quinoline core. These synthesized compounds exhibited potent activity against MCF-7 cells, indicating a possible impact of hormone receptors such as ER and PR on their effectiveness. Recognizing the crucial role of solubility in drug development, we endeavored to enhance solubility through pluronic nanomicelles. Initially, the synthesized compounds showed poor solubility, prompting the creation of compound-loaded nanoparticles to address this issue. Impressively, these loaded compounds in nanomicelles showed heightened activity against both MCF-7 and MDA-MB231 cells. This enhancement was likely due to the improved dispersion of the compounds in an aqueous environment facilitated by the nanomicelles, overcoming the low solubility of the free unloaded forms. Additionally, these formulations exhibited sustained release of the bioactive compounds from the nanomicelles

The data presented across these studies illustrates the diverse approaches in medicinal chemistry for combating different types of cancers. Through innovative strategies involving molecular design, compound synthesis, and nanoformulation techniques, these investigations have explored the potential of novel compounds and derivatives in targeting specific cancer types, showcasing the multifaceted nature of research aiming to tackle the complexities of cancer treatment. These varied approaches feature the importance of targeted therapy comprehensive approaches to address the diversity in cancer types and facilitate the treatment.

6. References

1. Sung, H., et al., *Global Cancer Statistics 2020: GLOBOCAN Estimates of Incidence and Mortality Worldwide for 36 Cancers in 185 Countries*. CA Cancer J Clin, 2021. **71**(3): p. 209-249.
2. Deo, S.V.S., J. Sharma, and S. Kumar, *GLOBOCAN 2020 Report on Global Cancer Burden: Challenges and Opportunities for Surgical Oncologists*. Ann Surg Oncol, 2022. **29**(11): p. 6497-6500.
3. Peczek, P., et al., *Cancer-associated inflammation: pathophysiology and clinical significance*. J Cancer Res Clin Oncol, 2023. **149**(6): p. 2657-2672.
4. Ostrand-Rosenberg, S., *Immune surveillance: a balance between protumor and antitumor immunity*. Curr Opin Genet Dev, 2008. **18**(1): p. 11-8.
5. Zhang, P.W., et al., *Classifying ten types of major cancers based on reverse phase protein array profiles*. PLoS One, 2015. **10**(3): p. e0123147.
6. Carbone, A., *Cancer Classification at the Crossroads*. Cancers (Basel), 2020. **12**(4).
7. Fitzgerald, R.C., et al., *The future of early cancer detection*. Nat Med, 2022. **28**(4): p. 666-677.
8. Zhong, L., et al., *Small molecules in targeted cancer therapy: advances, challenges, and future perspectives*. Signal Transduct Target Ther, 2021. **6**(1): p. 201.
9. Lin, M.J., et al., *Cancer vaccines: the next immunotherapy frontier*. Nat Cancer, 2022. **3**(8): p. 911-926.
10. Park, J.R., A. Eggert, and H. Caron, *Neuroblastoma: biology, prognosis, and treatment*. Hematol Oncol Clin North Am, 2010. **24**(1): p. 65-86.
11. Maris, J.M., *Recent advances in neuroblastoma*. N Engl J Med, 2010. **362**(23): p. 2202-11.
12. Yan, P., et al., *Comparison of Incidence and Outcomes of Neuroblastoma in Children, Adolescents, and Adults in the United States: A Surveillance, Epidemiology, and End Results (SEER) Program Population Study*. Med Sci Monit, 2020. **26**: p. e927218.
13. Mahapatra S. and C. KB. *Neuroblastoma*. 2023 Jul 10 [cited 2023 December]; Available from: <https://www.ncbi.nlm.nih.gov/books/NBK448111/>.
14. Cohn, S.L., et al., *The International Neuroblastoma Risk Group (INRG) classification system: an INRG Task Force report*. J Clin Oncol, 2009. **27**(2): p. 289-97.
15. Sokol, E. and A.V. Desai, *The Evolution of Risk Classification for Neuroblastoma*. Children (Basel), 2019. **6**(2).
16. Pugh, T.J., et al., *The genetic landscape of high-risk neuroblastoma*. Nat Genet, 2013. **45**(3): p. 279-84.
17. Fujita, T., et al., *CHD5, a tumor suppressor gene deleted from 1p36.31 in neuroblastomas*. J Natl Cancer Inst, 2008. **100**(13): p. 940-9.
18. Theissen, J., et al., *Chromosome 17/17q gain and unaltered profiles in high resolution array-CGH are prognostically informative in neuroblastoma*. Genes Chromosomes Cancer, 2014. **53**(8): p. 639-49.
19. Mosse, Y.P., et al., *Identification of ALK as a major familial neuroblastoma predisposition gene*. Nature, 2008. **455**(7215): p. 930-5.
20. Schulte, J.H., et al., *MYCN and ALKF1174L are sufficient to drive neuroblastoma development from neural crest progenitor cells*. Oncogene, 2013. **32**(8): p. 1059-65.
21. Qiu, B. and K.K. Matthay, *Advancing therapy for neuroblastoma*. Nat Rev Clin Oncol, 2022. **19**(8): p. 515-533.
22. Matthay, K.K., R.E. George, and A.L. Yu, *Promising therapeutic targets in neuroblastoma*. Clin Cancer Res, 2012. **18**(10): p. 2740-53.
23. Zafar, A., et al., *Molecular targeting therapies for neuroblastoma: Progress and challenges*. Med Res Rev, 2021. **41**(2): p. 961-1021.
24. Giordano, S.H., *Breast Cancer in Men*. New England Journal of Medicine, 2018. **378**(24): p. 2311-2320.
25. Arnold, M., et al., *Current and future burden of breast cancer: Global statistics for 2020 and 2040*. Breast, 2022. **66**: p. 15-23.
26. Lei, S., et al., *Global patterns of breast cancer incidence and mortality: A population-based cancer registry data analysis from 2000 to 2020*. Cancer Commun (Lond), 2021. **41**(11): p. 1183-1194.
27. Shiovitz, S. and L.A. Korde, *Genetics of breast cancer: a topic in evolution*. Ann Oncol, 2015. **26**(7): p. 1291-9.
28. Danaei, G., et al., *Causes of cancer in the world: comparative risk assessment of nine behavioural and environmental risk factors*. Lancet, 2005. **366**(9499): p. 1784-93.

29. Momenimovahed, Z. and H. Salehiniya, *Epidemiological characteristics of and risk factors for breast cancer in the world*. Breast Cancer (Dove Med Press), 2019. **11**: p. 151-164.
30. McPherson, K., C.M. Steel, and J.M. Dixon, *ABC of breast diseases. Breast cancer-epidemiology, risk factors, and genetics*. BMJ, 2000. **321**(7261): p. 624-8.
31. Key, T.J., P.K. Verkasalo, and E. Banks, *Epidemiology of breast cancer*. Lancet Oncol, 2001. **2**(3): p. 133-40.
32. Tsang, J.Y.S. and G.M. Tse, *Molecular Classification of Breast Cancer*. Adv Anat Pathol, 2020. **27**(1): p. 27-35.
33. Onitilo, A.A., et al., *Breast cancer subtypes based on ER/PR and Her2 expression: comparison of clinicopathologic features and survival*. Clin Med Res, 2009. **7**(1-2): p. 4-13.
34. Perou, C.M., et al., *Molecular portraits of human breast tumours*. Nature, 2000. **406**(6797): p. 747-52.
35. Harbeck, N., et al., *Breast cancer*. Nature Reviews Disease Primers, 2019. **5**(1).
36. Sun, Y.S., et al., *Risk Factors and Preventions of Breast Cancer*. Int J Biol Sci, 2017. **13**(11): p. 1387-1397.
37. Martin, A.M. and B.L. Weber, *Genetic and hormonal risk factors in breast cancer*. J Natl Cancer Inst, 2000. **92**(14): p. 1126-35.
38. Daly, A.A., et al., *A Review of Modifiable Risk Factors in Young Women for the Prevention of Breast Cancer*. Breast Cancer (Dove Med Press), 2021. **13**: p. 241-257.
39. Lukaszewicz, S., et al., *Breast Cancer-Epidemiology, Risk Factors, Classification, Prognostic Markers, and Current Treatment Strategies-An Updated Review*. Cancers (Basel), 2021. **13**(17).
40. den Hollander, P., M.I. Savage, and P.H. Brown, *Targeted therapy for breast cancer prevention*. Front Oncol, 2013. **3**: p. 250.
41. Ju, J., A.J. Zhu, and P. Yuan, *Progress in targeted therapy for breast cancer*. Chronic Dis Transl Med, 2018. **4**(3): p. 164-175.
42. Massague, J., *G1 cell-cycle control and cancer*. Nature, 2004. **432**(7015): p. 298-306.
43. Nurse, P., *A long twentieth century of the cell cycle and beyond*. Cell, 2000. **100**(1): p. 71-8.
44. Liu, J., Y. Peng, and W. Wei, *Cell cycle on the crossroad of tumorigenesis and cancer therapy*. Trends Cell Biol, 2022. **32**(1): p. 30-44.
45. Wang, Z., *Cell Cycle Progression and Synchronization: An Overview*. Methods Mol Biol, 2022. **2579**: p. 3-23.
46. Bertoli, C., J.M. Skotheim, and R.A. de Bruin, *Control of cell cycle transcription during G1 and S phases*. Nat Rev Mol Cell Biol, 2013. **14**(8): p. 518-28.
47. O'Connell, M.J., N.C. Walworth, and A.M. Carr, *The G2-phase DNA-damage checkpoint*. Trends Cell Biol, 2000. **10**(7): p. 296-303.
48. Lara-Gonzalez, P., F.G. Westhorpe, and S.S. Taylor, *The spindle assembly checkpoint*. Curr Biol, 2012. **22**(22): p. R966-80.
49. Malumbres, M., et al., *Cyclin-dependent kinases: a family portrait*. Nat Cell Biol, 2009. **11**(11): p. 1275-6.
50. Martinez-Alonso, D. and M. Malumbres, *Mammalian cell cycle cyclins*. Semin Cell Dev Biol, 2020. **107**: p. 28-35.
51. Wood, D.J. and J.A. Endicott, *Structural insights into the functional diversity of the CDK-cyclin family*. Open Biol, 2018. **8**(9).
52. Esposito, F., et al., *Wee1 Kinase: A Potential Target to Overcome Tumor Resistance to Therapy*. Int J Mol Sci, 2021. **22**(19).
53. Nakanishi, M., et al., *Identification and characterization of human Wee1B, a new member of the Wee1 family of Cdk-inhibitory kinases*. Genes Cells, 2000. **5**(10): p. 839-47.
54. Squire, C.J., et al., *Structure and inhibition of the human cell cycle checkpoint kinase, Wee1A kinase: an atypical tyrosine kinase with a key role in CDK1 regulation*. Structure, 2005. **13**(4): p. 541-50.
55. McGowan, C.H. and P. Russell, *Cell cycle regulation of human WEE1*. EMBO J, 1995. **14**(10): p. 2166-75.
56. Mueller, P.R., et al., *Myt1: a membrane-associated inhibitory kinase that phosphorylates Cdc2 on both threonine-14 and tyrosine-15*. Science, 1995. **270**(5233): p. 86-90.

57. Wells, N.J., et al., *The C-terminal domain of the Cdc2 inhibitory kinase Myt1 interacts with Cdc2 complexes and is required for inhibition of G(2)/M progression*. J Cell Sci, 1999. **112** (Pt 19): p. 3361-71.
58. Booher, R.N., P.S. Holman, and A. Fattaey, *Human Myt1 is a cell cycle-regulated kinase that inhibits Cdc2 but not Cdk2 activity*. J Biol Chem, 1997. **272**(35): p. 22300-6.
59. Nakajima, H., et al., *Myt1 protein kinase is essential for Golgi and ER assembly during mitotic exit*. J Cell Biol, 2008. **181**(1): p. 89-103.
60. Crncec, A. and H. Hochegger, *Triggering mitosis*. FEBS Lett, 2019. **593**(20): p. 2868-2888.
61. Suganuma, M., et al., *Sensitization of cancer cells to DNA damage-induced cell death by specific cell cycle G2 checkpoint abrogation*. Cancer Res, 1999. **59**(23): p. 5887-91.
62. Levine, A.J., *p53, the cellular gatekeeper for growth and division*. Cell, 1997. **88**(3): p. 323-31.
63. Wang, X., E.R. Simpson, and K.A. Brown, *p53: Protection against Tumor Growth beyond Effects on Cell Cycle and Apoptosis*. Cancer Res, 2015. **75**(23): p. 5001-7.
64. Kastan, M.B., C.E. Canman, and C.J. Leonard, *P53, cell cycle control and apoptosis: implications for cancer*. Cancer Metastasis Rev, 1995. **14**(1): p. 3-15.
65. Kastan, M.B. and J. Bartek, *Cell-cycle checkpoints and cancer*. Nature, 2004. **432**(7015): p. 316-23.
66. Bucher, N. and C.D. Britten, *G2 checkpoint abrogation and checkpoint kinase-1 targeting in the treatment of cancer*. Br J Cancer, 2008. **98**(3): p. 523-8.
67. Chen, T., et al., *Targeting the S and G2 checkpoint to treat cancer*. Drug Discov Today, 2012. **17**(5-6): p. 194-202.
68. Aarts, M., S. Linardopoulos, and N.C. Turner, *Tumour selective targeting of cell cycle kinases for cancer treatment*. Curr Opin Pharmacol, 2013. **13**(4): p. 529-35.
69. Ghelli Luserna di Rora, A., et al., *A WEE1 family business: regulation of mitosis, cancer progression, and therapeutic target*. J Hematol Oncol, 2020. **13**(1): p. 126.
70. Jeong, D., et al., *Protein kinase, membrane-associated tyrosine/threonine 1 is associated with the progression of colorectal cancer*. Oncol Rep, 2018. **39**(6): p. 2829-2836.
71. Sun, Q.S., et al., *Overexpression of PKMYT1 indicates the poor prognosis and enhances proliferation and tumorigenesis in non-small cell lung cancer via activation of Notch signal pathway*. Eur Rev Med Pharmacol Sci, 2019. **23**(10): p. 4210-4219.
72. Liu, L., et al., *PKMYT1 promoted the growth and motility of hepatocellular carcinoma cells by activating beta-catenin/TCF signaling*. Exp Cell Res, 2017. **358**(2): p. 209-216.
73. Wang, X.M., et al., *Effects of MCRS1 on proliferation, migration, invasion, and epithelial mesenchymal transition of gastric cancer cells by interacting with Pkmyt1 protein kinase*. Cell Signal, 2019. **59**: p. 171-181.
74. Magnussen, G.I., et al., *High expression of Wee1 is associated with poor disease-free survival in malignant melanoma: potential for targeted therapy*. PLoS One, 2012. **7**(6): p. e38254.
75. Chayka, O., et al., *Identification and pharmacological inactivation of the MYCN gene network as a therapeutic strategy for neuroblastic tumor cells*. J Biol Chem, 2015. **290**(4): p. 2198-212.
76. Zhang, Q., et al., *Overexpressed PKMYT1 promotes tumor progression and associates with poor survival in esophageal squamous cell carcinoma*. Cancer Manag Res, 2019. **11**: p. 7813-7824.
77. Dixon, H. and C.J. Norbury, *Therapeutic exploitation of checkpoint defects in cancer cells lacking p53 function*. Cell Cycle, 2002. **1**(6): p. 362-8.
78. Kawabe, T., *G2 checkpoint abrogators as anticancer drugs*. Mol Cancer Ther, 2004. **3**(4): p. 513-9.
79. Vogelstein, B., D. Lane, and A.J. Levine, *Surfing the p53 network*. Nature, 2000. **408**(6810): p. 307-10.
80. Castedo, M., et al., *Cell death by mitotic catastrophe: a molecular definition*. Oncogene, 2004. **23**(16): p. 2825-37.
81. De Witt Hamer, P.C., et al., *WEE1 kinase targeting combined with DNA-damaging cancer therapy catalyzes mitotic catastrophe*. Clin Cancer Res, 2011. **17**(13): p. 4200-7.
82. Russell, K.J., et al., *Abrogation of the G2 checkpoint results in differential radiosensitization of G1 checkpoint-deficient and G1 checkpoint-competent cells*. Cancer Res, 1995. **55**(8): p. 1639-42.
83. Powell, S.N., et al., *Differential sensitivity of p53(-) and p53(+) cells to caffeine-induced radiosensitization and override of G2 delay*. Cancer Res, 1995. **55**(8): p. 1643-8.

84. Ribeiro, J.C., et al., *Caffeine-increased radiosensitivity is not dependent on a loss of G2/M arrest or apoptosis in bladder cancer cell lines*. Int J Radiat Biol, 1999. **75**(4): p. 481-92.
85. Schmidt, M., et al., *Regulation of G2/M Transition by Inhibition of WEE1 and PKMYT1 Kinases*. Molecules, 2017. **22**(12).
86. Du, X., et al., *Structure-activity relationships of Wee1 inhibitors: A review*. Eur J Med Chem, 2020. **203**: p. 112524.
87. Fu, S., et al., *Strategic development of AZD1775, a Wee1 kinase inhibitor, for cancer therapy*. Expert Opin Investig Drugs, 2018. **27**(9): p. 741-751.
88. Kong, A. and H. Mehanna, *WEE1 Inhibitor: Clinical Development*. Curr Oncol Rep, 2021. **23**(9): p. 107.
89. Russell, M.R., et al., *Combination therapy targeting the Chk1 and Wee1 kinases shows therapeutic efficacy in neuroblastoma*. Cancer Res, 2013. **73**(2): p. 776-84.
90. Zhu, J.Y., et al., *Structural Basis of Wee Kinases Functionality and Inactivation by Diverse Small Molecule Inhibitors*. J Med Chem, 2017. **60**(18): p. 7863-7875.
91. Davis, M.I., et al., *Comprehensive analysis of kinase inhibitor selectivity*. Nat Biotechnol, 2011. **29**(11): p. 1046-51.
92. Platzer, C., et al., *Identification of PKMYT1 inhibitors by screening the GSK published protein kinase inhibitor set I and II*. Bioorg Med Chem, 2018. **26**(14): p. 4014-4024.
93. Szychowski, J., et al., *Discovery of an Orally Bioavailable and Selective PKMYT1 Inhibitor, RP-6306*. J Med Chem, 2022. **65**(15): p. 10251-10284.
94. Miller, W.L., *Steroidogenesis: Unanswered Questions*. Trends Endocrinol Metab, 2017. **28**(11): p. 771-793.
95. Delhez, A., et al., *Auditory function and dysfunction: estrogen makes a difference*. Cell Mol Life Sci, 2020. **77**(4): p. 619-635.
96. Jensen, E.V., *Basic guides to the mechanism of estrogen action*. Recent Prog Horm Res, 1962. **18**: p. 387-414.
97. Kuiper, G.G., et al., *Cloning of a novel receptor expressed in rat prostate and ovary*. Proc Natl Acad Sci U S A, 1996. **93**(12): p. 5925-30.
98. Thomas, P., et al., *Identity of an estrogen membrane receptor coupled to a G protein in human breast cancer cells*. Endocrinology, 2005. **146**(2): p. 624-32.
99. Schwabe, J.W. and S.A. Teichmann, *Nuclear receptors: the evolution of diversity*. Sci STKE, 2004. **2004**(217): p. pe4.
100. Nilsson, S. and J.-Å. Gustafsson, *Biological role of estrogen and estrogen receptors*. Critical reviews in biochemistry and molecular biology, 2002. **37**(1): p. 1-28.
101. Palacios, S., *Selective Estrogen Receptor Modulators (SERMs): State of the Art*. Postmenopausal Diseases and Disorders, 2019: p. 349-366.
102. Vrtačnik, P., et al., *The many faces of estrogen signaling*. Biochimica medica, 2014. **24**(3): p. 329-342.
103. Kumar, R., et al., *The dynamic structure of the estrogen receptor*. Journal of amino acids, 2011. **2011**.
104. Hamilton, K.J., et al., *Estrogen Hormone Biology*. Curr Top Dev Biol, 2017. **125**: p. 109-146.
105. Rani, A., et al., *Endocrine Resistance in Hormone Receptor Positive Breast Cancer-From Mechanism to Therapy*. Front Endocrinol (Lausanne), 2019. **10**: p. 245.
106. VanHook, A.M., *Ligand-Independent ER Activation*. 2010. **3**(117): p. ec112-ec112.
107. Giraldi, T., et al., *Steroid signaling activation and intracellular localization of sex steroid receptors*. J Cell Commun Signal, 2010. **4**(4): p. 161-72.
108. Bjornstrom, L. and M. Sjoberg, *Mechanisms of estrogen receptor signaling: convergence of genomic and nongenomic actions on target genes*. Mol Endocrinol, 2005. **19**(4): p. 833-42.
109. Hayashi, S. and Y. Yamaguchi, *Estrogen signaling pathway and hormonal therapy*. Breast Cancer, 2008. **15**(4): p. 256-61.
110. Marino, M., P. Galluzzo, and P. Ascenzi, *Estrogen signaling multiple pathways to impact gene transcription*. Curr Genomics, 2006. **7**(8): p. 497-508.
111. Cui, J., Y. Shen, and R. Li, *Estrogen synthesis and signaling pathways during aging: from periphery to brain*. Trends Mol Med, 2013. **19**(3): p. 197-209.
112. Zilli, M., et al., *Molecular mechanisms of endocrine resistance and their implication in the therapy of breast cancer*. Biochim Biophys Acta, 2009. **1795**(1): p. 62-81.

113. Fuentes, N. and P. Silveyra, *Estrogen receptor signaling mechanisms*. Adv Protein Chem Struct Biol, 2019. **116**: p. 135-170.
114. Arnal, J.F., et al., *Membrane and Nuclear Estrogen Receptor Alpha Actions: From Tissue Specificity to Medical Implications*. Physiol Rev, 2017. **97**(3): p. 1045-1087.
115. de Leeuw, R., J. Neefjes, and R. Michalides, *A role for estrogen receptor phosphorylation in the resistance to tamoxifen*. Int J Breast Cancer, 2011. **2011**: p. 232435.
116. Smith, C.L., *Cross-talk between peptide growth factor and estrogen receptor signaling pathways*. Biol Reprod, 1998. **58**(3): p. 627-32.
117. El-Tanani, M.K. and C.D. Green, *Two separate mechanisms for ligand-independent activation of the estrogen receptor*. Mol Endocrinol, 1997. **11**(7): p. 928-37.
118. Thomas, R.S., et al., *Phosphorylation at serines 104 and 106 by Erk1/2 MAPK is important for estrogen receptor- α activity*. Journal of molecular endocrinology, 2008. **40**(3): p. 173.
119. Belachew, E.B. and D.T. Sewasew, *Molecular Mechanisms of Endocrine Resistance in Estrogen-Positive Breast Cancer*. Front Endocrinol (Lausanne), 2021. **12**: p. 599586.
120. Parl, F.F., *Estrogens, estrogen receptor and breast cancer*. Vol. 36. 2000: IOS press.
121. Dallal, C.M., et al., *Estrogen metabolism and breast cancer risk among postmenopausal women: a case-cohort study within B~FIT*. Carcinogenesis, 2014. **35**(2): p. 346-55.
122. Samavat, H. and M.S. Kurzer, *Estrogen metabolism and breast cancer*. Cancer Lett, 2015. **356**(2 Pt A): p. 231-43.
123. Brufsky, A.M. and M.N. Dickler, *Estrogen receptor-positive breast cancer: exploiting signaling pathways implicated in endocrine resistance*. The oncologist, 2018. **23**(5): p. 528.
124. Travis, R.C. and T.J. Key, *Oestrogen exposure and breast cancer risk*. Breast Cancer Research, 2003. **5**(5): p. 1-9.
125. Kang, H., et al., *Potent aromatase inhibitors and molecular mechanism of inhibitory action*. European journal of medicinal chemistry, 2018. **143**: p. 426-437.
126. Deroo, B.J. and K.S. Korach, *Estrogen receptors and human disease*. J Clin Invest, 2006. **116**(3): p. 561-70.
127. Miyoshi, Y., et al., *Mechanisms of estrogen receptor- α upregulation in breast cancers*. Med Mol Morphol, 2010. **43**(4): p. 193-6.
128. Hilborn, E., O. Stål, and A. Jansson, *Estrogen and androgen-converting enzymes 17 β -hydroxysteroid dehydrogenase and their involvement in cancer: with a special focus on 17 β -hydroxysteroid dehydrogenase type 1, 2, and breast cancer*. Oncotarget, 2017. **8**(18): p. 30552.
129. Kumar, N., et al., *Most recent strategies targeting estrogen receptor alpha for the treatment of breast cancer*. Mol Divers, 2021. **25**(1): p. 603-624.
130. Nabieva, N. and P.A. Fasching, *Endocrine Treatment for Breast Cancer Patients Revisited-History, Standard of Care, and Possibilities of Improvement*. Cancers (Basel), 2021. **13**(22).
131. McDonnell, D.P., et al., *Elucidation of the molecular mechanism of action of selective estrogen receptor modulators*. The American journal of cardiology, 2002. **90**(1): p. F35-F43.
132. Watkins, E.J., *Overview of breast cancer*. Journal of the American Academy of PAs, 2019. **32**(10): p. 13-17.
133. Komm, B.S. and S. Mirkin, *An overview of current and emerging SERMs*. J Steroid Biochem Mol Biol, 2014. **143C**: p. 207-222.
134. Wiseman, H., *Tamoxifen; molecular basis of use in cancer; treatment and prevention*. General Pharmacology, 1996. **27**(5): p. 923.
135. Harper, M.J. and A.L. Walpole, *Contrasting endocrine activities of cis and trans isomers in a series of substituted triphenylethylenes*. Nature, 1966. **212**(5057): p. 87.
136. Harper, M.J. and A.L. Walpole, *Mode of action of I.C.I. 46,474 in preventing implantation in rats*. J Endocrinol, 1967. **37**(1): p. 83-92.
137. Klopper, A. and M. Hall, *New synthetic agent for the induction of ovulation: preliminary trials in women*. Br Med J, 1971. **1**(5741): p. 152-4.
138. Williamson, J.G. and J.D. Ellis, *The induction of ovulation by tamoxifen*. J Obstet Gynaecol Br Commonw, 1973. **80**(9): p. 844-7.
139. Obrero, M., D.V. Yu, and D.J. Shapiro, *Estrogen receptor-dependent and estrogen receptor-independent pathways for tamoxifen and 4-hydroxytamoxifen-induced programmed cell death*. J Biol Chem, 2002. **277**(47): p. 45695-703.

140. Liang, Y., et al., *CD36 plays a critical role in proliferation, migration and tamoxifen-inhibited growth of ER-positive breast cancer cells*. *Oncogenesis*, 2018. **7**(12): p. 1-14.
141. Kahraman, M., et al., *Maximizing ER- α degradation maximizes activity in a tamoxifen-resistant breast cancer model: identification of GDC-0927*. *ACS medicinal chemistry letters*, 2018. **10**(1): p. 50-55.
142. Early Breast Cancer Trialists' Collaborative, G., et al., *Relevance of breast cancer hormone receptors and other factors to the efficacy of adjuvant tamoxifen: patient-level meta-analysis of randomised trials*. *Lancet*, 2011. **378**(9793): p. 771-84.
143. Cuzick, J., et al., *Overview of the main outcomes in breast-cancer prevention trials*. *Lancet*, 2003. **361**(9354): p. 296-300.
144. Powles, T.J., et al., *Twenty-year follow-up of the Royal Marsden randomized, double-blinded tamoxifen breast cancer prevention trial*. *J Natl Cancer Inst*, 2007. **99**(4): p. 283-90.
145. Karn, A., et al., *Tamoxifen for breast cancer*. *JNMA J Nepal Med Assoc*, 2010. **49**(177): p. 62-7.
146. Viedma-Rodriguez, R., et al., *Mechanisms associated with resistance to tamoxifen in estrogen receptor-positive breast cancer (review)*. *Oncol Rep*, 2014. **32**(1): p. 3-15.
147. Jordan, V.C., *New insights into the metabolism of tamoxifen and its role in the treatment and prevention of breast cancer*. *Steroids*, 2007. **72**(13): p. 829-42.
148. Wu, X., et al., *The tamoxifen metabolite, endoxifen, is a potent antiestrogen that targets estrogen receptor alpha for degradation in breast cancer cells*. *Cancer Res*, 2009. **69**(5): p. 1722-7.
149. Furr, B.J. and V.C. Jordan, *The pharmacology and clinical uses of tamoxifen*. *Pharmacol Ther*, 1984. **25**(2): p. 127-205.
150. Katzenellenbogen, B.S., et al., *Bioactivities, estrogen receptor interactions, and plasminogen activator-inducing activities of tamoxifen and hydroxy-tamoxifen isomers in MCF-7 human breast cancer cells*. *Cancer Res*, 1984. **44**(1): p. 112-9.
151. Philipp Y. Maximov, R.E.M., V. Craig Jordan, *Tamoxifen Pioneering Medicine in Breast Cancer*. 2013.
152. Maximov, P.Y., et al., *Structure-function relationships of estrogenic triphenylethylenes related to endoxifen and 4-hydroxytamoxifen*. *J Med Chem*, 2010. **53**(8): p. 3273-83.
153. Shiau, A.K., et al., *The structural basis of estrogen receptor/coactivator recognition and the antagonism of this interaction by tamoxifen*. *Cell*, 1998. **95**(7): p. 927-37.
154. Brzozowski, A.M., et al., *Molecular basis of agonism and antagonism in the oestrogen receptor*. *Nature*, 1997. **389**(6652): p. 753-8.
155. Tzukerman, M.T., et al., *Human estrogen receptor transactivational capacity is determined by both cellular and promoter context and mediated by two functionally distinct intramolecular regions*. *Mol Endocrinol*, 1994. **8**(1): p. 21-30.
156. Ahmed, N.S., et al., *Structure-Activity Relationships of Triphenylethylene Derivatives and Their Evaluation as Anticancer and Antiviral Agents*. *ACS Omega*, 2023. **8**(29): p. 25903-25923.
157. Jordan, V.C., *Turning scientific serendipity into discoveries in breast cancer research and treatment: a tale of PhD students and a 50-year roaming tamoxifen team*. *Breast Cancer Res Treat*, 2021. **190**(1): p. 19-38.
158. Miller, C.P., *SERMs: evolutionary chemistry, revolutionary biology*. *Curr Pharm Des*, 2002. **8**(23): p. 2089-111.
159. Nelson, D.R., et al., *Comparison of cytochrome P450 (CYP) genes from the mouse and human genomes, including nomenclature recommendations for genes, pseudogenes and alternative-splice variants*. *Pharmacogenetics*, 2004. **14**(1): p. 1-18.
160. Brauch, H., et al., *Pharmacogenomics of tamoxifen therapy*. *Clin Chem*, 2009. **55**(10): p. 1770-82.
161. Wu, A.H., *Drug metabolizing enzyme activities versus genetic variances for drug of clinical pharmacogenomic relevance*. *Clin Proteomics*, 2011. **8**(1): p. 12.
162. Marechal, J.D., et al., *Insights into drug metabolism by cytochromes P450 from modelling studies of CYP2D6-drug interactions*. *Br J Pharmacol*, 2008. **153** **Suppl 1**: p. S82-9.
163. Goetz, M.P., A. Kamal, and M.M. Ames, *Tamoxifen pharmacogenomics: the role of CYP2D6 as a predictor of drug response*. *Clin Pharmacol Ther*, 2008. **83**(1): p. 160-6.
164. Sim, S.C. and M. Ingelman-Sundberg, *The Human Cytochrome P450 (CYP) Allele Nomenclature website: a peer-reviewed database of CYP variants and their associated effects*. *Hum Genomics*, 2010. **4**(4): p. 278-81.

165. Chan, C.W.H., et al., *Pharmacogenomics of breast cancer: highlighting CYP2D6 and tamoxifen*. J Cancer Res Clin Oncol, 2020. **146**(6): p. 1395-1404.
166. Ingelman-Sundberg, M., et al., *Influence of cytochrome P450 polymorphisms on drug therapies: pharmacogenetic, pharmacoeconomic and clinical aspects*. Pharmacol Ther, 2007. **116**(3): p. 496-526.
167. Stearns, A.B.V., *Pharmacogenomics of Tamoxifen: Ready for Prime Time?* Current Breast Cancer Reports, 2010.
168. Beverage, J.N., et al., *CYP2D6 polymorphisms and the impact on tamoxifen therapy*. J Pharm Sci, 2007. **96**(9): p. 2224-31.
169. Hoskins, J.M., L.A. Carey, and H.L. McLeod, *CYP2D6 and tamoxifen: DNA matters in breast cancer*. Nat Rev Cancer, 2009. **9**(8): p. 576-86.
170. Bijl, M.J., et al., *The CYP2D6*4 polymorphism affects breast cancer survival in tamoxifen users*. Breast Cancer Res Treat, 2009. **118**(1): p. 125-30.
171. Schroth, W., et al., *Association between CYP2D6 polymorphisms and outcomes among women with early stage breast cancer treated with tamoxifen*. JAMA, 2009. **302**(13): p. 1429-36.
172. Saladen, P., et al., *Tamoxifen metabolism predicts drug concentrations and outcome in premenopausal patients with early breast cancer*. Pharmacogenomics J, 2015. **15**(1): p. 84-94.
173. Rohe, A., et al., *In vitro and in silico studies on substrate recognition and acceptance of human PKMYT1, a Cdk1 inhibitory kinase*. Bioorg Med Chem Lett, 2012. **22**(2): p. 1219-23.
174. Najjar, A., et al., *Computer-aided design, synthesis and biological characterization of novel inhibitors for PKMYT1*. Eur J Med Chem, 2019. **161**: p. 479-492.
175. Rohe, A., et al., *A fluorescence anisotropy-based Myt1 kinase binding assay*. Assay Drug Dev Technol, 2014. **12**(2): p. 136-44.
176. Hajduk, P.J. and J. Greer, *A decade of fragment-based drug design: strategic advances and lessons learned*. Nat Rev Drug Discov, 2007. **6**(3): p. 211-9.
177. Chessari, G. and A.J. Woodhead, *From fragment to clinical candidate--a historical perspective*. Drug Discov Today, 2009. **14**(13-14): p. 668-75.
178. de Kloe, G.E., et al., *Transforming fragments into candidates: small becomes big in medicinal chemistry*. Drug Discov Today, 2009. **14**(13-14): p. 630-46.
179. Hossain, R., et al., *Natural-Derived Molecules as a Potential Adjuvant in Chemotherapy: Normal Cell Protectors and Cancer Cell Sensitizers*. Anticancer Agents Med Chem, 2022. **22**(5): p. 836-850.
180. Al-Sharif, I., A. Remmal, and A. Aboussekhra, *Eugenol triggers apoptosis in breast cancer cells through E2F1/survivin down-regulation*. BMC Cancer, 2013. **13**: p. 600.
181. Al Wafai, R., et al., *Chemosensitivity of MCF-7 cells to eugenol: release of cytochrome-c and lactate dehydrogenase*. Sci Rep, 2017. **7**: p. 43730.
182. Carrasco A, H., et al., *Eugenol and its synthetic analogues inhibit cell growth of human cancer cells (Part I)*. Journal of the Brazilian Chemical Society, 2008. **19**(3): p. 543-548.
183. Zheng, G.Q., P.M. Kenney, and L.K.T. Lam, *Potential anticarcinogenic natural products isolated from lemongrass oil and galanga root oil*. Journal of Agricultural and Food Chemistry, 1993. **41**(2): p. 153-156.
184. Chow, L.W. and W.T. Loo, *The differential effects of cyclophosphamide, epirubicin and 5-fluorouracil on apoptotic marker (CPP-32), pro-apoptotic protein (p21(WAF-1)) and anti-apoptotic protein (bcl-2) in breast cancer cells*. Breast Cancer Res Treat, 2003. **80**(3): p. 239-44.
185. Chumakova, O.V., et al., *Effect of 5-fluorouracil, Optison and ultrasound on MCF-7 cell viability*. Ultrasound Med Biol, 2006. **32**(5): p. 751-8.
186. Gao, F., et al., *Quinolone hybrids and their anti-cancer activities: An overview*. Eur J Med Chem, 2019. **165**: p. 59-79.
187. Yadav, V., et al., *Quinoline-derivatives as privileged scaffolds for medicinal and pharmaceutical chemists: A comprehensive review*. Chem Biol Drug Des, 2022. **100**(3): p. 389-418.

7. Appendix

Nehal Hany Elghazawy

Assistant Lecturer of Medicinal Chemistry/ Research Assistant



Work History

2022-01 - Current

● **Senior Research Associate – Chemistry Department- School of Sciences and Engineering**

American University in Cairo, Cairo, Egypt

- Responsible for Polymer Chemistry and Nanochemistry research and submission of publications in highly reputable peer-reviewed journals.

2022-02 - 2022-03

● **Ph.D. Researcher- Medicinal Chemistry Department**

Martin Luther University of Halle Wittenberg, Halle, Germany

Directed and performed computational studies and data analysis.

2015-02 - 2021-01

● **Research Assistant- Drug Design research lab**

Zewail City of Science and Technology, Giza, Egypt

- Performed Medicinal Chemistry wet lab experiments and documented results for reports, presentations, and peer-reviewed journal publications.

2019-09 - 2019-11

● **Ph.D. Researcher- Medicinal Chemistry Department**

Martin Luther University of Halle Wittenberg, Halle, Germany

- Directed and performed wet lab synthesis, product identification, data collection, evaluation, and analysis.

2017-11 - 2018-05

● **Ph.D. Researcher -Medicinal Chemistry Department**

Martin Luther University of Halle Wittenberg, Halle, Germany

- Work coordinately with a group of international drug designers on a project of development of a new series of anti-cancer agents.

2017-10 - 2017-11

● **Visiting Researcher – Organic Chemistry department**

Institut des Molécules et Matériaux du Mans, Le Mans Université, Le Mans, France

- Planned and optimized various organic chemistry protocols for developing new chemical moieties as potential anti-cancer agents

2016-02 - 2017-06

● **Teaching Assistant – Drug Design Department**

Biomedical Sciences, Zewail City of Science and Technology, Giza, Egypt

- Prepared and delivered tutorials for Drug Design classes, including Computational Drug Design and Advanced Organic Chemistry courses

2014-01 - 2014-08

- **Research Intern**
Helmholtz-Zentrum für Infektionsforschung - Saarland University, Saarbruecken, Germany
 - Performed Drug Design research and biological evaluation of novel anticancer agents.

2012-02 - 2015-02

- **Teaching Assistant- Faculty of Pharmacy and Biotechnology**
German University in Cairo, Cairo
 - Prepared and delivered tutorials of Drug Design, Pharmacology, and Clinical Pharmacy.

2011-10 - 2012-01

- **Quality Manager Administrator**
German University in Cairo, Cairo, Egypt
 - Handled the process of university's curriculum international accreditation.

2018-05 - Current

2013-02 - 2015-02

2006-07 - 2011-07



Education

- **Ph.D.: Medicinal Chemistry**
Martin-Luther University of Halle Wittenberg - Halle
- **Master of Science: Pharmaceutical chemistry**
German University in Cairo - Cairo
 - Thesis Grade (GPA): 0.7 (**Excellent**)
- **Bachelor of Science: Pharmacy and Biotechnology**
German University in Cairo
 - Cumulative GPA: 0.78 (**98.79 %**) (**Excellent with Highest Honors**)



Scholarships and Awards

- March 2019: DAAD Freelancer Scholarship, *Martin-Luther University of Halle Wittenberg, Halle (Saale), Germany.*
- September 2017: DAAD GERSS Scholarship, *Martin-Luther University of Halle Wittenberg, Halle (Saale), Germany.*
- February 2017: ASRT "IMHOTEP" grant, *Institut des Molécules et Matériaux du Mans, Le Mans Université, Le Mans, France*
- June 2016: Top 5 Shortlisted Candidates, local assessment, *Novartis International BioCamp 2016.*
- January 2014 – July 2014: DAAD GERSS Scholarship, *Saarland University, Saarbruecken, Germany*



Publications

Available at <https://orcid.org/0000-0002-9376-5410>

Speaker

Organization



Conferences

- September 2023: 18th International Conference of Biochemistry and Molecular Biology "Towards a Better Future for Humanity", **Cairo, Egypt** (**Best Poster award**)
- March 2019: 14th International Conference on Chemistry and its Role in Development ICCRD'14, **Mansoura, Egypt**
- September 2016: Prague Summer School - Advances in Drug Discovery, **Prague, Czech Republic**
- March 2016: 8th International Conference and Exhibition on Pharmaceutics & Novel Drug delivery system, **Madrid, Spain** (**Best Poster award**)
- March 2015: Dubai International Pharmaceuticals and Technologies Conference and Exhibition (DUPHAT), **Dubai, UAE**



Scientific events

- April 2019: Academic and industrial aspects of drug development, **Zewail city of Science and Technology, Cairo Egypt**
- August 2016: Drug Design and Development workshop, **Zewail city of Science and Technology, Cairo Egypt**
- September 2012: Organization committee of Humboldt Kolleg "Pharmaceutical & Biotechnological Therapies" Conference, **German University in Cairo, Cairo, Egypt**



Key skills

- Designing and implementing organic synthesis schemes and protocols
- Mastering different analysis techniques: IR, MS, NMR, HPLC, Elemental analysis.
- Analyzing data using different drug design software: Chemdraw, mnova.
- Planning research flow and organizing tasks effectively
- Mastering different molecular modeling techniques: Library design, Homology modeling, Docking, Pharmacophore, QSAR, Molecular Dynamics.
- Working with different computational software: MOE, Maestro, AMBER, GROMACS.
- Performing cell line assays: MTT assay
- Performing radioactive receptors binding assays
- Writing research grants, proposals, and publications.



Languages

- English (IELTS band: 7.5) Excellent
- Arabic Excellent
- German Good

List of publications related to the thesis

- [1] **N. H. Elghazawy**, S. Hagemann, F. Erdmann, S. Hüttelmaier, M. Schmidt, W. Sippl, Computer-aided design and Synthesis of novel anticancer agents: Introducing diaminopyrimidine derivatives with potential PKMYT-1 kinases inhibition - **Manuscript under preparation**
- [2] M.S. Nafie, **N.H. Elghazawy**, S.M. Owf, K. Arafa, M.A. Abdel-Rahman, R.K. Arafa, Control of ER-positive breast cancer by ERalpha expression inhibition, apoptosis induction, cell cycle arrest using semisynthetic isoeugenol derivatives, *Chemico-biological interactions* 351 (2022) 109753.
- [3] A. Najjar, C. Platzer, A. Luft, C.A. Assmann, **N.H. Elghazawy**, F. Erdmann, W. Sippl, M. Schmidt, Computer-aided design, synthesis and biological characterization of novel inhibitors for PKMYT1, *European journal of medicinal chemistry* 161 (2019) 479-492.
- [4] **N.H. Elghazawy**, A. Hefnawy, N.K. Sedky, I.M. El-Sherbiny, R.K. Arafa, Preparation and nanoformulation of new quinolone scaffold-based anticancer agents: Enhancing solubility for better cellular delivery, *European journal of pharmaceutical sciences : official journal of the European Federation for Pharmaceutical Sciences* 105 (2017) 203-211.
- [5] **N.H. Elghazawy**, M. Engel, R.W. Hartmann, M.M. Hamed, N.S. Ahmed, A.H. Abadi, Design and synthesis of novel flexible ester-containing analogs of tamoxifen and their evaluation as anticancer agents, *Future medicinal chemistry* 8(3) (2016) 249-56.
- [6] N.S. Ahmed, **N.H. Elghazawy**, A.K. ElHady, M. Engel, R.W. Hartmann, A.H. Abadi, Design and synthesis of novel tamoxifen analogues that avoid CYP2D6 metabolism, *European journal of medicinal chemistry* 112 (2016) 171-179.

List of All publications

- [1] J.J. Zhang, H. Fu, R. Lin, J. Zhou, A. Haider, W. Fang, **N.H. Elghazawy**, J. Rong, J. Chen, Y. Li, C. Ran, T.L. Collier, Z. Chen, S.H. Liang, Imaging Cholinergic Receptors in the Brain by Positron Emission Tomography, *J Med Chem* 66(16) (2023) 10889-10916.
- [2] M. Korff, A. Chaudhary, Y. Li, X. Zhou, C. Zhao, J. Rong, J. Chen, Z. Xiao, **N.H. Elghazawy**, W. Sippl, A.T. Davenport, J.B. Daunais, L. Wang, C. Abate, H. Ahmed, R. Crowe, T.J. Schmidt, S.H. Liang, S.M. Ametamey, B. Wunsch, A. Haider, Synthesis and Biological Evaluation of Enantiomerically Pure (R)- and (S)-[¹⁸F]OF-NB1 for Imaging the GluN2B Subunit-Containing NMDA Receptors, *J Med Chem* 66(23) (2023) 16018-16031.
- [3] A. Haider, L. Wang, L. Gobbi, Y. Li, A. Chaudhary, X. Zhou, J. Chen, C. Zhao, J. Rong, Z. Xiao, L. Hou, **N.H. Elghazawy**, W. Sippl, A.T. Davenport, J.B. Daunais, H. Ahmed, R. Crowe, M. Honer, A. Rominger, U. Grether, S.H. Liang, S.M. Ametamey, Evaluation of [(¹⁸F)RoSMA-18-d(6)] as a CB2 PET Radioligand in Nonhuman Primates, *ACS chemical neuroscience* 14(20) (2023) 3752-3760.
- [4] A. Haider, **N.H. Elghazawy**, A. Dawoud, C. Gebhard, T. Wichmann, W. Sippl, M. Hoener, E. Arenas, S.H. Liang, Translational molecular imaging and drug development in Parkinson's disease, *Molecular neurodegeneration* 18(1) (2023) 11.
- [5] J. Chen, W. Ran, Y. Huang, J. Wei, J. Rong, H. Wei, Y. Li, G. Li, Z. Chen, L. Collier, **N.H. Elghazawy**, W. Sippl, A. Haider, K. Liao, C. Dong, Y. Li, H. Xu, W. He, L. Wang, S.H. Liang, Evaluation of thiadiazine-based PET radioligands for imaging the AMPA receptor, *Biomed Pharmacother* 168 (2023) 115842.
- [6] H. Ahmed, R. Wallimann, L. Gisler, **N.H. Elghazawy**, S. Gruber, C. Keller, S.H. Liang, W. Sippl, A. Haider, S.M. Ametamey, Characterization of (R)- and (S)-[(¹⁸F)OF-NB1] in Rodents as Positron Emission Tomography Probes for Imaging GluN2B Subunit-Containing N-Methyl-d-Aspartate Receptors, *ACS chemical neuroscience* 14(24) (2023) 4323-4334.
- [7] M.S. Nafie, **N.H. Elghazawy**, S.M. Owf, K. Arafa, M.A. Abdel-Rahman, R.K. Arafa, Control of ER-positive breast cancer by ER α expression inhibition, apoptosis induction, cell cycle arrest using semisynthetic isoeugenol derivatives, *Chemico-biological interactions* 351 (2022) 109753.
- [8] I.M. El-Sewify, A. Radwan, **N.H. Elghazawy**, W. Fritzsche, H.M.E. Azzazy, Optical chemosensors for environmental monitoring of toxic metals related to Alzheimer's disease, *RSC advances* 12(50) (2022) 32744-32755.

- [9] **N.H. Elghazawy**, D. Zaafar, R.R. Hassan, M.Y. Mahmoud, L. Bedda, A.F. Bakr, R.K. Arafa, Discovery of New 1,3,4-Oxadiazoles with Dual Activity Targeting the Cholinergic Pathway as Effective Anti-Alzheimer Agents, *ACS chemical neuroscience* 13(8) (2022) 1187-1205.
- [10] H. Ahmed, L. Gisler, **N.H. Elghazawy**, C. Keller, W. Sippl, S.H. Liang, A. Haider, S.M. Ametamey, Development and Validation of [(3)H]OF-NB1 for Preclinical Assessment of GluN1/2B Candidate Drugs, *Pharmaceuticals* 15(8) (2022).
- [11] H.S.A. ElZahabi, M.S. Nafie, D. Osman, **N.H. Elghazawy**, D.H. Soliman, A.A.H. El-Helby, R.K. Arafa, Design, synthesis and evaluation of new quinazolin-4-one derivatives as apoptotic enhancers and autophagy inhibitors with potent antitumor activity, *European journal of medicinal chemistry* 222 (2021) 113609.
- [12] A. Najjar, C. Platzner, A. Luft, C.A. Assmann, **N.H. Elghazawy**, F. Erdmann, W. Sippl, M. Schmidt, Computer-aided design, synthesis and biological characterization of novel inhibitors for PKMYT1, *European journal of medicinal chemistry* 161 (2019) 479-492.
- [13] H. Mohammad, **N.H. Elghazawy**, H.E. Eldesouky, Y.A. Hegazy, W. Younis, L. Avrimova, T. Hazbun, R.K. Arafa, M.N. Seleem, Discovery of a Novel Dibromoquinoline Compound Exhibiting Potent Antifungal and Antivirulence Activity That Targets Metal Ion Homeostasis, *ACS infectious diseases* 4(3) (2018) 403-414.
- [14] **N.H. Elghazawy**, A. Hefnawy, N.K. Sedky, I.M. El-Sherbiny, R.K. Arafa, Preparation and nanoformulation of new quinolone scaffold-based anticancer agents: Enhancing solubility for better cellular delivery, *European journal of pharmaceutical sciences : official journal of the European Federation for Pharmaceutical Sciences* 105 (2017) 203-211.
- [15] R.K. Arafa, **N.H. Elghazawy**, Personalized Medicine and Resurrected Hopes for the Management of Alzheimer's Disease: A Modular Approach Based on GSK-3beta Inhibitors, *Advances in experimental medicine and biology* 1007 (2017) 199-224.
- [16] M.M. Ghorab, M.S. Alsaid, M. Higgins, A.T. Dinkova-Kostova, A.A. Shahat, **N.H. Elghazawy**, R.K. Arafa, Synthesis, molecular modeling and NAD(P)H:quinone oxidoreductase 1 inducer activity of novel 2-phenylquinazolin-4-amine derivatives, *Journal of enzyme inhibition and medicinal chemistry* 31(6) (2016) 1612-8.
- [17] M.M. Ghorab, M.S. Alsaid, M. Higgins, A.T. Dinkova-Kostova, A.A. Shahat, **N.H. Elghazawy**, R.K. Arafa, NAD(P)H:quinone oxidoreductase 1 inducer activity of some novel anilinoquinazoline derivatives, *Drug design, development and therapy* 10 (2016) 2515-24.

[18] **N.H. Elghazawy**, M. Engel, R.W. Hartmann, M.M. Hamed, N.S. Ahmed, A.H. Abadi, Design and synthesis of novel flexible ester-containing analogs of tamoxifen and their evaluation as anticancer agents, *Future medicinal chemistry* 8(3) (2016) 249-56.

[19] N.S. Ahmed, **N.H. Elghazawy**, A.K. ElHady, M. Engel, R.W. Hartmann, A.H. Abadi, Design and synthesis of novel tamoxifen analogues that avoid CYP2D6 metabolism, *European journal of medicinal chemistry* 112 (2016) 171-179.

Selbstständigkeitserklärung/Declaration of Authorship

Hiermit erkläre ich, dass ich die vorliegende Dissertationsschrift selbständig und ohne fremde Hilfe angefertigt, keine anderen als die angegebenen Quellen und Hilfsmittel benutzt und die aus ihnen wörtlich oder inhaltlich entnommenen Stellen als solche kenntlich gemacht habe. Die Arbeit wurde ausschließlich der Mathematisch-Naturwissenschaftlichen Fakultät der MartinLuther-Universität Halle-Wittenberg vorgelegt und an keiner anderen Universität oder Hochschule weder im In- und Ausland zur Erlangung des Doktorgrades eingereicht.

I hereby declare that I am the sole author of this thesis and that I have not used any sources other than those listed in the bibliography and identified as references. I further declare that I have not submitted this thesis at any other institution in order to obtain a degree.

Halle (Saale), 31.12.2023

Nehal Elghazawy